Università degli Studi di Camerino

International School of Advanced Studies

Mathematics Division

All wheel drive electric motorcycle modelling and control

Doctor of Philosophy in
Science and Technology - curriculum *Mathematics*
XXXII cycle

Ph.D. Candidate:

Verdiana Del Rosso

Advisors:

Prof. Simonetta Boria

Ing. Antonio Ranalli

Co-advisor:

Prof. Maria Letizia Corradini

Academic Year 2019/2020

"*Look wide, and even when you think you are looking wide - look wider still.*"

Sir Robert Baden-Powell

Abstract

Conventional motorcycles are powered through a chain or shaft linking the engine to the rear wheel. However, motorcycle riders are now facing riding conditions and obstacles where having only rear wheel drive can lead to vehicle damage, loss of control and an unstable front wheel during cornering and off-road riding in general. Traction and climbing ability are severely limited in extreme mountain conditions by only having the rear wheel to provide power. Accordingly, there is a need in the industry for a two-wheel drive motorcycle that efficiently and safely transfers power from the motor to the front wheel, because it provides the rider with increased ability to safely negotiate rough terrain.

In this background, the design of an optimal torque distribution strategy implemented by two separate electric motors in an all-wheel-drive electric motorcycle has many potentialities not fully explored and deeply understood for two wheel vehicles, that makes this study interesting from a scientific point of view.

With this in mind, the research project aims to design control systems for improving rider's safety and vehicle performance at low as well as high speeds, especially in critical situations and rough terrains, taking into account the presence of the front wheel torque generated by a hub-mounted electric motor.

At low speed the research investigates whether and how the front wheel torque helps the stabilization of the vehicle around the upright position, without any rider action required. The study is developed by deriving a simplified analytical model of the vehicle, which captures its lateral motion and a model-based control system, employing the sliding mode control technique. As further requirement, the motorcycle should be balanced in a small bounded area, by means of Multi Input control system.

At medium and high speeds the study explores how and how much the traction torque repartition can improve continuously the vehicle performances in combined longitudinal and lateral acceleration situations, such as the exit of a curve, especially in those conditions where a traditional motorcycle falls down because it overcomes tyre adherence limits. Last purpose is achieved deriving a dynamical optimal traction strategy which does not require the a priori knowledge of the friction

coefficient. Steady state analysis indicates outperformances of the all wheel drive motorcycle over the classical rear wheel drive one. Then, dynamical simulations of selected manoeuvres, in both flat and uneven road, corroborate the result.

Acknowledgments

This thesis is the result of a three years long research activity that I have carried out at the Department of Mathematics at University of Camerino and into the company Visionar srl. I would like to thank some people who made a contribution to this thesis and helped me in some way.

First of all, I would like to thank my advisor Simonetta Boria for her constant support and suggestions during all stages of my work and my co-advisor Maria Letizia Corradini for her guidance on control aspects. A special thanks to both of them for their constant availability, for the long meetings in front of my laptop trying to interpret all together the work results, the incitations towards new ways. I cannot forget to be also grateful to Roberto Giambò to help me on the mathematical model part and to have taught how much the mathematical analysis can assist you during research.

I wish to thank all members and colleagues of the company Visionar srl of Osimo (AN) to have found this project and to strongly believe in it and in me, starting from Antonio Ranalli and Andrea Andreucci. Your contribution has been essential for me to understand many features of the motorcycle behaviour and to find out every time a different point of view to solve a problem. In particular, I want to express my gratitude to my colleague Alessio Nardini for his support, his precious suggestions and explanations about mechanical engineering aspects and Matlab software and to share my desk and my lunch breaks. Thanks for all coffee cups you offered to me! One day I will find out a way to give you back the favour. All of you have tried to make me more practical and less theoretical, teaching me that the right trade off between them is the winner choice to solve problems and issues!

I would like to express my gratitude to Roberto Lot to have shared his invaluable knowledge about motorcycle and the software we used to validate the results as well as to have helped and guided me for a consistent part of this thesis. If my period abroad was particularly productive and positive, above all I owe you and your cordial hospitality at University of Southampton a debt of gratitude. I would also be thankful to Wahida and Penny for making me feel as at my department when I was in Southampton.

I am also glad to give a thank to my university colleagues Lorenza Spadoni, Mauro Bacaloni and Filippo Santarelli to let shine a smile on my face every day in the office. A special thanks to Josephin Giacomini, for her precious continuous advice: one day all your efforts on research will be clear to the department, the world and to your boss. You are a really special person.

One special thank goes to my best friend Gloria, the person who is with me in the good as well in the bad weather. Simply thank you for being here.

Last, but not the least I am particularly grateful to my parents Carmela and Stefano for their everlasting love and support during the whole period of studies, to my sister Chiara, and my brothers Cristiano and Sebastiano. Your suggestions and words are an invaluable source of inspiration to grow up and to improve myself. And finally, thank you to all the other members of my extended family!

This work was a great team job!

Contents

Abbreviations

ABS	Antilock Braking System
AWD	All Wheel Drive (vehicle)
CoG	Centre of Gravity
CoM	Centre of Mass
CoP	Centre of Pressure
DoF	Degrees of Freedom
ECU	Electronic Control Unit
ESC	Electronic Stability Control
ESP	Electronic Stability Program
FEA	Finite Element Analysis
IC	Internal Combustion (Engine)
MIMO	Multi Input Multi Output (control)
ODE	Ordinary Differential Equation
PI	Proportional-Integral (control method)
PID	Proportional-Integral-Derivative (control method)
PM	Permanent Magnet
PMSM	Permanent Magnet Synchronous Motor
RWD	Rear Wheel Drive (vehicle)
SISO	Single Input Single Output (control)
SOC	State of Charge
TC	Traction Control (System)

List of Symbols and Notations

General notation:

- a scalar: italic medium-face serif font, e.g. R, r, ω;
- a vector: italic bold serif font, e.g. $\boldsymbol{R}$, $\boldsymbol{r}$, $\boldsymbol{\omega}$;
  - a vector in a specific reference frame: reference frame is a subscript in capitol letter, e.g. $\boldsymbol{v}_{\Sigma}$;
- a matrix is represented in upright bold serif font, e.g. $\mathbf{R}$, $\mathbf{r}$;
- total time derivative: dot operator, e.g. $\dot{\boldsymbol{q}}, \dot{s}, \dot{\varphi}$;
- partial derivative: ∂ operator, e.g. $\partial s/\partial x$.
- scalar product: $\langle\ ,\ \rangle$;
- vectorial product: $\times$

It is adopted the SAE J670 convention for the reference frames.

Subscript	
r	rear
f	front
x, y, z	cartesian component

Superscript	
T	transpose matrix operation

Geometry	
W	wheelbase
ε	caster angle
a	trail
a_n	normal trail

d	front fork
R_r, R_f	rear and front wheel radius
ρ_r, ρ_f	rear and front tyre cross section radius

Kinematics

x, y, z	longitudinal, lateral and vertical position
$\boldsymbol{V} = (V_x, V_y, V_z)$	speed vector and components
$\boldsymbol{a} = (a_x, a : y, a_z)$	acceleration and components
$\varphi, \dot{\varphi}$	roll angle, roll rate
$\psi, \dot{\psi}$	yaw angle, yaw rate
μ	pitch angle
$\delta, \dot{\delta}$	handlebar steering angle, steer rate
δ_f	kinematic steering angle
ω_r, ω_f	rear and front wheel angular speed

Inertia

$\mathbf{G}$	centre of gravity
m	mass
m_r, m_f	rear and front mass
h	centre of gravity height
b	centre of gravity longitudinal position
I_{xx}, I_{yy}, I_{zz}	principal moments of inertia
I_{xy}, I_{xz}, I_{yz}	products of inertia
I_{wr}, I_{wf}	rear and front wheel spin moment of inertia

Tyres

$\mathbf{P}, \mathbf{Q}$	rear and front contact point
R_0	free nominal or unloaded tyre radius
R	loaded tyre radius
R_e	effective rolling radius
a_t	pneumatic trail
(F_x, F_y, F_z)	general tyre contact force
$(\boldsymbol{X}, \boldsymbol{Y}, -\boldsymbol{N})$	tyre contact force (with f, r subscripts)
$N, F_z \geq 0$	vertical load
(M_x, M_y, M_z)	tyre torque
κ	longitudinal slip
α	lateral or side slip

γ	camber angle
φ_t	turn slip
φ_s	spin slip
V_{sx}, V_{sy}	longitudinal and lateral slip speed
V_r	rolling speed
$\bar{V}_x$	conventional longitudinal speed
ω	rotational or spinning angular speed
δ_f	kinematic steering angle
ω_r, ω_f	rear and front wheel angular speed
K_x, K_α, K_γ	longitudinal, lateral and camber stiffness
c_γ, K_ψ	twisting and rotational stiffness
μ	friction coefficient (with x, y subscripts)
u_y	rolling friction
B, C, D, E, S_H, S_V	Pacejka 'Magic Formula' parameters (with x, y subscripts)
(F_{xo}, F_{yo}, M_{zo})	pure slip tyre contact force, torque
(F_{sx}, F_{sy}, M_{sz})	combined slip tyre contact force, torque
$G_{x\alpha}, G_{yk}$	scaling factors in combined slip
$\sigma_\kappa, \sigma_\alpha$	tyre relaxation lengths

Rider controls

T_S	steer torque
T_r, T_f	rear and front wheel torque

Others

g	gravity acceleration
F_D	drag force
F_L	lift force
$\boldsymbol{q}, \dot{\boldsymbol{q}}$	generalized coordinate and velocity vector
$K(\boldsymbol{q}, \dot{\boldsymbol{q}})$	kinetic energy
$V(\boldsymbol{q})$	potential energy
$L(\boldsymbol{q}, \dot{\boldsymbol{q}})$	Lagrangian fuction
Q_q	generalized force vector
$(\hat{\boldsymbol{\imath}}, \hat{\boldsymbol{\jmath}}, \hat{\boldsymbol{k}})$	unit vector

Chapter 1

Introduction

1.1 Background and motivations

Key aims of motorcycle designers are to enhance vehicle performances, handling, stability, efficiency and safety, especially when the vehicle is approaching the limit of adhesion of its tyres and one way to influence these features is the development of advanced vehicle dynamics control systems. In particular, engineers have strived for more control over the distribution of torque to manage the individual rotations of the wheels.

Over the years previous objectives has been pursued in different ways. For example, limited wheel slip control strategies have improved traction when one of the wheels is slipping and electronically controlled braking systems have improved the stability of vehicles in dangerous situations. Now, through the use of advanced mechanical or electric drivelines and the trend towards the use of electric propulsion in road vehicles, there is the opportunity to design All Wheel Drive (AWD) vehicles and actively control drive-torque distribution to influence the handling and performance of the vehicle itself. Indeed, since lateral force-generating capacity is limited when the wheel is generating high longitudinal forces, enhancements in handling and stability can be made by transferring torque to a different wheel. For example, in the automotive industry a vehicle equipped with an efficient electronically controlled torque management system, able to distribute the available driving torque between the axles/wheels independently, can suitably shift the drive torque between outer and inner wheels, to improve its transient performances in turning (see e.g. [1]). More precisely, in a corner, drive torque might be increased at the outside wheel, and reduced at the inside wheel, to help the vehicle turns into the curve, then, as the vehicle straightens up, more torque might be applied to the inside wheels to help prevent excessive oversteer. Similarly, changing the distribution of power between front and rear wheels of a motorcycle could give the driver more control over its

vehicle: powering the front wheel makes the motorcycle feeling more stable in a turn, gives more traction when accelerating on slippery surfaces or when vertical load is reduced on a wheel, and helps vehicle stabilization at low speeds.

Altering the handling of real vehicle is not so simple because it is affected by speed, severity of a manoeuvre, vehicle properties such as tyre conditions, and external influences such as friction coefficient. Over the years, there have been significant efforts to make vehicles more predictable in extreme situations and many control systems have been designed for this purpose: Anti-lock Braking System (ABS) to prevent locked wheels under braking, Traction Control (TC) System to prevent wheels spinning under acceleration and in cornering situations, Electronic Stability Program (ESP) to keep a vehicle in a controllable condition by limiting the power of the engine, or by applying brakes at one, or more, of the wheels. In the last years, these systems and devices have become available in motorcycles too. However, all of them act basically reducing vehicle speed counteracting the rider's intention that can experience an uncomfortable driving, as a result. This aspect should not be underestimated in the riding world where motorcycles are primarily recreational vehicles for the thrill seeking rather than commuter ones.

With this in mind, studying the optimal way to redistribute the power between wheels and analysing its effects on the handling and stability of the bike become an interesting and attractive field of research for motorcycles manufacturers. The rider has the full control of the vehicle if the drive torque is redistributed between rear and front wheels instead of reduced, because in this way the vehicle keeps the driver's desired speed, and consequently the control strategy becomes acceptable and not invasive for the rider himself and for his driving feeling. At the same time, a suitable torque management system has the positive feature of increasing the bike traction performances as well as driver's safety, as it will be demonstrated into this dissertation. For these reasons, it might be used in parallel with conventional safety systems.

Another potential advantage of an electric all-wheel drive motorcycle with active torque distribution is related to the energy saving and environmental sustainability, both hot topics nowadays. Indeed, a full electric motorcycle can be seen as a solution for sustainable mobility, and what is more, torque distribution helps to control the vehicle in a manoeuvre without the application of wheel brakes, which waste energy both through heat, and through subsequent acceleration to recover the lost speed. When a wheel slips over the ground, energy is dissipated as heat; choosing the distribution of torque to minimise the slip will minimise the amount of energy lost. Clearly, it is important to minimise the energy consumed not only for environmental reasons, but also for monetary ones.

In face of the main advantages of a torque management system explained so far, the feasibility of an all-wheel drive architecture in a vehicle is not a secondary matter. The adoption of AWD architecture is increasing in automobiles [2] where various types of torque vectoring drivelines have been implemented; the same it has not been yet seen in motorcycles market mainly because of two reasons: firstly, the difficulty of motorizing the front wheel, especially keeping content manufacturing costs; secondly, the lack of convenience of front wheel traction in the matter of fact that modern road bikes are so powerful that can lift the front wheel off ground. This explains why there are almost no studies on the topic related to motorcycles, unlike four wheel vehicles. Nonetheless, few exceptions of all wheel drive motorcycles, primarily for off-road use, exist. They apply a portion of the drive torque at the front wheel using mechanical or hydraulic actuations, as it will be reported later. However, electric traction with two separate motors and throttle-by wire control are probably the most viable technical solution to implement AWD architecture on motorcycles. The reduction of costs and size of electric motors, the increase of battery life, the reduction of recharge times and the availability of smaller, lighter and more cost-effective electromechanical actuators such as electronic throttle or actuated brakes might make two-wheel-drive motorcycles more cost competitive and attractive for their potentialities in the two-wheelers market. Thus, it is worth investigating about safety and performances of an electric AWD motorcycle with respect to a conventional one.

Within the outlined context, it is therefore appropriate and important to investigate the effects of torque distribution and its potential benefits on performances, handling, and efficiency of a motorcycle. For all the aforementioned reasons, the design of electronically controlled torque management systems in an electric all wheel drive motorcycle for performance enhancement rather than oriented to the safety in limit-handling scenarios including off-road low-traction conditions, on-road high-speed cornering and low speed driving, has become an interesting area of research both for academic and industry sectors. This thesis investigates mainly on performance and safety. For a preliminary analysis on efficiency see [3].

1.2 All wheel drive electric motorcycles: state of art

In this Section the history and issues related to All Wheel Drive motorcycles will be reviewed and the use of electric motors for vehicle propulsion discussed. Indeed, electric traction provides an opportunity to instantly and accurately control

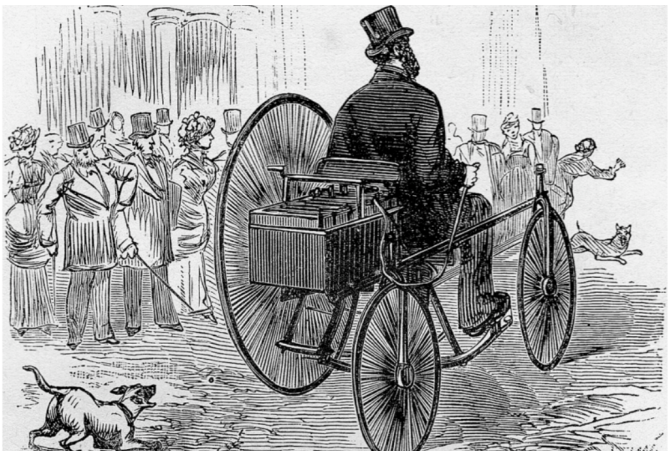

Figure 1.1: Gustave Trouve pioneers electric transport in 1881: the first electric vehicle demonstrated to the world, on April 19, using a Starley tricycle with Trouvé's own batteries and electric motor attached [4].

the amount of torque the wheels receive, especially if separate motors are used for each wheel and therefore, it is also worth a comment. Special attention will be paid to off-road motorcycles, where the all-wheel-drive electric architecture can be mainly exploited because of low friction surfaces and limit-handling scenarios.

1.2.1 Electric motorcycles

Electric vehicles have a full electric propulsion system or, in other words no other engines than an electric motor/s. Today, electric motorcycles are a real product of automotive industry, even if it took decades to embrace this progress. The idea for the electric motorcycle was first suggested (it seems) in 1870s by the fellow who first patented the concept of the motorcycle itself, Louis-Guillame Perreaux, but the first successful demonstration of an electric vehicle was a tricycle built by Gustave Trouvé, demonstrated on 19 April 1881 on the Rue Valois in Paris [4] (Figure 1.1). The vehicle had an autonomy between 16 and 40 kilometers and a maximum speed of 14 km/h. However, the first patent for an "electrical bicycle" was only issued in the 1890s: on 19 September 1895, a patent application was filed by Ogden Bolton Jr. of Canton Ohio [5].

Decades upon decades, technology has made giant steps in the production of two-wheeled vehicles equipped with an electric motor. Recently, it is even become an important part of the international market. Briefly, in the years following the first patent, new constructions, adequate to the state of technology of the time, were created. These vehicles could achieve range of 100 km at speeds up to 60 km/h, having a mass of about 100 kg [6]. In the 1919, the Ransomes, Sims e Jefferies company created a prototype of an electric motorbike powered from a battery

located in a sidecar [7]. In the 1936 the Limelette brothers created a company called Socovel, which built electric motorcycles until 1948 [8]. In the 1967, Karl Kordesch designed a fuel cell which he used to power a motorcycle [9]. In the 1974, Mike Corbin adapted an electric starter motor from a Douglas A-4B fighter jet and created a motorcycle called Quick Silver, which established a record speed in the electric motorcycle category, at 266.16 km/h [10] (a contemporary record from 2011 stands at 316.899 km/h and was established by SWIGZ Electric Superbike). As the construction and materials technology progressed, new constructions were created, and presently there is a wide choice of models of electric motorcycles from makers including: BMW, Brammo, Brutus2, Bultaco, Electric Motorsport, Energica Motor Company, Gogoro, Harley-Davidson, Honda, Hollywood Electrics, Johammer, Lightning Motorcycle, Lito Green Energy, Quantya, Sora, Sarolea, Terra Motors, Yamaha, Yo and Lito, Z Electric Vehicle and Zero Motorcycles.

Electric scooter and motorcycles of the aforementioned manufacturers might be quite different one each other due to vehicle's applications: commuting into cities, sport racing, off-road competitions, and so on. Independently from the specific application, for most of electric vehicles, the electric powertrain consists of three main parts (a battery pack, a motor drive controller and a motor), as shown for example in Figure 1.2a in the drawing of an electric motorcycle prototype designed in the Gdynia Maritime University [11] and in the electric power architecture scheme of Figure 1.2b. These items constitute a system that has to be optimized in design phase in order to meet the desired performance and specific requirements imposed by the vehicle's application. Improvements of the efficiency and technology in this perspective have been achieved through intensive research and innovation throughout years using computer modelling, simulation, laboratory and prototype testing, as shown for instance in [12–15]. Because of the zero emission goal present in many government regulations for the next future, research and investigations on this topic are going on. Special attention in this sense is also rising towards off-road motorcycles [16, 17].

For an electric motorbike crucial requirements are related to system weight, volume, and size, which should be kept sufficiently low and small to achieve best bike performances. All of them depend mainly on the battery pack, therefore its selection plays a key role not only for bike autonomy, but also for overall bike development, because it affects directly speed, manoeuvrability and power consumption. Selecting the batteries, main energy source of the propulsion system, requires choosing a suitable compromise between the needed stored energy and the power densities [12]. Indeed, high specific energy is required from a source to provide a long driving range, whereas high specific power helps to increase the acceleration. Figure 1.3

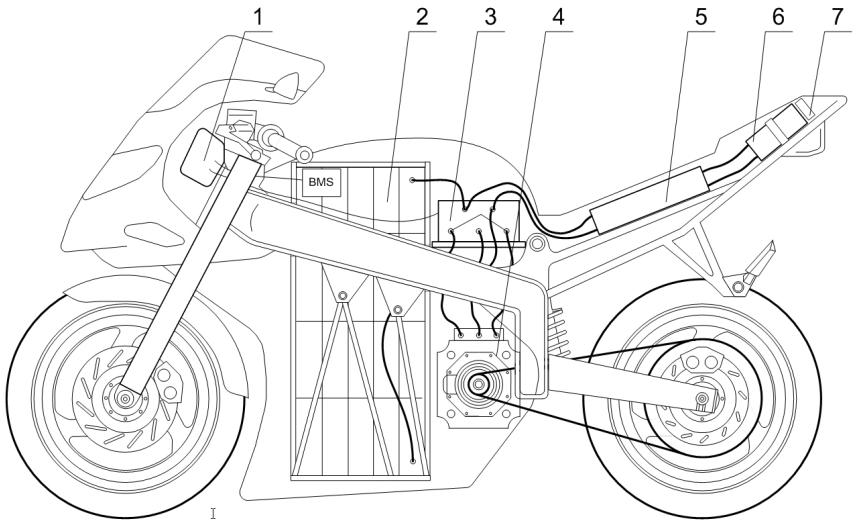

(a) Electric motorcycle prototype designed in Gdynia Maritime University [11]: 1. instrumented cluster, 2. battery pack with BMS, 3. power inverter, 4. PMSM motor, 5. DC/DC converter, 6. auxiliary 12V battery, 7. battery charger connector.

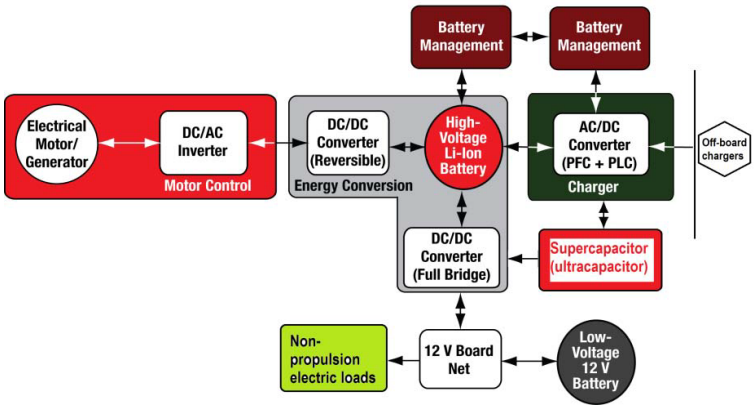

(b) Typical power system architecture scheme.

Figure 1.2: Focus on powertrain of an electric motorcycle.

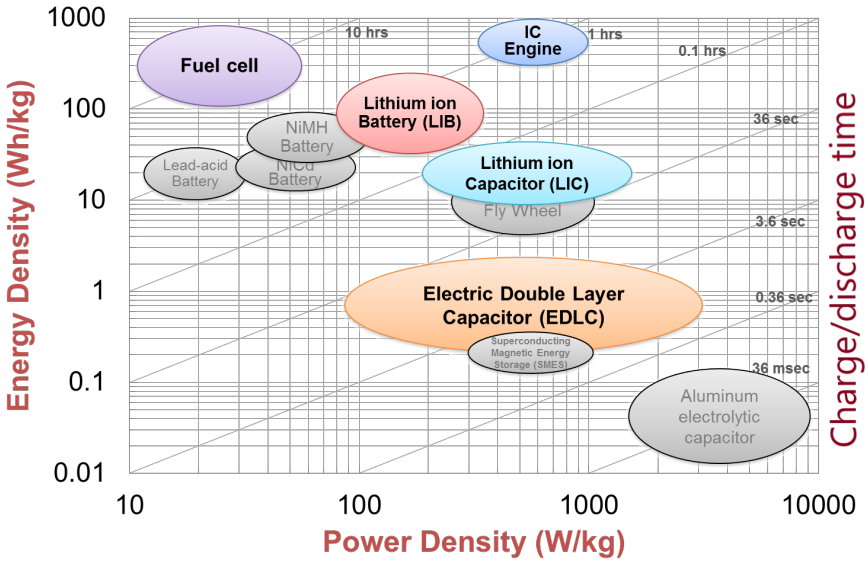

Figure 1.3: Energy storage systems: energy vs power density. [18]

Battery type	Number of cycles	Specific energy (Wh/kg)	Specific power (kW/kg)
Lead-acid	500 - 800	33 - 42	0.18
Li-Ion	3500	130 - 140	2.4

Table 1.1: Evolution of battery characteristics. Data from [19].

illustrates a (not exhaustive) overview of the current situation of energy storage devices in an energy-power density graph. Although high energy density and high power density are two of the most important criteria of battery choice that have led the battery evolution from lead-acid to Lithium-Ion ones, as reported in Table 1.1, there are other characteristics that are sought after to make a perfect energy source: fast charging, long service and cycle life, low cost, and maintenance are a few of them.

Different battery types have their own pros and cons, and in the selection phase, these things have to be kept in mind. In [20], Khaligh et al., provide key features of some known batteries which are demonstrated in Table 1.2.

The second element of the electric propulsion system is the motor, the core of the powertrain: it converts electrical energy that it gets from the battery into mechanical energy which enables the vehicle to move. In [21] some requirements of a motor for electric vehicle application are cited. The most relevant are high power, high torque, wide speed range, high efficiency, reliability, robustness, reasonable cost, low noise and small size. Although DC motor seems a logical choice for electric vehicle's propulsion, as it is powered from DC batteries, their lack in efficiency, bulky

Table 1.2: Advantages and disadvantages of common battery types. Data from [21]

Battery type	Advantages	Disadvantages
Lead-acid	• Available in production volume • Comparatively low in cost • Mature technology as used for over fifty years	• Cannot discharge more than 20% of its capacity • Has a limited life cycle if operated on a deep rate of SOC (state of charge) • Low energy and power density • Heavier • May need maintenance
NiMH (Nickel-Metal Hydride)	• Double energy density compared to lead-acid • Harmless to the environment • Recyclable • Safe operation at high voltage • Can store volumetric energy and power • Cycle life is longer • Operating temperature range is long • Resistant to over-charge and discharge	• Reduced lifetime of around 200-300 cycles if discharge rapidly on high load currents • reduced usable power because of memory effect
Li-Ion (Lithium-Ion)	• High energy density, twice of NiMH • Good performance ar high temperature • Recyclable • Low memory effect • High specific power • High specific energy • Long battery life, around 1000 cycles	• High cost • Recharging still takes quite a long time, though better than most batteries
Ni-Zn (Nickel-Zinc)	• High energy density • High power density • Uses low cost materials • Capable of deep cycle • Friendly to environment • Usable in a wide temperature range from -10°C to 50°C	• fast growth of dendrite, preventing use in vehicles
Ni-Cd (Nickel-Cadmium)	• Long lifetime • Can discharge fully without being damage • Recyclable	• Cadmium can cause pollution in case of not being properly disposed of • Costly for vehicular application

structure, lack in reliability because of the commutator or brushes present in them and associated maintenance requirement have made them less attractive [22] over time. With the advance of power electronics and control systems, different motor types have emerged to meet the needs of the electric propulsion sector: induction and permanent magnet (PM) types [23] based on AC motors being the most favoured ones as traction motors, due to their lower weight and costs, higher reliability and lower maintenance needs [19]. For high power propulsion, induction motors are used. In view of a torque distribution implementation on motorcycles, another not negligible feature is the location of the electric motor and its motion transmission to the wheel. Electric motors can either be hub-mounted or mounted in board with a simple transmission. Motor mounted as a part of a wheel structure eliminates mechanical gears resulting more efficient and allows to control directly the wheel torque. That makes the hub-mounted motor the preferable configuration for torque distribution. However, it is not free from drawbacks because this configuration increases the unsprung mass of the bike with detrimental effects on vehicle ride and handling that can be compensate with a better suspension system. A type of motor suitable for this kind of configuration is the Permanent magnet synchronous motor (PMSM) [19, 21].

An example of battery and motor components sizing for an off-road motorcycle is illustrated in [16]. After many simulations with various motorcycle configurations in many different driving cycles, the setup with the best ratio of performance (driving range), energy consumption and weight in that case is the one with the lithium polymer technology battery and 4.8 mAh combined with the permanent magnet synchronous machine. The final battery pack consists of 200 cells and weights about 20 kg. The voltage is between 173 V and 217 V depending on the state of charge. The overall mass of the motorcycle is about 90 kg.

Last main component of the electric powertrain is the motor drive controller. It is based on electronic components which interact with the power converter to control the electric parts, i. e. electric motor and battery. Therefore, a motor drive controller includes both an energy management system able to regulate the use of energy on board and a driving control strategy in order to control the power to be supplied to the electric motor or motors, based mainly on the required power of the driver and the vehicle speed. In case of all-wheel-drive motorcycle, specific algorithms to properly manage relative power in the two motors and activate rear and front wheels in drive or braking mode have to be allocated in the drive controller. These strategies are basically divided in two type: torque distribution and torque reduction. A suitable management of these strategies in the motor controller might improve vehicle driving. More details on drive control strategies

will be handled later, because they constitutes the core of the problems analysed in this dissertation. A deeper discussion on the other components of propulsion system in electric motorcycles is not in the aims of the present thesis: for a more comprehensive study on the electric vehicle technology refers to [21, 24].

Behind the brief overview on electric motorcycle design features that vehicle engineers need to keep in mind in the perspective of an all wheel drive implementation, it is worth mentioning other reasons that had led to this rising interest of electric powered two wheelers from consumers, manufacturers and governments. First of all, traditional fuelled vehicles constitutes a major source of urban pollution and other environmental problems, whereas the electric motorcycle has no tilepipe emissions associated to high efficiency and therefore it can be see as an environmental friendly solution for sustainable mobility of the future [25] as long as cleaner grid energy production and battery recycling are implemented. Indeed, as Kerdlap and Gheewala [26] assert in their study related to Thailand's electric motorcycle production, the realization of a power development plan can reduce total impacts of the electric motorcycle fleet to global warming by 6% to 10%, but it is crucial that batteries from electric motorcycles are recycled to avoid 98% of impacts to toxicity, released by some battery components (especially lead). Electric motorcycle could also be an appealing solution to reduce the risk of human exposure to excessive high traffic noise in a motorcycle city. Sheng *at al.* [27] demonstrate that in a modern urban area in which the total traffic volume is high and traffic noise levels at majority of sites overcome 75 dB(A), the proportion of noise levels above 75 dB(A) decreases significantly from 82.6% to 59.9% when 100% of gasoline motorcycles in the real traffic scenario is replaced by the electric ones. Furthermore, the lack of noise in electric motorcycles can be a benefit in off-road rural activities where noise engine is a hurdle for fauna protection and local restrictions. Finally, it is worth highlighting that advantages of electric motorcycle are not only related to environmental problems, but also to operation and convenience. In face of their high initial manufacturing cost (mainly due to battery), the electric machines enjoy an enormous fuel cost advantage with respect to the Internal Combustion (IC) engines, because of a much low price of electricity than gasoline. In addition, these vehicles require a very little maintenance, factors which make them convenient from economic point of view.

Despite of the explained positive aspects, the adoption of electric motorcycles is not free from limitations such as increasing manufacturing cost, entailing significant additional unsprung mass (especially for hub-mounted motor configuration) or gyroscopic effects, issues on energy storage system capacity and vehicle range, and finally long charging times as well as currently insufficient number of charging stations and

inadequate power grid for a large number of electric vehicles. Limitations in battery autonomy, longevity and charging times make them practical for short and local journeys compared to internal combustion engine's vehicles or for off-road activities and competitions. However, on battery drawbacks and technological problems a lot of work is being done by academia, private manufacturers, and governments, especially about range or battery autonomy [28]. Additionally, number of charging stations are increasing [29], thus electric mobility can be a valid alternative in automotive industry for near future (the Paris Declaration on electro-mobility and climate change expresses the ambition to exceed globally the threshold of 100 million electric cars and 400 million electric two-wheelers by 2030 [29]).

The great and rapid progression in electric mobility outlined in this Section is a further incentive to scientifically investigate on all wheel drive technology and find out the benefits this kind of bike has over the conventional one, which is the main objective of the whole dissertation.

A full electric propulsion system is not the one and only technology that can be exploited to design an all wheel drive architecture on a motorbike. For completeness, in the next Section solutions to power both motorcycle wheels will be reviewed, investigating benefits and limitations of each proposed approach.

1.2.2 All-Wheel-Drive motorcycle architecture

Despite of recognized potentialities of the front wheel power on vehicle dynamic control and soft off-road terrain riding capabilities [30], the two wheel drive architecture for motorcycles has not experienced the same spread into the market as in four wheel vehicles world. In industry only few exceptions exist [31–34], although many patented solutions to motorize the front wheel of the two wheelers have been proposed since the 1960s, even from main motorbike manufacturers. They can basically be split up into three broad groups; those with mechanical drive by means of chains, sprockets or shafts, those with hydraulic drive that exploit pressurised fluid and finally, those with a full electric or hybrid motor. This division essentially follows the historical development of this technology. Follow a summary based on type of power transfer system.

Mechanical AWD motorcycles

Mechanical two wheel drive motorcycles are by no means a new idea - the first all wheel drive motorcycle prototype dates back to 1958. It had a mechanical drive designed by Charles Fehn of Rokon [32] with his patented power transfer system [35] and hollow drum wheels (see Figure 1.4). The front wheel was mechanically

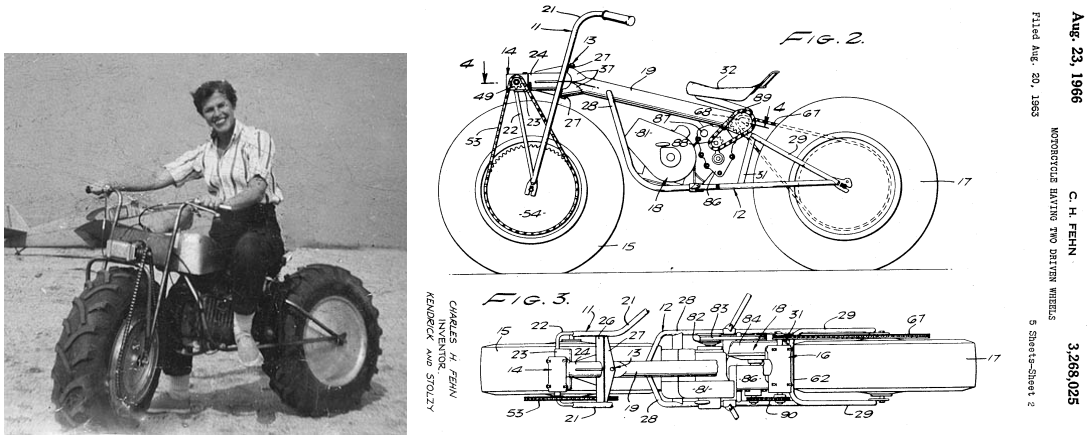

Figure 1.4: The first AWD motorcycle had mechanical system with chains to power the front wheel. On the right, original patent drawing of the vehicle [35].

powered by the following system: a shaft run up the backbone with a bevel drive gearbox in the steering head and a chain down to the front wheel. It seems that Rokon motorbike was the first to use the one way clutch idea to drive the front wheel. It has now become a standard issue on chain drive AWD's. The designed front wheel power system worked, also proved by the fact that its evolution is still in production by Rokon, even though powering the front wheel drive by means of a chain severely limits the motorcycle capacity of any high speed manoeuvring. Anyway, this is the first example of AWD motorcycle produced for the market.

An alternative mechanical all-wheel-drive system is patented in U.S. Patent 5113964 [36]. The document describes a motorcycle with a different mechanical front wheel power system consisted of a series of belts, chains, gears, or sprockets from the motor to the front fork and then to the front wheel along one side of the fork. Although a motorcycle does not need the same broad range of steering required by a bicycle, the presence of a bulky drive chain on one side of the front fork would cause problems with both steering as well as unwanted torque reactions that would make the motorcycle potentially uncontrollable at high speeds.

Last mechanical front wheel drive powertrain that is worth mentioning is mounted on AWD off-road motorbikes (enduro, motocross, and superbikes) manufactured by the Christini Inc. [31]. The company has developed a kit to convert single track motorcycles into all-wheel-drive ones (see Figure 1.5). Christini-equipped bikes have a second drive chain, running from the countershaft to a point high on the frame beam. From there, a shaft transmits power under the fuel tank. Bevel gears in the steering head transfer power down the steering stem to the lower triple clamp. Two small drive chains in the clamp transfer power out to a pair of telescoping shafts, running parallel to the fork legs [37]. At the front hub, a

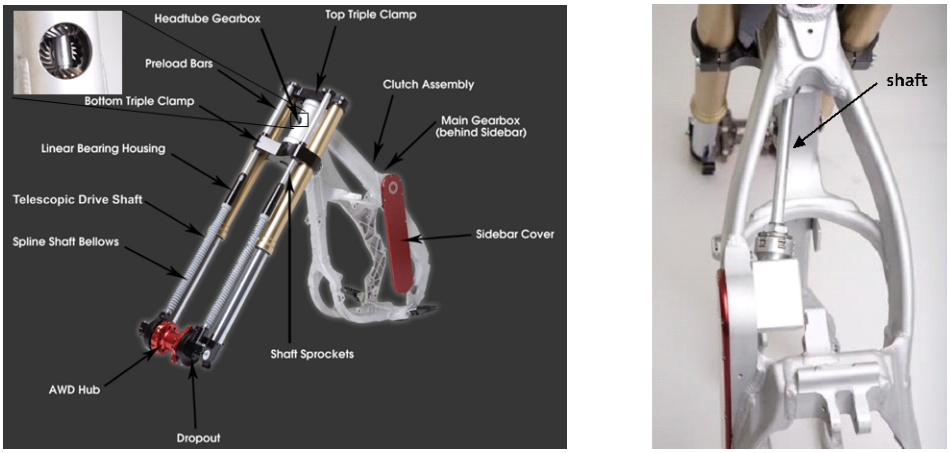

Figure 1.5: Christini all-wheel-drive motorcycle mechanical kit. Pictures illustrate the components of the power system.

sprag clutch – similar to the freewheel mechanism in a bicycle's rear hub – transfers power to the front wheel when rear-wheel speed exceeds front-wheel speed by more than a prescribed ratio. Notice that any system that applies positive torque to the front wheel in a turn generates a "steer-torque" in the motorcycle, making the bike leaned in. That "steer-torque" complicates enough the handling, so Christini has decided to minimize the torque effects of its own system by using counter-rotating shafts, which cancel each other out. Those two shafts also provide an unexpected benefit: they act as gyroscopic steering dampers, reducing the bump steer effects produced by other front-hub motors.

The presented powertrains have their drawbacks common to all mechanical front wheel power systems; indeed, in addition to handling limits on high speed manoeuvres cited so far, mechanical drives have at least three drive chains, with related difficulties on their maintenance, and limitations on steering lock, gearing hassles and front suspension design problems, which has to be properly modified compared to a conventional bike.

Hydraulic two wheel drive motorcycles

Second type of AWD architecture uses hydraulic pressure to transmit the power to the front wheel. It was developed after the first mechanical systems; a wide research on this type of front drive was carried out in Nineties, mainly because at that time, four wheel drive was the technology of the day in cars. The basic idea of this front power transfer system is the following: an internal combustion engine drives a hydraulic pump rather than a gearbox as in a conventional motorcycle; the pump pressurises oil directed to the hydraulic motor located in the wheel hub, which finally converts the high pressure oil's energy into rotary motion. Variations of

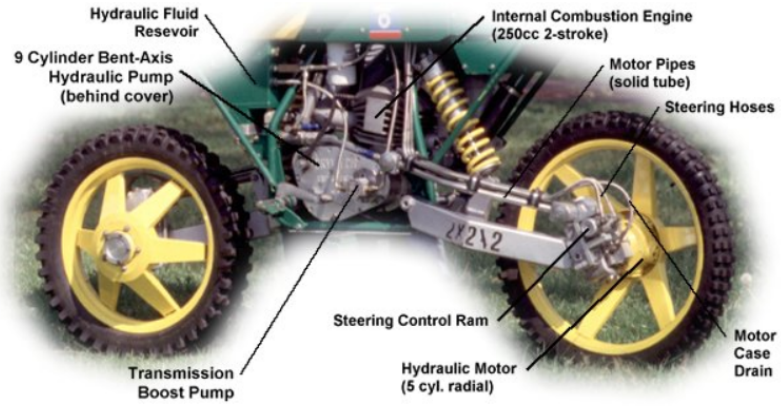

Figure 1.6: All-wheel-drive motorcycle with hydraulic drive: components of the power system are pointed out.

this basic principle actuated on motorcycles have been patented over years [38–40]. Every proposal attempts to overcome some technical issues intrinsically related to hydraulic drive such as steerability of the front assembly, improvements on the suspension system, additional weight or bulk or damage exposure to external obstacle if oil motor is mounted outside the wheel hub.

In the mass-market perspective, hydraulic drive system to power the front wheel was also explored by Swedish suspension specialists Öhlins [33], convinced that two-wheel-drive promised a motorcycling revolution. In 1992 the company began to work on a two wheel drive system that came closer than one might have thought to reach mass-market production. The firm's technology reached off-road success and production in the short-lived Yamaha WR450F 2-Trac, shown in Figure 1.7. The motorcycle, still in circulation, has the following system. A small hydraulic pump is attached to the engine and is driven by an extra chain running from the front sprocket of the stock gearbox. It uses six or more tiny pistons to pump hydraulic fluid through flexible, Kevlar-reinforced hoses to a hydraulic motor mounted on the front hub. This simply turns the wheel via a cog mounted inside the hub [39, 41]. Because the pump is driven from the gearbox sprocket, the front wheel can never turn faster than the rear – so it won't spin. But, if the rear tyre loses grip and spins, the pump will run faster – increasing the hydraulic pressure and therefore the amount of power going to the front wheel. Last remark constitutes a common feature in both hydraulic and mechanical systems: they require excess of slip at the rear wheel before a drive torque is applied at the front wheel, and the amount of torque transferred is fixed by the design of the system, which limits the application of traction control systems.

Hydraulic motor can be mounted in or out the front wheel hub. Both con-

Figure 1.7: Yamaha WR450F 2-Tracs, hydraulic two-wheel-drive dirtbike owned by the USGP winner (Marty Moates) in 2004 and zoom in the front wheel hydraulic motor.

figurations have specific troubles in addition to suspension and front assembly manoeuvrability such as exposure to damages during running in the latter case and additional weight and bulk in the former one. None of these issues are, in themselves, terminal flaws. Problems that are harder to solve include the additional cost that the hydraulic drive added. The system may have been relatively simple but it requires a precision manufacturing expensive to achieve. Moreover, a motorcycle with a front wheel driven by a hydraulic drive system would have significantly less efficient power transfer than a rigid-shaft drive system [42].

Most probably the limitations and drawbacks of the mechanical and hydraulic power transfer systems were obstacles to mass production of this kind of vehicles. Finding a way to drive a front wheel that steers, without compromising the suspension or adding too much weight or bulk, is the key to make it a success. A decade later than Nineties, electronic traction control was on the rise as well as a revolution in tyre technology. It could be that the coming revolution in electronics and electric power, delineated in the previous Section 1.2.1, finally triggers a mass movement to AWD two wheelers.

Electric and hybrid electric AWD motorcycles

Lightweight in-hub motors and the fact they only need a couple of wires to be fed rather than precision hydraulics or complex shafts, could make easy to add front-drive to virtually any bike. These are macro reasons why recently AWD motorbike design and prototypes consider almost exclusively electric front power systems in a hybrid or full electric version rather than hydraulic or mechanical ones.

Firstly, all-wheel drive powertrain design in a hybrid electric motorcycle is

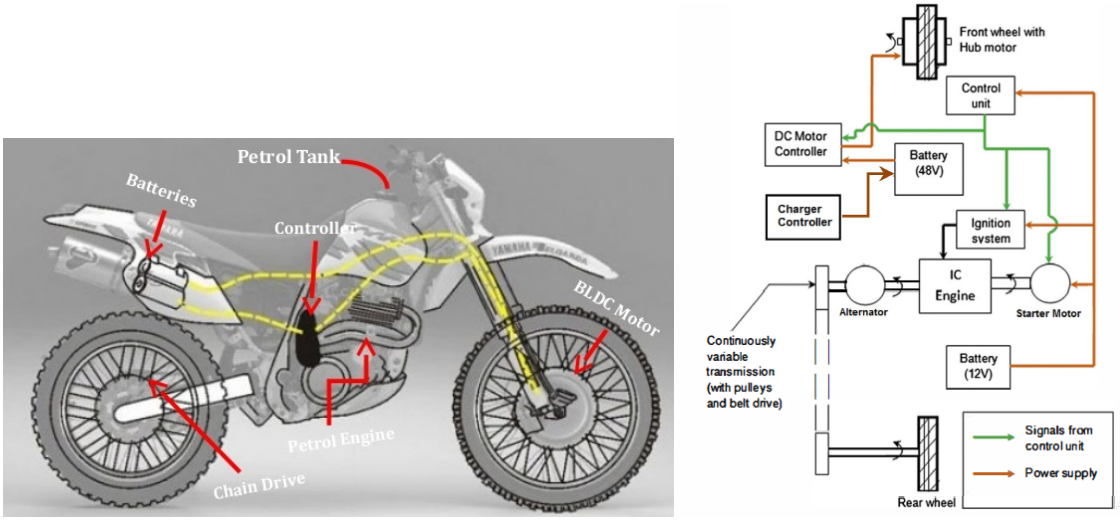

Figure 1.8: Basic scheme of a hybrid electric all-wheel-drive motorcycle (left) and its parallel configuration powertrain block diagram (right). The diagram is from [45].

analysed, since this kind of motorcycles are of growing interest due to environmental concerns and fuel efficiency. Indeed, even a well known automotive manufacturer has launched a AWD hybrid electric travel enduro model in the second half of 2017 [43]. The efficiency of a hybrid electric motorbike can be optimised managing in a suitable way the energy sources - the internal combustion engine and the electric motor/s - used to power the wheels. Notice that for electric or hybrid electric motorcycles due to the space and weight limitations, electric motors mounted into the wheel hub are highly recommended as traction unit. For hub motors, their electromagnetic fields are supplied to the stationary windings of the motor. The outer part of the motor follows, or tries to follow, those fields, turning the attached wheel, that in this way it results directly driven. Two types of hybrid electric powertrains exist, parallel and series configurations, and both of them can be modified for attaining a two wheel driven bike. Chen *et al.* [44] and Nguyen *et al.* [45] in their works describe two examples of AWD hybrid motorcycle in parallel configuration. Figure 1.8 shows in a simple way the idea of this architecture and the parallel configuration block scheme. Basically, this all wheel drive powertrain uses a direct-driven front wheel motor, while rear wheel is driven by a gasoline engine through continuously variable transmission. The battery constitutes the energy storage system for the electric motor and in the control unit is stored the control strategy to provide individual or simultaneous traction to both wheels. Differences between the two proposed designs are minimal and concern mainly the generator, the use of electric motor in regenerative mode when the vehicle is decelerating, and the type of battery, lead-acid in one case and Lithium-Ion in the other.

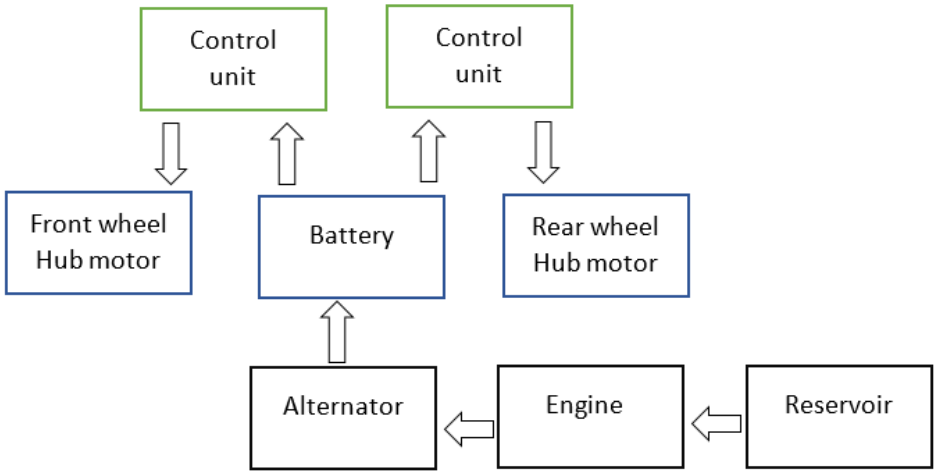

Figure 1.9: Series hybrid electric motorcycle configuration scheme.

Alternatively, the internal combustion engine can be exclusively used to drive an alternator to provide electricity and recharge the battery when its charge becomes low, without directly drives any wheel. Then, the vehicle is only driven by electric motor/s with the generator set providing the electric power to them. Considering one hub motor for each wheel, a series hybrid all wheel drive electric motorcycle [46] is realized. Figure 1.9 visualises its configuration scheme. Other detailed two wheel drive hybrid electric configurations can be found out for instance in [47–49]. In [48] the front wheel drive may be adapted to conventional telescoping (or shock-absorbing) front fork suspension system and the whole embodiment still work for a full electric motorcycle.

Moving from hybrid electric to full electric AWD motorcycle does not involve such a great difference. The overall layout of full current electric motorcycles is identical to hybrid ones where the body houses the motor instead of the engine (see Figure 1.2a). Therefore, an all-wheel-drive electric motorcycle can be conceived similar to an AWD hybrid electric one, even if in this case the traction capacity of the bike fully depends on the state of charge of the battery and there is no engine to recharge it during running. Consequently, as in the hybrid configuration, the front wheel is always driven by an hub motor [48, 50], whereas the rear wheel can be driven through a chain [34, 51] or another electric hub motor [52, 53]. In both cases the controller sends the instructions to motor actuators to activate individually or simultaneously the wheels in traction or braking mode. Indeed, in full electric motorcycle both wheels motion can be controlled accurately and instantly by means of electric motors making this type of architecture the best choice to exploit the benefits of the all-wheel-drive technology. What is more, the front wheel motor could also serve as a generator for recuperation during braking.

Although the great benefits in term of wheel spin controllability, in addition to the technical limitations of an electric vehicle (range, battery charging time, and so on), it is relevant to highlight that the use of hub motors increases unsprung mass, add gyroscopic effects and raise concerns for the suspension that could be enhanced and redesigned in most of the cases. More specifically, the adding high weight of front hub motor could adversely affect the driving behaviour, whereas the built-in rear wheel hub motor is combined in a disadvantageous manner only with exposed, low-maintenance chain circuits. All these drawbacks are worth being further investigated, but they do not reduce in any way the advantage of using two separate electric hub motors for an all-wheel drive powertrain respect to other mechanical or hydraulic solutions, especially in term of torque distribution system design.

1.2.3 All-Wheel-Drive motorcycle summary

From 1960s to nowadays, many solutions have been proposed to motorized the front wheel of a motorcycle and all of them have pros and cons. Issues on vehicle manoeuvrability due to additional weight and bulk, and on front suspension system are common in a different manner to all designs. Moreover, the mechanical and hydraulic methods can activate the front wheel drive only when the rear wheel spins faster than the front one and the ratio of rear-front torque is fixed by the design. Thus, in such powertrains it is hard to implement a torque distribution strategy, that can be easily actuated by means of two separate electric hub motors in an electric all-wheel-drive architecture. Another crucial factor that has limited their diffusion is the additional cost for precision manufacturing of hydraulic and mechanical solutions that is hard to reduce. All these aspects contribute to adopt the electric powertrain with two separate motors, one for each wheel, as the best candidate for an all wheel drive two wheeler architecture.

Furthermore, the recent environmental concerns have conducted to an increasing interest and research in electric propulsion with great enhancements on autonomy, charging grid and time of the battery, main obstacles to social acceptance of the electric vehicles. This coming revolution on electric power technology could trigger a mass movement to the all-wheel drive motorcycle diffusion, in parallel to an increased awareness on its benefits in improving the dynamics over conventional rear single-track motorcycle. Practical advantages could involve both vehicle performances and safety on low adherence terrains, but further scientific investigations are necessary on these aspects.

1.3 Objectives and contributions

After discussing the motivations and implementability of an all-wheel-drive electric motorcycle, it is clear that a motorized front wheel as well as a torque distribution strategy implemented by two separate electric motors have many potentialities not fully explored and deeply understood that can be applied for different purposes into a motorbike. This makes the study of active torque distribution interesting from a scientific point of view where a certain gap exists, especially in cornering traction conditions. Most of the known dynamic control systems designed for cars and motorcycles such as Traction Control system, Antilock Braking System, Electronic Stability Control (ESC), and ABS cornering act on emergency situations cutting off the engine or motor power. However, reducing power is not the only possible action on motors: they can also be actuated distributing the overall traction torque. If in the first case the control action could not follow the driver's intention, most probably annoying the rider himself, a drive or brake torque repartition should be able to guarantee a smoother driving feeling because the system distributes the overall torque demanded by the rider.

Nonetheless, the actual technological limitations on motorizing the motorcycle front wheel have limited until now the idea of analysing and designing active torque distribution systems and their effects, at least for improving vehicle performances instead of its efficiency. Indeed, the only traction strategies for AWD bikes that have been studied refer to straight line manoeuvres to prevent spinning under traction or fixed rear-front drive ratios.

The PhD project wants to explore whether the adoption of an all-wheel drive architecture in an electric motorcycle can reduce this gap or, in other words,

- can improve continuously and smoothly the vehicle performances in combined longitudinal and lateral acceleration manoeuvres, especially in those situations where a traditional motorcycle falls down because it overcomes its tyre adherence limits;

- can enhance the stability at low speed exploiting the individual or simultaneous activation of wheel torques in a suitable dynamic ratio.

Within these purposes, the terms for comparison will be the traditional rear wheel drive (RWD) motorcycle along the entire dissertation.

Go into more details. Minimizing the lap time is the first step to win a race; the goal is achieved with a combination of the rider ability and motorcycle acceleration performances. The rider capacities on the track can be enhanced just by training and experience; however, the additional degree of freedom of an all-wheel-drive

architecture could be exploited to improve the second one, that is the acceleration performances. Therefore, one objective of this thesis is to determine an optimal traction strategy to distribute the overall traction torque between rear and front wheels when the motorcycle is running. In this context "optimal" means achieving the best motorcycle performances in straight running as well as in cornering, where combined lateral and longitudinal accelerations occur, over a conventional rear single-track motorbike, possibly taking into account the driving conditions.

On the other hand, balancing a motorcycle at low-speed is challenging, especially for new riders because it is unstable below a certain critical speed [54]. The rider becomes very cautious at such speeds as a continuous input is necessary to balance the motorcycle [55]; moreover, the required steering input increases as speed reduces [56]. It is interesting to understand if the front wheel motorization could facilitate the driver in this balancing process. Thus, the other objective of the thesis focuses on the low-speed stability of the motorcycle due to the above-mentioned reasons. Specifically, the effects and benefits of involving positive or negative front wheel torque to self-balance the vehicle at zero-low speed (0 - 1 m/s) will be investigated. The process should be carried out, if possible, without any rider action on the handlebar and the need he puts his feet on the ground. To better understand the influence of the front wheel torque in the vehicle stabilization, the action of the steer torque will be limited, locking the handlebar. For an application in real situations such as during a red traffic light, the stabilization should be achieved in a small bounded area of the ground.

1.4 Methodologies and thesis outline

1.4.1 Methodology

Both problems we want to deal with are control ones. In general, a model-based control strategy is robuster against uncertainties (such as unmeasurable or variable parameters) or external plant disturbances than a model-free one. Therefore, model-based controllers are highly recommanded in automotive sector where the system is nonlinear and subjected to unknown road friction or variable wind force, just to mention few examples of involved uncertainties. Based on these remarks, both problems will be managed with a common approach:

1. studying the current state of art related to both modelling and control strategy;

2. developing a simplified mathematical model oriented to control which focuses on the bike dynamics of interest;

3. designing a control strategy from it;

4. validating and testing the strategy in a complex multibody motorcycle model by means of selected numerical simulations;

5. critically analysing and evaluating the results, making comparisons with the rear wheel drive motorcycle performances to find out any benefit of the all-wheel-drive architecture against its single-track equivalent.

Each part of this common scheme is then declined in a specific way to assess the two different objectives.

1.4.2 Thesis outline

The thesis structure follows the methodology outline, described so far.

A general introduction on motivations and background of powering the front wheel of a motorcycle is discussed in **Chapter 1** as well as the design and adoption problems of an all-wheel-drive architecture on these kind of vehicles. The discussion indirectly outlines the current state of art on this technology too.

Chapter 2 introduces the motorcycle geometry and develops the simplified mathematical models to design the control strategies for the introduced problems. In the same chapter it is also described the comprehensive multibody model of the motorcycle selected for control validation. Finally, a short discussion about virtual rider modelling, required to simulate the driver action to follow a path, is presented.

Tyres are the only component of a motorcycle in contact with the ground, thus the forces generated into them affects relevantly the vehicle dynamical behaviour, making them one of the most important component of the vehicle itself. Therefore, their modelling deserves a separate **Chapter 3**.

The design and assessment of the control strategies for the two problems are carried out in the following chapters. Specifically, **Chapter 4** focuses on designing the stability control strategy for the self-balancing problem, using two control techniques, the sliding mode and the Partial-Integral-Derivative (PID). As preliminary investigation, the stabilization is achieved using only one input, the front wheel torque. Both strategies are validated by means of the multibody model and a comparison of numerical simulations is reported. Then, the chapter concludes with a discussion about the design of a Multi Input Multi Output (MIMO) controller able to stabilize the motorcycle in a small bounded area. The control strategy uses both rear and front wheel torques for self-balancing the vehicle.

The optimal traction repartition strategy is derived in **Chapter 5**. A steady state analysis is firstly conducted and then the strategy is tested in some manoeuvres

by means of dynamical simulations. Because the traction repartition law does not require the knowledge of road friction coefficient, it is interesting to test it for off-road tracks: results of manoeuvres with an uneven road profile are reported at the end of the chapter. Even if tests on a real motorcycle are out of scope of the present research, a discussion about the implementation of the torque repartition law in the perspective of its application on a real vehicle is conducted too.

Finally, conclusions about the work and future research lines are outlined in the conclusive **Chapter 6** .

Chapter 2

Motorcycle modelling

2.1 Introduction

The advantages due to the additional degrees of freedom of an all-wheel drive powertrain have already been identified and exploited for safety in braking manoeuvres, especially in cornering, for instance in [57] and [58]. On the contrary, the effects of an active traction torque repartition on performances and handling in a turn have not been investigated yet, at least for two wheel vehicles.

In this perspective, the analysis requires a model of a motorcycle that can independently vary the drive torque at its wheels. In order to use it for control purposes, it should not be a complex mathematical model like those ones required for high-fidelity simulations, but a simplified, reliable and manageable analytical model that enable to design control laws as well as to capture the main behaviours of the real system under study. A good trad-off between accuracy and simplicity has to be pursue. Because each control problem under attention focuses on specific vehicle dynamics - low speed lateral dynamic for the stabilization problem and high accelerating combined in-plane and out-of-plane dynamics for cornering performance analysis - in order to achieve simplicity in modelling, ad hoc models for each of them will be created, taking into account specific assumptions.

Furthermore, since validation of the vehicle models and controls with a real AWD motorcycle is out of scope for this research, the models will be verified using a complex multibody model taken from the literature, suitably adapted to the two wheel drive architecture.

A literature review on all aspects of motorcycle modelling for both control purposes and accurate dynamic simulations will be discussed firstly. Then, the main geometrical parameters of the motorcycle and its kinematics quantities will be introduced and a four-DoF model for the low speed stabilization problem will be developed using a Lagrangian approach. Conversely, a straightforward steady-state

motorcycle model to derive the optimal traction distribution control law will be directly developed in Chapter 5 to improve the readability of the performance analysis. The multibody motorcycle model used for control validation will be then outlined. It is based on the work of Cossalter and Lot [59]. Simple driver model, capable of controlling the bike to achieve a specified manoeuvre will be finally described.

2.2 Literature review on motorcycle modelling

Recent advances in the field of ride-by-wire technology for motorcycle (namely active braking and full electronic throttle) has opened the way to the design of innovative control strategies to improve two-wheeled vehicles stability and performances. As such, it has become of growing importance to devise mathematical models of bike dynamics to be employed for control design purposes. The designed control strategies based on such models have to be numerically tested before applying them on a prototype bike. The increasing computational power of computers allows to save time and money by means of numerical simulations of the system, which could be carried out before experimental tests. Necessary condition for this step is to be provided of a highly accurate bike model (usually a multibody one), which is able to predict a realistic system-controller response to bike inputs. Then, the analysis of simulation results is used to correct the control system itself, if something is not properly controlled or does not behave as desired. In conclusion, both simple analytical and complex multibody models are required to correctly develop a control system, really capable of influencing and controlling the vehicle motion, avoiding undesired or unexpected responses of the dynamic system under control.

2.2.1 Mathematical control-oriented models

Multibody models are suitable for simulation purposes, closed-loop validation, and modal and sensitivity analysis, as they faithfully describe the dynamical behaviour of the vehicle; however, they are too complex for model-based control systems design. Indeed, the design of such a control system requires models that can be synthetically described, in the perspective of using them in on-board controllers to directly influence the vehicle dynamics.

Many different dynamics exist on a vehicle: its lateral instabilities, the longitudinal motion, the suspension system, a coupling between longitudinal variables (i.e. brake and traction torque) and out-of-plane modes, and so on; the phenomenon under control determines the type of model and the approach to derive it. For the

present thesis, the low speed stability problem mainly involves the capsize mode and the lateral motion, whereas the optimal traction repartition law requires a steady state model able to capture the coupled lateral and longitudinal motion and valid for high acceleration manoeuvres. Remember that the control strategies want to utilize the rear and front wheel torques, thus the control-oriented models have to consider both positive and negative wheel torques as inputs.

Control-oriented models presented in the literature do not completely fit for these purposes, since they mainly focus on the design of steering controller and do not consider both wheel torques as inputs. This is because the first solution to balance a two-wheeled vehicle is to act on the steer handlebar.

For example, in [60] Seffen *et al.* aim to capture the lateral motion of the bike and study its controllability. In order to do that lateral displacement, yaw, roll, and steer angles are selected as generalized coordinates and the bike is considered as a system of four rigid bodies. A set of 4th second order equations of motion based on Lagrangian approach is then derived. The steer torque applied by the rider to the handlebar is the only control input to study the bike lateral controllability. Similarly, in Tanelli [61], a 4th order model of the weave and wobble dynamics of the motorcycle is developed. The model presented in that work is then used to design algorithms to control a semi-active steering damper: this explains why the author again considers the steering torque as unique control input and chooses the side slip angle, the yaw rate, the steer angle, and the steer rate as generalized coordinates.

Since a motorcycle is intrinsically unstable, keeping the balance on a bike is always the primary control objective that cannot be neglected. Consequently, a lateral stability controller is also included in path tracking control or autonomous driving problems. From these two fields, other relevant models for the low speed stability problem can be found out [62, 63]. In his work, Getz [62] designs a controller which, using steering and rear wheel torque as control inputs, induces a model of an automatically controlled riderless bicycle to approximately track a time-parametrized path in the horizontal ground plane while retaining its balance. The bicycle is modelled as a single body system with two nonholonomic constraints for the wheel-ground contact points. In body frame the reduced equations of motion result in a 3rd order model with steer and rear wheel torque as control inputs. Starting from Getz, Saccon [63] presents a Sliding Plane Model (SPM), which differs from Getz's model in the way the tyre-road contact is modelled. While Getz's model assumes nonholonomic contact, the SPM model includes a more realistic tyre-ground interaction model, accounting for lateral sliding and normal load. The generalized coordinates are the rear contact point coordinates and the roll and yaw

angles, whereas the control inputs to the model are the thrust force and the effective steering angle. Similarly but for autonomous motorcycle, Yi *et al.* [64] propose a 5th order mathematical model based on constrained Lagrangian, which includes roll, lateral, and longitudinal dynamics and a linear tyre model. This model has a larger complexity with respect to the previous ones because the motorcycle is modelled as two rigid bodies instead of a lumped mass: the steering assembly and the rear body. The model is designed for trajectory tracking and stability control for agile manoeuvres. The stability is achieved by steering control and gyroscopic actuators. Additionally, it is interesting that the model works at low speed too.

Another control-oriented motorcycle analytical model for stability purposes is presented in Corno [65]. The model considers both longitudinal and lateral forces exerted by the tyres and has as inputs the steering torque as well as the front and rear wheel torques in the perspective of designing active stability control of two-wheeled vehicles. The resulting model is an 11th order nonlinear system. Although seemingly high in order, the availability of the actual equations represents an advantage to employ the model with advanced nonlinear model-based control techniques and analysis tools.

In [58, 66] control strategies that increase the stability of the motorcycle by acting only on driving and braking torques are presented. In both cases the mathematical model is obtained with a black-box approach by identifying the motorcycle dynamics as modelled by Bikesim®, an experimentally validated multibody simulator. Similarly, Baumann [57] develops an explicit mathematical model for enhancing safety, especially in cornering, minimizing the brake steer torque. Such a torque acts on the steering axis such that the motorcycle further turns in the curve if it is not compensated by the driver. Therefore, braking while cornering leads to a righting of the motorcycle whereby the desired trajectory cannot be followed. Consequently, the author wants to minimize this undesired torque to reduce its negative effects on the system handling in cornering. The presented systems are MIMO ones and the related control strategies, applied for cornering stability, take into account the rider intentions, even though the control action mainly focuses on braking rather than on traction manoeuvres.

A specific study on low speed stability of a motorcycle is in [67]. Assuming that during balancing the motorcycle roll and steer angles remain small, which could be reasonably true, a linear motorcycle model is developed, deriving equations in roll direction both for open-loop and close-loop systems. The significance of steering mechanism on bike stability is explained.

Finally, Yang and Murakami [68] propose an interesting electric motorcycle model to self-balance the bike without the active use of handlebar by the rider

in a full-speed range. The motorcycle includes two steering actuators and two driving ones, one for each wheel, so the proposed solution is not applicable on a conventional motorcycle, which has only front steering. When the motorcycle stops or moves with slow speed, the front and rear wheel are rotated of the same angle, parallel to each other, but no more parallel to the bike rear symmetry plane. In this configuration the front and rear wheel motors can be effectively controlled by swaying to keep the balance in a way similar to Segway stabilization control system.

Summarizing, in most of the aforementioned studies the developed motorcycle models for vehicle stabilization involve in some way the steering torque or steering angle as main input variable, except for Yang and Murakami work [68] where the low speed self-balancing is achieved setting the bike in a "Segway mode" and actuating two in-wheel motors. In few cases both wheel torques are considered; however, the front wheel torque is activated only in brake mode, whereas this research wants to understand the advantages of a driving front wheel torque in lateral stability and cornering performance. So, new motorcycle models are essential to investigate benefits of front wheel torque for low speed stability as well as high acceleration performances.

2.2.2 Multibody models

By creating accurate models of dynamic systems, one can precisely predict responses of the system itself to a range of inputs, getting rid of the necessity for empirical testing with the associated cost savings. High fidelity vehicle models are generally derived using multi-body dynamics, which is a logical continuation of the classical mechanics introduced by Newton. The system is modelled as a set of connected rigid bodies that may undergo translational and rotational motions relative to each other. The number of components and subsystems in a typical real vehicle makes comprehensive modelling impossible; however, considering a reasonable number of parameters and bodies, accurate models can be developed. Of course, the more precise the model should be, the larger the number of bodies will be.

The multi-body model for computer simulations can be built either by developing a mathematical model of the vehicle or by using commercial software for vehicle system dynamics. Even though the first method is more difficult and time consuming in developing phase than the second, maximum flexibility in the description of the features of the model can be obtained only by using a mathematical model. Moreover, mathematical modelling has a high computation efficiency, while multi-body software requires a lot of time to carry out simulations. Solving the

mathematical equations of motion of the generated dynamical system is not a trivial task; however, many programs now allow the computation of numerical solutions to complex mathematical problems and systems of ordinary differential equations (ODE) behind the multibody modelling.

Several multibody models based on analytical approach have been derived along the years [54, 59, 69–73]. A milestone, developed by the Lagrangian approach, is the Sharp's work [54] where the bicycle consists in two rigid bodies, the rear and the front assembly and its motion is represented by seven coordinates: rear contact point coordinates, roll, yaw and steer angles, and finally the wheel spins. Explicit derivation of the equations of motion is reported in the article. Based on Sharp's work, an analytical model of a two wheel drive motorcycle is developed in [74]. The model reliability is verified by an ad hoc multibody model built in a MSC Adams environment; however, the model needs of other validation tests. Other validated multibody models that are worth mentioning are [59, 70, 73]. In Ooms's thesis[73] the presented eleven degrees of freedom (DoF) model simulates the rolling wheel not as a nonholonomic constraint, but through a simple linear tyre model, that is capable of predicting tyre forces at large camber angles. The wheels are not restricted to the ground surface, so that wheelies and stoppies can be simulated with this model. Furthermore, the model is fully nonlinear and lateral and longitudinal dynamics are interconnected. Finally, Cossalter and Lot [59] develop another eleven DoF mathematical model based on natural coordinate approach. Each rigid body is described with a set of fully cartesian coordinates. Then, links between the bodies are obtained by means of algebraic equations. The model is implemented in a Fortran code and tested carrying out both simulated and real experimental manoeuvrers. Notice that the nonlinearity is a fundamental feature of a multibody model for high fidelity simulations because it allows to obtain a system response closer to reality, even if the system becomes more complex. For other interesting models see the literature review drawn up by Limebeer and Sharp [75].

Different commercial programs are available for multibody modelling: Simscape Multibody [76], CarSim [77], Dymola [78] and MSC Adams [79] are some of them. In particular, Simscape Multibody is useful for the three-dimensional modelling of rigid bodies in user defined geometries and it has been successfully employed by Ooms to develop a thirteen DoF multibody model - evolution of the previous one [73] - to test the reliability of its analytical equations of motion. The code of both analytical and multibody models are freely downloadable from Mathworks website [80]. CarSim and BikeSim are programs that derive the equations of motion symbolically and can then simulate the dynamic behaviour of the vehicles using the model to produce animations and plots of variables. By means of these programs

Sharp and others have developed one of the most known and used multibody models [81, 82], starting from Koenen's work [69]. The vehicle is considered composed of seven rigid bodies: front and rear wheel, front and rear unsprung mass, the chassis which includes the rider's lower body, the handlebar and the rider's upper body. The forces at the tyre/road contact point are computed according to the Magic Formula [83] and relaxation equations with a time-varying time constant. Both programs allow the user to investigate transient and steady state behaviour of systems under various inputs. Modelica [84] is an object-oriented open-source modelling language providing the language definition as well as a standard library for modelling in different physical domains. Schmitt in his master's thesis [85] provides an example of motorcycle modelling with Dymola, an advanced Modelica environment, capable of performing all necessary symbolic transformations. MSC Adams has been used to model a scooter with good success [86].

2.2.3 Motorcycle modelling review summary

This Section has introduced a review about vehicle modelling for investigations in motorcycle stability and performance. The discussion has highlighted that a good insight can be gained into the handling and balancing of motorcycles using relatively simple mathematical models, but the influence of torque repartition could be analysed with some changes to these models. However, to obtain more accurate results and realistic simulations, especially as the vehicle approaches the limit of adhesion, more complex models are required. They are also beneficial to assess and validate the control strategies designed starting from simplified mathematical models of the vehicle.

In the following Sections the mathematical model used for control design as well as the multibody models employed for validation assessmente will be presented and described in detail.

2.3 Motorcycle geometry

Motorcycles are composed of a great variety of mechanical parts, including some complex ones; however, considering the suspensions to be rigid, a motorcycle can be defined as a mechanical system of four rigid bodies: the rear assembly (frame or chassis, saddle, tank and motor-transmission drivetrain group), the front assembly (the fork, the steering head and the handlebars), the front wheel, and the rear wheel. These rigid bodies are connected by three revolute joints (the steering axis and the two wheel axles) and are in contact with the ground at two wheel/ground contact

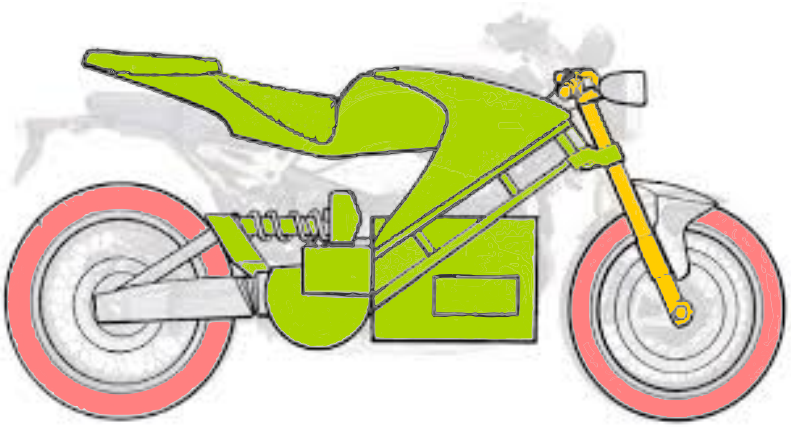

Figure 2.1: Most important bodies of a motorcycle: chassis (green), steering system (yellow) and front and rear wheels (salmon).

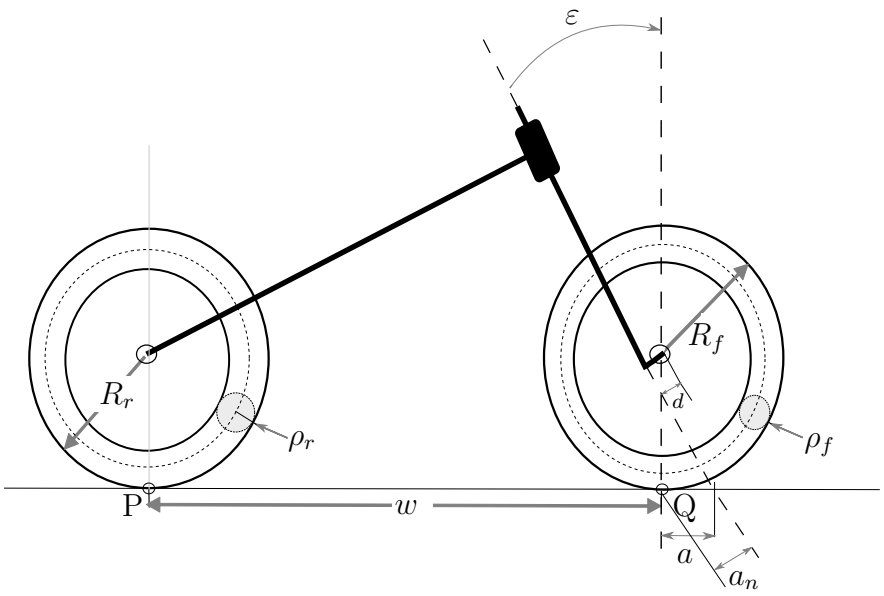

Figure 2.2: Motorcycle geometry.

points, as illustrated in Figure 2.1.

To introduce the basic geometric parameters a rigid motorcycle is considered, i.e. one without suspensions with the wheels fitted to non-deformable tyres, and schematized as two toroidal solid bodies with circular sections, as in Figure 2.2. The geometric parameters involved are: the *wheelbase* w that is the distance between the contact points of the tyres on the road, indicated by P and Q into the mentioned Figure; the *caster angle* ε, i. e. the angle between the vertical axis and the rotation axis of the steering head; the *trail* a, defined as the distance between the contact point of the front wheel and the intersection point of the steering head axis with the road measured in the ground plane; the *normal trail* a_n which is the distance between the front contact point and the steering axis. Trail and normal trail are

related each other by means of the caster angle ε:

$$a_n = a \cos \varepsilon. \tag{2.1}$$

They play a key role in the stability of a motorcycle, especially in rectilinear motion, as well explained in [71]. Observe that usually the steering axis does not pass through the centre of the wheel: the perpendicular distance between the axis of the steering head and the centre of the front wheel is named *fork offset d*. R_r and R_f are the radius of the rear and front wheel respectively, whereas ρ_r and ρ_f indicate the radius of rear and front cross section.

All these parameters are measured with the motorcycle in a vertical position and the steering angle of the handlebar set to zero. This motorcycle position is named *nominal configuration*.

2.4 Low speed self-balancing model

Balancing a motorcycle at low-speeds is challenging, because the bike is unstable below a certain critical speed [54]. On this dissertation an analysis is conducted to find out whether the front wheel torque can help in some way the stabilization of a riderless bike when the vehicle moves at zero-low speed (0.1 - 1 m/s), especially applied in those situations like a red traffic light where the vehicle is on but halted. The process has to be carried out, if possible, without any rider action on the handlebar and the need he puts his feet on the ground. To better understand the influence of the wheel torque in the vehicle stabilization, the action of the steer torque is limited, locking the handlebar at a positive angle. Indeed, a positive steering angle guarantees the vehicle motion on a curve and the rotation of the wheel on a corner generates a gyroscopic moment around the horizontal axis of the contact points, which has the desired effect of straightening the wheel.

The basic idea for vehicle balancing is to reproduce a configuration similar to Segway or wheelchair which are stable at low speed [87]. When the steering axis is rotated up to its maximum and then locked, the swaying front wheel driving torque actuation should help motorbike balancing even if the steer torque is not available.

In this perspective this Section presents a control-oriented model, dynamically similar to an inverted pendulum, able to capture the lateral motion of the vehicle. It considers both rear and front wheel driving torques instead of the rear driving torque and the steering one, unlike most of the works proposed into literature. The model is not far from the four DoF model presented in [88], with some simplifications. Indeed for instance, at low speed the aerodynamics effects can be neglected. Moreover,

steering axis is initially set on a strictly positive steering angle and is kept constant over time to facilitate the straightening effect. In the presented model the analytical equations of motion are obtained by the Lagrangian approach: the result is a non linear second order ODE system; for a better understand of the phenomenon under study the model will not be linearised.

2.4.1 Model Assumptions

A simplified motorcycle model illustrated in Figure 2.3 is considered. It consists in two bodies: a rear frame and a front steering assembly. Some simplifying hypotheses are made.

1. The wheels of the motorcycle are considered to have negligible inertial moments, mass, radii, and width, and to roll with neither lateral nor longitudinal slip.

2. The rigid frame of the bicycle is assumed to be symmetric about a plane containing the rear wheel.

3. The front contact point and instantaneous rotation axis do not change when the lean angle changes.

4. The vertical motion is neglected (no suspension motion), because its contribution is not so significant and consistent at low speeds, unlike in high accelerating or decelerating manoeuvres.

5. The bicycle is assumed to have a steering-axis fixed in the bicycle's plane of symmetry, and perpendicular to the flat ground when the bicycle is upright.

Remark. Assuming that the steering axis is vertical simplifies the motorcycle dynamics and neglects a significant geometric stabilization mechanism, which is the "motorcycle trail" (denoted as a in Figure 2.2), as discussed in [71]. The resulting model of the motorcycle dynamics cannot capture the influence of the steering angle on the roll dynamics when the longitudinal velocity is zero. Namely, the steering cannot be used to stabilize the motorcycle. However, the stabilization control variable is not the steer torque, but the front wheel; consequently, the assumption of null caster angle is not so restrictive for the developed analysis.

2.4.2 Reference Frames, Generalized Coordinates and Forces

Figure 2.3 shows the coordinate systems for a motorcycle turning with a lean angle. Let P and Q denote rear and front contact point, respectively. To identify

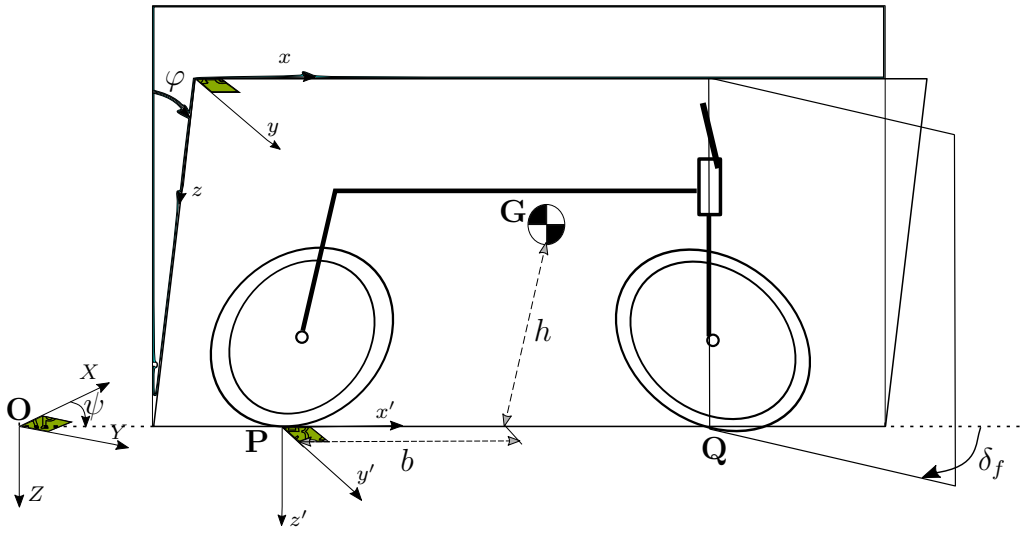

Figure 2.3: Motorcycle model scheme with reference frames and roll, kinematic steer and yaw angles φ, δ_f, ψ.

the motorcycle in a generic configuration and derive the model, three different reference frames are adopted.

- The *global* inertial reference frame $\Sigma = (OXYZ)$: it is fixed in space with its origin at arbitrary point. The Z-axis points vertically downwards in the same direction of the force of gravity and the $X - Y$ plane is horizontal and coincident with the ground.

- The *body fixed* reference frame $F = (Px'y'z')$: moves with the vehicle and has its origin at the rear contact point P. The x'-axis indicates the forward direction of the vehicle and the z'-axis remains orthogonal to the ground at all times and parallel to Z-axis, pointing downwards. The y'-axis completes a right-handed frame. The reference frame origin P has coordinates $(x_0, y_0, 0)^T$ in the global inertial coordinate system.

- The *body vehicle* reference frame $S = (Pxyz)$: a reference system with origin again in the rear contact point P of the main frame of the motorcycle and z-axis parallel to the vehicle vertical axis and pointing downwards; when the vehicle leans, the z-axis follows it and remains parallel to the motorcycle's plane of symmetry. The x-axis indicates the forward direction and the y-axis completes a right-handed frame.

Now on, where subscript is given in capitol letter, the quantity represents a vector in that coordinate system (e.g., v_Σ is velocity vector in the global reference frame). Where subscripts are given individually, the quantity refers to the specific component of the vector (e.g., $v_{x\Sigma}$ is the velocity in the longitudinal direction of the

inertial reference frame). Simultaneously, the following convention will be followed in mathematical expressions: a scalar is represented in italic medium-face serif font, e.g., R, r, ω; a vector is represented in italic bold serif font, e.g., $\boldsymbol{R}$, $\boldsymbol{r}$, $\boldsymbol{\omega}$; and a matrix is represented in upright bold serif font, e.g., $\mathbf{R}$, $\mathbf{r}$.

Coordinates The intersection of the vehicle's plane of symmetry with the ground plane forms its contact-line. In a generic configuration the contact line is no more parallel to X-axis, but it is rotated about the Z-direction of an angle ψ, named *yaw-angle*. The contact-line is considered directed, with its positive direction from the rear to the front of the bike. The yaw-angle ψ is zero when the contact-line is parallel to the X-axis and is positive in the clockwise direction. The angle that the motorcycle's plane of symmetry makes with the vertical direction is the *roll angle*, $\varphi \in (-\pi/2, \pi/2)$. The roll angle φ is positive when the vehicle leans to the right according to right hand rule (see Figure 2.3). Neglecting the suspension motion reduces one degree of freedom to the system: the rotation of the chassis around the axis of the rear wheel; the associate angle is named *pitch angle* μ and is not included in the described model. Finally, consider the line of intersection between the plane of the front wheel and the ground plane. Let $\delta_f \in (-\pi/2, \pi/2)$ be the *kinematic steering angle* between this intersection and the contact-line, as shown in Figure 2.3.

Remarks. 1. Note that the kinematic steering angle δ_f is not the angle of rotation of the steering axis of the motorcycle with respect to the chassis, indicated as *handlebar steering angle* δ. The difference is due to the caster inclination ε and the motorcycle roll φ [71]. Then, δ_f and δ are related by

$$\tan\delta_f = \frac{\cos\varepsilon \sin\delta}{\cos\varphi\cos\delta - \sin\varphi\sin\varepsilon\sin\delta} \tag{2.2}$$

Neglecting the term $\sin\varphi\sin\varepsilon\sin\delta$ with respect to $\cos\varphi\cos\delta$, the approximate equation for the kinematic steering angle δ_f becomes

$$\tan\delta_f = \frac{\cos\varepsilon}{\cos\varphi}\tan\delta. \tag{2.3}$$

In the model assumptions the steering axis is vertical, that is the bike has null caster angle; furthermore, the control objective is the bike stabilization around the vertical position, thus small roll angles are involved. With these considerations, in the simplified model the kinematics and handlebar steering angles are supposed equals $\delta_f = \delta$ and called steering angle without any distinction. This further assumption is valid along the dissertation unless declared differently.

2. A second observation is a term clarification about the roll angle φ, sometimes confused with the camber angle. By definition, the roll angle is that angle the motorcycle's plane of symmetry makes with the vertical direction indicated by the Z-axis, whereas the *camber angle* γ is that one the wheel's plane makes with the vertical direction, so refers to a specific wheel. For the rear wheel these two angles coincides; however, when the steering angle δ is other than zero, the roll angle differs from the angle the front wheel plane makes with the vertical direction and for this reason they are named differently. The relationship between the roll φ and front camber angle γ_f reads

$$\gamma_f = \arcsin(\cos\delta \sin\varphi + \cos\varphi \sin\delta \sin\varepsilon). \tag{2.4}$$

Notice it also depends on the caster inclination ε in addition to the steer angle δ.

The coordinates x, y of the contact point between the rear tyre and the road expressed in the global reference frame, the yaw angle ψ, the roll angle φ, and steer angle δ describe a complete set of generalized coordinates for the motorcycle. Notice that no longitudinal tyre slip assumption eliminates the requirement of wheels rotation ω_r and ω_f as further generalized coordinates as well as the related equations. Furthermore, for the investigated control problem the steering angle is kept fixed over time because it is assumed that the handlebar is locked over time as specific model feature. So, the steering angle becomes a model parameter instead of a generalized coordinate, transforming the model into a single body one with four degrees of freedom x, y, ψ, φ.

The generalized coordinates definitions introduced so far justify why the reference frames use the right hand rule with the Z-axis in the same direction of gravity force. Indeed, according to this convention, described by the US Society of Automotive Engineers into the SAE J670 standard [89], if the vehicle travels along a cornering manoeuvre in a clockwise direction, its forward speed, the yaw angle, the roll angle and the steering angle result all positive, which is the most natural way to describe its motion. Into this convention positive wheel rotations corresponds to counter-clockwise rotations.

Notice that it could be convenient to use a coordinates system instead of another, especially to simplify calculations, thus a change in coordinates needs to be introduced. Let $(\hat{\boldsymbol{\imath}}_\Sigma, \hat{\boldsymbol{\jmath}}_\Sigma, \hat{\boldsymbol{k}}_\Sigma)$, $(\hat{\boldsymbol{\imath}}_F, \hat{\boldsymbol{\jmath}}_F, \hat{\boldsymbol{k}}_F)$ and $(\hat{\boldsymbol{\imath}}_S, \hat{\boldsymbol{\jmath}}_S, \hat{\boldsymbol{k}}_S)$ be the unit vector sets

for the three coordinate systems and $\mathbf{R}_\psi$ and $\mathbf{R}_\varphi$ the rotation matrices:

$$\mathbf{R}_\psi = \begin{bmatrix} \cos\psi & -\sin\psi & 0 \\ \sin\psi & \cos\psi & 0 \\ 0 & 0 & 1 \end{bmatrix}, \qquad \mathbf{R}_\varphi = \begin{bmatrix} 1 & 0 & 0 \\ 0 & \cos\varphi & -\sin\varphi \\ 0 & \sin\varphi & \cos\varphi \end{bmatrix}. \tag{2.5}$$

To move from the global reference frame Σ to the body fixed one F a rotation into the ground plane around the Z-axis of the yaw angle ψ is required

$$\begin{bmatrix} \hat{\boldsymbol{\imath}}_F \\ \hat{\boldsymbol{\jmath}}_F \\ \hat{\boldsymbol{k}}_F \end{bmatrix} = \mathbf{R}_\psi^T \begin{bmatrix} \hat{\boldsymbol{\imath}}_\Sigma \\ \hat{\boldsymbol{\jmath}}_\Sigma \\ \hat{\boldsymbol{k}}_\Sigma \end{bmatrix} \tag{2.6}$$

in addition to a translation of a vector $(x_0, y_0, 0)$ (the superscript T indicates the transpose matrix operation), whereas to move from the body fixed reference frame F to body vehicle one S a rotation of a roll angle φ around the x'-axis is necessary

$$\begin{bmatrix} \hat{\boldsymbol{\imath}}_S \\ \hat{\boldsymbol{\jmath}}_S \\ \hat{\boldsymbol{k}}_S \end{bmatrix} = \mathbf{R}_\varphi^T \begin{bmatrix} \hat{\boldsymbol{\imath}}_F \\ \hat{\boldsymbol{\jmath}}_F \\ \hat{\boldsymbol{k}}_F \end{bmatrix}. \tag{2.7}$$

The composition $[\mathbf{R}_\psi \mathbf{R}_\varphi]^T$ can be used to write the components of a velocity vector, expressed in the global reference frame Σ, into the body vehicle coordinate system S:

$$\begin{bmatrix} \hat{\boldsymbol{\imath}}_S \\ \hat{\boldsymbol{\jmath}}_S \\ \hat{\boldsymbol{k}}_S \end{bmatrix} = [\mathbf{R}_\psi \mathbf{R}_\varphi]^T \begin{bmatrix} \hat{\boldsymbol{\imath}}_\Sigma \\ \hat{\boldsymbol{\jmath}}_\Sigma \\ \hat{\boldsymbol{k}}_\Sigma \end{bmatrix} = \begin{bmatrix} \cos\psi & \sin\psi & 0 \\ -\sin\psi\cos\varphi & \cos\psi\cos\varphi & \sin\varphi \\ \sin\psi\sin\varphi & -\cos\psi\sin\varphi & \cos\varphi \end{bmatrix} \begin{bmatrix} \hat{\boldsymbol{\imath}}_\Sigma \\ \hat{\boldsymbol{\jmath}}_\Sigma \\ \hat{\boldsymbol{k}}_\Sigma \end{bmatrix} \tag{2.8}$$

Although the model has no steering assembly, since the steering angle is a model parameter greater than zero, a rotation matrix related to this angle is introduced to determine the orientation relative to the main body of the (massless) front assembly:

$$\mathbf{R}_\delta = \begin{bmatrix} \cos\delta & -\sin\delta & 0 \\ \sin\delta & \cos\delta & 0 \\ 0 & 0 & 1 \end{bmatrix} \tag{2.9}$$

It will be used to express a vector $\boldsymbol{v}$, applied at the front contact point Q in the direction of wheel plane such as the front thrust, into the body fixed frame F: $\boldsymbol{v}_F = \mathbf{R}_\delta^T \boldsymbol{v}$.

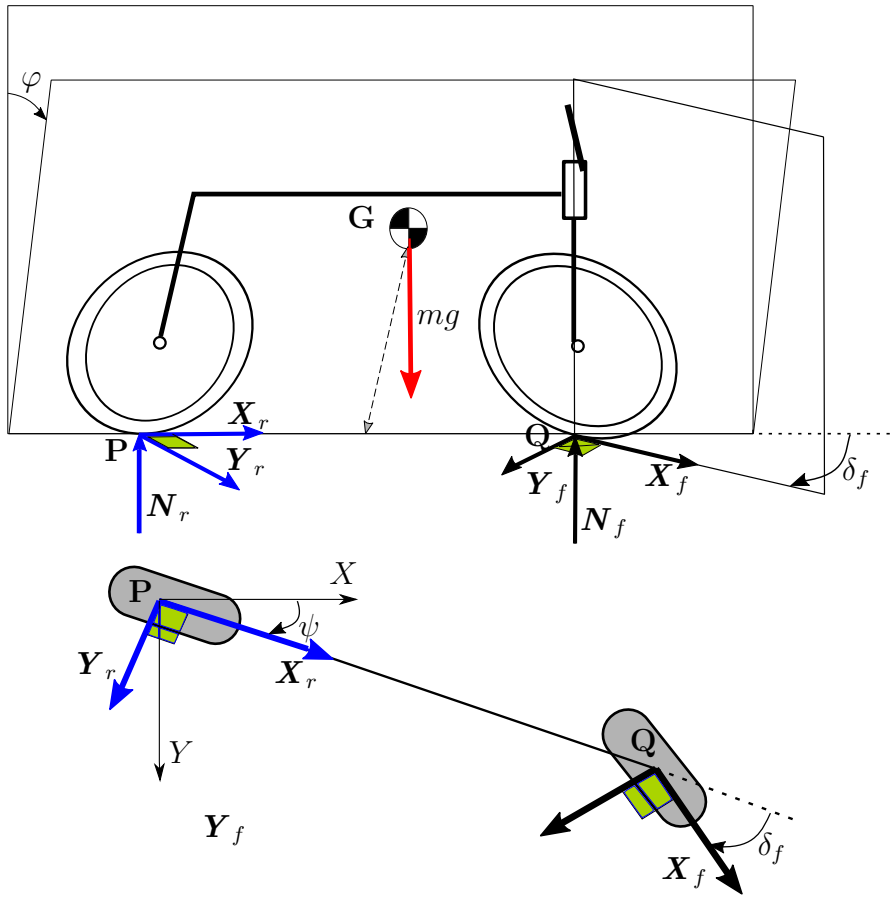

Figure 2.4: Forces acting on the vehicle: generic configuration (above) and top view (below).

Inputs and forces

Final ingredients before deriving the equations of motion are the forces and torques. Remember the presence of an electric motor in the front wheel hub of motorcycle to use for stabilization, in addition to the rear one. Thus, the control inputs of the model are the rear and front wheel torques T_r and T_f: both of them can be positive or negative, that is used as driving torque as well as braking one. This feature makes the final system a Multi Input model, so MIMO advanced control techniques can be designed based on it. By means of the wheel radii the wheel torques can be related to tyre reaction force $\boldsymbol{X}$ that the ground exerts on the motorcycle at its rear and front wheel contact points P and Q when vehicle moves forward (see Figure 2.4)

$$X_f = \frac{T_f}{R_f} \tag{2.10a}$$

$$X_r = \frac{T_r}{R_r} \tag{2.10b}$$

These reaction forces $\boldsymbol{X_f}$ and $\boldsymbol{X_r}$ act along the contact-line, as indicated in Figure 2.4.

Lateral tyre forces $\boldsymbol{Y_r}$ and $\boldsymbol{Y_f}$, which are friction forces, are also included in the model. These forces are generated at the contact patch between tyre and road and are the consequence of the sliding of the tread rubber on the asphalt surface. For this reason, these forces can be calculated using wheel kinematics and in particular, the velocity of the contact point (see Fig. 2.4). In the presented model it is adopted a linear tyre model - the simplest available - where all equations are linearised with respect to a straight running configuration. Let N_i, $i = r, f$ be the tyre static load. In the considered linear tyre model the lateral force has the roll angle φ and slip angle α contributions:

$$Y = (k_\varphi \varphi + k_\alpha \alpha) N \tag{2.11}$$

with α the slip angle, k_φ and k_α the roll and cornering stiffness, respectively. However, the slip angle contribution is smaller than the roll angle one at low speed and for this reason this second term is neglected here [71, 83]. Longitudinal slips are ignored as well. So, lateral tyre forces are reduced to

$$Y = k_\varphi \varphi F_z \tag{2.12a}$$

$$F_z = -N. \tag{2.12b}$$

The adopted linear tyre model will be presented more in detail in Section 3.4.

Unlike the lateral tyre forces, the tyre moments are neglected. Two are the main moments acting on the tyre: the overturning moment and the yawing moment. The overturning torque around the x-axis is usually included to take into account the displacement of the contact point with the roll angle, but it has been assumed no contact point migration with lean angle, so it can be neglected. The yaw torque around the z-axis is the sum of two terms, the self-aligning torque, which depends on the sideslip angle, but by hypothesis no lateral slip occurs, and the twisting torque, which depends on the camber angle, but its contribution is small. Thus, the tyre moments are not taken into account in model derivation. Further details in Chapter 3.

The motorcycle is also subjected to other external forces: the force of gravity mg - g denoted the acceleration of gravity - and the aerodynamics forces. The former acts on the point mass m of the bike at its centre of gravity, indicated by the point **G** in Figure 2.4. Among the aerodynamic forces, the drag resistance $\boldsymbol{F}_D$ has the most significant effects on the motorcycle motion. It is expressed by the

following formula

$$F_D = \frac{1}{2}\rho C_D A v^2 \tag{2.13}$$

where v is the vehicle speed, A the frontal area, ρ the air mass density, and C_D aerodynamics constant that depends on vehicle geometry. This term mainly depends on the vehicle speed: the higher the speed is, the greater the drag force and its effect on the vehicle dynamics is. However, in the discussed problem the motorbike balancing happens at low speeds; thus, aerodynamics effects can be neglected too into the model derivation.

Summarizing, the motorcycle is riderless and under automatic control, driven by two wheel torques, subjected to the force of gravity and the tyre friction forces. The steer torque is not a control input.

2.4.3 Mathematical model derivation

The equations of motion are given by Lagrange's equations:

$$\frac{\mathrm{d}}{\mathrm{d}t}\frac{\partial L(\boldsymbol{q}, \dot{\boldsymbol{q}})}{\partial \dot{\boldsymbol{q}}} - \frac{\partial L(\boldsymbol{q}, \dot{\boldsymbol{q}})}{\partial \boldsymbol{q}} = Q_q, \tag{2.14}$$

where $\boldsymbol{q} = [x\ y\ \varphi\ \psi]^T$ and $\dot{\boldsymbol{q}} = [\dot{x}\ \dot{y}\ \dot{\varphi}\ \dot{\psi}]$ are the generalized coordinates and velocities vectors, $L(\boldsymbol{q}, \dot{\boldsymbol{q}}) = K(\boldsymbol{q}, \dot{\boldsymbol{q}}) - V(\boldsymbol{q})$ is the Lagrangian function, $K = K(\boldsymbol{q}; \dot{\boldsymbol{q}})$ is the kinetic energy, $V = V(\boldsymbol{q})$ is the potential energy, $Q_q = [Q_x\ Q_y\ Q_\varphi\ Q_\psi]^T$ is the vector of the generalized external forces. The equations of motion are symbolically derived with Wolfram Mathematica® and published in [90].

Model Lagrangian function

The kinetic energy of a multibody system is equal to the sum of the kinetic energy of each of the rigid bodies which compose the system. Each kinetic energy is computed by König's theorem [91], which states that the kinetic energy of each body is the sum of the kinetic energy associated to the movement of the centre of mass and the kinetic energy associated to the movement of the particles relative to the centre of mass, that is,

$$K = K_{\text{trasl}} + K_{\text{rot}} = \frac{1}{2} m_i \boldsymbol{v}_i^2(P_i) + \frac{1}{2}\langle \boldsymbol{\omega}_i, I_i(P_i)\boldsymbol{\omega}_i \rangle \tag{2.15}$$

where $\boldsymbol{\omega}_i$ is the angular velocity, m_i is the mass of the i-th body of the system, P_i its centre of mass, $I_i(P_i)$ its inertia tensor in the local reference frame of the body and $\langle\, , \rangle$ the scalar product.

The kinetic quantities needed to compute the kinetic energy (2.15) are the mass centre velocity $\boldsymbol{v}_i(P_i)$ and angular velocity $\boldsymbol{\omega_i}$ for each body. The angular velocity can be determined remember that, in the body moving reference frame, it can be expressed by the relation:

$$\boldsymbol{\omega}_S = \langle \frac{\mathrm{d}\hat{\boldsymbol{\jmath}}_S}{\mathrm{d}t}, \hat{\boldsymbol{k}}_S \rangle \hat{\boldsymbol{\imath}}_S + \langle \frac{\mathrm{d}\hat{\boldsymbol{k}}_S}{\mathrm{d}t}, \hat{\boldsymbol{\imath}}_S \rangle \hat{\boldsymbol{\jmath}}_S + \langle \frac{\mathrm{d}\hat{\boldsymbol{\imath}}_S}{\mathrm{d}t}, \hat{\boldsymbol{\jmath}}_S \rangle \hat{\boldsymbol{k}}_S \tag{2.16}$$

To obtain this quantity into the inertial reference frame Σ its is sufficient to express the moving unit vectors with respect to the fixed ones.

The velocity of the centre of mass it is obtained either differentiating the centre of mass coordinates with respect to time or applying the *fundamental formula of rigid motion*:

$$\boldsymbol{v}(P) = \boldsymbol{v}(O) + \boldsymbol{\omega} \times (P - O) \tag{2.17}$$

where $\boldsymbol{\omega}$ is the body angular velocity and $\times$ denotes the vector product. Of course, the three vectors in (2.17) have to be expressed in the same reference frame.

For the problem assumption on the steering angle, the motorcycle model consists in a single body, thus the kinetic energy (2.15) has to be computed for a single body mass. Let **G** be the mass centre of the motorcycle body (see Figure 2.4). The kinetic quantities needed to compute kinetic energy are the mass centre velocity $\boldsymbol{v}(G)$ and the system angular velocity $\boldsymbol{\omega}$. The angular velocity $\boldsymbol{\omega}$ of the system can be obtained by the relation (2.16). To apply it, the derivative of the body unit vectors with respect to time is required. From the inverse of (2.8), the unit vectors in body vehicle reference frame S can be expressed with respect to the global Σ, then differentiating

$$\frac{\mathrm{d}\hat{\boldsymbol{\imath}}_S}{\mathrm{d}t} = -\dot{\psi}\sin\psi\hat{\boldsymbol{\imath}} + \dot{\psi}\cos\psi\hat{\boldsymbol{\jmath}} \tag{2.18a}$$

$$\begin{aligned}\frac{\mathrm{d}\hat{\boldsymbol{\jmath}}_S}{\mathrm{d}t} = &(-\dot{\psi}\cos\psi\cos\varphi + \dot{\varphi}\sin\psi\sin\varphi)\hat{\boldsymbol{\imath}} + (-\dot{\psi}\sin\psi\cos\varphi - \\ &- \dot{\varphi}\cos\psi\sin\varphi)\hat{\boldsymbol{\jmath}} + \dot{\varphi}\cos\varphi\hat{\boldsymbol{k}}\end{aligned} \tag{2.18b}$$

$$\begin{aligned}\frac{\mathrm{d}\hat{\boldsymbol{k}}_S}{\mathrm{d}t} = &(\dot{\psi}\cos\psi\cos\varphi + \dot{\varphi}\sin\psi\cos\varphi)\hat{\boldsymbol{\imath}} + (\dot{\psi}\sin\psi\sin\varphi - \dot{\varphi}\cos\psi\cos\varphi)\hat{\boldsymbol{\jmath}} - \\ &- \dot{\varphi}\sin\varphi\hat{\boldsymbol{k}}.\end{aligned} \tag{2.18c}$$

To compute the scalar product in (2.16), the two vectors have to be expressed in the same reference frame, thus, referring to the global one Σ, the coordinate of

the angular velocity in the body moving coordinate system S read:

$$\omega_{xS} = \left\langle \frac{\mathrm{d}\hat{\boldsymbol{\jmath}}_S}{\mathrm{d}t}, \hat{\boldsymbol{k}}_S \right\rangle = \dot{\varphi} \tag{2.19a}$$

$$\omega_{yS} = \left\langle \frac{\mathrm{d}\hat{\boldsymbol{k}}_S}{\mathrm{d}t}, \hat{\boldsymbol{\imath}}_S \right\rangle = \dot{\psi}\sin\varphi \tag{2.19b}$$

$$\omega_{zS} = \left\langle \frac{\mathrm{d}\hat{\boldsymbol{\imath}}_S}{\mathrm{d}t}, \hat{\boldsymbol{\jmath}}_S \right\rangle = \dot{\psi}\cos\varphi, \tag{2.19c}$$

whereas, in the global reference frame it reads

$$\boldsymbol{\omega}_\Sigma = \dot{\varphi}\cos\psi\hat{\boldsymbol{\imath}}_\Sigma + \dot{\varphi}\sin\psi\hat{\boldsymbol{\jmath}}_\Sigma + \dot{\psi}\hat{\boldsymbol{k}}_\Sigma \tag{2.20}$$

which expresses the rotation of the body around the z'-axis and the x-axis of Figure 2.3.

On the other hand, the mass centre velocity $\boldsymbol{v}(G)$ with respect to the inertial frame Σ is obtained by differentiating the expression of its global position with respect to time. In the body moving coordinate system S, the centre of mass $G_S = (b, 0, -h)$ (see Figure 2.3), which into the global system Σ becomes

$$\begin{aligned}\boldsymbol{G}_\Sigma = {} & (x + b\cos\psi - h\sin\psi\sin\varphi)\hat{\boldsymbol{\imath}}_\Sigma + (y + b\sin\psi + h\cos\psi\sin\varphi)\hat{\boldsymbol{\jmath}}_\Sigma \\ & - h\cos\varphi\hat{\boldsymbol{k}}_\Sigma.\end{aligned} \tag{2.21}$$

Thus, by differentiating (2.21) with respect to time, the velocity vector reads:

$$\begin{aligned}\boldsymbol{v}_\Sigma(G) = {} & (\dot{x} - (h\cos\varphi\sin\psi)\dot{\varphi} - (h\sin\varphi\cos\psi + b\sin\psi)\dot{\psi})\hat{\boldsymbol{\imath}}_\Sigma + \\ & + (\dot{y} + h\cos\varphi\cos\psi\dot{\varphi} + (b\cos\psi - h\sin\varphi\sin\psi)\dot{\psi})\hat{\boldsymbol{\jmath}}_\Sigma + \\ & + (h\sin\varphi)\dot{\varphi}\hat{\boldsymbol{k}}_\Sigma.\end{aligned} \tag{2.22}$$

Now, we have all the quantities to calculate the kinetic energy as in (2.15), that is,

$$K = K_{\text{trasl}} + K_{\text{rot}} = \frac{1}{2}m\boldsymbol{v}_\Sigma^2(G) + \frac{1}{2}\langle\boldsymbol{\omega}_S, I(G)\boldsymbol{\omega}_S\rangle \tag{2.23}$$

where m is the body mass, $I(G)$ its inertia tensor in the local reference frame S, and $\boldsymbol{v}_\Sigma^2(G)$ is equal to $\langle\boldsymbol{v}_\Sigma(G), \boldsymbol{v}_\Sigma(G)\rangle$. Substituting the kinematics quantities (2.22)

and (2.19) in (2.23), the kinetic energy terms become

$$\begin{aligned} K_{\text{trasl}} = \frac{1}{2} m \Big[& \dot{x}^2 + \dot{y}^2 + h^2\dot{\varphi}^2 + \left(h^2 \sin^2\varphi + b^2\right)\dot{\psi}^2 + 2(hb\cos\varphi)\dot{\varphi}\dot{\psi} - \\ & - 2\dot{x}\left(h\cos\varphi\sin\psi\dot{\varphi} + (h\sin\varphi\cos\psi + b\sin\psi)\dot{\psi}\right) + \\ & + 2\dot{y}\left(h\cos\varphi\cos\psi\dot{\varphi} + (b\cos\psi - h\sin\varphi s_\psi)\dot{\psi}\right)\Big], \end{aligned} \tag{2.24a}$$

$$\begin{aligned} K_{\text{rot}} = \frac{1}{2} \Big[& I_{\text{xx}}\dot{\alpha}^2 + 2(I_{\text{yy}}\sin\varphi + I_{\text{xz}}\cos\varphi)\dot{\alpha}\dot{\theta} + \\ & + (I_{\text{yy}}\sin^2\varphi + 2I_{\text{yz}}\sin\varphi\cos\varphi + I_{\text{zz}}\cos^2\varphi)\dot{\theta}^2\Big], \end{aligned} \tag{2.24b}$$

and, using (2.21), the potential energy is

$$V = mgG_{z\Sigma} = mgh\cos\varphi. \tag{2.25}$$

Using the expressions (2.24) and (2.25), the Lagrangian function L of the motorcycle is

$$L = K_{\text{trasl}} + K_{\text{rot}} - V. \tag{2.26}$$

Generalized external forces

The potential term $V(q)$ of Lagrangian function L is the potential associated to external conservative forces such as the gravity force, whereas, the non-conservative external forces (e.g. friction forces) contribute to generalized forces term Q_q

$$Q_q = \sum_h \langle \boldsymbol{F}_h, \frac{\partial \mathbf{P}_h}{\partial q} \rangle, \tag{2.27}$$

where $\mathbf{P}_h$ is the application point of the force $\boldsymbol{F}_h$ and $\frac{\partial P_h}{\partial q}$ is the vector consisted of partial derivatives of point $\mathbf{P}_h$ components for each generalized coordinate in $\boldsymbol{q}$. Both vectors involved into the formula (2.27) have to be expressed in the same reference frame.

The contribution of the force of gravity has already been taken into account into the system by the potential energy term V (2.25). Thus, in this Section the contribution of the other forces acting on the system is computed. As discussed in Section 2.4.2, the active forces acting on the body are the rear and front wheel thrusts $\boldsymbol{X_r}$ and $\boldsymbol{X_f}$ applied at the rear and front contact points $\mathbf{P}$ and $\mathbf{Q}$, respectively. They act along the intersection of the wheel plane with the ground, as reported in Figure 2.4. To compute the generalized forces (2.27), the application point coordinates and force components are needed. In the global reference frame Σ, the

wheel contact points $\mathbf{P}$ and $\mathbf{Q}$ have coordinates (refer to Figure 2.4)

$$\mathbf{P} = x\hat{\boldsymbol{\imath}}_\Sigma + y\hat{\boldsymbol{\jmath}}_\Sigma, \tag{2.28a}$$
$$\mathbf{Q} = (x + w\cos\psi)\hat{\boldsymbol{\imath}}_\Sigma + (y + w\sin\psi)\hat{\boldsymbol{\jmath}}_\Sigma \tag{2.28b}$$

with w the motorcycle wheelbase, whereas the thrust forces $\boldsymbol{X_r}$ and $\boldsymbol{X_f}$ components are

$$\boldsymbol{X_r}_\Sigma = X_r\cos\psi\hat{\boldsymbol{\imath}}_\Sigma + X_r\sin\psi\hat{\boldsymbol{\jmath}}_\Sigma \tag{2.29a}$$
$$\boldsymbol{X_f}_\Sigma = X_f\cos(\psi+\delta)\hat{\boldsymbol{\imath}}_\Sigma + X_f\sin(\psi+\delta)\hat{\boldsymbol{\jmath}}_\Sigma. \tag{2.29b}$$

Remember that the thrust forces magnitude is related to the wheel torque inputs by (2.10) and the steer angle δ is a model parameter, thus does not change over time.

Other forces included in the model are the tyre lateral forces $\boldsymbol{Y_r}$ and $\boldsymbol{Y_f}$, which have the same application points $\mathbf{P}$ and $\mathbf{Q}$ of the thrust forces $\boldsymbol{X_r}$ and $\boldsymbol{X_f}$, but direction of action orthogonal to them:

$$\boldsymbol{Y_r}_\Sigma = -Y_r\sin\psi\hat{\boldsymbol{\imath}}_\Sigma + Y_r\cos\psi\hat{\boldsymbol{\jmath}}_\Sigma \tag{2.30a}$$
$$\boldsymbol{Y_f}_\Sigma = -Y_f\sin(\psi+\delta)\hat{\boldsymbol{\imath}}_\Sigma + Y_f\cos(\psi+\delta)\hat{\boldsymbol{\jmath}}_\Sigma. \tag{2.30b}$$

Then, substituting (2.29), (2.30), and the partial derivatives of the application points (2.28) in $Q_q = \sum_h \langle \boldsymbol{F}_h, \frac{\partial P_h}{\partial q}\rangle$ yields to the generalized force terms

$$\begin{aligned} Q_x &= (\boldsymbol{X_r} + \boldsymbol{Y_r})\cdot\frac{\partial\mathbf{P}}{\partial x} + (\boldsymbol{X_f} + \boldsymbol{Y_f})\cdot\frac{\partial\mathbf{Q}}{\partial x} = \\ &= X_r\cos\psi + X_f\cos(\psi+\delta) - Y_f\sin(\psi+\delta) - Y_r\sin\psi; \end{aligned} \tag{2.31a}$$

$$\begin{aligned} Q_y &= (\boldsymbol{X_r} + \boldsymbol{Y_r})\cdot\frac{\partial\mathbf{P}}{\partial y} + (\boldsymbol{X_f} + \boldsymbol{Y_f})\cdot\frac{\partial\mathbf{Q}}{\partial y} = \\ &= X_r\sin\psi + X_f\sin(\psi+\delta) + Y_f\cos(\psi+\delta) + Y_r\cos\psi; \end{aligned} \tag{2.31b}$$

$$Q_\varphi = (\boldsymbol{X_r} + \boldsymbol{Y_r})\cdot\frac{\partial\mathbf{P}}{\partial\varphi} + (\boldsymbol{X_f} + \boldsymbol{Y_f})\cdot\frac{\partial\mathbf{Q}}{\partial\varphi} = 0; \tag{2.31c}$$

$$Q_\psi = (\boldsymbol{X_r} + \boldsymbol{Y_r})\cdot\frac{\partial\mathbf{P}}{\partial\psi} + (\boldsymbol{X_f} + \boldsymbol{Y_f})\cdot\frac{\partial\mathbf{Q}}{\partial\psi} = w(X_f\sin\delta + Y_f\cos\delta). \tag{2.31d}$$

For a light notation the scalar product has been indicated by the symbol $\cdot$.

Equations of motion

Finally, using the Lagrangian function $L(\boldsymbol{q}, \dot{\boldsymbol{q}})$ obtained substituting the (2.25) and (2.24) in (2.26) and the generalized forces vector (2.31), the Lagrange's equations of motion (2.14) of the model can be calculated.
Equation of motion related to x: $\frac{\mathrm{d}}{\mathrm{d}t}\frac{\partial L}{\partial \dot{x}} - \frac{\partial L}{\partial x} = Q_x$

$$\begin{aligned} &m(\ddot{x} - (h\cos\varphi\sin\psi)\ddot{\varphi} - (h\sin\varphi\cos\psi + b\sin\psi)\ddot{\psi} + (h\sin\varphi\sin\psi)\dot{\varphi}^2 - \\ &- 2(h\cos\varphi\cos\psi)\dot{\varphi}\dot{\psi} + (h\sin\varphi\sin\psi - b\cos\psi)\dot{\psi}^2) = \\ &= X_r\cos\psi + X_f\cos(\psi+\delta) - Y_f\sin(\psi+\delta) - Y_r\sin\psi; \end{aligned} \tag{2.32}$$

Equation of motion related to y: $\frac{\mathrm{d}}{\mathrm{d}t}\frac{\partial L}{\partial \dot{y}} - \frac{\partial L}{\partial y} = Q_y$

$$\begin{aligned} &m(\ddot{y} + (h\cos\varphi\cos\psi)\ddot{\varphi} - (h\sin\varphi\sin\psi - b\cos\psi)\ddot{\psi} - (h\sin\varphi\cos\psi)\dot{\varphi}^2 - \\ &- 2(h\cos\varphi\sin\psi)\dot{\varphi}\dot{\psi} - (h\sin\varphi\cos\psi + b\sin\psi)\dot{\psi}^2) = \\ &= X_r\sin\psi + X_f\sin(\psi+\delta) + Y_f\cos(\psi+\delta) + Y_r\cos\psi; \end{aligned} \tag{2.33}$$

Equation of motion related to roll angle φ: $\frac{\mathrm{d}}{\mathrm{d}t}\frac{\partial L}{\partial \dot{\varphi}} - \frac{\partial L}{\partial \varphi} = Q_\varphi$

$$\begin{aligned} &- (mh\cos\varphi\sin\psi)\ddot{x} + (mh\cos\varphi\cos\psi)\ddot{y} + \left(h^2 m + I_{\mathrm{xx}}\right)\ddot{\varphi} + \\ &+ ((mhb + I_{\mathrm{xz}})\cos\varphi - I_{\mathrm{yz}}\sin\varphi)\ddot{\psi} - ((mh^2 + I_{\mathrm{yy}} - I_{\mathrm{zz}})\sin\varphi\cos\varphi + \\ &+ (2\cos^2\varphi - 1)I_{\mathrm{yz}})\dot{\psi}^2 = mgh\sin\varphi; \end{aligned} \tag{2.34}$$

Equation of motion related to yaw angle ψ: $\frac{\mathrm{d}}{\mathrm{d}t}\frac{\partial L}{\partial \dot{\psi}} - \frac{\partial L}{\partial \psi} = Q_\psi$

$$\begin{aligned} &- m(h\sin\varphi\cos\psi + b\sin\psi)\ddot{x} + m(b\cos\psi - h\sin\varphi\sin\psi)\ddot{y} + \\ &+ ((mhb + I_{\mathrm{xz}})\cos\varphi + I_{\mathrm{xy}}\sin\varphi)\ddot{\varphi} + ((-mh^2 - I_{\mathrm{zz}})\cos^2\varphi + \sin(2\varphi)I_{\mathrm{yz}} + \\ &+ m(b^2 + h^2) + I_{\mathrm{yy}}\sin^2\varphi)\ddot{\psi} - ((mhb + I_{\mathrm{xz}})\sin\varphi - I_{\mathrm{xy}}\cos\varphi)\dot{\varphi}^2 + \\ &+ 2((mh^2 - I_{\mathrm{yy}} - I_{\mathrm{zz}})\sin 2\varphi + I_{\mathrm{yz}}\cos(2\varphi))\dot{\varphi}\dot{\psi} = w(X_f\sin\delta + Y_f\cos\delta). \end{aligned} \tag{2.35}$$

Equations (2.32) - (2.35) constitute a non-linear ODE system with front and rear longitudinal forces X_f and X_r as inputs; the lateral forces Y_r and Y_r, which appear into the equations, are not system inputs, since they are functions of the roll angle φ and wheel vertical load N_r and N_f, modelling the contact points with the linear tyre model (2.12). Notice that the nonlinearity of the system is a key model feature to capture the complexity of the system response to an external input; hence, for control design the system will not be linearised, as in the most of cases, but a nonlinear control technique will be applied.

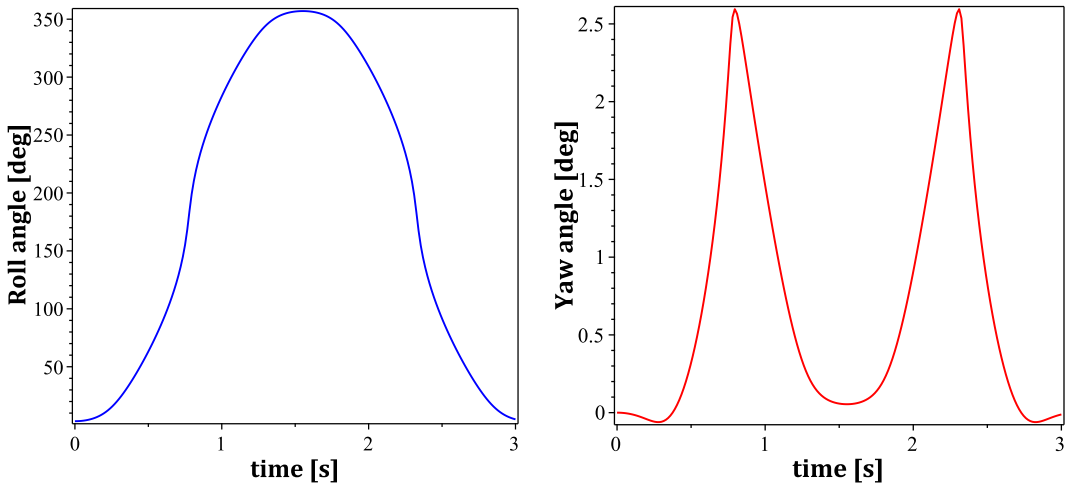

(a) Free response with no physical limitations.

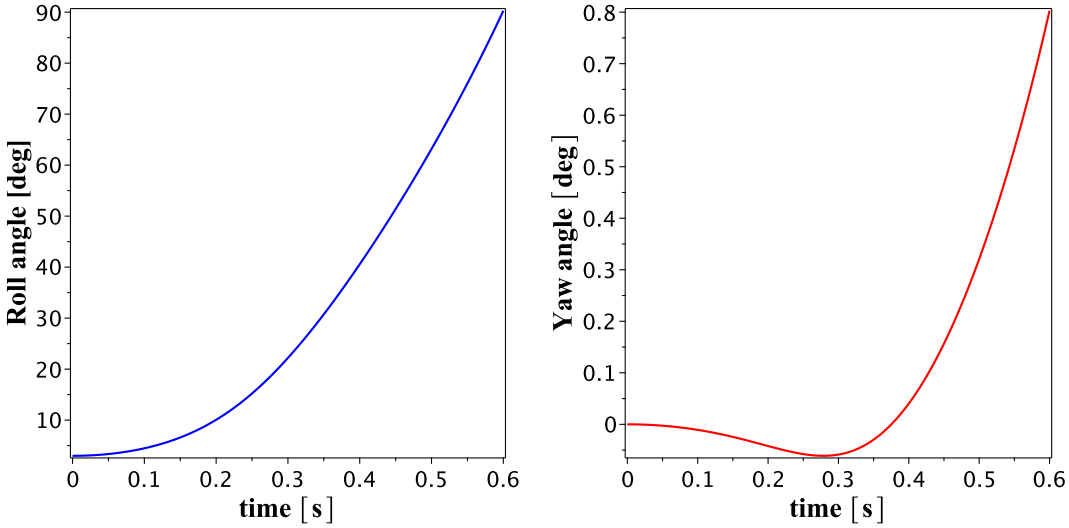

(b) Zoom in with roll angle limited to 90°.

Figure 2.5: Roll and yaw angle response of the motorcycle model (2.32) - (2.32) in free evolution: the response is similar to an inverted pendulum.

The derived non linear model (2.32) - (2.35) of the motorcycle is similar to an inverted pendulum. Figure 2.5 shows the free response of the system: at the beginning of simulation the vehicle is leaned by 3° towards right with respect to the vertical plane and all the other generalized coordinates and velocities are equal to zero. In Figure 2.5b maximum roll angle is limited to ninety degrees, which represents the physical limit when the bike reaches the ground. It is clear that the vehicle falls down because no external forces are engaged to contrast the force of gravity. The values of the model parameters are reported in the Appendix A.

The model derived in this Section will be engaged to design the lateral stability control system for the self-balancing problem.

2.5 Multibody model

Experimental tests of designed control strategies are not in the scope of the present research, thus numerical simulations with a multibody model as close as possible to the real vehicle behaviour play a key role for the control validation assessment. Among the several multibody models described in the literature review of Section 2.2.2, the multibody software, developed by the Cossalter's team at the University of Padua for investigating two wheeled vehicles dynamics [92], fits with thesis testing purposes. The very good agreement between the model response and the experimental data confirms indeed the high reliability and fidelity of the model itself, named FastBike, to a real bike behaviour. Secondly, it uses a nonlinear mathematical model based on the natural coordinates approach [93] with explicit equations of motion, symbolically derived using Maple® and its library MBSymba [94], which removes calculation errors and guarantees the maximum flexibility in the description of the motorcycle features as well as high computational efficiency and better performances with respect to other similar commercial software [59]. Finally, it is provided of a user-friendly interface for inputting the bike data and planning simulations and can be integrated as a block into Simulink/MatLab® environment. Last feature makes possible to design custom advanced control systems for the vehicle model that can be tested in dynamical simulations. All these features make this multibody model suitable for the validation assessment.

In FastBike code, the motorcycle is modelled as a system of four rigid bodies, as shown in Figure 2.6, each with an associated mass and rotary inertia:

- the rear assembly, including chassis, engine, and fuel tank;
- the front steering assembly, including steering column, and handlebar;

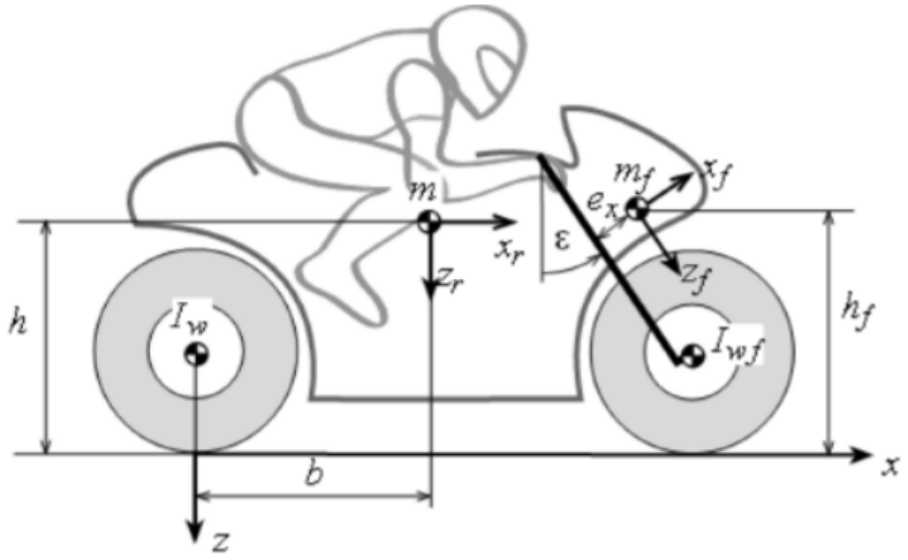

Figure 2.6: Vehicle mass distribution of FastBike software - version 1 [92] . Subscripts r and f indicate the rear and front part respectively.

- the rear wheel;
- the front wheel.

The rider is considered rigidly attached to the rear frame, thus its mass is included into the rear assembly one.

There are nine degrees of freedom to describe the motion of the bodies:

- the system can move with six degrees of freedom, both translational and rotational:
  - longitudinal, lateral and vertical coordinates of the overall centre of mass;
  - roll motion of the rear frame with respect to the vertical direction, i.e. the rotational motion about the x-axis (see Figure 2.6 for reference frame);
  - yaw motion, i.e. the rotation around the z-axis;
  - pitch motion around the y-axis;
- the front frame can steer with respect to the rear frame;
- both wheels spin about their axle.

The wheels can have different dimensions and to them different drive torques can be applied. Separate front and rear tyre models are used for the calculation of tyre forces and moments. The tyre model included in FastBike takes into account

the geometry, the position of the contact point and the deformability of the carcass [95]. It has been designed for working properly up to very large camber angle, and for providing exactly the forces/torques both in stationary and transient conditions. Further details on tyre model will be presented in Chapter 3.

The software includes aerodynamic effects of course. The aerodynamic drag force for the combined motorcycle and rider is calculated for the current vehicle speed and applied at a point specified on the motorcycle mainframe corresponding to the centre of pressure.

The virtual rider can control the vehicle by means of the handlebar, the brakes and the accelerator. The rider's movement away from the saddle and the corresponding control actions are not included in the model. In this way the motorcycle's direction is controlled only by the torque exerted on the handlebar (steering torque). The forward speed is controlled by applying the brakes (rear and front brake torques) and by acting on the accelerator lever (propulsive force). Therefore, the motorcycle has four inputs: the steering torque, the front and rear brake torques and the engine torque. In order to analyse the benefits of the front wheel traction torque on the vehicle dynamics, the last input has been customized adding a further input to the model: the front driving torque. The developers have also suitably modified the mathematical model to adapt it for low speed motion and both forward and backward manoeuvres.

Further parameters and initial conditions are specified by the user in the software interface. Data from the bodies and tyre models can be logged for post-processing, representing a further advantage of FastBike software.

The suspensions are not included in this version of the software, but at low speed the swingarm as well as the front fork do not travel relevantly, so their motion can be neglected and the model remains still valid for stability control system validation anyway. However, this lacked feature is not so irrelevant for off-road motorcycles and high acceleration motions, thus an updated version is required in order to test the optimal traction strategy in selected manoeuvres close to tyre limits.

In the second version the most relevant improvement is related to the suspension motion. The motorcycle is modelled as a system of six bodies instead of four: unsprung masses related to the suspension motion are added to the rigid bodies of the first version, the front unsprung mass (i.e. the lower part of the front suspension, the front brake caliper, etc.) and the rear unsprung mass (e.g. the swing arm). Specifically, the front suspension is telescopic, whereas the rear one is a swinging arm type, both modelled as linear spring-damper system. Once again the driver is considered to be rigidly attached to the rear assembly.

Adding two further rigid bodies the degrees of freedom of the new multibody

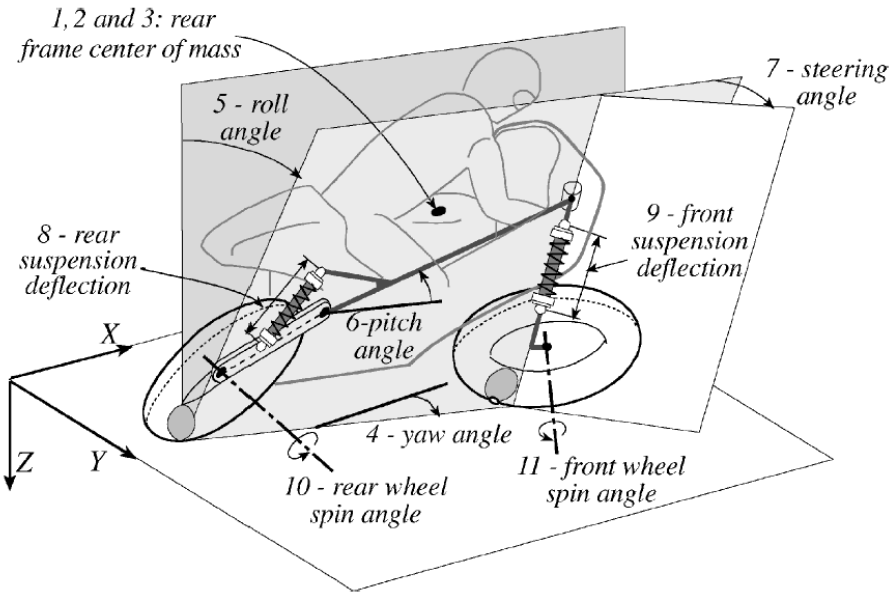

Figure 2.7: Degrees of freedom of the multibody model FastBike - version 2 [59]. With respect to the first version of the code, the rear swingarm and front fork degrees of freedom have been added to take into account the suspension motion.

model increase from nine to eleven: the old ones plus the front suspension travel and the rear suspension deflection, as depicted in Figure 2.7. However, the number of variables required for describing the system is larger than the number of degrees of freedom, more precisely they are seventeen: the roll and the pitch angles, the height of the centre of mass, the front fork travel and the swingarm angle and their derivatives, the steer angle and steer rate, the three centre of gravity speeds in chassis reference frame and the three chassis angular speeds in body fixed reference frame and finally, the rear and front wheel angular speeds.

The following forces and torques act on the motorcycle elements: suspensions forces due to springs and shock-absorbers, tyre forces and torques, aerodynamic forces, rider steering torque, steer damper torque, rear and front brake torques and finally rear and front traction torques. The rear wheel torque is transmitted from the sprocket to the rear wheel by means of the chain, also modelled in detailed. Notice that the control inputs are not changed with respect to the first version. More details on the second multibody model can be found on reference [59].

2.6 Driver model

In the self-balancing problem the rider can be considered as a system disturbance rather than a further control input, because the steering is locked and the stabilization should be achieved without any rider active intervention neither on the

handlebar nor on the acceleration lever. In this case a virtual rider is not required and because it is a preliminary study no external disturbance is added to the system during numerical simulations. Conversely, the optimal traction torque repartition strategy actively works when the vehicle is running along a path, following the rider's intention. Therefore, the rider's ability cannot be neglected and a virtual rider capable of generating challenging manoeuvres and simulating the real driver's actions to follow a path has to be designed.

Usually, the rider acts on the handlebar and leans the vehicle to carry out a cornering manoeuvre and rotates the acceleration lever to achieve the desired travel speed, or in other words he modifies the motorcycle inputs - steering, throttle and brake torques. This justifies why the rider is modelled as a steering torque controller, able to activate of course also the engine torque. The upper torso movement can also be taken into account, but it has a secondary relevance in the present study. Many control techniques can be chosen to design such controllers [96], sometimes matched with the Optimal Maneouvre Method [97] to determine the ideal speed and roll angle for the specific path. Model Predictive Control (MPC) is considered particularly suitable for virtual rider design [88], since the way a human rides a bike is very similar to that of MPC, i.e. using local preview information in a receding horizon fashion, but also a PID architecture with gain scheduling can be successfully used for this task [98].

To evaluate the performance of the traction repartition control law compared to the traditional rear traction motorcycle it should not be simulated an expert rider performing an optimal manoeuvre, since the focus is on the results obtained by the rider-vehicle system when the wheel torque distribution is applied. The rider model should be kept as simple as possible and its role should be to follow prescribed speed and roll angle profiles, even though following the speed reference is easier than following a roll angle profile because the lateral motion is more complex due to the motorcycle intrinsic instability.

For sake of simplicity the speed and the path control have separated loops and the control objectives are achieved by a PID architecture, as shown in Figure 2.8. The speed and the longitudinal motion on the vehicle are controlled by the throttle and brakes. The speed control uses a simple proportional and integral (PI) correction on the speed error to determine the required total brake or traction torque T:

$$T = K_{Pv}(V_{\text{ref}} - V) + K_{Iv} \int (V_{\text{ref}} - V)dt \tag{2.36}$$

where V_{ref} and V are the reference and actual speed, K_{Pv} and K_{Iv} are respectively

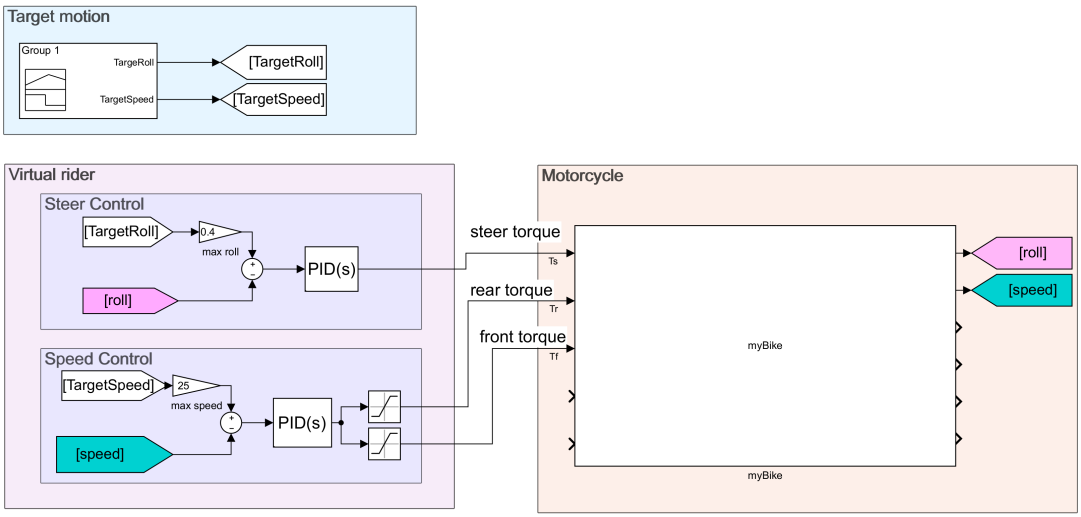

Figure 2.8: PID architecture for the virtual rider model: separate loops for speed and steering torque control.

the proportional and integral gains. Since motorcycle has front and rear independent brakes and wheels motors, then the control law properly distributes the total torque between the rear and front wheel motors.

To control the lateral stability and the path following, it is introduced the following PI steering torque controller:

$$T_S = K_{P\varphi}(\varphi_{\text{ref}} - \varphi) + K_{I\varphi} \int (\varphi_{\text{ref}} - \varphi) dt \tag{2.37}$$

where T_S is the steering torques, φ_{ref} and φ are the reference and actual roll angles, $K_{P\varphi}$ and $K_{I\varphi}$ are respectively the proportional and integral gains. The scheme is in Figure 2.8. Both PI controllers are tuned by trial and errors

2.7 Motorcycle modelling summary

This Chapter has presented the vehicle model for investigations in motorcycle stability at low speed. Good insight can be gained into balancing of motorcycles using a simplified mathematical model, which can be used for control design purposes. However, to obtain more accurate results and test control strategies, more complex models are required: multibody models work very well for this task. Many multibody models have been developed in literature, but that ones based on explicit equations of motion allow more flexibility in vehicle features description as well as complete control on the model itself. With this in mind the FastBike software has been selected for this research, suitable adapted for low speed motion

and two wheel drive torques architecture.

Chapter 3

Tyre modelling

3.1 Introduction

A pneumatic tyre is usually the only component interfacing with the road from a vehicle and its function is to generate proper forces during cornering or traction/braking manoeuvres. Therefore, the contact patch modelling and the computation of tyre forces F_x, F_y and F_z and moments M_x, M_y and M_z are an essential part of the motorcycle model. As for the vehicle modelling, many tyre models has been developed, from simpler to very complex ones and the choice among them is associated to its application and the level of accuracy required by the problem.

Low speed self-balancing problem and the optimal traction strategy work at different simulation conditions, therefore they need different tyre models. During stabilization with speed close to zero simulations do not achieve high levels of combined longitudinal and lateral slip, thus a relative simple tyre model can be enough; it can even be linearised with respect to the straight running in case of the analytical model for the control design. However, it might have the feature to manage low and negative speed to simulate the swaying motion. On the other hand, the traction distribution acts in straight running as well as in cornering manoeuvres where combined longitudinal and lateral slips occur; consequently, the tyre model has to works in this further condition too.

In this Chapter tyre models of increasing level of complexity for both the analytical and multibody motorcycle models of Sections 2.4 and 2.5 will be described after a literature review on the topic.

3.2 Tyre models: state of art

A large number of tyre models has been introduced in literature, based on theories with different perspectives and objectives for vehicle dynamics studies. This Section will summarise the available methods of calculating forces and moments generated by a tyre, given the current conditions.

In general, two approaches are employed to construct this type of tyre models: the theoretical approach and the empirical one [83]. Empirical models are based on experimental data and mathematical formulas to fit them; whereas theoretical or physical models are based on mathematical modelling of physics of the tyre as a system and seek for analytical or numerical solutions. A detailed review on tyre modelling approaches may be found in [99].

3.2.1 Analytical and Physical models

These models describe the kinematics and dynamics of the tyre contact patch in detail. The parameters that describe the tyre behaviour are of physical and geometrical nature and full-scale tyre measurements are not necessary.

An example of this kind of model is in [100]. At low slip ratios, the response of the tyre to a vertical load can be calculated easily, as the tyre material deforms elastically in the contact patch. The model can be extended to allow for sliding in the contact patch, using the so called *brush model* [100]: its simplest version consists of a belt with attached a single row of bristles and it can explain how contact forces and torques are generated and related to the macroscopic tyre motion. For basic simulations, with small slip magnitudes, this simple model might suffice; however, at large slip or high camber angle magnitudes, it no longer accurately predicts the relationship between slip and force, narrowing its application range.

Other models based on the brush concept represent its evolution [101, 102] and attempt to overcome its limits. Gim's analytical tyre model [101] divides the contact region into the adhesion region and sliding one; it includes the camber angle and can be used for both pure and combined slip cases as well as for on and off-road conditions. On the other hand, in the physical based analytical model of Pacejka and Sharp [102] the experimental data do not fit at combined slip, but a transition region is introduced.

The physical tyre models are good enough for making quantitative, still approximated, prediction of vehicle behaviour. Thus, their application is almost unlimited: they are used for quasi-static behaviour, non-linear handling, ride, comfort, durability. However, the attempt to derive equations that model all the processes in

the contact patch, such as heat dissipation, would be impractical and results in very complex models, often tailored for a specific area of application; therefore for in depth analysis and simulations, more sophisticated semi-empirical methods are recommended and often used.

3.2.2 Semi-empirical models

This kind of tyre model is based on nonlinear mathematical approximations of tyre forces and moments and interpolation of test data. Empirical tyre models require full-scale tyre measurements, data processing and parameter identification. These tyre models are in general very accurate, and are used for vehicle dynamics analysis in a broad sense, ranging from nonlinear handling to ride simulations.

Pacejka and others at TU-Delft has developed the most famous and widely spread Magic Formula tyre model [83] to address the large deviations observed in experimental results from analytical models such as the brush model. This semi-empirical model is a set of equations that relate tyre load, lateral and longitudinal slips, camber angle and vehicle speed to the generated forces and moments, using a large set of parameters which are determined by means of a least square error regression, or other similar techniques, from experimental data.

The definition of the fitting formulas is largely arbitrary, indeed many versions of the Magic Formula have been proposed along the years [70, 83, 102, 103], from the four-parameter model for approximating only lateral or longitudinal forces, to complex models, accounting for combined slip and camber angle. The Magic Formula calculates all six principle forces and moments in both steady state and transient conditions. Its equations can capture the non linearity in tyre behaviour at very low as well as very high slip conditions, making it valid in a wide range of situations. High accuracy and efficiency in the results are the further ingredients to candidate it as predominant tyre model in multibody simulations.

The Magic Formula was extended to improve its applicability to motorcycle tyres, and the large camber angles they experience and recently, a new unified version, the MF-Tyre 6.2 [103], that can handle both cars and motorcycles tyre has been presented. Modifications to its equations to take into account some other phenomena such as the temperature [104] or tyre wear [105] has been proposed, highlighting the flexibility of this model, still under development.

In most of the cases in literature the proposed models are suitable for high speed performances, but not for low speed manoeuvres, such as in the self-balancing problem. A Magic Formula correction for low speed is proposed in [106], whereas in other cases the kinematics quantities definition are directly adjusted [107].

The high number of parameters to estimate in the formulas represents the main difficulty in the use of this empirical model, even if they have a physical background. In this perspective Meijaard and Popov [70] present a simpler, but, perhaps, more usable model with fewer parameters and a simplified version of the MF-Tyre 6.2 with a small set of parameters will be presented in this research too.

3.2.3 Finite Element models

Finally, finite element analysis (FEA) of the contact patch can provide an accurate representation of the processes involved in the tyre over actual operation conditions, which makes it a powerful tool for tyre parameter identification. Indeed, the tyre is modelled by a detailed finite-element mesh for the complete tyre structure including the compressed air. The factors described by FEA method include the tyre geometry, material, dynamic, and structure components properties, so their use is mostly restricted to detailed structural analysis with high nonlinear deformations, hydroplaning and acoustic analysis. However, these physical models are computationally too expensive to be used in multibody dynamics simulations.

3.2.4 Tyre models review summary

For vehicle dynamics analysis and simulation, different types of mathematical models for describing the tyre behaviour have been presented in literature, each type for a specific application. These types are different in complexity and accuracy depending on the area of application. The dynamical simulations for vehicle performance analysis require an efficient tyre model. On one hand, finite elements models are computationally too expensive for multibody simulations and describe an excessive level of detail for the present application, whereas physical models lead to very complex and impractical equations in combined slip conditions. Thus none of them is adequate for our purposes. On the other hand, the Magic Formula, developed by the Delft University, is capable of fitting experimental data using relatively simple mathematical formulas with a set of parameters, making it computationally efficient for multibody simulations as well as extremely flexible in range of applications. It might be successfully applied to model the tyre behaviour in the different conditions and situations involved in the present research.

3.3 Tyre model inputs: kinematic quantities

In order to derive the tyre model input quantities, the tyre is assumed to behave like a thin rigid disk, as depicted in Figure 3.1. In this Figure, two planes are

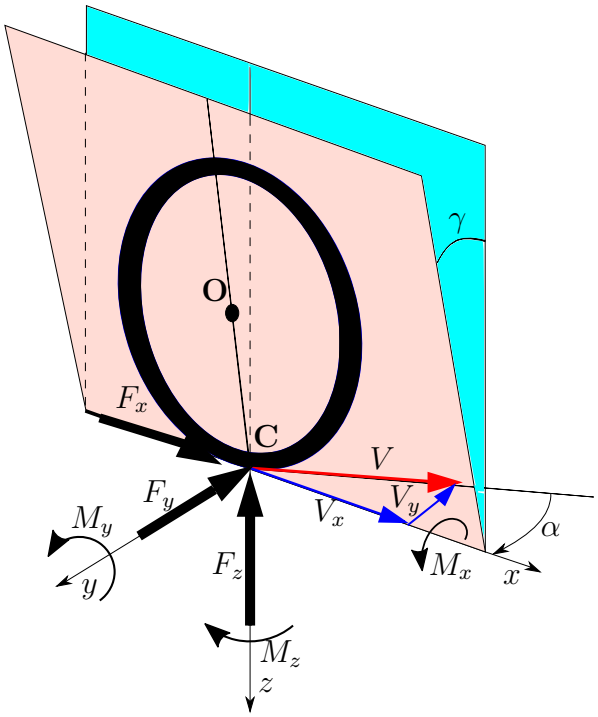

Figure 3.1: Definition of kinematic quantities of the wheel: camber γ, sideslip angle α and contact patch velocity V with its longitudinal and lateral components V_x and V_y. Forces and moments, output of tyre model, are represented too.

drawn, the wheel plane and the vertical plane, in addition to the line of the ground. The wheel–road contact point **C** is the intersection point of these planes with the plane orthogonal to the vertical one that passes through the centre **O** of the wheel. To have a clearer picture the last plane has not been drawn. Remember that wheel inclination angle (or wheel camber) γ is defined as the angle between the wheel plane and the normal to the road. Tyre deflection ρ is defined as the difference between the free nominal R_0 and loaded actual tyre radius R, illustrated in Figure 3.2. The loaded tyre radius is the distance between the wheel centre point **O** and the wheel–road contact point **C**:

$$\rho = R_0 - R. \tag{3.1}$$

The longitudinal slip velocity V_{sx} in the tyre–road contact point **C** is defined by the longitudinal wheel centre velocity V_x, the wheel rotational velocity ω and the effective rolling radius R_e:

$$V_{sx} = V_x - \omega R_e. \tag{3.2}$$

The effective rolling radius R_e is the ratio between the tyre centre velocity V_x and the spinning angular speed ω, when the tyre is in pure rolling motion, i.e. its motion

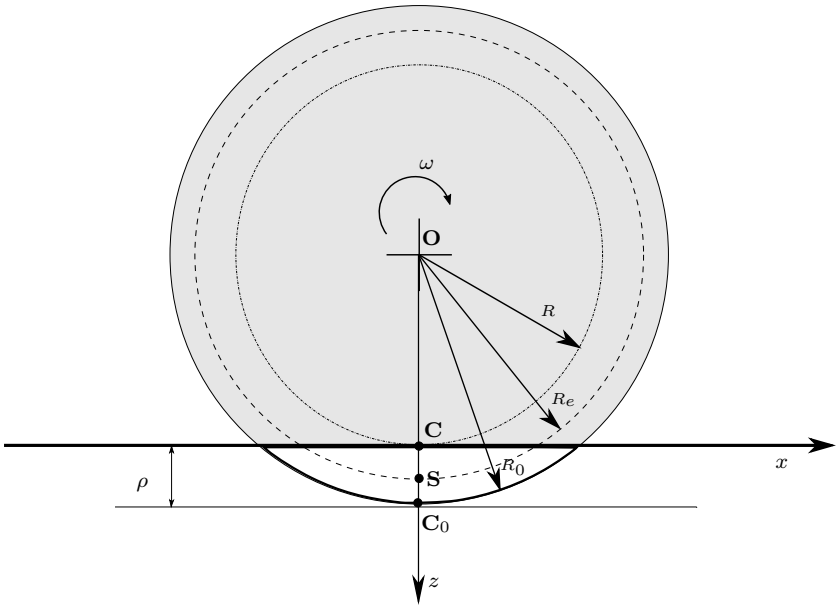

Figure 3.2: Wheel radii for pure rolling and loaded tyre. S is the slip point.

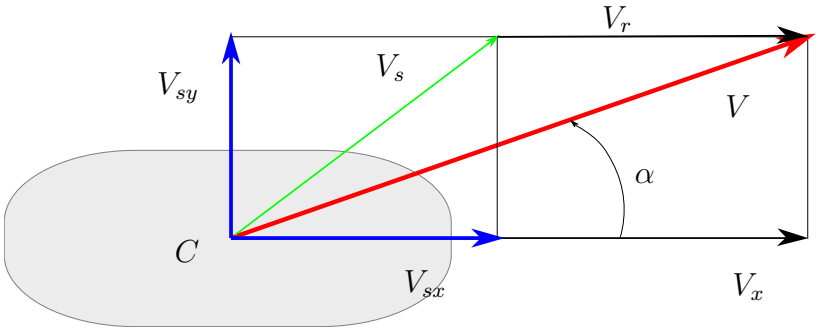

Figure 3.3: Wheel velocities at combined cornering and braking/traction.

occurs without any longitudinal force:

$$R_e = \frac{V_x}{\omega} \tag{3.3}$$

and usually it is comprises between the free nominal and loaded tyre radius, see Figure 3.2.

The lateral slip velocity V_{sy} is equal to the lateral velocity along the y-axis V_y of the wheel–road contact point **C** with respect to the road plane:

$$V_{sy} = V_y \tag{3.4}$$

In addition to the slip velocities, the rolling velocity V_r is determined by the wheel

angular speed ω and the effective rolling radius R_e:

$$V_r = \omega R_e. \tag{3.5}$$

In Figure 3.3 the wheel velocities are depicted for clarification.

Different definitions of slip exist in the literature and since tyre slip is an input of the tyre model, the slip quantities and model description cannot be separated. To better describe the longitudinal tyre motion, the *longitudinal slip* κ is defined as:

$$\kappa = -\frac{V_{sx}}{V_x} \tag{3.6}$$

with V_{sx} the longitudinal slip velocity (3.2). If the longitudinal slip velocity definition (3.2) is substituted in (3.6), the longitudinal slip can be written as

$$\kappa = -\frac{V_{sx}}{V_x} = \frac{\omega R_e}{V_x} - 1. \tag{3.7}$$

According to it, three different situations are represented:

- in pure rolling (3.3), the longitudinal slip $\kappa = 0$ because the forward speed V_x is equal to the rolling speed V_r;
- in traction, the wheel spins faster than in pure rolling, i.e. the rolling speed V_r is greater than the forward speed V_x, and $\kappa > 0$;
- in braking, the wheel spins slower than in pure rolling and $\kappa < 0$.

As depicted in Figure 3.3, the *sideslip angle* α is by definition the angle between the speed $V = \sqrt{V_x^2 + V_{sy}^2}$ and the x-axis, that is

$$\tan \alpha = \frac{V_{sy}}{|V_x|} \tag{3.8}$$

where V_{sy} is the lateral slip velocity (3.4) and V_x the forward velocity along the x-axis. This angle is involved in the generation of the lateral force. The sign of this angle is given by the right hand rule applied about the z-axis, i.e. the sideslip is positive if the wheel is turned to the right with respect the direction of motion.

In addition to longitudinal slip and sideslip angle, a third slip quantity is used as input for a tyre model, the *turn slip*. Turn slip is one of the two components that contribute to the spin of the tyre. Turn slip φ_t is calculated using the wheel yaw rate $\dot{\psi}$, which is the angular velocity of the wheel around the direction normal to the road:

$$\varphi_t = -\frac{\dot{\psi}}{V_x}. \tag{3.9}$$

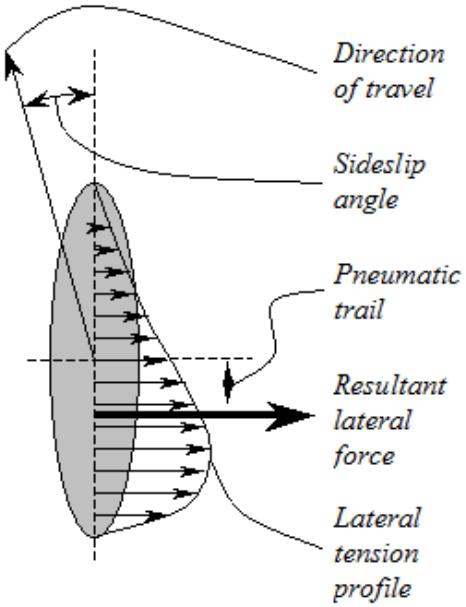

Figure 3.4: Bike tyre contact patch in a turn.

Even turn slip affects the lateral force generation, but its contribution is small and may be neglected in most of the cases.

Another kinematic quantity involved in the tyre model is the *spin slip* φ_s. It is defined as the ratio between the vertical components of the wheel angular speed ω_z and the longitudinal forward speed V_x

$$\varphi_s = -\frac{\omega_z}{V_x} = -\frac{1}{V_x}(\dot{\psi} - \omega \sin\gamma) \tag{3.10}$$

Spin slip may be neglected in most of the cases too.

The lateral force does not pass through the contact patch centre **C** of the tyre, thus due to this offset, named *pneumatic trail*, it creates a yaw moment around the vertical axis. More technically, the pneumatic trail a_t is the distance that the resultant force of side-slip occurs behind the geometric centre of the contact patch, as depicted in Figure 3.4 It is at its maximum when the slip angle is zero and decreases as slip angle increases. Pneumatic trail increases with vertical load.

3.3.1 Tyre kinematics for low speed motion

The behaviour of tyres at low and null speed requires particular modelling care. Indeed, all the kinematic quantities equations (3.6), (3.8), (3.9) and (3.10) break down when the forward speed is close to zero because the longitudinal speed appears at denominator in their definitions.

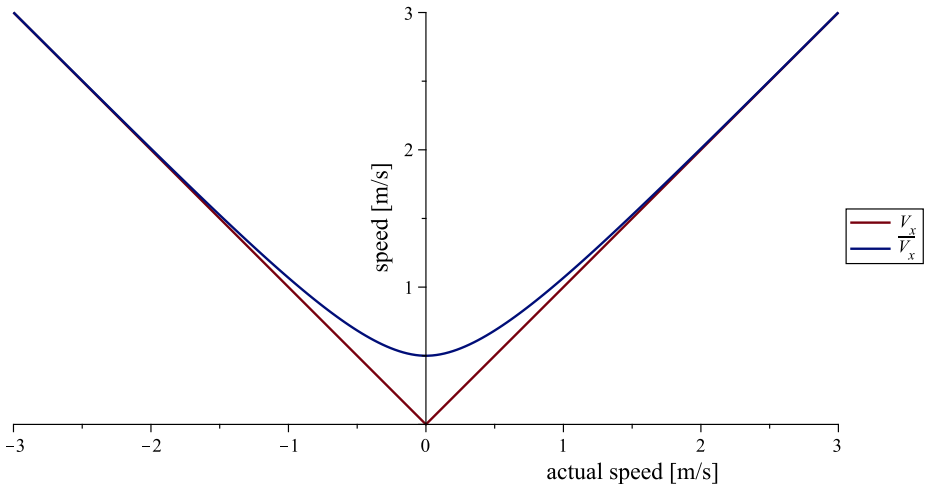

Figure 3.5: Longitudinal speed regularization for small or zero values. For speed values less than 1 m/s, the actual longitudinal speed V_x (red line) is replaced by the conventional longitudinal speed $\bar{V}_x$ (blue line).

There are few tyre models available in literature specifically developed for null and low speed situation; however, they are more complicated and the transition from low to higher speeds is not straightforward.

In the present research the velocity correction proposed in [92] is adopted. The tyre model ensures a smooth transition between low and medium-high speed by considering a conventional value $\bar{V}_x$ instead of the actual longitudinal speed V_x

$$|\bar{V}_x| = |V_x| + \epsilon e^{(-|V_x|/\epsilon)}, \qquad \epsilon = 0.5, \tag{3.11}$$

to calculate tyre slips. The correspondence between $\bar{V}_x$ and the actual longitudinal speed V_x is depicted in Figure 3.5. When the actual speed V_x is null, $\bar{V}_x$ is set to its minimum value of 0.5 m/s. As the speed increases the differences between V_x and $\bar{V}_x$ gradually decreases and are practically negligible above 1.5 m/s.

This model will be used for the self-balancing problem which involves speed close to zero.

3.4 Linear tyre model

The linear tyre model is the simplest model available, where all equations are linearised with respect to a straight running configuration. When the magnitude of the wheel slip is small, the sideslip angle α can be approximated as

$$\alpha = -\frac{V_{sy}}{V_x} \tag{3.12}$$

and the longitudinal and lateral forces F_x and F_y as well as the yaw torque M_z generated by the wheel are roughly proportional to the kinematic quantities and the tyre load N:

$$F_x = K_\kappa \kappa N, \tag{3.13a}$$
$$F_y = (K_\alpha \alpha + K_\gamma \gamma) N, \tag{3.13b}$$
$$F_z = -N, \tag{3.13c}$$
$$M_y = u_y N, \tag{3.13d}$$
$$M_z = -a_t F_y + (c_\gamma \gamma + K_\psi \varphi_t) N, \tag{3.13e}$$

where K_κ, K_α and K_γ, are the longitudinal, lateral and camber stiffnesses of the tyre and c_γ and K_ψ the twisting and rotational stiffnesses, and u_y the rolling friction. All this parameters can be calculated from experimental data. From (3.13b), notice that the lateral force has two contributions: it is generated both by the sideslip angle and the camber angle. The contribution of each force is reported in Figure 3.6, normalized with respect to the vertical load. Similarly, the yaw torque expression M_z includes three different terms: the self-aligning torque, which depends on the sideslip angle, the twisting torque, which depends on the camber angle and the rotational torque, which depends on rotational slip.

Both the longitudinal and lateral forces must not exceed the friction limit. They are saturated at the maximum lateral and longitudinal tyre-road friction coefficients μ_x and μ_y, according to

$$\begin{aligned} \bar{F}_x &= \min(\mu_x, \frac{|F_x|}{F_z}) \operatorname{sign}(\kappa) F_z = \\ &= \min(\mu_x, K_\kappa |\kappa|) \operatorname{sign}(\kappa) F_z \end{aligned} \tag{3.14a}$$

$$\begin{aligned} \bar{F}_y &= \min(\mu_y, \frac{|F_y|}{F_z}) \operatorname{sign}(K_\alpha \alpha + K_\gamma \gamma) F_z = \\ &= \min(\mu_y, |K_\alpha \alpha + K_\gamma \gamma|) \operatorname{sign}(K_\alpha \alpha + K_\gamma \gamma) F_z \end{aligned} \tag{3.14b}$$

where the sign operator is the signum function and $\bar{F}$ indicates the saturated force. However, notice that before the saturation occurs, the tyre forces have the expected linear behaviour. For further information, see the brush model [83].

The linear tyre model will be used into the control oriented mathematical model for the self-balancing problem to model the lateral forces. Tyre torques are neglected because their contribution is small with respect to the longitudinal and lateral forces.

As the slip magnitude increases, there is more relative motion between the tread

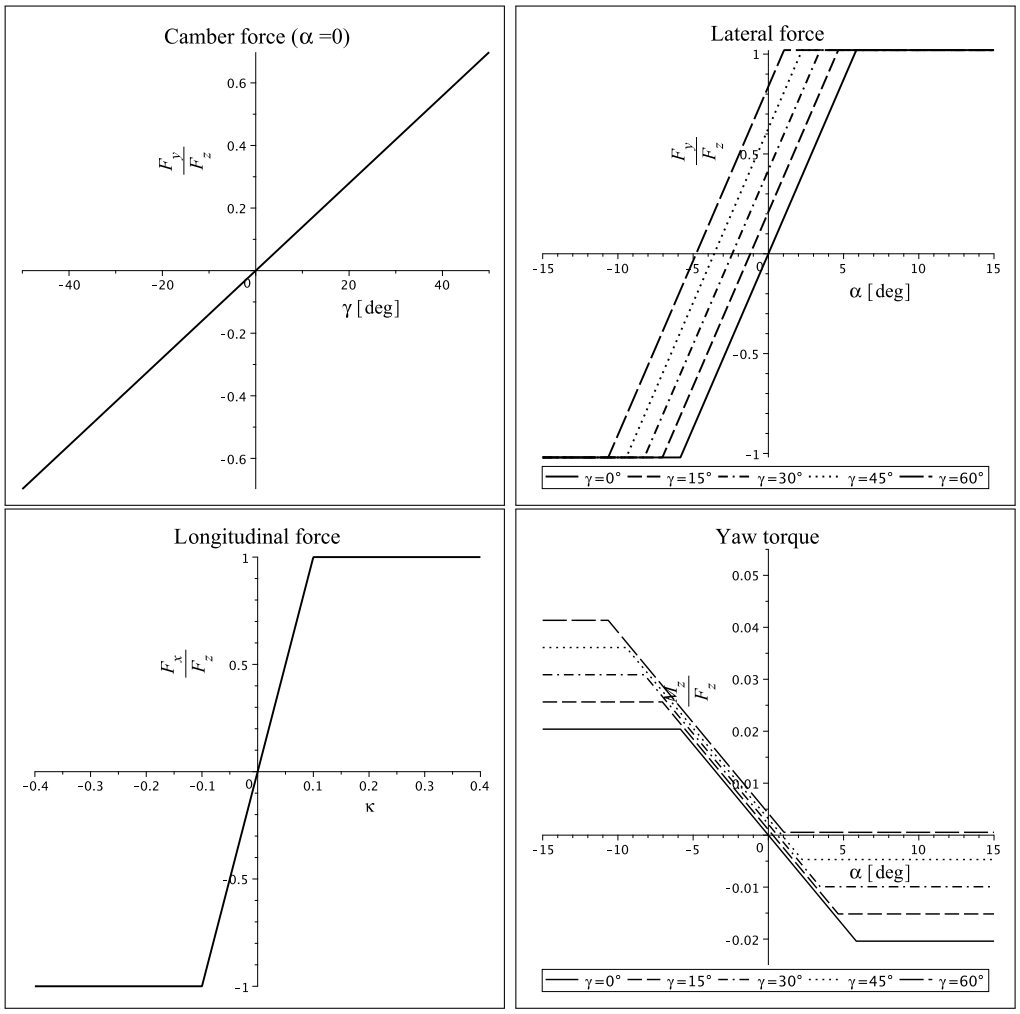

Figure 3.6: Linear tyre model with saturation. The lateral force plot with $\gamma = 0$ (on top right) is the side slip force; the yaw torque curve with $\gamma = 0$ (below right) describes the self-aligning torque.

material and the road surface. Heat is generated in the contact patch, and the response of the tyre force to the slip becomes nonlinear; thus, the above equations are no longer valid. Since traction torque repartition needs to be investigated in high-speed situations close to friction limit, a more realistic tyre model that is valid for larger slip magnitudes is required. The Pacejka Magic Formula tyre model will be empoyed for this purpose, since it satisfies a good trade-off between the relative simplicity of the mathematical formulation that can be included in dynamical simulations and the capacity of fitting the experimental data. The two versions used in this research for the tyre modelling in multibody model will be described in following Sections after a general introduction on the Magic Formula.

3.5 Magic Formula basics

The Magic Formula [83] is a type of mathematical expression that is capable of describing basic tyre characteristics surprisingly well. It produces characteristics that closely match measured curves for the side force F_y, the yaw torque M_z and the longitudinal force F_x as functions of their respective slip quantities, the slip angle α and the longitudinal slip κ, with the effect of load F_z and camber angle γ included in the parameters. The fitting is valid when the time rate of the slip quantities, i.e. slip and slip angle velocity, can be neglected, that is in the so-called steady-state cornering and braking/driving conditions.

A tyre force or torque F is modelled as a function of slip X in the following way

$$x = X + S_H \tag{3.15a}$$

$$F(X) = y(x) + S_V \tag{3.15b}$$

$$y(x) = D \sin[C \arctan(Bx - E(Bx - \arctan Bx))] \tag{3.15c}$$

with B, C, D, E, S_H and S_V parameters, which are functions tyre load F_z and camber angle γ. The parameters, or factors, have a specific influence on the Magic Formula characteristic:

- B, the stiffness factor, stretches the curve and is left to determine the slope at the origin;
- C, the shape factor, mainly influences the shape of the curve and controls the limits of the range of the sine function appearing in the formula (3.15c);
- D, the peak factor, determines the peak value of the curve, that is the

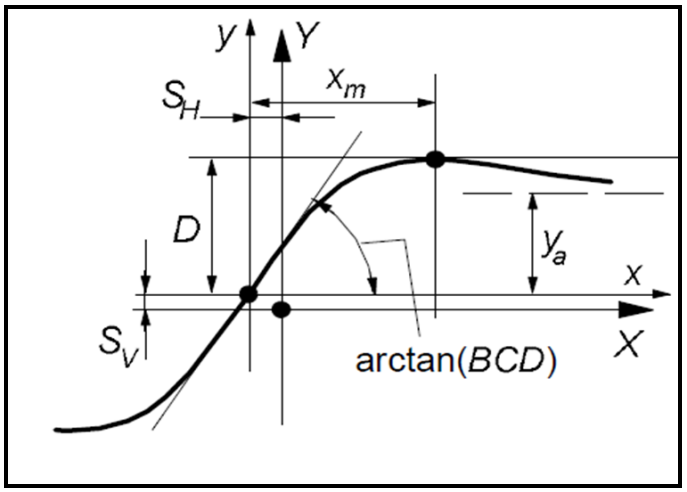

Figure 3.7: Curve produced by the Magic Formula function (3.15). The meaning of the curve parameters is indicated.

maximum of the function. For the longitudinal and lateral forces it is related to friction coefficient;

- E, the curvature factor, influences the characteristic around the peak of the curve and the horizontal position of the peak;
- S_H and S_V, the horizontal and vertical shifts, introduce an offset to the origin.

The Magic Formula $y(x)$ typically produces a curve that passes through the origin $x = y = 0$, reaches a maximum and subsequently tends to a horizontal asymptote y_a (see Figure 3.7). For given values of the coefficients B, C, D and E the curve shows an anti-symmetric shape with respect to the origin. A typical qualitative shape of this function is depicted in Figure 3.7.

The Figure 3.7 also illustrates the meaning of the parameters. The shape factor C controls the limit value of the curve and thereby the shape of the curve, according to:

$$C = 2 - \frac{2}{\pi} \arcsin\left(\frac{y_a}{D}\right). \tag{3.16}$$

The product BCD corresponds to the slope of the curve at the origin:

$$K_x = y'(x) = BCD \tag{3.17}$$

With known C and D, the stiffness factor B is left to control the slope of curve at the origin.

From B and C, the location of the peak value is directly determined by the

curvature factor E, which is related to the peak location x_m as defined in equation:

$$E = \frac{Bx_m - \tan(\pi/(2C))}{Bx_m - \arctan Bx_m} \tag{3.18}$$

The equations above illustrate that the Magic Formula factors can indeed have a physical interpretation and changing their values can vary a lot the shape of the generated function (force or torque). This illustrates the great flexibility of the formulation and explains why it is so widely spread. For further details on the Magic Formula see Pacejka handbook [83].

3.6 Basic Tyre Model

Many versions of the general formula (3.15), differing in complexity and range of validity, are widely used in numerical simulations. The first model - presented in this Section - is a simple non linear generalization [92] of the linear tyre model (3.13), which involves few parameters. As the linear model, it is valid when the slips occur principally in one direction, either lateral or longitudinal, in the so-called *pure slip* condition, that is when the tyre is either cornering or braking/driving. This assumption considerably simplifies the function expression, but limits the validity range of the model. However, at low speed for the self-balancing problem the approximation is realistic enough, thus the model can be used in the multibody software for the self-balancing control strategy validation.

Under pure slip conditions, in the Basic Tyre Model the general forms of the Magic Formula (3.15) is reduced to

$$y(x) = D \sin \arctan(Bx) N. \tag{3.19}$$

Specifically, the longitudinal and lateral steady-state forces F_{x0} and F_{y0} read

$$F_{x0} = D_x \sin\left(\arctan \frac{K_\kappa \kappa}{D_x}\right) N, \tag{3.20a}$$

$$F_{y0} = D_y \sin\left(\arctan \frac{K_\alpha \alpha + K_\gamma \gamma}{D_y}\right) N, \tag{3.20b}$$

$$F_z = -N \tag{3.20c}$$

where D_x and D_y represent the longitudinal and lateral adherence limits respectively.

The yaw torque M_{z0} becomes

$$M_{z0} = -a_t \left(1 - \frac{|\alpha|}{a_0}\right) F_{y0} + c_\gamma \gamma (1 + t_w \gamma^2) N + K_\psi \varphi_t N \tag{3.21}$$

Symbol	Unit	Description
D_x		longitudinal adherence
K_κ	1/rad	longitudinal stiffness
D_y		lateral adherence
K_α	1/rad	sideslip stiffness
K_γ	1/rad	camber stiffness
a_t	m	pneumatic trail
c_γ	m	twisting stiffness
K_ψ		rotational slip stiffness
a_0	rad	self-aligning non-linear coefficient
t_w	$1/\text{rad}^2$	twisting non-linear coefficient

Table 3.1: Description of the Basic Tyre Model parameters.

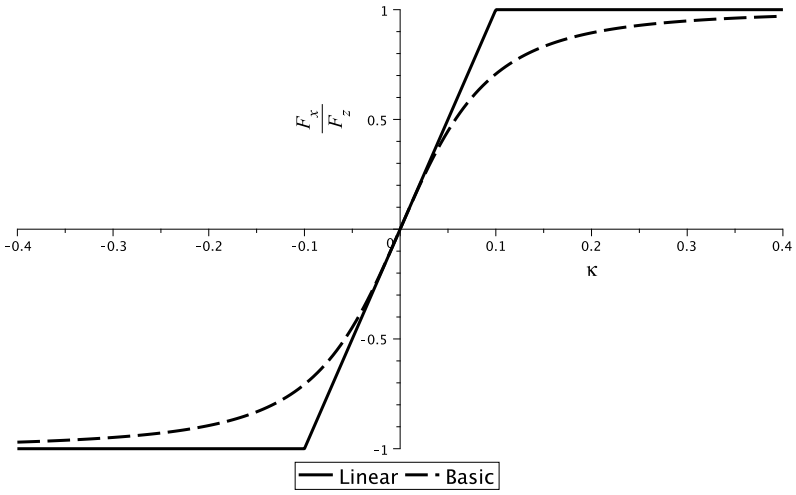

Figure 3.8: Basic vs linear tyre model. The figure reports the longitudinal force, as example. Similar behaviour holds for the other tyre quantities too.

where parameters a_0 and t_w has been introduced to take into account the non linear dependence of the yaw torque on sideslip and camber angles. The list of full set of parameters involved in the Basic Tyre Model and their description is reported in Table 3.1. For numeric values see Table A.5 in Appendix A.

Unlike the linear tyre model (3.14), the Basic Tyre Model guarantees a smooth transition between the linear region and the limit of adhesion, as highlighted by the plots in Figure 3.8. The behaviour of the lateral force F_{y0} and the yaw torque M_{z0} are reported in Figure 3.9. The camber angle introduces an offset into the self-aligning torque.

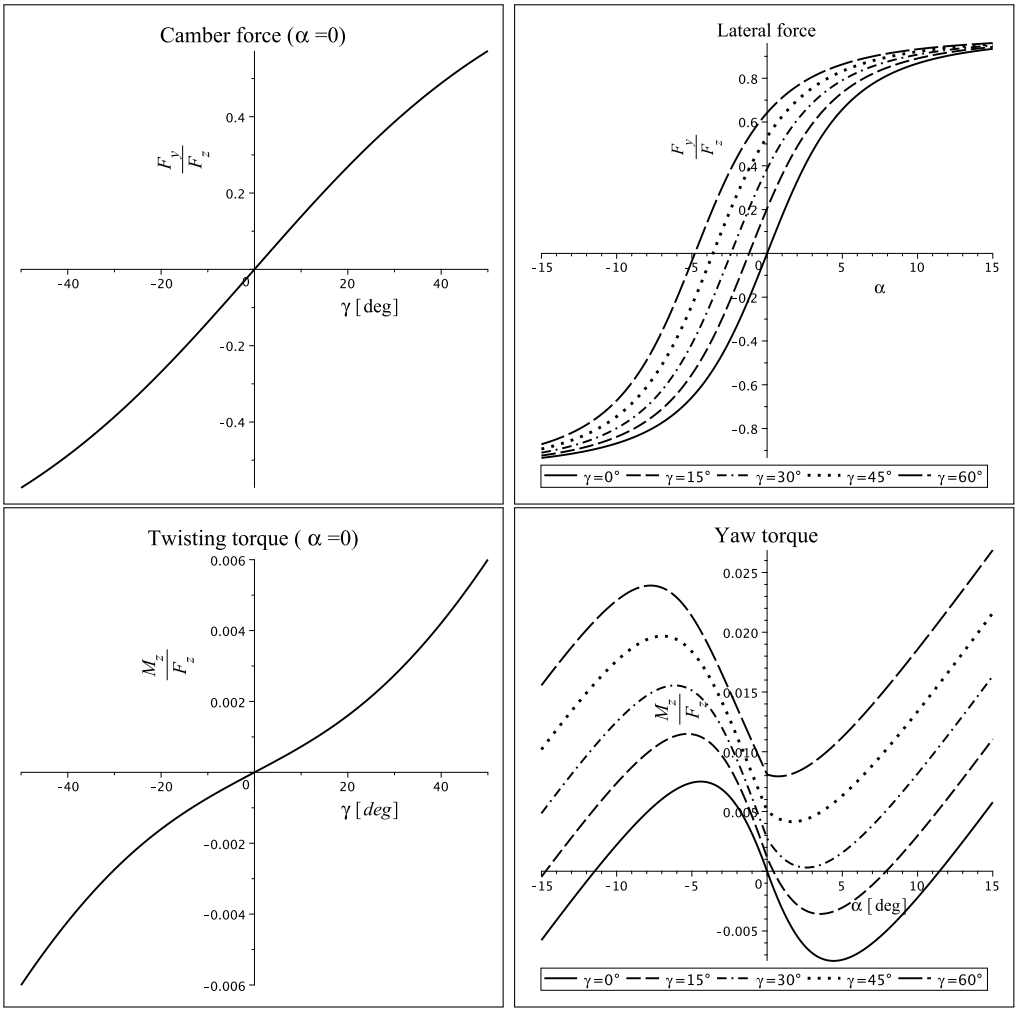

Figure 3.9: Basic Tyre Model: lateral force and yaw torque. The lateral force plot with $\gamma = 0$ (on top right) is the side slip force; the yaw torque curve with $\gamma = 0$ (below right) describes the self-aligning torque. The behaviour of the longitudinal force is shown in Figure 3.8.

3.7 Full Tyre Model

The Basic (and linear) Tyre Model discussed so far are based on the assumption that pure slip curves remain approximately similar in shape when the tyre runs at conditions different from the reference condition. The *reference condition* is defined as the state where the tyre runs at its nominal load F_{zo}, at camber equal to zero ($\gamma = 0$), at either free rolling ($\kappa = 0$) or at side slip equal to zero ($\alpha = 0$) and on a given road surface (μ_o). A similar shape means that the characteristic that belongs to the reference condition is regained by vertical and horizontal multiplications and shifting of the curve for a different tyre load or friction coefficient. It occurs because the Magic Formula parameters B, C, D involved are effectively constants.

According to the experimental data, the Magic Formula coefficients B, C, D, and E are not constant, but vary depending on a series of factors, including the tyre load and the camber angle as the most important, and consequently, the curve shape should change if tyre runs at conditions different from the reference one. Therefore, the Basic Tyre Model is good enough in describing the tyre behaviour when the conditions do not differ quite a lot from the reference ones, but for example in high longitudinal or lateral acceleration manoeuvres where high load transfer between wheels is involved, the model prediction could be inaccurate. Furthermore, the effects of the optimal traction distribution have also to analysed in cornering while tyre is driven. In this condition, lateral and longitudinal forces coexist at once. However, the basic tyre model presented in Section 3.6 does not work any more in this situation, since it is valid in pure slip conditions. Concluding, for the optimal traction strategy problem it is required a new tyre model with parameters depending on tyre load as well as camber angle and which works in combine slip conditions.

A new Magic Formula version with validity for combined slip conditions too will be presented in this Section. The Magic Formula is based on a recent version called MF-Tyre 6.2 (see [103]). The choice of the version is not only because it is the latest version available, but mainly because it offers a unified model that can handle both cars and motorcycle tyres. The last feature should not be underestimate: indeed, the Magic Formula was initially developed for cars and thus could handle only small camber angles, since a wheel of car does not roll with high angles during running. But, especially for motorcycles, the camber angle plays a crucial role in generating forces and torques, thus it has been introduced an explicit dependence of the Magic Formula coefficients by this angle. For sake of simplicity, a quite simplified version of the Magic Formula proposed in [103] will be described here, while the full model uses more than one hundred of parameters to calculate tyre forces and torques

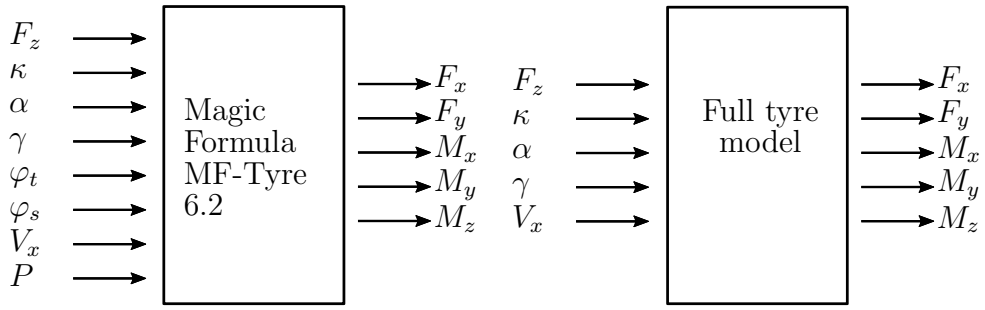

Figure 3.10: Full Magic Formula inputs and outputs (on right), against the MF-Tyre 6.2 (on left) version.

as a function of the kinetic quantities κ, α, γ, φ_t and φ_s as well as tyre load and inflation pressure P. Among the features neglected, both the turn slip φ_t and the spin slip φ_s have only a secondary influences on the tyre forces compared to the slips κ, α, and the camber angle γ. The final inputs and outputs of the Full Tyre Model are represented in the diagram block of Figure 3.10, against the Delft version [103] of the model. Another interesting feature of the MF-Tyre 6.2 Magic Formula version is that it introduces into the formula the dependence of the outputs - force or moment - on the tyre inflation pressure P. This dependence is not crucial for the present scopes, thus all the related parameters has been set equal to zero and are neglected in the presented formulas; however, the effect of inflation pressure is not negligible if the operating pressure is sensibly different from the tested one. In this perspective, the full set of Magic Formula equations [103] has been coded in Simulink so that the features neglected in this research can be taken into account in future works, if necessary.

3.7.1 Pure slip conditions

Firstly, it is presented the simplified version of MF-Tyre 6.2 for pure slip conditions: the Magic Formula coefficients will be functions of tyre load as well as camber angle.

Pure longitudinal force The Magic Formula (3.15) may be used to calculate a pure longitudinal force F_{xo} as a function of longitudinal slip κ:

$$F_{xo} = D_x \sin[C_x \arctan(B_x\kappa - E_x(B_x\kappa - \arctan B_x\kappa))]. \tag{3.22}$$

The Magic Formula coefficients B_x, C_x, D_x and E_x reflect the tyre load and camber dependency in the following way:

$$\begin{aligned} C_x &= p_{Cx1} \\ \mu_x &= (p_{Dx1} - p_{Dx2} df_z)(1 - p_{Dx3}\gamma^2) \\ D_x &= \mu_x F_z \\ K_\kappa &= (p_{Kx1} + p_{Kx2} df_z) F_z \\ B_x &= \frac{K_\kappa}{p_{Cx1} D_x} \end{aligned} \tag{3.23}$$

where df_z is a non-dimensional load increment defined with respect to the nominal load F_{z0}

$$df_z = \frac{F_z - F_{z0}}{F_{z0}}. \tag{3.24}$$

The explicit effects of the tyre load and camber angle on the longitudinal force F_x are illustrated in Figure 3.11 where the ratio between the longitudinal and vertical force F_x/F_z as function of the longitudinal slip κ is depicted: load variation affects the friction coefficient μ_x (and indirectly the maximum D_x of the function, see Figure 3.11a) as well as slightly the longitudinal stiffness K_κ, i.e. the slope of the curve at origin. On the other hand, the greater the camber angle is, the smaller the capacity of generating the longitudinal force becomes (Figure 3.11b). Notice that using the Basic Tyre Model, the same function in Figure 3.8 is valid for different tyre loads and camber angles, highlighting the first improvement of the new tyre model.

Pure lateral force As shown in the Basic Tyre model, the lateral force (3.20) depends on both the sideslip α and the camber angle γ, while the Magic Formula (3.15c) is a function of a single variable. To overcome this difficulty, Pacejka and De Vries [108], [83] proposed a Magic Formula version specifically adapted to motorcycle tyres. The pure lateral force is obtained as summation of two different contributions, the side slip and the camber angle:

$$\begin{aligned} F_{yo} = D_y \sin[&C_\alpha \arctan(B_\alpha \alpha - E_\alpha(B_\alpha \alpha - \arctan B_\alpha \alpha)) \\ &+ C_\gamma \arctan(B_\gamma \gamma - E_\gamma(B_\gamma \alpha - \arctan B_\gamma \gamma))]. \end{aligned} \tag{3.25}$$

In (3.25) the side slip and camber stiffness K_α, K_γ are defined separately. However, having different tyre models for car and motorcycle is not so practical, especially for dynamic analysis software developers point of view. Also for this reason, last Magic Formula version MF-Tyre 6.2 [103] has unified the two models writing the pure

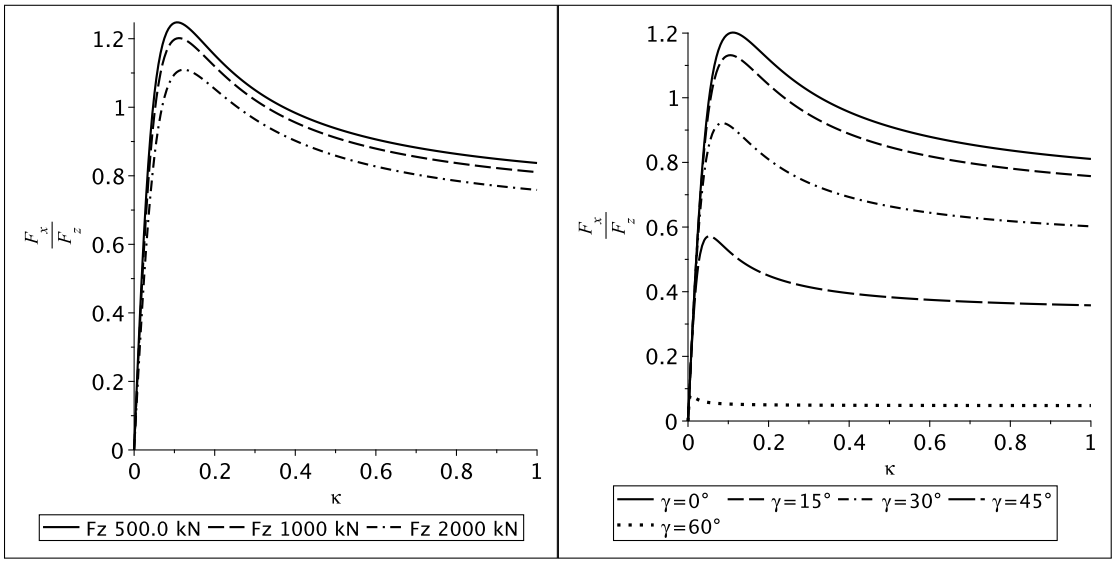

(a) Tyre load effects ($\gamma = 0$).

(b) Camber angle effects: nominal load $F_{z0} = 1000$ N.

Figure 3.11: Tyre load and camber angle effects on pure longitudinal force F_{xo}. Magic Formula parameter values in Table A.7 in Appendix A.

lateral force with an equation similar to the general Magic Formula form (3.15c). In order to do that, the side slip and camber angle are linearly combined into an *equivalent sideslip* α_y:

$$\alpha_y = \alpha + \frac{K_\gamma}{K_\alpha(\gamma)}\gamma \tag{3.26}$$

with explicit dependence of the side slip stiffness on the camber angle $K_\alpha(\gamma)$, and the pure lateral force F_{yo} reads:

$$F_{yo} = D_y \sin[C_y \arctan(B_y\alpha_y - E_y(B_y\alpha_y - \arctan B_y\alpha_y))]. \tag{3.27}$$

Even for the pure lateral force F_{yo}, the Magic Formula coefficients B_y, C_y, D_y and E_y are functions of the load F_z too:

$$\begin{aligned}
C_y &= p_{Cy1} \\
\mu_y &= (p_{Dy1} - p_{Dy2}df_z)(1 - p_{Dy3}\gamma^2) \\
D_x &= \mu_y F_z \\
K_\alpha &= p_{Ky1} \sin(p_{Ky4} \arctan \frac{F_z}{p_{Ky2}F_{z0}})(1 - p_{Ky3}|\gamma|)F_{z0} \\
K_\gamma &= (p_{Ky6} + p_{Ky7}df_z)F_z \\
B_x &= \frac{K_\alpha}{p_{Cy1}D_y}
\end{aligned} \tag{3.28}$$

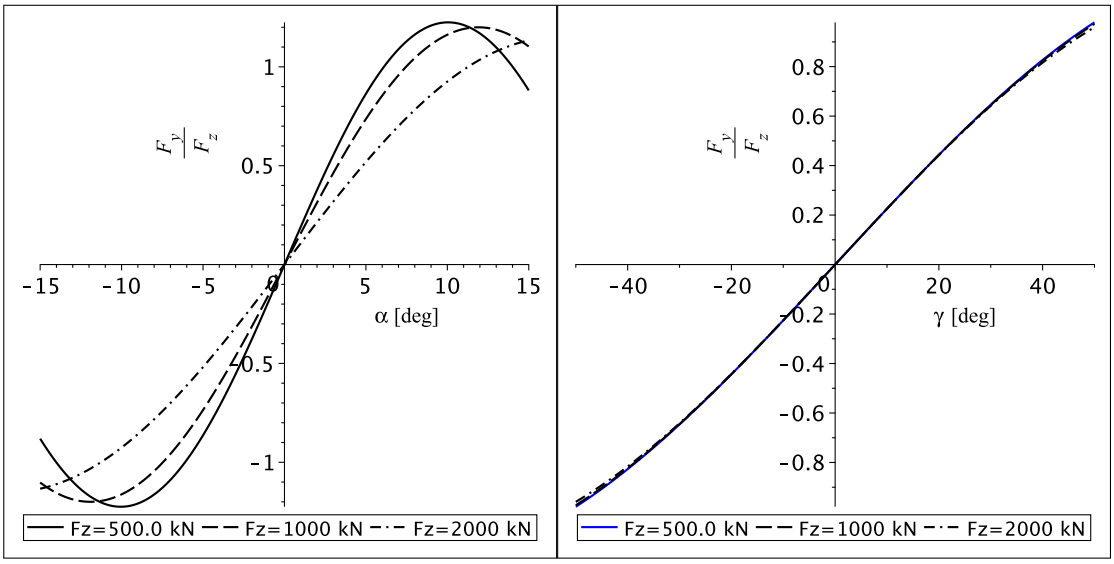

(a) Sideslip force ($\gamma = 0$). (b) Camber force ($\alpha = 0$).

Figure 3.12: Tyre load effects on pure lateral force force F_{yo}. The camber force (on the right) is almost not influenced by load variations.

From the coefficients expressions (3.28) notice that generally the friction coefficient μ_y decreases both with load and camber.

The load effects on the lateral force are depicted in Figure 3.12, setting the same Magic Formula parameters used for dynamical simulations (see values in Table A.7 in Appendix A). The camber force is almost not influenced by load variations, but adds an off-set on pure sideslip force, shifting the location of the peak. The pure lateral force F_{yo} can be visualized in Figure 3.13. The camber angle has the effect of a backward translation of the side force along the sideslip axis.

Remark. An observation about the motorcycle equilibrium on a steady cornering: as depicted in Figure 3.14a, when the vehicle is leaned, tyre has to generate the lateral force necessary to contrast the gravity force momentum. Figure 3.14b shows that in steady state cornering the camber force already generates most of the lateral force necessary to guarantee the equilibrium, so the remaining part is produced by non null sideslip angles, explaining their main function on vehicle motion. However, notice that tyre sideslip α required in the steady cornering remain very small.

A comparison among the Magic Formula versions and the linear model in pure slip conditions is reported in Figure 3.15. Main differences are visible in the asymptotic behaviour and when the force is close to saturation.

Pure yaw torque The overall yaw torque M_z is the sum of two terms:

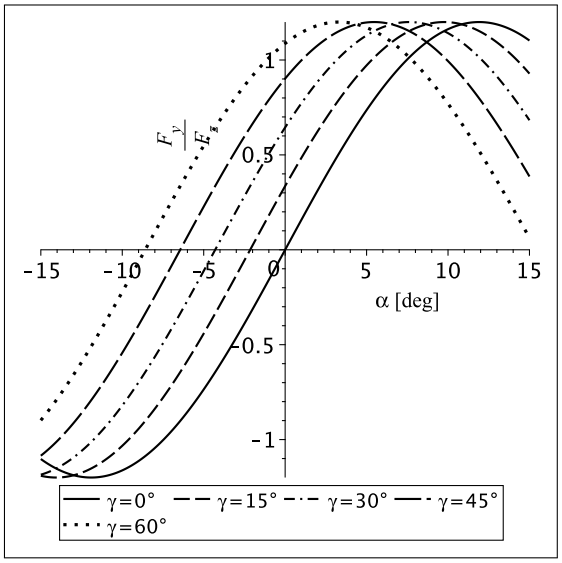

Figure 3.13: Pure lateral force force F_{yo} at nominal load $F_{z0} = 1000$ N for different camber angles γ.

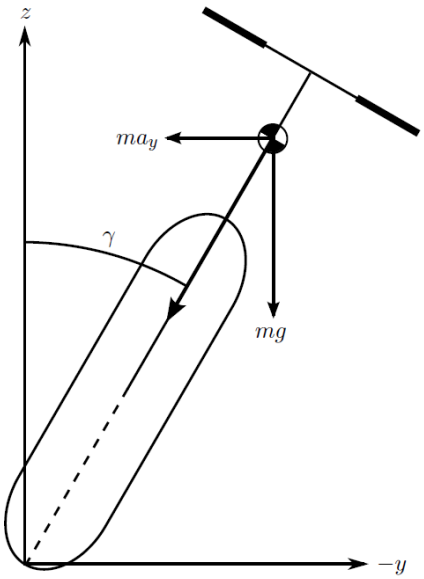

(a) Equilibrium in steady cornering: rear view of the motorcycle.

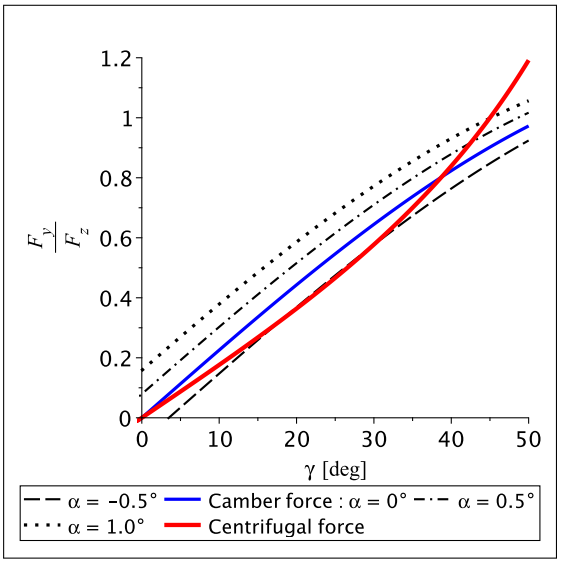

(b) Centrifugal force and camber force: a small sideslip is reqired to guarantee that lateral force matches the centrifugal one.

Figure 3.14: Steady state cornering.

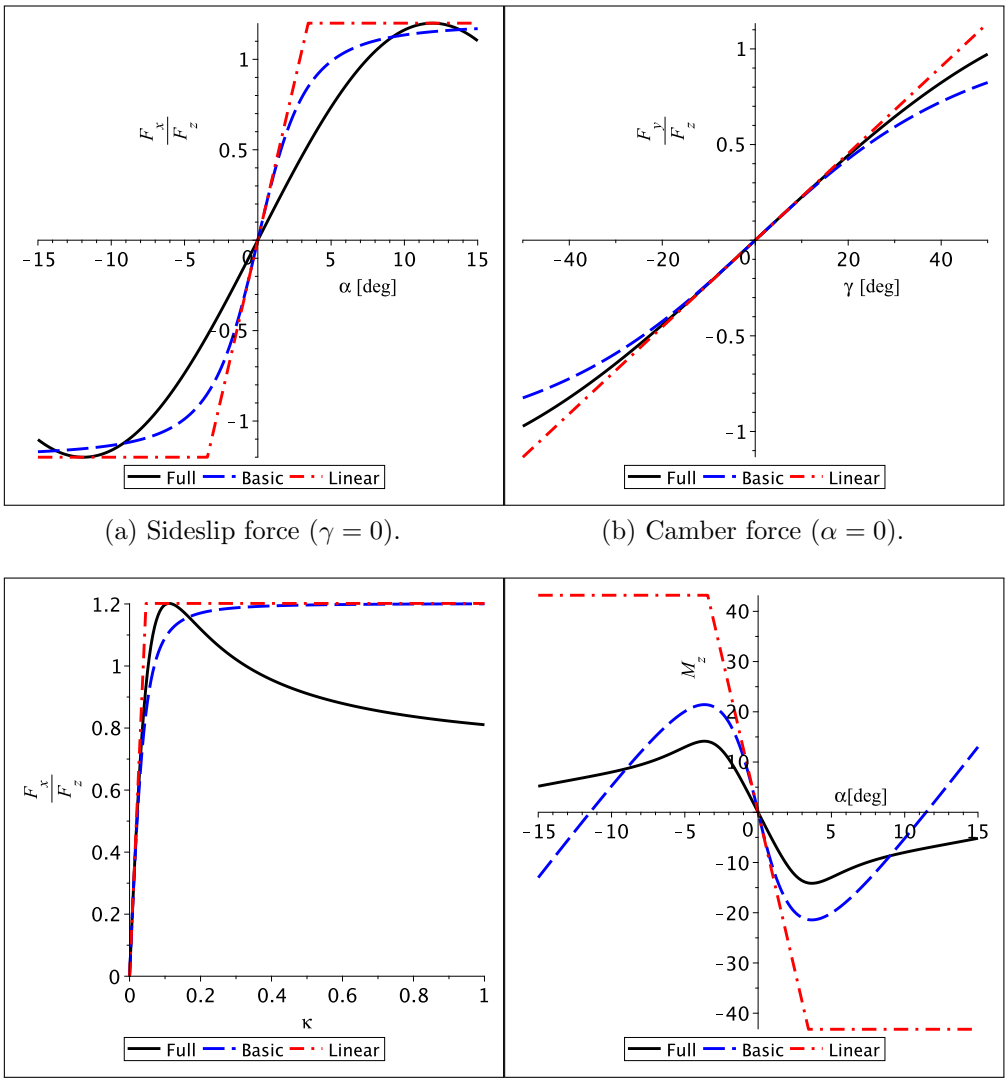

(a) Sideslip force ($\gamma = 0$).

(b) Camber force ($\alpha = 0$).

(c) Longitudinal force.

(d) Self-align torque ($\alpha = 0$).

Figure 3.15: Comparison among the different versions of Magic Formula (Basic (3.20) and MF-Tyre 6.2 ((3.22), (3.27)) and the linear model (3.14). For all cases Magic Formula parameters are: $F_{z0} = 1000$ N, $\mu_x = p_{Dx1} = \mu_y = p_{Dy1} = 1.2$,$K_\kappa = p_{Kx1} = 26$, $K_\alpha = p_{Ky1} = 20$, $K_\gamma = p_{Ky6} = 1.3$. Other parameter values in Appendix A.

- the *self-aligning torque* $M_{z\alpha}$, depending on the sideslip angle α and generated by the sideslip force because it does not pass through the centre of contact patch **C**;
- the *twisting torque* M_{zr}, created when the wheel is cambered. It tends to move the wheel along a trajectory with a smaller curvature radius, thereby acting to twist the wheel out of alignment.

Mathematically, the yaw torque is

$$M_{zo} = M_{z\alpha} + M_{zr} = -a_t \, F_{yo}|_{\gamma=0} + M_{zr} \tag{3.29}$$

with the self-aligning torque $M_{z\alpha}$ expressed as the product of the pneumatic trail a_t by the lateral force $F_{yo}|_{\gamma=0}$ calculated by putting $\gamma = 0$ into (3.27). The minus sign into the yaw torque formula (3.29) stresses the self-aligning effect of the lateral force. In the Basic Tyre Model the dependence of pneumatic trail on the sideslip angle α has been considered introducing a new parameter α_0 (3.21). In this case, the tyre trail variation with the sideslip angle can be expressed by the Magic Formula itself:

$$a_t = D_t \cos[C_t \arctan(B_t\alpha - E_t(B_t\alpha - \arctan B_t\alpha))] \cos\alpha. \tag{3.30}$$

To introduce the effect of the tyre load on the pneumatic trail, the D_t factor is written as

$$D_t = R_0 q_{Dz1} \frac{F_z}{F_{z0}} \tag{3.31}$$

where R_0 is the unloaded tyre radius. The result is depicted in Figure 3.16a: the pneumatic trail a_t increases with the load and, as stated in Section 3.3, a_t is maximum at null sideslip angle $\alpha = 0$, then decreases as sideslip increases. In the meanwhile, the lateral force increases as well (see Figure 3.12), creating a self aligning torque $M_{z\alpha}$, as shown in Figure 3.16b.

The twisting torque M_{zr}, second term in yaw torque M_z is calculated as follow

$$M_{zr} = D_r \cos(\arctan B_r\alpha). \tag{3.32}$$

To stress the dependence of this term on the camber angle, the coefficient D_r has been simplified in

$$D_r = R_0 \cos\alpha(q_{Dz8} + q_{Dz10}|\gamma|)\gamma F_z, \tag{3.33}$$

deleting its tyre load dependency with respect to the original version reported in [103]. The twist effect of the camber angle γ on the wheel is depicted in Figure 3.16c. Its action contrasts the self-aligning torque $M_{z\alpha}$ (see Figures 3.16b and

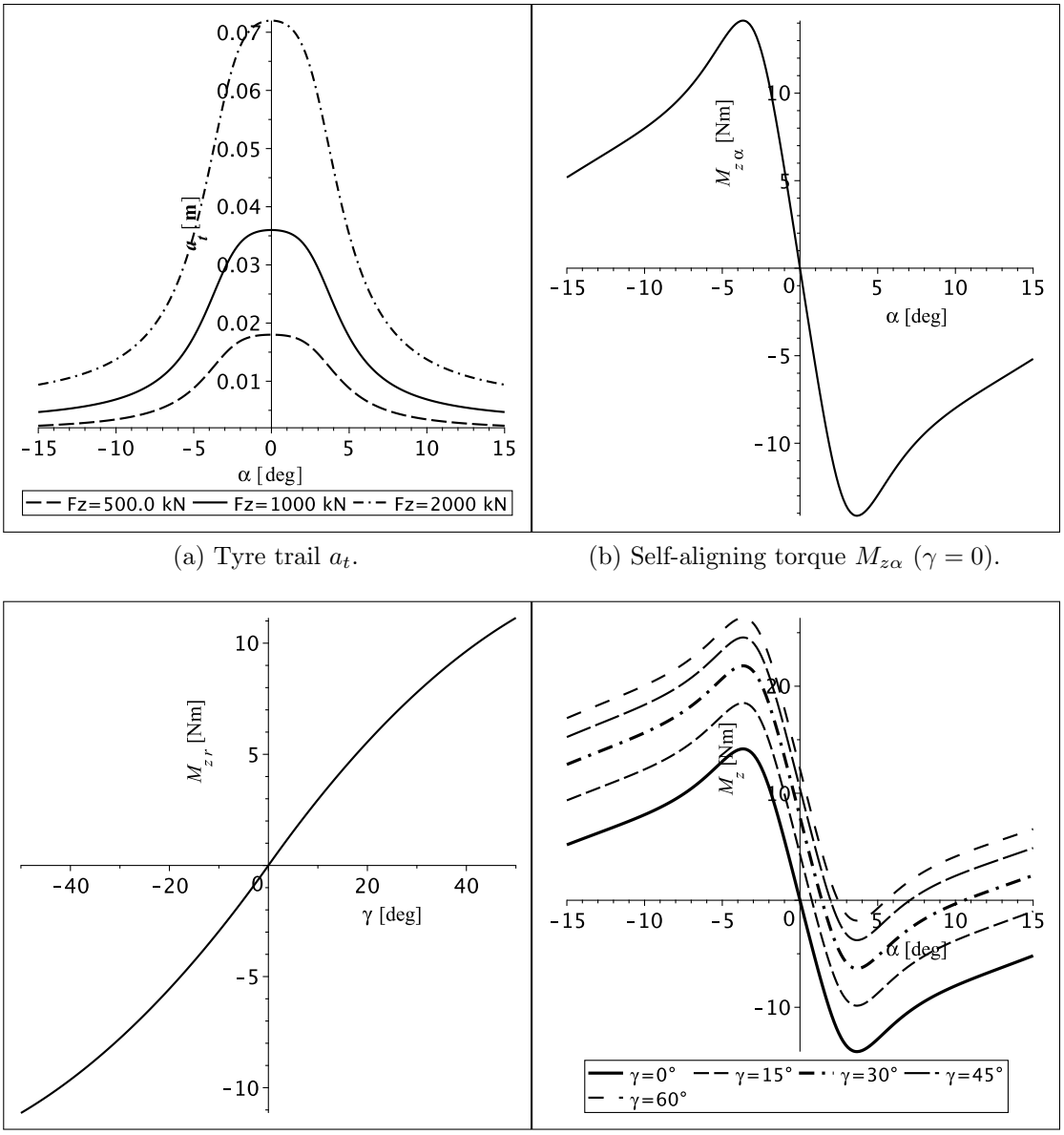

(a) Tyre trail a_t.

(b) Self-aligning torque $M_{z\alpha}$ ($\gamma = 0$).

(c) Twisting torque M_{zr} ($\alpha = 0$).

(d) Yaw torque M_r for different values of camber γ.

Figure 3.16: Yaw torque in pure slip conditions at $F_{z0} = 1000$ N and $R_0 = 0.3$ m.

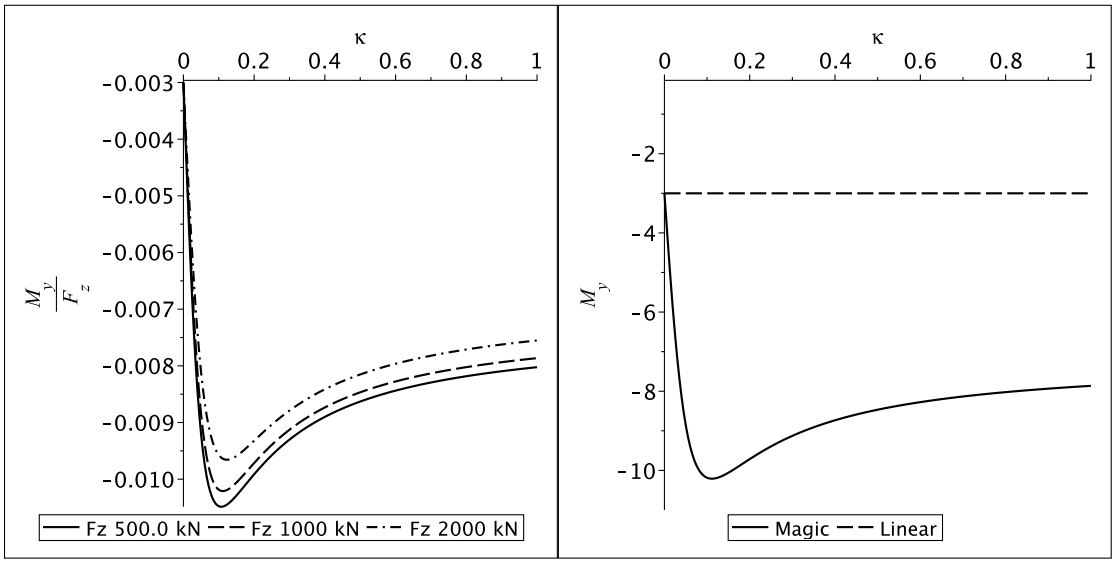

(a) Effect of tyre load. (b) Comparison of linear and full version.

Figure 3.17: Rolling resistance M_y. Magic Formula parameters are: $q_{sy1} = 0.01$, $q_{sy2} = 0.02$, $q_{sy3} = q_{sy4} = q_{sy5} = 0$.

3.16c). The final result is the overall yaw torque M_r, reported in Figure 3.16d as function of sideslip α at different camber γ: the twist torque adds an off-set to the self-aligning torque.

Rolling resistance To move the wheel at constant forward speed, it is necessary to overcome a rolling resistance M_y proportional to the vertical load F_z:

$$M_y = u_y F_z = q_{sy1} R_0 F_z \tag{3.34}$$

as expressed by the linear model (3.13). The rolling friction u_y is proportional to the unload radius, thus the dependence can be explicitly expressed by introducing the non dimensional parameter q_{sy1}.

To take into account the presence of the longitudinal force F_x and the dependence on the speed V_x and the camber angle γ, the rolling resistance formula (3.34) can be evaluated by:

$$M_y = -\left(q_{sy1} + q_{sy2}\frac{F_x}{F_{z0}} + q_{sy3}\left|\frac{V_x}{V_{x0}}\right| + q_{sy4}\left|\frac{V_x}{V_{x0}}\right|^4 + q_{sy5}\gamma^2\right) R_0 F_z \tag{3.35}$$

introducing four non-dimensional parameters q_{sy2}, q_{sy3}, q_{sy4} and q_{sy5}. An example is depicted in Figure 3.17.

Overturning torque The overturning moment is especially important to investigate the vehicle roll-over occurrence and the curving behaviour of a motorcycle. Due to the lateral deflection connected with the side force F_y, the point of application of the vertical force F_z moves in the direction of the side force generating a negative couple M_x. Similarly, when the wheel is cambered, even the lateral force F_y does not passes through the nominal contact point, creating an overturning moment. Therefore, the overall overturning moment M_x is evaluated by

$$M_x = R_0[-q_{sx12}\gamma|\gamma|F_z + (q_{sx13} + q_{sx14}|\gamma|)F_y]. \tag{3.36}$$

It is usually included to take into account the displacement of the contact point with the roll angle. However, in the multibody model presented in Section 2.5 the actual contact point position is used and there is no need to take into account for such term.

3.7.2 Combined slip conditions

The above equations of forces and torques are designed for use when slip is principally in one direction only, either lateral or longitudinal. However, in high lateral and longitudinal acceleration motions, that is when the tyre is driven or braked while it is cornering, both longitudinal and lateral forces are present at once, and the model proposed till now becomes less accurate in describing the behaviour of a real tyre. Indeed, using the above equations in situations of combined slip can give a resultant force that exceeds the friction limit. In an attempt to increase the range of validity of the model to include these situations, it is required a correction to guarantee that the friction limit is not exceeded in any direction. Thus, the concept of friction circle is introduced.

In order to remain inside the tyre adherence region, the longitudinal and lateral forces F_x and F_y are constrained to

$$\left(\frac{F_x}{F_z}\right)^2 + \left(\frac{F_y}{F_z}\right)^2 \leq \mu^2 \tag{3.37}$$

i.e. are confined into a circle of radius μ.

If different friction limits along the x and y-axes are considered, previous inequality becomes

$$\left(\frac{F_x}{\mu_x F_z}\right)^2 + \left(\frac{F_y}{\mu_y F_z}\right)^2 \leq 1 \tag{3.38}$$

which is the equation of an ellipse with semi-minor axes $\mu_x F_z$ and $\mu_y F_z$, the so-called *ellipse of adherence* or *friction ellipse* (see Figure 3.18). The above

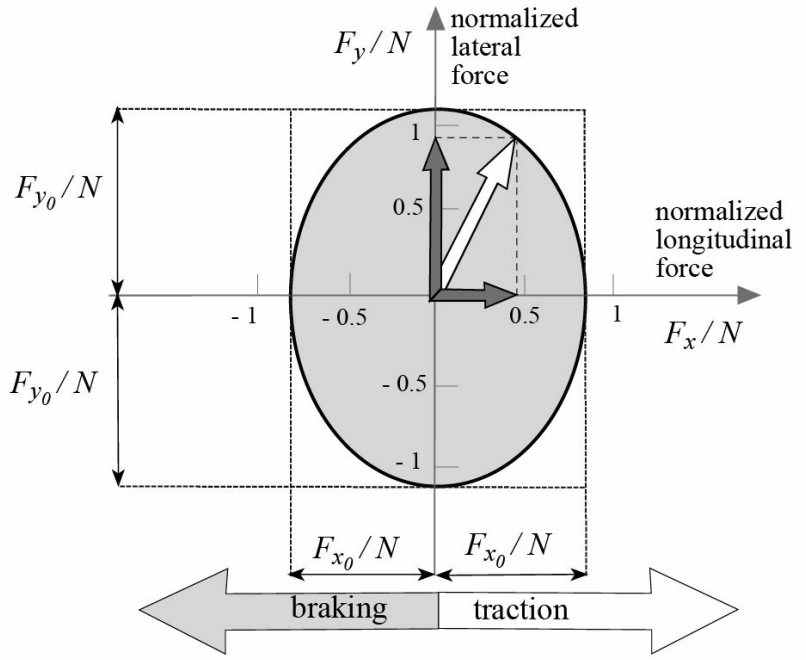

Figure 3.18: Friction ellipse.

inequality establishes that the lateral force F_y that can be exercised is reduced by the simultaneous presence of the longitudinal force F_x, because their resultant must be within the friction ellipse. Note that the length of the semi-minor axes is equal to the maximum longitudinal, and lateral forces respectively, when they act alone, as depicted in Figure 3.18.

Longitudinal and lateral forces in combined slip To ensure that the resultant force does not exceed the friction ellipse, then lateral and longitudinal forces are scaled to be within the maximum by a scale factor G, named *weighting function*, which depends on the slip on the other axis. In this sense, the force formulas for combined slip are based upon the expressions of lateral and longitudinal forces F_{xo} and F_{yo} (3.22), (3.27) for pure slip conditions:

$$F_{sx} = G_{x\alpha}(\kappa, \alpha, F_z)F_{xo} \tag{3.39a}$$

$$F_{sy} = G_{y\kappa}(\kappa, \alpha, F_z)F_{yo}. \tag{3.39b}$$

The general expression of the weighting function G as reported in [103] reads

$$G = \frac{\cos[C\arctan(Bx - E(Bx - \arctan(Bx)))]}{\cos[C\arctan(BS_H - E(BS_H - \arctan(BS_H)))]} \tag{3.40}$$

where x is the slip of the other axis. In this dissertation the horizontal offset S_H of the curves to the origin has not been considered. With this assumption, the

denominator of (3.40) becomes equal to one and the weighting factor G can be expressed with the cosine version of the Magic Formula (3.15c). Then the proposed simplified version of (3.40) is:

$$G_{x\alpha}(\kappa, \alpha, F_z) = \cos[C_{x\alpha} \arctan(B_{x\alpha}\alpha] = \cos\left(r_{Cx1} \arctan \frac{r_{Bx1}\alpha}{\sqrt{1 + r_{Bx2}\kappa^2}}\right) \quad (3.41a)$$

$$G_{y\kappa}(\kappa, \alpha, F_z) = \cos[C_{y\kappa} \arctan(B_{y\kappa}\kappa] = \cos\left(r_{Cy1} \arctan \frac{r_{By1}\kappa}{\sqrt{1 + r_{By2}\alpha^2}}\right) \quad (3.41b)$$

Since these factors are comprises by zero and one and depend on both the longitudinal κ and lateral slip α, then the longitudinal force is reduced by the presence of some sideslip as well as the lateral force is reduced by the presence of some longitudinal slip, as clearly depicted in Figure 3.19. Notice that the camber dependence is not considered in the scaling factor, because it is included into the friction coefficients μ_x, μ_y.

As result, these scaling factors create a coupling between the lateral and longitudinal force F_{sx} and F_{sy}, that can be visualized in Figure 3.20. It is clear that when the tyre is generating large forces in one direction, its ability to generate them in the other is diminished. The force envelop is close to the friction ellipse, thus the adherence limit is guaranteed in any direction both in traction and braking.

Yaw torque in combined slip When both lateral and longitudinal forces are present at once, the yaw torque expression becomes more complicated:

$$M_{sz} = -a_t \, F_{sy}|_{\gamma=0} + M_{zr} - sF_{sx}, \quad (3.42)$$

where $F_{sy}|_{\gamma=0}$ is the lateral force in combined slip (3.39b) calculated once again by putting the camber angle $\gamma = 0$. In combined slip conditions the pneumatic trail a_t and twisting torque M_{zr} formulas (3.30) and (3.32) employ the *equivalent sideslip* α_{eq}

$$\alpha_{eq} = \arctan \sqrt{\tan^2\alpha + \left(\frac{K_\kappa}{K_\alpha}\right)^2 \kappa^2} \operatorname{sign} \alpha \quad (3.43)$$

becoming

$$a_t = D_t \cos[C_t \arctan(B_t\alpha_{eq} - E_t(B_t\alpha_{eq} - \arctan B_t\alpha_{eq}))] \cos\alpha \quad (3.44a)$$

$$M_{zr} = D_r \cos(\arctan B_r\alpha_{eq}). \quad (3.44b)$$

More interesting to notice in the combined slip yaw torque formula (3.42) is the presence of a new contribution: the moment generated by driving or braking

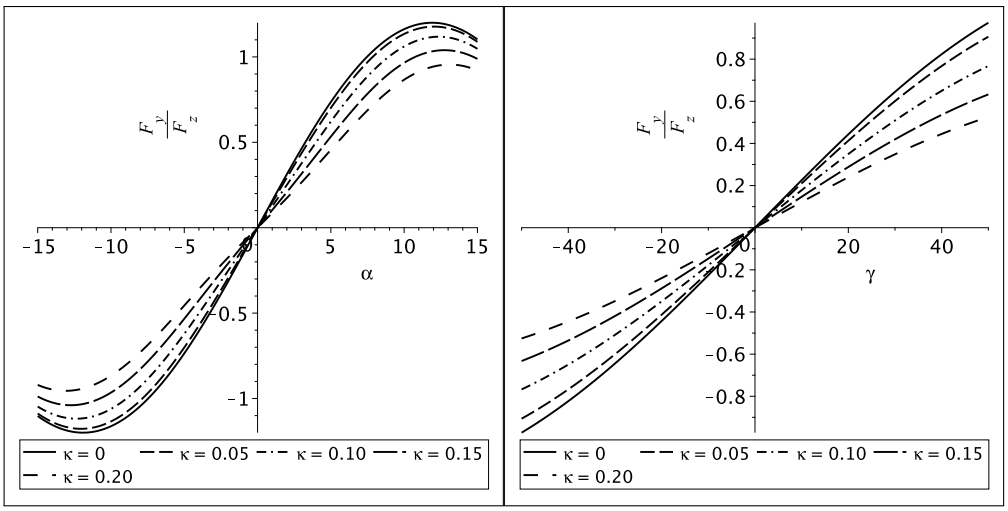

(a) Sideslip force ($\gamma = 0$).

(b) Camber force ($\alpha = 0$).

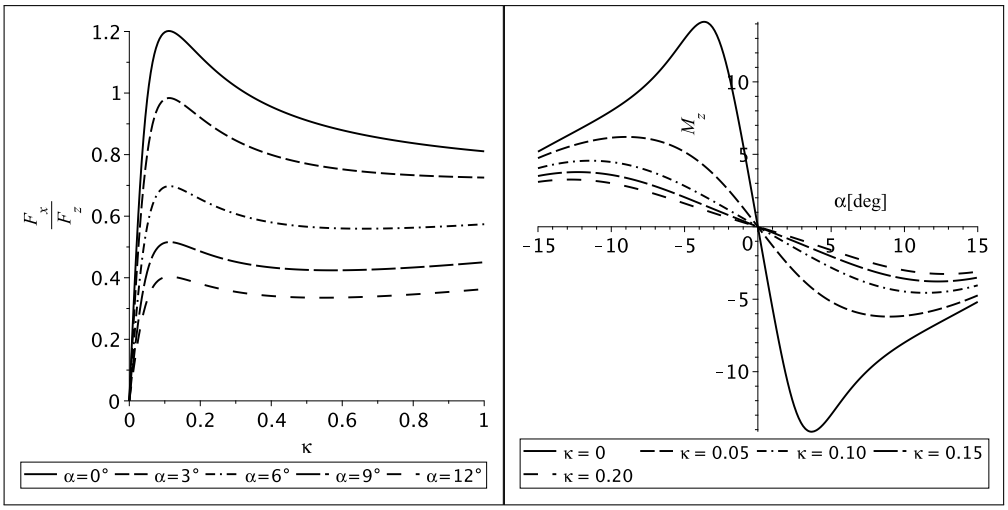

(c) Longitudinal force.

(d) Self-aligning torque.

Figure 3.19: Combined slip. For all cases Magic Formula parameters are: $F_{z0} = 1000$ N, $\mu_x = p_{Dx1} = \mu_y = p_{Dy1} = 1.2$,$K_\kappa = p_{Kx1} = 26$, $K_\alpha = p_{Ky1} = 20$, $K_\gamma = p_{Ky6} = 1.3$. Other parameter values in Appendix A.7.

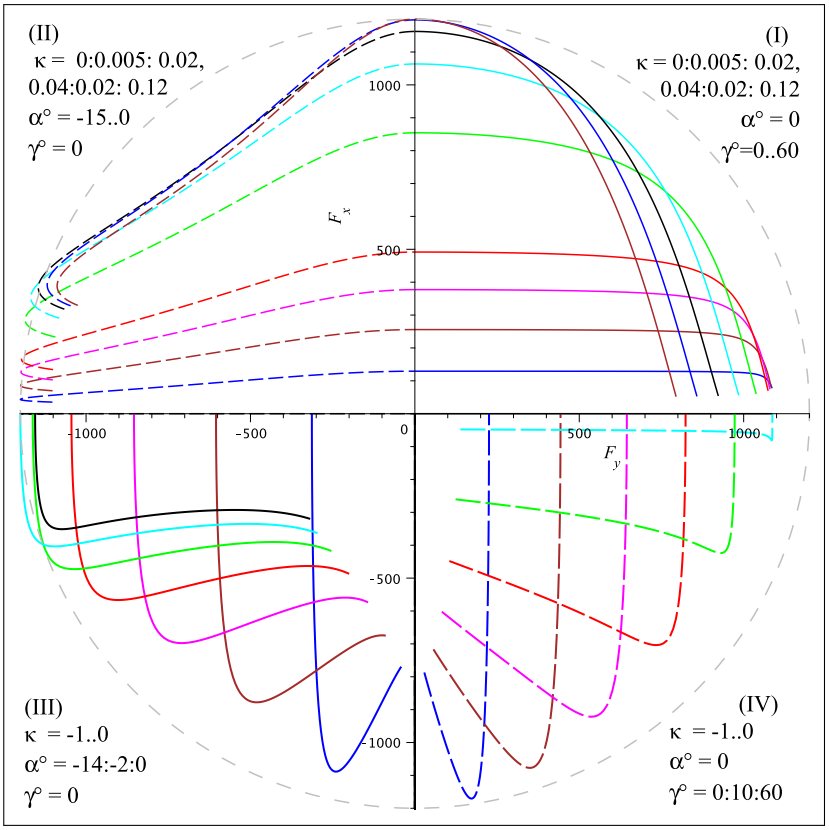

Figure 3.20: Friction ellipse and coupling between lateral and logitudinal force. The force envelope is close to the friction ellipse. Magic Formula parameters for combined slip are: $r_{Bx1} = 13.5$, $r_{Bx2} = 1$, $r_{Cx1} = 1$, $r_{By1} = 7.8$, $r_{By2} = 8.2$, $r_{Cy1} = 1$.

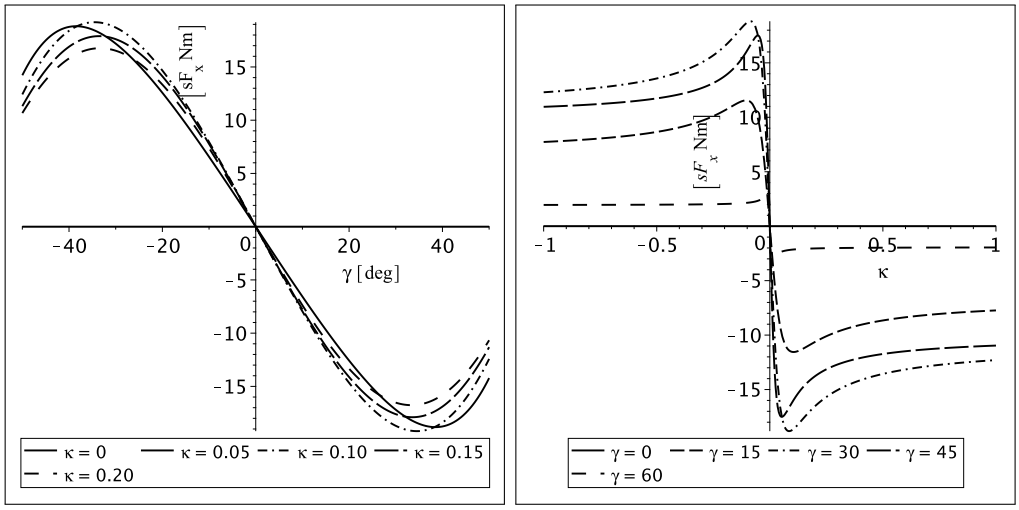

Figure 3.21: Moment generated by the longitudinal force sF_x. Lateral displacement parameters: $s_{sz1} = s_{sz2} = 0$, $s_{sz3} = 0.13$.

force F_{sx}. Indeed, the driving force generates a moment that tends to align the plane of the tyre in the direction of velocity (see Figure 3.21 on the right), while the braking force generates a moment of opposite sign which therefore moves it out of alignment. This moment is created because of the moment arm s that arises through the side force induced lateral deformation, a possibly initial offset of the line of action and the sideways rolling of the tyre cross section due to camber:

$$s = \left(s_{sz1} + s_{sz2} \frac{F_{sy}}{F_{z0}} + s_{sz3} \gamma \right) R_0. \tag{3.45}$$

For the sake of simplicity, these effects are assumed not to be influenced by the wheel load. In general, the lateral deformation has a negligible value with respect to the lateral displacement of the contact point of the tyre due to the camber.

An example of yaw moment torque in combined slip conditions is depicted in Figure 3.19d. The self-aligning moment decreases as the longitudinal slip increases.

3.8 Transient tyre behavior

The Magic Formula equations are only valid for steady-state operating conditions. Under realistic vehicle driving conditions however, the influence of the input velocities cannot be neglected.

Since the tyre carcass is deformable not only in the vertical direction, but also in the lateral, a tyre does not respond instantaneously to a change in sideslip angle: a certain time lag occurs during transient manoeuvres before the steady-state levels of side force and moment are reached (similar for F_x). Thus, to a more realistic analysis of transient manoeuvres, the tyre transient behaviour needs to be modelled. Many non-steady state tyre models exist such as the contact-mass model or the stretched-string one (see [83]). A typical solution represents the tyre's behaviour in transient state by a spring-damper model of the contact patch [71, 95]. The spring represents the tyre's lateral (longitudinal) stiffness (C_y, C_x expressed in N/m) which depends mainly on the form and characteristics of the tyre's carcass, while the damper describes the tyre behaviour under conditions of lateral (longitudinal) slip. After some manipulations, the transient forces are described by a first-order differential equation

$$\frac{\sigma_\kappa}{V_x} \dot{F}_x + F_x = F_{sx}(\kappa, \alpha, \gamma, F_z) \tag{3.46a}$$

$$\frac{\sigma_\alpha}{V_x} \dot{F}_y + F_y = F_{sy}(\kappa, \alpha, \gamma, F_z) \tag{3.46b}$$

where F_{sx} and F_{sy} are the steady state forces computed by the Magic Formulas (3.39b) and σ_κ, σ_α are called *relaxation lengths*, calculated using both the overall tyre stiffnesses C_x, C_y and slip stiffnesses K_κ, K_α

$$\sigma_\kappa = \frac{K_\kappa}{C_x}, \tag{3.47a}$$

$$\sigma_\alpha = \frac{K_\alpha}{C_y} \tag{3.47b}$$

The relaxation length represents the distance the wheel has to cover in order for the force to reach 63% of the steady state force. Integrating the differential equation gives the force once a temporal variation to the slip has been assigned. For detailed description of the relaxation model see [95].

3.9 Tyre models summary

This Chapter has described various tyre models that can be used with the vehicle models described in Sections 2.4 and 2.5. They range from simple linear models suitable for simulations with the simplified analytic model, where vertical load does not change, to complex ones suitable for conditions of combined slip and large camber angles in steady state conditions.

Specifically, the Basic Tyre Model is appropriate in the multibody model to assess the self-stability problem. The presented Full Tyre Model with the relaxation length equation for transient manoeuvring will be engaged as tyre model in the update version of the multibody model to test the optimal strategy of traction torque distribution in dynamical simulations.

Chapter 4

Low speed stability

4.1 Introduction

In motorcycles, at medium - high speed, the roll stability is usually maintained by the restoration force generated by self-steering effect. However, when the vehicle is stationary or travelling at low speed, sufficient restoring force does not occur because some of the forces, such as centrifugal force, become small. Thus, balancing a motorcycle at low-speeds is challenging, especially for new riders because it is unstable below the certain critical speed [54], as mentioned. The rider becomes very cautious at such speeds as it requires continuous input to balance the motorcycle [55]; moreover, the required steering input increases as speed reduces. Thus, at low speed the rider could benefit by any type of passive or active riding assist system.

The layout of a motorcycle influences its stability [71, 109]. However, it cannot be tuned entirely for stability because it also determines other performance requirements such as manoeuvrability, ride comfort, ergonomics, acceleration feel, braking, etc. Hence, it is necessary to explore other methods to improve stability. There are many research studies on improving and assessing the stability (weave and wobble) and handling characteristics of the motorcycle at high speeds [110, 111]. On the other hand, only a limited number of studies exists on low-speed stability of motorcycle, which is the scope of the present research. In [112] the relations between input and output parameters of a motorcycle at low speed are examined. The work assumes that the motorcycle has steering support sub-system; control systems able to keep a motorcycle in upright standing state are presented. The work proves that both steering angle control or steering torque control have possibility of bike stabilization. In research studies [113, 114], the low-speed stability of a bicycle is proposed using a theoretical approach. On the other hand, the low-speed stability of a motorcycle is specifically studied in [67] using a theoretical and experimental approach to identify the parameters that can reduce the rider's

effort. Such parameters are again steering angle and steering torque.

A small humanoid robot can balance and steer a bicycle by providing input to the handlebar, using the lateral dynamics of the bicycle [115]. Both simulations and experiments verify that the proposed controller can automatically counteract the mass imbalance in the system and allow the robot to perform straight-line steering. In research [116], the bicycle is balanced using both, flywheel and balancer; the balancer is configured as a flywheel, when disturbances to the system are large, and it will switch to the balancer when the position of the centre of gravity should be shifted. The work shows that stabilizing bicycle with the flywheel has better performance than the balancer, but it cannot be controlled to shift the bicycle angle to track the desired value, unlike the balancer which can do this motion. In Tanaka and Murakami's research [117], the bicycle is self-balanced by controlling its steering, using the dynamic model derived from the equilibrium of gravity and centrifugal force. Similarly, the work [118] proposes two handle control algorithms for autonomous stable running with the aim of developing a stable human assistance bicycle and in [119], a rear wheel torque controller gets a stable speed and a steering angle balance control method keeps the system upright. Yi *et al.* [120] propose a trajectory tracking and stability control for autonomous motorcycle for agile manoeuvres using steering angular velocity and rear thrust as control inputs; the control strategy works fine at low speed too.

The steering input required to improve the low-speed stability heavily used in all the previous studies can be reduced by adding an extra degree of freedom to a motorcycle such as a two wheel steering mechanism [121]. The test results into the cited work confirm that the two-wheel steering system is capable of changing the motion characteristics of the motorcycle in actual riding. Furthermore, the research also theoretically demonstrates that these changes in motion characteristics are caused by variation of caster and trail. Both parameters are strictly involved in bike stability. A similar two-steering system is also employed in lateral motion control into research [68] on an electric two wheel driven motorcycle. The low-speed stability of the motorcycle is achieved by providing steering and driving torques to both front and rear wheels, unlike a typical motorcycle. When the vehicle stops or moves at low speed, the front and rear steering axes are rotated in the same direction and the self-balancing is achieved by swaying the driving motors. Notice that it is one of the first studies which involves electric two wheel drive motorcycle for stability purposes. However, these changes on steering axes may not retain the conventional form and dynamics of the motorcycle.

The change of motorcycle trail length has been applied to design a riding assist system for stationary and low speed self-standing roll stability by the well-known

motorcycle company Honda [122]. In the research a control model is built to represent dynamics of roll motion; it has equivalent two point masses (upper and lower from the vehicle's centre of gravity). When the vehicle steers, the roll moment direction generated by the shift of the lower point mass becomes the same as the direction generated by the ground contact point shift of the front tyre. Thus, if the trail length has a negative value, only by steering control, the total roll moment, which is large enough to restore the imposed inclination of the vehicle, is producible. So, the possibility of establishing a viable self-standing control for the stationary state is indicated in that work. The results are successfully tested on a real prototype equipped with a mechanically arranged switching function able to change from negative to positive trail lengths. In negative trail length, the roll stability cannot be maintained because the self-steering effect does not work in medium to high speed and a switch is required.

Some researchers have applied other different external apparatuses to counteract the force of gravity and keep the bicycle balanced at upright position. In [123] an autonomous bicycle is simulated by assuming that a rotor is mounted on a crossbar that generates a tilting torque. This torque is the inverse of the gravitational torque on the bicycle. Lee and Ham [124] propose a control law to control a load mass balance system mounted on the middle of the bicycle to achieve stabilization. Exploiting a similar principle strictly related to the idea of the inverted pendulum, Yamaha has launched its own prototype, named MOTOROiD, that stands upright even when stopped [125]. The MOTOROiD body has a rotating axis that is capable of shifting the position of the centre of gravity of the motorcycle as a whole, restoring the vehicle stability. The mechanism is called the Active Mass Center Control System (AMCES).

The low-speed stability of a bicycle or motorcycle can also be achieved by adding a device that provides gyroscopic moments. In [126] alternative systems are considered, including single and twin counter-rotating gyroscopes either freely (passive stabilisers) or in a controlled way (active stabilisers). It is proved that the most effective configuration is one where the gyroscope spins with respect to an axis parallel to the wheels' spin axis and swings with respect to the vehicle yaw axis. Furthermore, it is demonstrated that actively controlled gyroscopes are capable of stabilising the vehicle in its whole range of operating speed, from zero or low speed to medium high ones as well as during braking. Beznos *et al.* [127] describe a bicycle with a gyroscopic stabilization capable of autonomous motion along a straight line as well as along a curve. A sliding mode controller to control the gyroscopic moment and stabilize a bicycle at zero-forward velocity is presented in [128].

Recently, the research has investigated whether two wheel drive architecture helps a better management of vehicle stabilization. In [58], [57] control strategies that increase the stability of electric motorcycle by acting only on driving and braking torques are presented. These strategies take into account the rider's intentions and are applied for cornering stability. In mentioned articles the front wheel torque is only braking one, whereas the present research is interested in bike stabilization by means of driving front wheel torque. Notice that all of the aforementioned studies involve in some way either the steering actuation or external apparatuses that may not retain the conventional form of the motorcycle. In some cases only the rear driving torque or a braking not driving front wheel torque are involved in balancing and investigating its influence on vehicle stabilization is worth a study. So, this Chapter will focus on the low-speed stability of the motorcycle due to the above-mentioned reasons. It explores whether the use of two wheel drive torques can affect the low speed stability of the motorcycle as alternative to the steering input and other external apparatuses.

For a better comprehension of the interaction between the roll motion at low speed (about 0 - 1 m/s) and the front wheel drive torque, the study is carried out locking the steering handlebar at a positive angle and under this assumption a lateral stability control is designed: when the steering axis is rotated up to its maximum and then locked, front wheel driving torque actuation should help motorbike balancing for gyroscopic effects even if steer torque is not available. Thus, the steer angle is considered as model parameter instead of a degree of freedom of the motorcycle. The main focus of the research is about the vehicle stability; however, in view of an application at real situations a brief discussion on the vehicle self-standing in a small bounded area is carried out too.

Since the vehicle lateral stability is the not negligible control priority, firstly the study will focus on designing Sigle Input Single Output (SISO) roll motion controller, based on PID technique. Due to the difficulty to keep the vehicle self-balanced at low speed the problem will be also explored throughout a model-based nonlinear control technique, the sliding mode control, to better account and neutralize the nonlinear influences of the system dynamics. The starting model for sliding mode control design is the 4 DoF analytical model presented in Section 2.4. It considers both rear and front wheel driving torques as model inputs. Then, the designed control systems will be compared and tested on a multibody software and simulation results presented. Once balancing has been guaranteed a second control objective can be added to the control system requirements: stabilization in a small bounded area. Thus, MIMO controller will be designed to try to confine the longitudinal motion into a small bounded area during stabilization process.

4.2 State space model representation

The mathematical model presented in Section 2.4 is an analytical model - dynamically similar to an inverted pendulum - tuned to capture the coupling between longitudinal variables (both rear and front driving and braking torques) and capsize mode. The model has been derived to be specifically employed for control design purposes in the present low speed stabilization problem. For that reason the model has been developed as simple as possible with only four degrees of freedom: x and y coordinates of rear contact point, the roll angle φ and the yaw angle ψ. Once again notice that steering angle is not considered as generalized coordinate. For further details on the analytical model see Section 2.4. Since the four DoF model has not been validated yet, its assessment by multibody motorcycle model will be discussed in the present Chapter conjointly to control systems validation.

The equations of motion (2.32) - (2.35) of the simplified model as derived in Section 2.4 are given in the matrix form

$$\mathbf{M}(\boldsymbol{q}, \dot{\boldsymbol{q}})\ddot{\boldsymbol{q}} = \mathbf{C}(\boldsymbol{q}, \dot{\boldsymbol{q}}) + \mathbf{D}(\boldsymbol{q})\boldsymbol{u} \tag{4.1}$$

where $\mathbf{M}$ is the mass matrix, $\boldsymbol{q} = [x\ y\ \varphi\ \psi]^T$ and $\dot{\boldsymbol{q}} = [\dot{x}\ \dot{y}\ \dot{\varphi}\ \dot{\psi}]$ denote the generalized coordinate and velocity vectors and $\boldsymbol{u} = [X_r\ X_f]^T$ the control input vector of the rear and front thrust forces (related to the wheel torques T_r and T_f by the expressions (2.10)). Matrices $\mathbf{M}$, $\mathbf{C}$ and $\mathbf{D}$ are functions of generalized coordinates $\boldsymbol{q}$ and velocities $\dot{\boldsymbol{q}}$.

System (2.32) - (2.35) or its equivalent matrix form (4.1) is a second order ODE one, but control techniques work better on first order ODE systems. Defining the state vector

$$\begin{aligned} \boldsymbol{X} &= [x\ \ y\ \ \varphi\ \ \psi\ \ \dot{x}\ \ \dot{y}\ \ \dot{\varphi}\ \ \dot{\psi}]^T = \\ &= [x_1\ x_2\ x_3\ x_4\ x_5\ x_6\ x_7\ x_8]^T, \end{aligned} \tag{4.2}$$

it is possible to recast the proposed model as:

$$\overline{\mathbf{M}}(\boldsymbol{X})\dot{\boldsymbol{X}} = \bar{\mathbf{A}}(\boldsymbol{X}) + \bar{\mathbf{B}}(\boldsymbol{X})\,\boldsymbol{U} \tag{4.3}$$

where $\bar{\mathbf{M}}(\boldsymbol{X}) \in M^{8\times 8}$ is the new mass matrix, $\bar{\mathbf{A}} \in M^{8\times 1}$ is a column vector obtained from the Christoffel matrix $\mathbf{C}(\boldsymbol{q}, \dot{\boldsymbol{q}})$ after recasting and $\bar{\mathbf{B}} \in M^{8\times 2}$ is the

input matrix of the input vector $\boldsymbol{U} = \boldsymbol{u}$. Inverting $\bar{\mathbf{M}}(\boldsymbol{X})$ the system becomes:

$$\dot{\boldsymbol{X}} = \mathbf{A}(\boldsymbol{X}) + \mathbf{B}(\boldsymbol{X})\,\boldsymbol{U}, \tag{4.4}$$

or more explicitly

$$\begin{aligned}
\dot{x}_1 &= x_5 \\
\dot{x}_2 &= x_6 \\
\dot{x}_3 &= x_7 \\
\dot{x}_4 &= x_8 \\
\dot{x}_5 &= \mathbf{A}_5 + \mathbf{B}_5\boldsymbol{u} \\
\dot{x}_6 &= \mathbf{A}_6 + \mathbf{B}_6\boldsymbol{u} \\
\dot{x}_7 &= \mathbf{A}_7 + \mathbf{B}_7\boldsymbol{u} \\
\dot{x}_8 &= \mathbf{A}_8 + \mathbf{B}_8\boldsymbol{u}
\end{aligned} \tag{4.5}$$

This is the general state-space representation of the proposed model used in control design. Notice that the matrix $\mathbf{A}$ directly depends by $\boldsymbol{X}$, so the system (4.4) or its explicit form (4.5) is nonlinear, as stated above.

4.3 Front wheel torque control

This Section will show the design of control systems to balance the previous unstable model and avoid motorcycle falling down. The lateral stability is the only control priority in this Section, that has to be achieved regardless of the final behaviour of the other state variables.

Firstly, a discussion of possible control and controlled variables is presented. Generally in two-wheeled vehicles, even before assuring that the motorcycle can follow a desired trajectory, it is important to prevent falls. Thus, the most natural controlled variable is the roll angle. At low speed if the motorcycle roll angle is kept close to zero (control objective setpoint) in face of external disturbances, the overall stability of the vehicle is improved. As stated in introductory Section 4.1, most of models and stability control systems presented in literature are based on steering actuation, which is not available in this project. However, a direct way to restore vehicle stability is acting on the wheel torques to generate rotational torques around the bike roll axis. Thus, only wheel torques can be used as control inputs to achieve stabilization.

As stated in [66], the front wheel torque has a greater authority on the roll

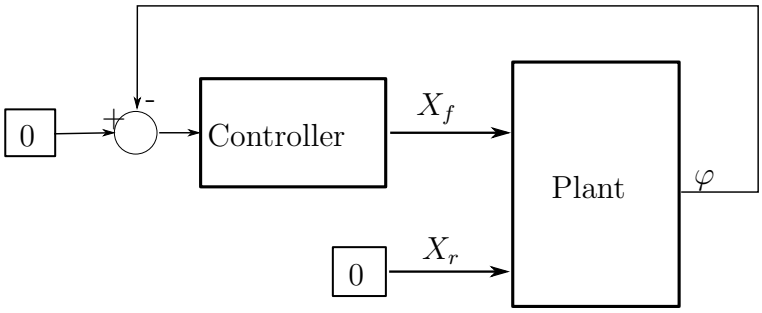

Figure 4.1: SISO control scheme when vehicle stabilization is the only control priority. The roll angle φ is controlled by the front thrust force X_f, whereas the rear wheel thrust X_r is identically zero during simulations.

angle than the rear wheel one and the front and rear wheel torque have a similar influence on the longitudinal acceleration. According to these considerations, the front wheel torque is employed to control the roll angle only, while the rear wheel torque mainly controls the longitudinal motion. However, at first the requirement on path length is neglected, focusing only in vehicle stability. Thus in this Section the front wheel thrust X_f is chosen as single control input, whereas the rear one X_r is set identically zero during simulations, as depicted in control scheme in Figure 4.1.

Two control strategies are designed: a PID control and a sliding mode controller. Control systems have to test whether vehicle can be self-balanced when its initial velocity is zero and its steering axis is locked at a positive angle. The described conditions represent the motorcycle initial configuration when the controllers are activated.

4.3.1 PID control design

As preliminary investigation on the problem a Proportional-Integrative-Derivative feedback controller is chosen and designed as vehicle stability control strategy for its easiness in implementation and its simplicity - a good result can be achieved by tuning only three parameters.

The stability controller works in the following way: the total amount of drive torque to be delivered to the front wheel is controlled to bring the vehicle's roll angle φ to the target angle for stabilization, i.e. $\varphi_{\text{ref}} = 0$. The amount of drive torque is determined using a PID control of the vehicle roll angle relative to the

reference angle, φ_{ref}, with the following equations and equivalent Simulink blocks:

$$e_\varphi = \varphi_{\text{ref}} - \varphi \tag{4.6a}$$

$$T_f = G_p e_\varphi + G_i \int_0^t e_\varphi(\tau)\,\mathrm{d}\tau + G_d \frac{\mathrm{d}}{\mathrm{d}t} e_\varphi(t) \tag{4.6b}$$

where φ is the current vehicle roll angle, T_f is front drive torque, G_p, G_i and G_d are the proportional, integral and derivative gains, tuned by trial-and-error. Notice that the inputs of system (2.32) - (2.35) are the rear and front thrust force and not the wheel torques, thus the control output T_f (4.6b) is then divided by the front wheel radius R_f, according to (2.10), to obtain the amount of the required front thrust force X_f to transfer to the plant.

4.3.2 Sliding mode control design

The control of dynamical systems in presence of uncertainties and disturbances such as our motorcycle system is a common problem to deal with when considering real plants. The effect of these uncertainties on the system dynamics should be carefully taken into account in the controller design phase since they can worsen the performance or even cause system instability.

For this reason, during recent years, the problem of controlling dynamical systems in presence of heavy uncertainty conditions has become an important subject of research. As a result, considerable progresses have been attained in robust control techniques, such as non linear adaptive control, model predictive control, backstepping, sliding model control and others. These techniques are capable of guaranteeing the attainment of the control objectives in spite of modelling errors and/or parameter uncertainties affecting the controlled plant. Among the existing methodologies, the Sliding Mode Control (SMC) technique turns out to be characterized by high simplicity and robustness.

Sliding mode control was first proposed and elaborated by several researchers from the former Russia, starting from the sixties [129–131]; however, the ideas did not appear outside of Russia until the seventies when a book by Itkis [132] and a survey paper by Utkin [133] were published in English. Since then, sliding mode control has developed into a general design control method applicable to a wide range of system types including non linear systems, MIMO systems, discrete time models, large-scale and infinite-dimensional systems.

Essentially, sliding mode control utilizes discontinuous feedback control laws to force the system state to reach, and subsequently to remain on, a specified surface within the state space (the so-called *sliding or switching surface*), as depicted in

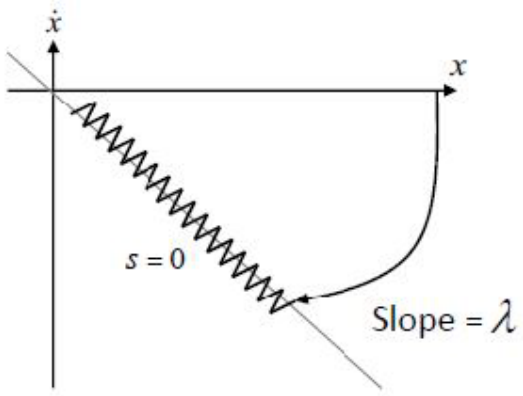

Figure 4.2: Sliding surface.

Figure 4.2. The system dynamics when confined into the sliding surface is described as an ideal sliding motion and represents the controlled system behaviour.

The advantages of obtaining such a motion are twofold: firstly, the system behaves as a system of reduced order with respect to the original plant; and secondly the movement on the sliding surface of the system is insensitive to a particular kind of perturbation and model uncertainties. This latter property of invariance towards so-called matched uncertainties - that ones included into the image of control matrix **B** - is the most distinguish feature of sliding mode control and makes this methodology particular suitable to deal with uncertain non linear systems [134], like the control-oriented system (2.32) - (2.35) under study where unmodelled dynamics and parameters uncertainties may be included rather than external disturbances, not so significant in the considered quasi-static situation. For these reasons one of the main fields of application of this control technique is the automotive [135, 136]. Moreover, this strategy can be implemented for both SISO and MIMO systems, so it could be applied to achieve more than one control target taking into account the system interconnected dynamics.

It could be interesting to compare the PID and sliding mode performances for parametric variations. It should be noticed, however, that the complexity of the equations of motion (2.34)-(2.33) hinder an easy analytical verification that the parametric variations into equations (4.4) satisfy the matching hypothesis.

Control design

Consider a nonlinear system affine in control

$$\dot{x}(t) = A(x) + B(x)u, \tag{4.7}$$

like (4.4), where $x(t) \in \mathbb{R}^n$ and $u \in \mathbb{R}^m$. The components of the discontinuous feedback are given by

$$u_i = \begin{cases} u_i^+(x), & \text{if } s_i(x) > 0 \\ u_i^-(x), & \text{if } s_i(x) < 0 \end{cases} \quad i = 1, ..., m \tag{4.8}$$

where $s_i(x)$=0 is the $i-$th sliding surface, and

$$s(x) = [s_1(x),\ s_2(x), ...,\ s_m(x)]^T = 0 \tag{4.9}$$

is the m-dimensional sliding manifold.

The control problem consists in developing continuous function u_i^+ and u_i^-, and the sliding surface $s(x) = 0$ so that the closed-loop system (4.7) - (4.8) exhibits a sliding mode on the m-dimensional sliding manifold $s(x) = 0$.

The design of the sliding mode control law can be divided in two phases:

1. Phase 1 consists in the construction of a suitable sliding surface so that the dynamic of the system confined to the sliding manifold produces a desired behaviour;

2. Phase 2 entails the design of a discontinuous control law which forces the system trajectory to the sliding surface and maintains it there.

More precisely, a (discontinuous) control law u_N should force the system trajectory to intersect the surface in a finite time and a continuous control u_{eq} guarantees that system trajectories stay on it. A possible structure for the final control system (4.8) is a combination of these two control laws:

$$u_i = u_{i_{eq}} + u_{iN} \tag{4.10}$$

For further details see [134].

Phase 1: sliding surface design The switching surface $s(x)$ is designed such that the system response restricted to $s(x) = 0$ has a desired behaviour. Although general nonlinear switching surfaces (4.9) are possible, linear ones are more prevalent in design; so linear switching surface of the form

$$s(x) = Sx(t) = 0 \tag{4.11}$$

are considered.

Remark. Remember that now in the single input case the low speed self-balancing problem has a unique control objective that is to achieve the vehicle equilibrium, i.e. the achievement of a null roll angle (expressed by the variable x_3) regardless the behaviour of the other variables of the system. In other words, the analysis restricts the attention on the reduced states $(\varphi, \dot{\varphi}) = (x_3, x_7)$ and in order to achieve the control objective the front wheel thrust X_f is employed as single control input.

Thus here $m = 1$. Since the control priority is to keep the roll angle $\varphi = x_3$ (see (4.2)) close to zero, the proposed sliding surface of the form (4.11) is

$$s(\boldsymbol{X}) = \dot{x}_3 + \lambda x_3 = x_7 + \lambda x_3, \qquad \lambda > 0 \tag{4.12}$$

where the last equality is obtained by (4.5) and λ is a design parameter that determines the velocity in which system reaches the surface. On the sliding surface, control objective is achieved. Indeed, as mention before, now the problem focuses on the stability of the reduced states (x_3, x_7) rather than on the global stability of the system. Actually, it can be formally proved that establishing a sliding motion on the chosen sliding surface does not necessarily guarantee stability of the overall system. Some developed analytical calculations seem to suggest that systems stability is not ensured on the sliding surface, at least *a priori*, but this is not of interest for the problem under study.

After switching surface design, the next important aspect of sliding mode control is guaranteeing the **existence of a sliding mode**. A sliding mode exists, if in the vicinity of the switching surface, $s(x) = 0$, the velocity vectors of the state trajectory are always directed toward the switching surface. Consequently, if the state trajectory intersects the sliding surface, the value of the state trajectory remains within a neighbourhood of $\{x|s(x) = 0\}$. From a geometrical point of view, the tangent vector or time derivative of the state vector must point toward the sliding surface in the region of attraction. An ideal sliding mode exists only when the state trajectory $x(t)$ of the controlled plant satisfies $s[x(t)] = 0$ at every $t \geq t_0$ for some t_0. Starting from time instant t_0, the system state is constrained on the discontinuity surface, which is an invariant set after the sliding mode has been established.

In general, the existence problem can be seen as a generalized stability problem, hence the second method of Lyapunov provides a natural setting for analysis. Specifically, stability to the switching surface requires to choose a generalized Lyapunov function $V(x)$ which is positive definite and has a negative time derivative in the region of attraction. For all single input systems a suitable Lyapunov function

is

$$V(x) = \frac{1}{2}s^2(x) \tag{4.13}$$

which clearly is positive definite. In sliding mode control, $\dot{s}$ will depend on the control and hence if switched feedback gains can be chosen so that

$$\dot{V}(x,s) = s\dot{s} < 0 \tag{4.14}$$

in the domain of attraction, then the state trajectory converges to the surface and is restricted to the surface for all subsequent time. This latter condition is called the *reaching or reachability condition* and ensures that the sliding manifold is reached asymptotically.

Condition (4.14) is often replaced by the so-called *η-reachability condition*

$$\dot{V}(x,s) = s\dot{s} \leq -\eta|s|, \qquad \eta > 0 \tag{4.15}$$

which ensures finite time convergence to $s(x) = 0$. Indeed, by integration of (4.15) one has

$$|s(x(t))| - |s(x(0))| \leq -\eta t \tag{4.16}$$

showing that the time required to reach the surface, starting from the initial condition $s(x(0))$ is bounded by

$$t_s = \frac{|s(x(0))|}{\eta} \tag{4.17}$$

making $\eta > 0$ another control design parameter. The equivalent and discontinuous control laws has to be designed such that the η-reachability condition (4.15) (chosen in this design problem) is satisfied.

Phase 2: discontinuous control law The controller design is the second phase of the sliding mode control design procedure mentioned earlier. The problem is to choose switched feedback gains capable of forcing the plant state trajectory to the switching surface (u_N) and of maintaining a sliding mode condition (u_{eq}). The assumption is that the sliding surface has already been designed. In the discussed problem, the control law is obtained applying the method of the equivalent control: the control vector u (4.8) will be a combination of a continuous u_{eq} control and discontinuous terms u_N of the form (4.10). Now these two terms are separately designed.

The first step of the equivalent control approach is to find the input u_{eq} such that the state trajectory stays on the switching surface $s(x) = 0$. The existence of

the sliding mode implies that $s(x) = 0$, for all $t \geq t_0$, and $\dot{s}(x) = 0$.

By differentiating $s(x)$ with respect to time along the trajectory (4.7) it yields

$$\dot{s}(x) = \left[\frac{\partial s}{\partial x}\right] \dot{x} = \left[\frac{\partial s}{\partial x}\right] [A(x) + B(x)u_{eq}] = 0 \tag{4.18}$$

where u_{eq} is the so-called *equivalent control*. Note that, under the action of the equivalent control u_{eq} any trajectory starting from the manifold $s(x) = 0$ remains on it, since $\dot{s}(x) = 0$. As a consequence, the sliding manifold $\dot{s}(x) = 0$ is an invariant set.

To compute u_{eq}, the matrix product $[\partial s/\partial x]B(x)$ must be nonsingular for all x. This is the *sliding hypothesis*. Then

$$u_{eq} = -\left[\frac{\partial s}{\partial x}B(x)\right]^{-1} \frac{\partial s}{\partial x}A(x). \tag{4.19}$$

Applying this procedure to the designed sliding surface (4.12), it is obtained

$$\dot{s}(\boldsymbol{X}) = \dot{x}_7 + \lambda \dot{x}_3 = \mathbf{A}_7 + \mathbf{B}_7 u_{eq} + \lambda x_7 = 0 \tag{4.20}$$

using the trajectory of system (4.5). To solve with respect to u_{eq} the term $\mathbf{B}_7 \neq 0$ must be nonsingular for all x:

$$\begin{aligned}
\mathbf{B}_7 =& (h\,(Izz - Iyy)\sin\delta\cos^3\varphi - h\,(-2\,\sin\delta\sin\varphi Iyz + \cos\delta Ixy)\cos^2\varphi + \\
&+ (\cos\delta\sin\varphi h Ixz - (-Iyy\,h + Ixz\,(b-w))\sin\delta)\cos\varphi - \\
&- Ixy\;(\sin\delta\,(b-w)\sin\varphi - \cos\delta h))/(h^2 m(Izz - Iyy)\cos^4\varphi + \\
&+ 2h^2 m\,Iyz\,\sin\varphi\cos^3\varphi + \left(-m(Izz - 2\,Iyy)h^2 - Ixx\,Izz + Ixx\,Iyy - \right. \\
&\left. - Ixy^2 + Ixz^2\right)\cos^2\varphi - 2\,\sin\varphi\left(Iyz\,h^2 m + Ixx\,Iyz - Ixy\,Ixz\right)\cos\varphi - \\
&- Iyy\,h^2 m - Ixx\,Iyy + Ixy^2)
\end{aligned} \tag{4.21}$$

It depends only on the generalized coordinate φ, i.e. the roll angle. The plot in Figure 4.3 assures that this term $\mathbf{B}_7$ is always non zero into the physical limit of the roll angle $\varphi \in \left(-\frac{\pi}{2}; \frac{\pi}{2}\right)$.

Solving (4.20) with respect to u_{eq}, the designed equivalent control is

$$u_{eq} = -\mathbf{B}_7^{-1}(\mathbf{A}_7 + \lambda x_7). \tag{4.22}$$

Therefore, given $s(x(t_0)) = 0$, the dynamics of the system on the switching surface for $t \geq t_0$, is obtained by substituting (4.22) in (4.4). The motion on the switching surface results governed by a reduced order dynamics because of the set of state

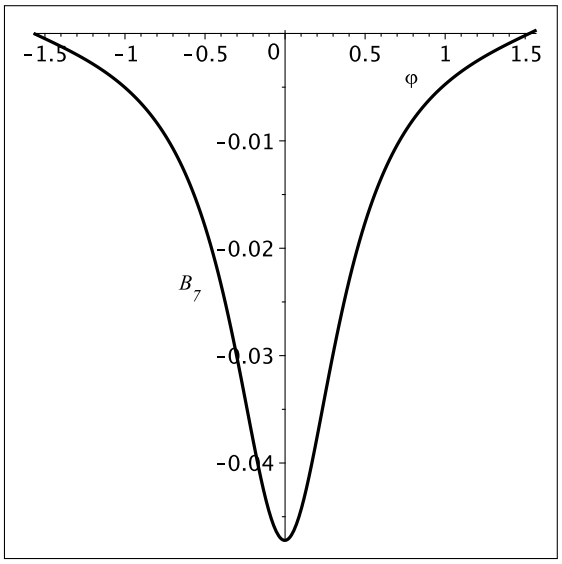

Figure 4.3: Sliding hypothesis to compute the equivalent control u_{eq}: the term $\mathbf{B}_7$ is invertible into the physical limits of the roll angle $\varphi \in \left(-\frac{\pi}{2}; \frac{\pi}{2}\right)$.

variable constraints $s(\boldsymbol{X}) = 0$.

The next step is to choose switched discontinuous feedback gain u_N capable of forcing the plant state trajectory to the switching surface $s(\boldsymbol{X}) = 0$.

For controllers having the structure of $u = u_{eq} + u_N$, it results that

$$\begin{aligned} \dot{s}(x) &= \left[\frac{\partial s}{\partial x}\right] \dot{x} = \left[\frac{\partial s}{\partial x}\right] [A(x) + B(x)(u_{eq} + u_N)] = \\ &= \left[\frac{\partial s}{\partial x}\right] [A(x) + B(x)u_{eq}] + \frac{\partial s}{\partial x} B(x)u_N = \\ &= \frac{\partial s}{\partial x} B(x)u_N \end{aligned} \tag{4.23}$$

This result allows an easy verification of the existence and reachability of a sliding mode, i.e., the condition that $s(x)\dot{s}(x) < -\eta|s|$ when $s(x) \neq 0$:

$$s(x)\dot{s}(x) = s(x)\frac{\partial s}{\partial x} B(x)u_N < -\eta|s(x)|. \tag{4.24}$$

Dividing by $s(x)$,

$$\frac{\partial s}{\partial x} B(x)u_N < -\eta\frac{|s|}{s} = -\eta \operatorname{sign} s. \tag{4.25}$$

Thus, a possible discontinuous control structure for u_N is

$$u_N = -\left[\frac{\partial s}{\partial x} B(x)\right]^{-1} \eta \operatorname{sign} s(x). \tag{4.26}$$

where the sign function is defined as

$$\operatorname{sign} s(x) = \frac{s(x)}{|s(x)|} = \begin{cases} 1 & \text{if } s(x) > 0 \\ -1 & \text{if } s(x) < 0 \\ 0 & \text{if } s(x) = 0 \end{cases} \tag{4.27}$$

Declined in the discussed problem it becomes

$$u_N = \mathbf{B}_7^{-1} \eta \operatorname{sign}(s) \tag{4.28}$$

and the control law u is the sum of the discontinuous control u_N (4.28) and the equivalent control u_{eq} (4.22).

This control law requires infinitely fast switching to maintain the sliding mode motion. In real-life applications, it is not reasonable to assume that the control signal can switch at infinite frequency. On the contrary, it is more realistic, due to the inertias of the actuators and sensors and to the presence of noise and/or exogenous disturbances, to assume that it switches at a very high (but finite) frequency. Then the system state oscillates within a neighbourhood of the switching surface (see Figure 4.2). This oscillation is the so-called *chattering effect*.

In many situations, especially when dealing with mechanical systems, the chattering and the need for discontinuous control signal would not be considered acceptable, since rapidly changing control actions induce stress and wear in mechanical parts and the system could be damaged in a short time.

To avoid implementing problems and reduce control signal chattering it can be applied the so-called *boundary layer method* [134]: a natural solution is to smooth the discontinuity in signum function to obtain an arbitrarily close but continuous approximation

$$u_N = -\mathbf{B}_7^{-1} \eta \begin{cases} \operatorname{sign}(s(x)), & \text{if } |s| > \epsilon \\ \frac{s(x)}{\epsilon} & \text{if } |s| < \epsilon \end{cases} \qquad \epsilon > 0 \tag{4.29}$$

where ϵ is a small positive scalar, which denotes the boundary layer width and a third design parameter. The approximation is shown in Figure 4.4.

4.3.3 Numerical validation and analysis of results

This Section will show some simulation results of the two control strategies designed above starting from the simplified motorcycle model (2.32) - (2.35) and their validation using the multibody model. Both model and controllers have been

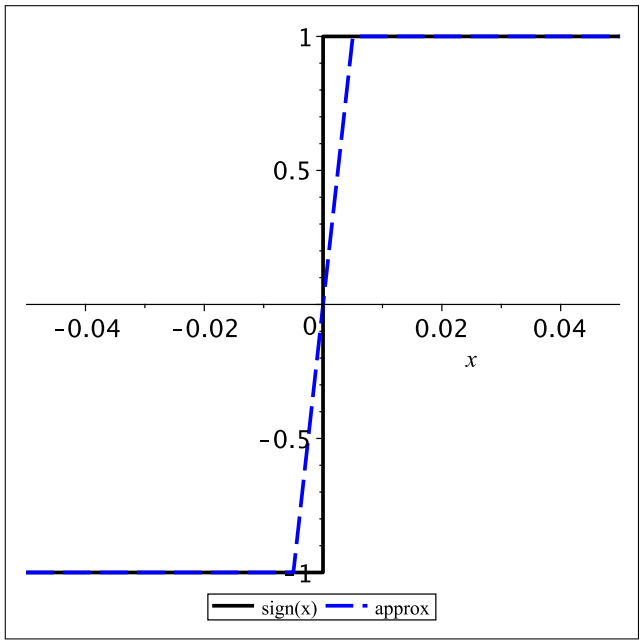

Figure 4.4: A differentiable approximation of the signum function to avoid implementing problems in discontinuous part of sliding mode control.

implemented in Matlab/Simulink. The results herein has been published in two conference papers [137, 138].

As multibody model the first version of FastBike software is adopted. Remind that the mathematical model behind it is fully nonlinear and the motorcycle is modelled as a system of four rigid bodies - the rear and front assemblies and the rear and front wheels. The front fork and the swingarm angle are not included in the current version; however, their motion can be neglected in self-standing control at low speed. The road contact patch forces are computed by means of the Basic Tyre Model of Section 3.6. The multibody model includes the steering torque among control inputs, in addition to front and rear wheel torque, but the investigation requires to apply the stabilizing control strategies to the front wheel with the front steering axis rotated at its maximum value ($\delta = 40°$) and locked during simulations. This condition is easily reproduced into the analytical model considering the steering angle δ as a further model parameter; conversely, in the multibody model the steering angle is set equal to 40 degrees as initial condition and then it has been added a further feedback PI controller on the steering torque using the steer error $e_\delta = \delta - 40°$ with gains $K_P = 150$ and $K_I = 1e3$ to maintain the steering axis in the same angle.

To validate analytical model and analyse whether it captures roll vehicle dynamics, an equal set of parameters of a real motorcycle - manufactured by Visionar srl - has been used in both models: these parameters are listed in Appendix A.

PID	Value	**Sliding**	Value
G_p	1.5e5	λ	5
G_i	3e5	η	-5
G_d	9e3	ϵ	$1e-3$

Table 4.1: Control design parameters for both sliding mode controller and PID one when the front wheel force X_f is the only control input.

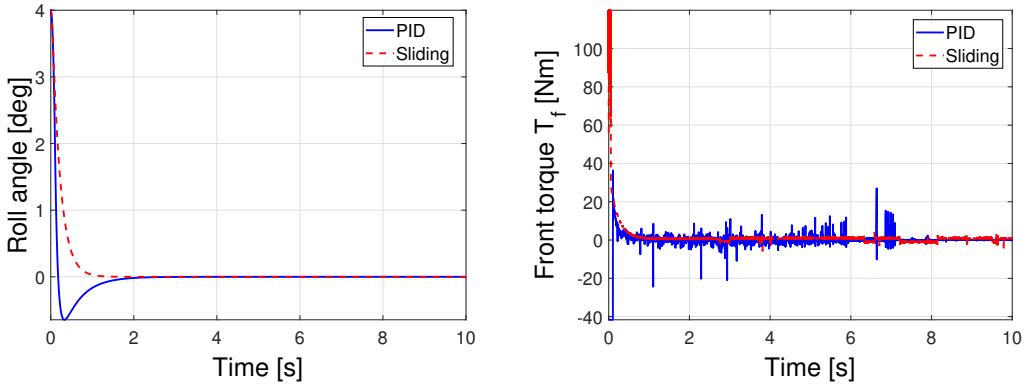

(a) Roll angle response.

(b) Front wheel torque applied by the controller.

Figure 4.5: Response of the analytical model to the single input control strategies: PID (solid blue line) and sliding mode (dashed red line).

Moreover, roll angle is set equal to $\varphi = 4°$ at the beginning of simulation and the sliding mode controller as well as the PID one of front wheel force X_f - designed by analytical model - have been tested in the multibody software applying same control design parameters, reported in Table 4.1.

The single input controllers have to test whether motorcycle can be self-balanced starting with null initial velocity and keeping steering axis locked over time. Figure 4.5a answers positively to this question. Indeed, after less than 2 seconds both PID and sliding mode control stabilize the vehicle achieving a null roll angle, even though the sliding mode controller requires a lower front wheel torque (see Figure 4.5b). Notice that introducing the continuous approximation (4.29) in the discontinuous part of the sliding mode control law, the front wheel torque T_f results less oscillating than the control input applied by the PID controller. In addition, as shown in Figure 4.6 for the sliding mode controller, the system begins its evolution with null velocity and then evolves keeping a low speed - about 0.2 m/s - and so it remains in the model framework. In this case the requirement on path length has been neglected, but since its reduction will be a control objective later, the motorcycle trajectory with the two control strategies is worth an analysis. The track of the motorcycle equipped with the PID and sliding mode controllers is depicted in Figure

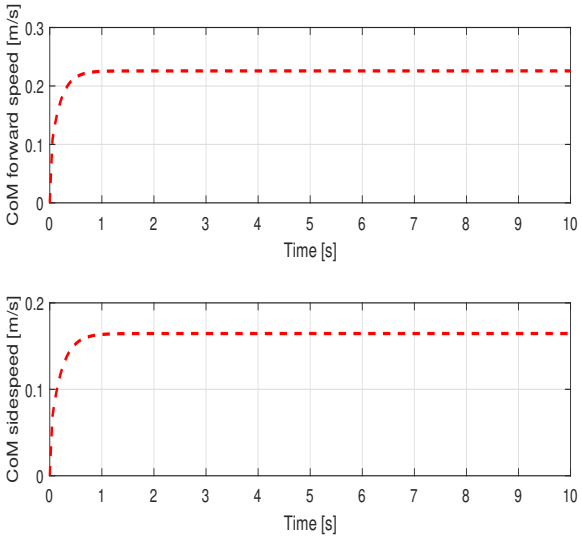

Figure 4.6: Simulation results of forward (top) and side (bottom) speed of centre of mass in the analytical model with the single input sliding mode controller.

4.7: rear contact point track shows that vehicle moves on a curve, as expected due to the rotation of the steering axis. If we compare the motorcycle trajectories of sliding mode and PID controllers, the latter performs better than the former. This remark will be useful in the control design when the stability action would be limited in a small bounded area.

Until now it seems that the model captures the lateral stability motion and the control strategies agree on self-balancing the bike by means of the front wheel torque only. However, the analytical model is quite simple, thus a validation on a more realistic model is required.

Control validation

Validation tests are carried out comparing analytical model response to the multibody software one when same control strategy is applied.

Figure 4.8a shows that both in analytical and multibody models the roll angle response to the PID controller achieves the reference value $\varphi_{ref} = 0$ in less than 2 seconds. That means the controller stabilizes the vehicle giving once again a positive preliminary result for motorcycle stabilization without the use of steering torque. Moreover, roll angle time history of the two models has an impressive good match using the PID controlller as well as the sliding mode control technique: in both cases the same controller can stabilize the motorcycle multibody model of the software - which is a more complex model - behaving in a similar way with respect to the response of the analytical one. This indicates that the analytical

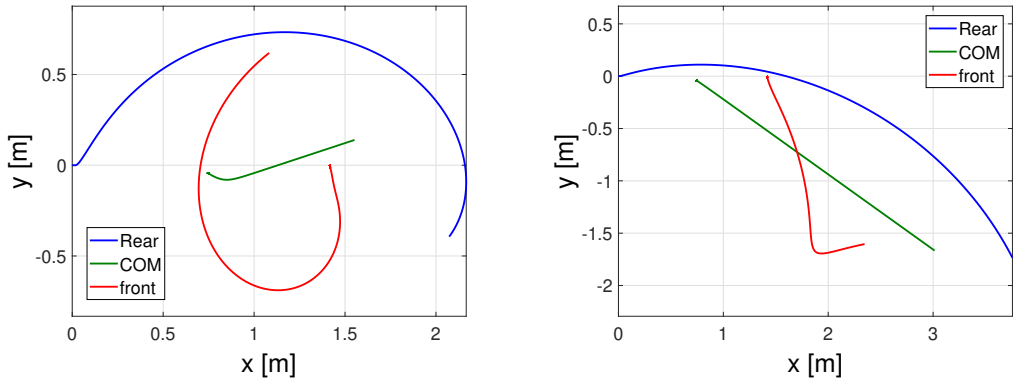

(a) PID controller. (b) Sliding mode controller.

Figure 4.7: Motorcycle trajectory of single input control system in the simplified analytical model: rear contact point (blue), centre of mass (green) and front contact point (red).

model captures the main vehicle roll dynamics, predominant with respect to the other out-of-plane modes at low speed. Also in the yaw angle response both models reproduce the same linear behaviour to the PID controller, as reported in Figure 4.8b, even though in FastBike it is slightly smaller. Similarly, the yaw angle has a linear growth in both models for the sliding mode control too, but in this case in FastBike software the angle results slightly bigger.

The mathematical model has been developed for simulations at low speed, thus this feature has to be verified: Figure 4.9 shows vehicle forward velocity keeps low (less than 0.7 m/s in absolute value) during the whole control action in both models, remaining in the work assumptions.

Finally, in Figure 4.10a it can be seen that the two models control signal has a comparable magnitude with both control strategies and remains below the physical limit imposed by the problem ($T_f = 120$ Nm) during the whole simulation time. However, it can be noticed that after achieving vehicle stabilization, the multibody software enters in a steady state circular motion, requiring a constant positive front wheel torque. This is probably an effect of the presence of steer torque controller, needed to maintain a constant steering angle at 40°.

Concluding, as preliminary study the whole validation analysis has highlighted that the presented analytical model captures the main lateral motion dynamics and can be used for model-based control systems. More important, the good match of the balancing variable (the roll angle) in both control strategies, achieved by actuating the front wheel torque only, confirms the intuitive idea that the front wheel torque can affect the stability of the vehicle in addition to its longitudinal motion, thus it can be proficiently utilized in stability systems.

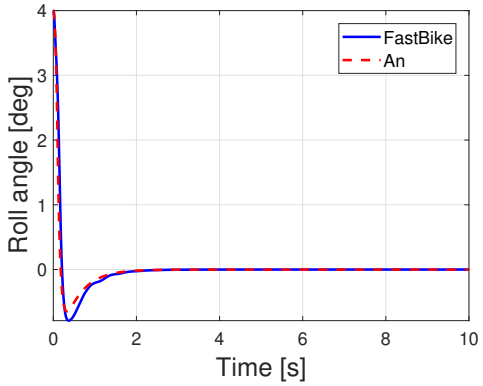

(a) Roll angle φ with PID controller.

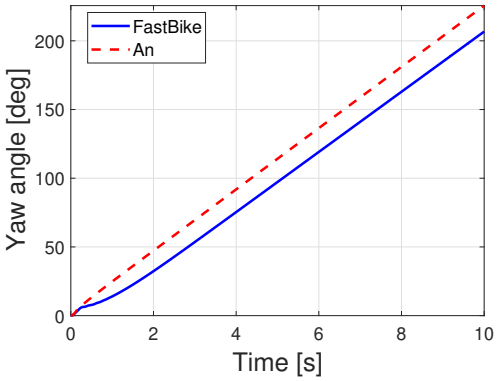

(b) Yaw angle ψ with PID controller.

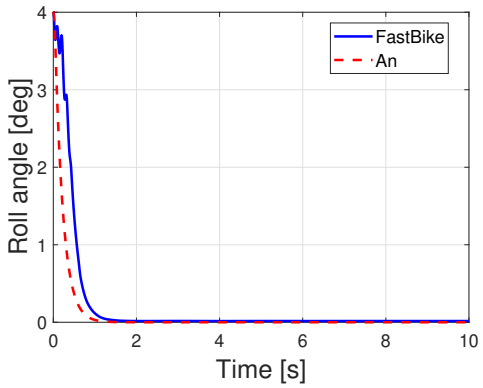

(c) Roll angle φ with sliding mode controller.

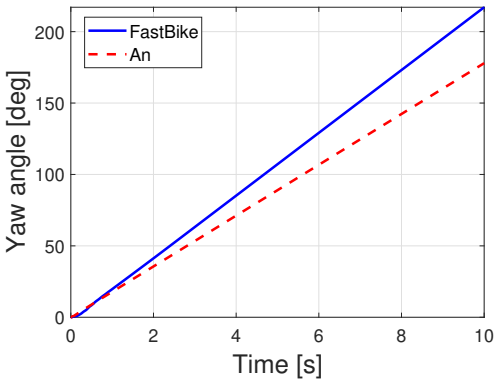

(d) Yaw angle ψ with sliding mode controller.

Figure 4.8: Comparison of roll and yaw angle simulation responses to Single Input PID and sliding mode control systems: analytical model (red dashed line) and multibody one (blue solid line).

4.4 Two wheel torque control

In the present Section, the longitudinal acceleration is also considered as second output, as its regulation is needed in order to overcome the drawbacks of the preliminary single input controllers related to the distance required for the vehicle stability. Indeed, the front wheel torque not only restores the stability generating a rotational torque around the roll axis, but also moves the vehicle forward.

According to the considerations given in Section 4.3, the front wheel torque is employed to control the roll angle and vehicle balance, so the rear wheel torque can be used to counteract the forward motion since it controls the longitudinal motion. Thus, the control system acts so as to recover stability and reduces the travelled distance during stabilization. Ideally, the rear wheel torque should apply a suitable amount of torque in sign opposite to front one in order to produce a swaying motion of the vehicle similar to the inverted pendulum balancing. The

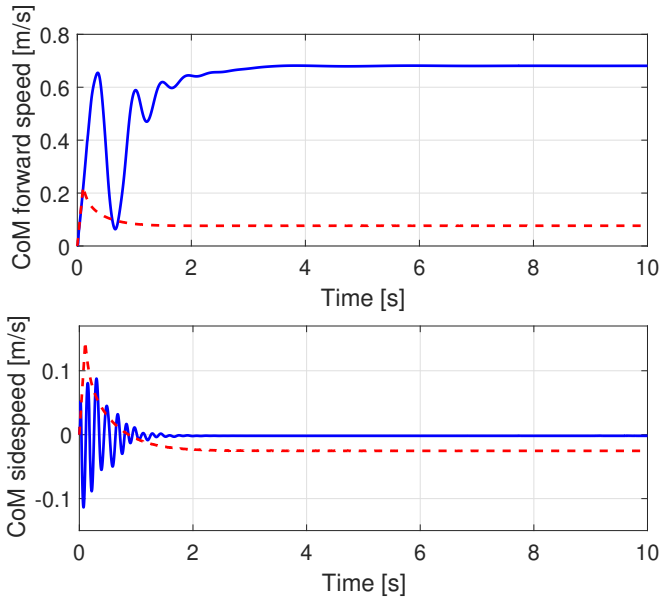

Figure 4.9: Simulation results of longitudinal (above) and lateral (below) centre of mass velocity for Single Input PID controller: model (red dashed line) and simulator (blu line).

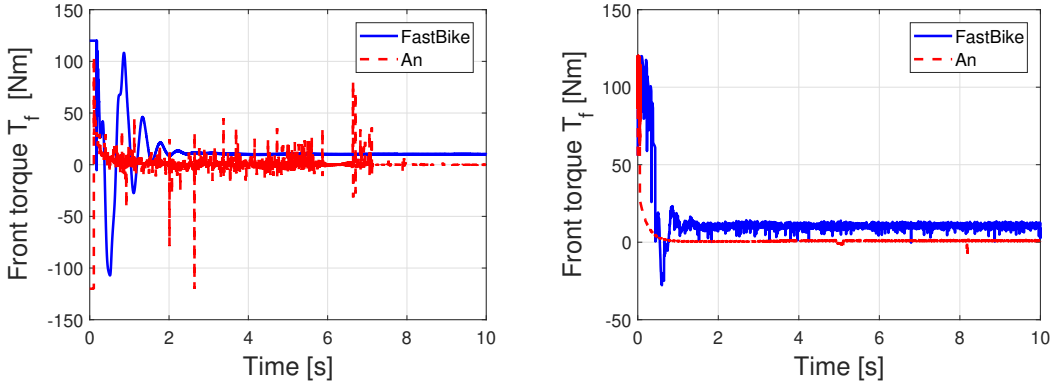

(a) PID controller.

(b) Sliding mode controller.

Figure 4.10: Front wheeò torque control input T_f simulation results in SISO strategies: analytical model (red dashed line) and multibody one (blue solid line).

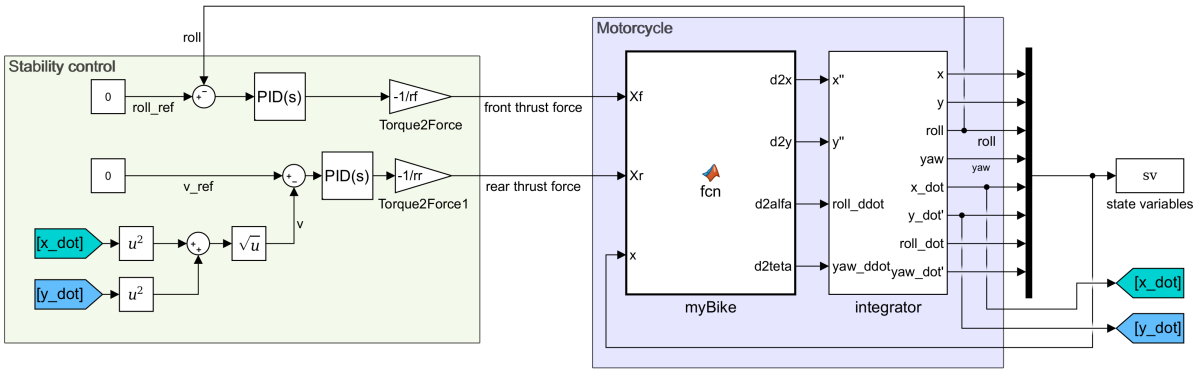

Figure 4.11: MIMO control architecture for self-balancing problem: the front wheel torque restores the stability, whereas the rear one reduces the travelled distance tracking a null rear contact point speed.

desired behaviour can be realized by a MIMO control architecture.

After balancing the motorcycle, the roll angle is small enough, but not exactly zero as well as the front control input. Thus, its longitudinal component moves the vehicle forward and consequently, the further controller should reduce bike speed. For these reasons, the rear contact point speed $v = \sqrt{\dot{x}^2 + \dot{y}^2}$ is set as the second controlled variable, whereas the other one remains the roll angle φ.

4.4.1 MIMO PID control design

For its simplicity and applicability, the control strategy consists in two uncoupled feedback loops of PID controllers: one for each wheel torque. The control technique choice is also influenced by the simulation results on the trajectory of the SISO problem: Figure 4.7 shows that the system is balanced in a shorter path by the PID controller than the sliding mode one. The control strategy is the following: front wheel torque controller tracks a null roll angle ($e_\varphi = \varphi_{ref} - \varphi = -\varphi$)

$$T_f = G_{p\varphi} e_\varphi + G_{i\varphi} \int_0^t (e_\varphi(\tau)) d\tau + G_{i\varphi} \frac{\mathrm{d}e_\varphi}{\mathrm{d}t}; \tag{4.30}$$

the rear one the null speed ($e_v = v_{ref} - v = -v$)

$$T_r = G_{pv} e_v + G_{iv} \int_0^t (e_v(\tau)) d\tau + G_{iv} \frac{\mathrm{d}e_v}{\mathrm{d}t}. \tag{4.31}$$

The control scheme of the MIMO control architecture is depicted in Figure 4.11, whereas front and rear wheel torque PID gains of the two controllers are reported in Table 4.2. The results of this strategy are presented in [138].

PID Gains	Rear Torque	Front torque
G_p	10	1e4
G_i	5	1e5
G_d	-8	5e3

Table 4.2: Control design parameters for the two PID controllers of the MIMO control architecture in the self-balancing problem.

4.4.2 MIMO Sliding mode control design

For completeness a feasibility study about controlling the interconnected dynamics of the system through a Multi Input sliding mode controller is investigated in this Section.

The design of such a sliding mode control law, also in the multi input case, follows the phases outlined into the Section 4.3.2, i.e. the construction of a suitable sliding surface so that the dynamics of the system confined into the sliding manifold produces a desired behaviour and the design of a discontinuous control law to force the system trajectory into the sliding surface. In this case both the sliding surface and the control law will be vectors instead of scalar formulas.

The first problem is the choice of the sliding surface. Remember once again that in the two wheel torque case as further control objective the controller should reduce the distance travelled by the vehicle acting on the bike speed. The first control priority remains the roll angle stability.

In order to do that it seems quite natural to select the following sliding surface

$$s_1(\boldsymbol{X}) = \begin{bmatrix} \dot{\varphi} + \lambda\varphi \\ \dot{x}^2 + \dot{y}^2 \end{bmatrix} = \begin{bmatrix} x_7 + \lambda x_3 \\ x_5^2 + x_6^2 \end{bmatrix} \qquad \lambda > 0 \tag{4.32}$$

with λ design parameter and the roll angle φ and the rear contact point velocity as controlled variables, similar to the MIMO PID architecture presented in Section 4.4.1. Notice that unlike the SISO case where $s(\boldsymbol{X})$ (4.12) was linear, the designed sliding surface $s_1(\boldsymbol{X})$ (4.32) is nonlinear in the second component.

The next step is the design of the equivalent control $\boldsymbol{u}_{eq}$ necessary to maintain the system on the sliding surface once it has been reached. Considering the state vector (4.2) and the model (4.5), the time derivative of the sliding surface $s_1(\boldsymbol{X})$

becomes

$$\dot{s}_1(\boldsymbol{X}) = \begin{bmatrix} \ddot{\varphi} + \lambda\dot{\varphi} \\ 2\dot{x}\ddot{x} + 2\dot{y}\ddot{y} \end{bmatrix} = \begin{bmatrix} \dot{x_7} + \lambda x_7 \\ 2(x_5\dot{x_5} + x_6\dot{x_6}) \end{bmatrix} = \begin{bmatrix} \mathbf{A}_7 + \lambda x_7 \\ 2(x_5\mathbf{A}_5 + x_6\mathbf{A}_6) \end{bmatrix} + \\ + \begin{bmatrix} \mathbf{B}_{71} & \mathbf{B}_{72} \\ 2(x_5\mathbf{B}_{51} + x_6\mathbf{B}_{61}) & 2(x_5\mathbf{B}_{52} + x_6\mathbf{B}_{62}) \end{bmatrix} \boldsymbol{u}_{eq} = 0 \tag{4.33}$$

where $\boldsymbol{u}_{eq} = [X_f, X_r]^T$ is the equivalent control input. To apply the equivalent control method, the sliding hypothesis must be satisfied, that is the matrix $\frac{\partial s(x)}{\partial x}B(x)$ which multiplies the vector $\boldsymbol{u}_{eq}$ in (4.33) must be nonsingular or, in other words, its determinant must be not equal to zero:

$$\det \begin{bmatrix} \mathbf{B}_{71} & \mathbf{B}_{72} \\ 2(x_5\mathbf{B}_{51} + x_6\mathbf{B}_{61}) & 2(x_5\mathbf{B}_{52} + x_6\mathbf{B}_{62}) \end{bmatrix} \neq 0. \tag{4.34}$$

However, this condition cannot be guaranteed. Indeed, it becomes singular and the relative matrix not invertible when the rear contact point velocity $\dot{x}^2 + \dot{y}^2 = x_5^2 + x_6^2$ is zero, which is exactly the second control objective of the problem, thus the controller cannot be designed.

As alternative the rear contact point velocity $\dot{x}^2 + \dot{y}^2$ can be substituted by the rear contact point position $x^2 + y^2$ and this quantity can be considered as second controlled variable of the problem. Now the related new sliding surface is

$$s_2(\boldsymbol{X}) = \begin{bmatrix} \dot{\varphi} + \lambda\varphi \\ x^2 + y^2 \end{bmatrix} = \begin{bmatrix} x_7 + \lambda x_3 \\ x_1^2 + x_2^2 \end{bmatrix} \qquad \lambda > 0 \tag{4.35}$$

Calculating its time derivative to design the equivalent control,

$$\dot{s}_2(\boldsymbol{X}) = \begin{bmatrix} \ddot{\varphi} + \lambda\dot{\varphi} \\ 2x\dot{x}2y\dot{y} \end{bmatrix} = \begin{bmatrix} \dot{x_7} + \lambda x_7 \\ 2(x_1x_5 + x_2x_6) \end{bmatrix} = \\ = \begin{bmatrix} \mathbf{A}_7 + \lambda x_7 \\ 2(x_1x_5 + x_2x_6) \end{bmatrix} + \begin{bmatrix} \mathbf{B}_{71} & \mathbf{B}_{72} \\ 0 & 0 \end{bmatrix} \boldsymbol{u}_{eq} = 0 \tag{4.36}$$

it can be noticed that the control input $\boldsymbol{u}_{eq}$ does not enter in the second component of the sliding surface vector and no equivalent control can be designed with reference to this sliding surface $s_2(\boldsymbol{X})$.

Remark. It is worth emphasizing that, according to standard sliding mode control theory, the signum of sliding surface is essential for designing the discontinuous part of the control law. Nonetheless, both previous sliding surfaces $s_1(\boldsymbol{X})$ and $s_2(\boldsymbol{X})$ (4.32), (4.35) are such that the second component is always positive, this suggesting

that they are not a good choice for the considered control problem.

Taking into account this remark, in the last attempt a control on longitudinal position only instead of the rear contact point position $x^2 + y^2$ is conceived. The chosen (linear) sliding surface reads

$$s_3(\boldsymbol{X}) = \begin{bmatrix} \dot{\varphi} + \lambda_1 \varphi \\ \dot{x} + \lambda_2 x \end{bmatrix} = \begin{bmatrix} x_7 + \lambda_1 x_3 \\ x_5 + \lambda_2 x_1 \end{bmatrix} \qquad \lambda_1, \lambda_2 > 0 \tag{4.37}$$

where λ_1 and λ_2 are two design parameters.

By differentiating $s_3(\boldsymbol{X})$ with respect to time along the trajectory it yields

$$\dot{s}_3(\boldsymbol{X}) = \begin{bmatrix} \dot{x}_7 + \lambda_1 \dot{x}_3 \\ \dot{x}_5 + \lambda_2 \dot{x}_1 \end{bmatrix} = \begin{bmatrix} \mathbf{A}_7 + \lambda_1 x_7 \\ \mathbf{A}_5 + \lambda_2 x_5 \end{bmatrix} + \begin{bmatrix} \mathbf{B}_{71} & \mathbf{B}_{72} \\ \mathbf{B}_{51} & \mathbf{B}_{52} \end{bmatrix} \boldsymbol{u}_{eq} = 0. \tag{4.38}$$

The equivalent control $\boldsymbol{u}_{eq}$ required to guarantee that the system stays on the sliding surface is

$$\boldsymbol{u}_{eq} = - \begin{bmatrix} \mathbf{B}_{71} & \mathbf{B}_{72} \\ \mathbf{B}_{51} & \mathbf{B}_{52} \end{bmatrix}^{-1} \cdot \begin{bmatrix} \mathbf{A}_7 + \lambda_1 x_7 \\ \mathbf{A}_5 + \lambda_2 x_5 \end{bmatrix}, \tag{4.39}$$

but it can be designed if and only if the matrix

$$\tilde{B} = \begin{bmatrix} \mathbf{B}_{71}(x_3) & \mathbf{B}_{72}(x_3) \\ \mathbf{B}_{51}(x_3, x_4) & \mathbf{B}_{52}(x_3, x_4) \end{bmatrix} \tag{4.40}$$

is invertible or, equivalently is not singular. Since the explicit expressions of $\mathbf{B}_{71}(x_3)$, $\mathbf{B}_{72}(x_3)$, $\mathbf{B}_{51}(x_3, x_4)$, $\mathbf{B}_{52}(x_3, x_4)$ terms are quite long, especially the terms $\mathbf{B}_{51}(x_3, x_4)$, $\mathbf{B}_{52}(x_3, x_4)$, the expression of resulting determinant of matrix $\tilde{B}$ (4.40) is not reported here. Despite of the missed explicit expression, it is interesting to notice that terms in the previous matrix $\tilde{B}$ (4.40) depend only on x_3 and x_4 state variables (i.e. on roll and yaw angles), hence the curve of the couples (x_3, x_4) which make singular the matrix $\tilde{B}$ can be plotted and visualized into a $x_3 - x_7$ plane. Such a curve is depicted in Figure 4.12: around the null roll angle - required to achieve vehicle stabilization - the sliding hypothesis is violated for some values of yaw angle.

No guarantees exist that the system will avoid that set of states which makes the input distribution matrix $\tilde{B}$ singular. Consequently, theoretically the simulation could possibly work and stabilize the vehicle for a time interval, but a singularity could instantaneously occur. The above considerations show that this approach cannot be effectively used to solve the problem.

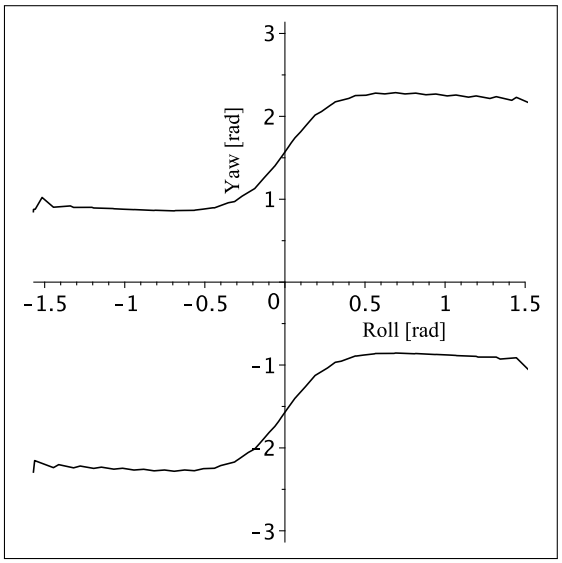

Figure 4.12: Curves where the determinant of the sliding hypothesis matrix $\tilde{B}$ (4.40) for the multi input sliding surface $s_3(\boldsymbol{X})$ (4.38) is zero.

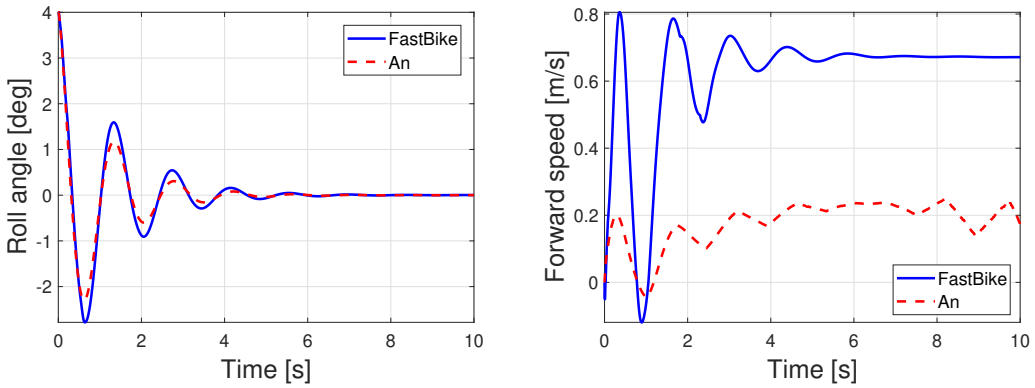

(a) Roll response.

(b) Longitudinal velocity of rear contact point.

Figure 4.13: Numerical simulation with two inputs control strategy: analytical model (red dashed line) and multibody model (blue solid line).

For the aforementioned difficulties it has been decided not to include numerical simulations of the multi input sliding mode controller into the dissertation, but the discussion has highlighted that the topic is worth a in-depth analysis in a possible future work.

4.4.3 Numerical validation and analysis of results

In this Section only the numerical results of the multi input PID architecture are reported, since the multi input sliding mode controller presents some technical issues as described in the previous Section 4.4.2.

The first control priority of the new control system is again the vehicle stability.

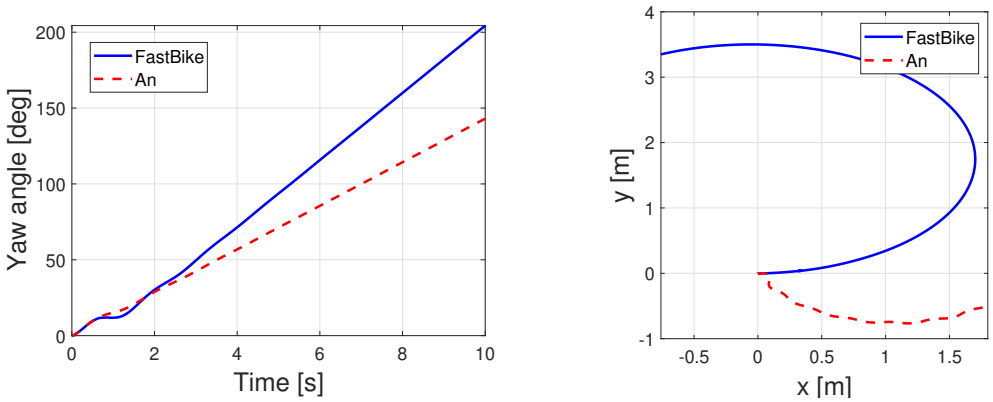

(a) Yaw response.

(b) Centre of mass trajectory.

Figure 4.14: Numerical simulation with two inputs control strategy: analytical model (red dashed line) and multibody model (blue solid line).

The balancing aim is satisfied, as illustrated by the roll response in Figure 4.13a, even though in a longer lapse of time with respect to the corresponding single input strategy (see Figure 4.8a). In the same Figure the validation with the multibody model is depicted too: the two models register a qualitatively similar behaviour in roll angle response, corroborating the analytical model validity with respect to the lateral motion.

As second aim of the control strategy, the self-balancing action should occur at very low speed remaining almost in the same point. In order to do that an oscillating behaviour of the rear contact point velocity around zero would be expected. However, as reported in Figure 4.13b, although in absolute value the speed is kept low (less than 1 m/s) during the whole control action, in both models it asymptotically reaches a positive value, different between the two cases. This means that the swaying motion does not occur and the second control aim is not completely satisfied, highlighting a weakness on the control strategy. Indeed, the speed behaviour has direct consequences on vehicle trajectory. The issue can be related to the choice of the controlled variable $v = \sqrt{\dot{x}^2 + \dot{y}^2}$, which does not take into account the motion direction because it is always a positive quantity.

Due to the previous consideration, since after a transient the vehicle moves at almost constant speed and the handlebar is rotated of 40 degrees, the motorcycle proceeds along a curve in both cases, as shown in Figure 4.14b. This evidence is also confirmed by the time history of the yaw angle which increases linearly, even if with different slopes in the two models (see Figure 4.14a); in the analytical model this variable grows more slowly, explaining the shorter trajectory of the bike. The highlighted discrepancy makes think of a possible limitation of the analytical model.

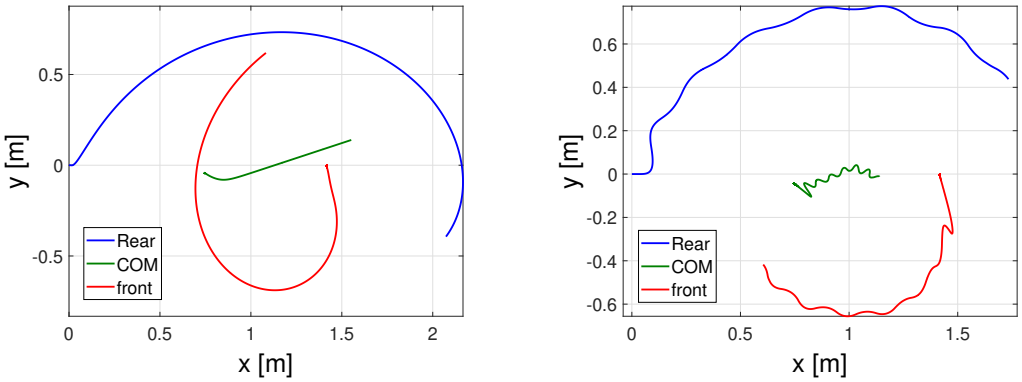

(a) Single input control.

(b) Two inputs control.

Figure 4.15: Comparison of motorcycle track with PID control systems. Figure shows rear contact point (blue), centre of mass (green) and front contact point (red).

Although the vehicle motion does not result as desired (swaying), an improvement of track length is obtained by the two inputs control system. Figure 4.15 shows a comparison of this strategy with the single input PID control one: in same lapse of time, motorcycle with two control inputs moves in a shorter track.

For completeness, it is worth an analysis the rear and front wheel torques, i.e. the control inputs of the system required to achieve the control aims. Their time history is reported in Figure 4.16. The Figure shows that the control strategy acts differently into the two models. In the multibody model, after a transient where the motorbike is balanced, the control system activates a negative rear wheel torque to counteract the action of the positive front one, as expected. Notice that the front wheel torque is different than zero, remaining activated in order to keep the bike upright, because the roll angle will be never exactly null. Moreover, its magnitude is higher than the front torque with the analytical model because the roll angle oscillates with higher amplitude. On the other hand, in the analytical model if the front wheel torque tends to zero, the rear wheel torque presents a discontinuous action with high frequency switching between positive and negative values. Furthermore, it is increasing the oscillation amplitude through time. This behaviour is apparently not justified by other evidences, so it could be related to a weakness of the model, which probably does not consider other fundamental dynamics or of the controller itself. However, it should be in-depth investigated.

Concluding, the second requirement on the distance has shown some difficulties and possible limitations of the model. However, the study on the problem is only preliminary and further improvements are required.

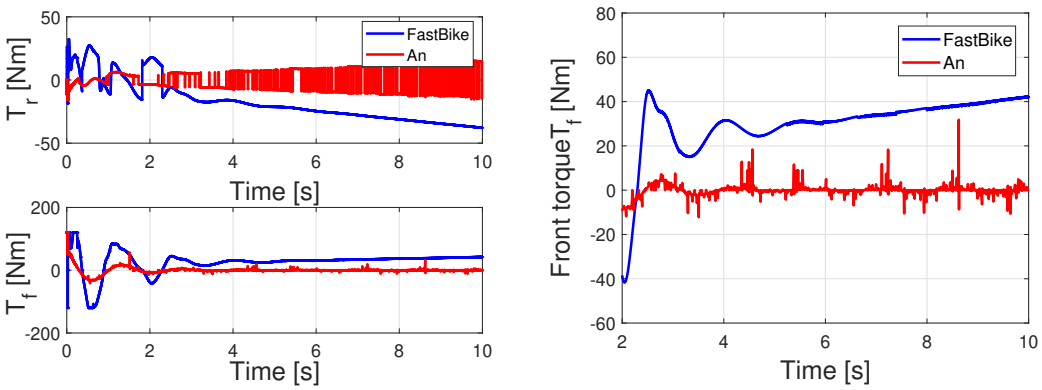

Figure 4.16: Rear (above) and front (below) wheel torque control inputs in two inputs control strategy: analytical model (red dashed line) and multibody model (blue solid line). The picture on the right represents a zoom of the front wheel torque.

4.5 Conclusions

Four kinds of control systems for self-standing two wheel drive electric motorcycle have been presented under the hypothesis that both rear and front wheel torque are available, but the handlebar cannot be actuated. The control strategies have to guarantee vehicle stabilization in a shorter trajectory for an application on real situations. At first, the second objective has been ignored and the front wheel torque has been chosen as unique control input able to generate rotational torques around the bike control axis. A PID control has been compared to sliding mode one: positive simulation results has been obtained by both of them in motorcycle balancing, showing that the front wheel torque can affect the vehicle stability. Then, the introduction of the rear wheel torque as a further control input has reduced the trajectory length, achieving the second control goal. In this case the control system has consisted in two uncoupled PID controllers. The attempt of designing a MIMO sliding mode controller has been also discussed, but some structural issues and possible singularities on sliding hypothesis have been analysed.

The model validation with a multibody software has highlighted a good match of the balancing variable (the roll angle) and this indicates that the presented analytical model captures the main dynamics of capsize motion. The availability of non linear equations represents an advantage with respect to the classical Jacobian linearisation approach commonly used in the literature. Furthermore, the model can be employed to design advanced non linear model-based control systems and analysis tools and it is also suitable for MIMO control strategies taking into account both rear and front torques, eventually satisfying more than one control aim.

The presented work is a positive preliminary study on the topic, even though

confining motorcycle trajectory in a small area requires further analysis and work to apply the system in real situations as well as other tests on the analytical model. A possible solution is to try designing control strategies using more advanced control techniques than the PID taking into account the presence of two control inputs - both front and rear wheel torque - instead of a single one as well as the interconnected dynamics of the model to better achieve both motorcycle balancing and its track confinement and exclude limitations in the model validity.

Chapter 5

Optimal traction strategy

5.1 Introduction

Motocross and motorcycle riders are now facing riding conditions and obstacles where having only rear wheel drive can lead to vehicle damage, loss of control and an unstable front wheel during cornering and off-road riding in general. For professional riders, precious race time is lost avoiding obstacles or losing traction in loose rocks, sand, dirt, mud, or ice. Traction and climbing ability are severely limited in extreme mountain conditions by only having the rear wheel that provides power. Accordingly, there is a need in the industry for a two-wheel drive motorcycle that efficiently and safely transfers power from the motor through the transmission to the front wheel, that provides the rider with increased ability to safely negotiate rough terrain and improve their performances.

The adoption of AWD architecture poses the problem of the appropriate distribution between front and rear propulsion torque. Since lateral force-generating capacity is limited when the wheel is generating high longitudinal forces, enhancements in handling and stability can be made by transferring torque to the front wheel. Changing the distribution of power between the wheels of a motorcycle could give the driver more control over its vehicle: powering the front wheel makes the motorcycle feeling more stable in a turn and gives more traction when accelerating on loose surfaces. These important advantages have already been identified and applied in braking manoeuvres encouraged by the matter of fact all motorcycles have both front and rear brakes, so it is possible to build systems of braking repartition. Analysis and optimal braking control systems, also applied to electric motorcycles, are presented for example in [57, 58, 139, 140]. On the other hand, probably due to few prototypes of all wheel drive motorcycles almost no literature exists about two wheel traction repartition systems, even though it is interesting as well as challenging to find out optimal traction strategies. First studies on this

topic aim at understanding performances of this kind of bikes in limit handling scenarios. Griffin and Popov [3] develop an analysis on AWD motorcycles focusing on energy efficiency. The investigation is conducted with fixed torque ratio instead of presenting an optimal traction torque strategy. An optimal driving strategy for electric two wheeled vehicles is presented in [141] as well as [142]. In the first case the distribution law is based on a model predictive approach taking into account the nonlinearities of the system and its objective is to prevent the traction wheel from spinning under traction. In the second one, a different slip control system is proposed taking into account different road conditions. However, both strategies have been developed and validated only in straight running, even though traction repartition can be particular interesting also in combined lateral and longitudinal acceleration such as the exit of a curve.

This Chapter will illustrate a novel optimal traction strategy for an AWD electric motorcycle that improves performances both in straight running and cornering, taking into account the rider's intentions. The performances will be compared to the traditional single track motorcycle to analyse quantitatively the improvements. The potential implementation of the presented traction distribution law in a real AWD electric motorcycle will be explored, highlighting that the proposed algorithm does not require any additional sensor or actuator.

At first, the optimal all wheel drive traction strategy will be derived from a simple analytical model and a discussion about its practical implementation will be conducted too. Then, the proposed strategy will be validated by a multibody model both with a steady state analysis and by time domain numerical simulations of straight and cornering manoeuvres in flat and uneven roads.

5.2 All-wheel drive optimal distribution strategy

This Section defines the distribution of traction torque between the rear and front motors which maximises riding performance.

First it is necessary to define an objective matrix which quantifies motorcycle performance. There are several options, for example it could be minimized the time to accelerate from 0 to 100 km/h [139], or the lap time on a circuit [143]. For this study, it is selected an objective that is simple and at the same time can enhance both straight and cornering manoeuvres. These are the main reasons why motorcycle performances are evaluated by $g - g$ diagrams.

A $g - g$ diagram, i.e. the plot of longitudinal versus lateral accelerations of a vehicle, is a useful tool to evaluate the rider's and motorcycle performances and to compare different motorbikes. When a vehicle is moving, its motion is characterized

by a longitudinal and a lateral acceleration (a_x, a_y). This couple (a_x, a_y) constitutes a point into the $g-g$ diagram. The maxima lateral and longitudinal accelerations physically achievable by the bike (limited by the friction of the road) define the set of admissible motions and vehicle manoeuvrability and appear as a sort of ellipse or circle, that is for a single tyre. It is clear the bigger the $g-g$ diagram of a motorcycle is, the better its performances are. Thus, it has to be designed a suitable distribution of driving torque between rear and front wheels that results in the biggest $g-g$ diagram for traction. In this sense *optimal* means the strategy which maximally engages the tyres giving the biggest set of admissible motions (i.e. the set of longitudinal and lateral acceleration) in $g-g$ diagram or in other words which maximizes the tyre adherence expressed by the vectorial sum of the normalized longitudinal and lateral tyre forces. Ideally, if the tyres are maximally engaged, the resulting $g-g$ diagram should coincide with the overall internal area of the friction ellipse, real physical limit imposed by the interaction between the tyre and the road. Moreover, this tool helps to quantify how and how much the AWD bike outperforms the RWD. Another advantage of this kind of analysis is that it does not require any driver model.

Remark. Before deriving the method of traction torque distribution which maximizes the set of admissible motion, a remark on terminology used in this Chapter is necessary to avoid confusion. The *optimal traction strategy* will be designed as an optimization policy rather than as result of an optimal control problem. Thus, even though the terms are the same used in control theory the design of traction strategy will not follow the traditional approaches proposed in this field of research.

In order to derive a simplified $g-g$ diagram, the motorcycle is modelled as a lumped mass, which is subjected to steady-state longitudinal and lateral accelerations (a_x, a_y) with geometrical parameters and centre of mass (CoM) position of the whole system shown in Figure 5.1. The suspension motion is neglected and, for simplicity, the aerodynamics centre is assumed to coincide with the CoG. Longitudinal, lateral, and vertical forces are considered at the rear and front contact points. The rider can control the motorcycle dynamics modifying the longitudinal and lateral accelerations in the following way: acting on the throttle he can produce the necessary longitudinal forces to accelerate the vehicle and rotating the handlebar he can impose the suitable lateral forces to achieve the desired lateral acceleration.

The dynamic equations of motion are obtained by Newton-Euler approach.

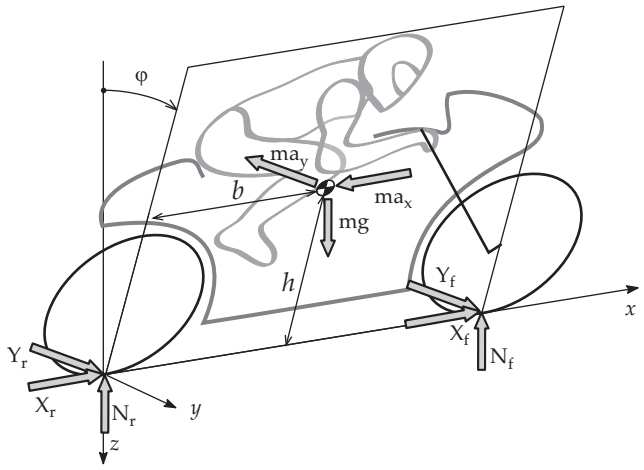

Figure 5.1: Inverted pendulum motorcycle model for performance envelope analysis.

Newton's equations are the following:

$$ma_x + F_D = X_r + X_f \tag{5.1a}$$

$$ma_y = Y_r + Y_f \tag{5.1b}$$

$$mg = N_r + N_f \tag{5.1c}$$

where F_D is the drag resistance. Euler's equations with respect to the centre of gravity **G** are:

$$ma_y h \cos\varphi = mgh \sin\varphi \tag{5.2a}$$

$$(ma_x + F_D)h \cos\varphi = (w - b)N_f + bN_r \tag{5.2b}$$

$$(ma_x + F_D)h \sin\varphi = (w - b)Y_f + bY_r \tag{5.2c}$$

where a_x and a_y are the longitudinal and lateral accelerations, φ the roll angle, m the mass of the whole system (both vehicle and rider), w the wheelbase, b and h the coordinates of CoM. X, Y, and N are the longitudinal, lateral and vertical tyre forces respectively with subscripts r and f used for referring to rear and front tyres. A traction bias β is now introduced as:

$$\beta = \frac{X_f}{X_r + X_f} \tag{5.3}$$

that indicates the percentage of the total longitudinal force applied at the front wheel, therefore $\beta = 0$ means the force is applied only at the rear wheel. It may be immediately calculated the roll angle from (5.2a):

$$\varphi = \arctan \frac{a_y}{g} \tag{5.4}$$

and solved the system (5.1) - (5.2), which is linear with respect to tyre forces as functions of accelerations a_x, a_y, and speed V. For the sake of simplicity, it is provisionally assumed that the speed is small, so $F_D = 0$ and the tyre forces become:

$$X_f = \beta m a_x \tag{5.5a}$$

$$Y_f = \left(\frac{b}{w} - \frac{h}{w} \frac{a_x}{\sqrt{g^2 + a_y^2}} \right) m a_y \tag{5.5b}$$

$$N_f = \left(\frac{b}{w} - \frac{h}{w} \frac{a_x}{\sqrt{g^2 + a_y^2}} \right) m g \tag{5.5c}$$

$$X_r = (1 - \beta) m a_x \tag{5.5d}$$

$$Y_r = \left(\frac{w - b}{w} + \frac{h}{w} \frac{a_x}{\sqrt{g^2 + a_y^2}} \right) m a_y \tag{5.5e}$$

$$N_r = \left(\frac{w - b}{w} + \frac{h}{w} \frac{a_x}{\sqrt{g^2 + a_y^2}} \right) m g. \tag{5.5f}$$

In conclusion, equations (5.5) give the tyre forces at equilibrium for any arbitrary accelerations couple (a_x, a_y). However, when accelerations are high, it is not granted that tyres are capable of generating the requested forces because friction is limited. Consequently, not every set of given longitudinal and lateral accelerations (a_x, a_y) is physically achievable.

A friction "ellipse" constraint must be written for both the front and rear tyres as follows:

$$\frac{X_f^2}{N_f^2} + \frac{Y_f^2}{N_f^2} \leq \mu^2 \tag{5.6a}$$

$$\frac{X_r^2}{N_r^2} + \frac{Y_r^2}{N_r^2} \leq \mu^2 \tag{5.6b}$$

where μ denotes the friction coefficient. By introducing tyre forces (5.5) into adherence inequalities (5.6a) and (5.6b), front and rear tyre adherence constraints

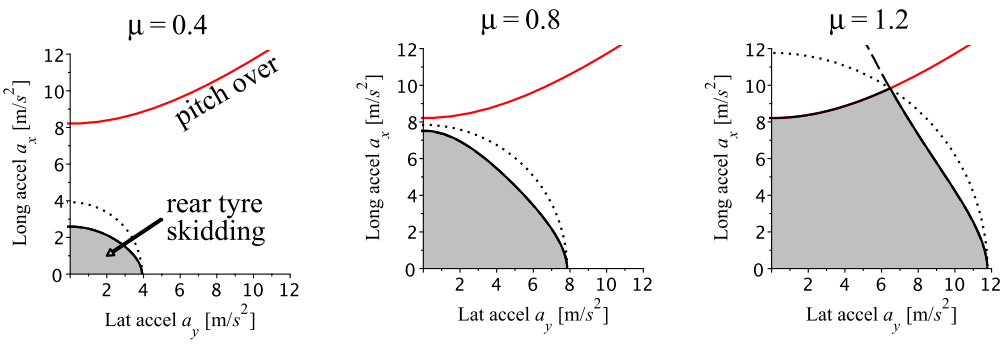

Figure 5.2: $g-g$ performance of a rear wheel drive motorcycle for various friction coefficients μ.

become:

$$\frac{\beta^2 a_x^2}{g^2\left(\frac{b}{w}-\frac{h}{w}\frac{a_x}{\sqrt{g^2+a_y^2}}\right)^2}+\frac{a_y^2}{g^2}\leq\mu^2 \tag{5.7a}$$

$$\frac{(1-\beta)^2 a_x^2}{g^2\left(\frac{w-b}{w}+\frac{h}{w}\frac{a_x}{\sqrt{g^2+a_y^2}}\right)^2}+\frac{a_y^2}{g^2}\leq\mu^2. \tag{5.7b}$$

In conclusion, these inequalities represent feasible adherence areas for each tyre in the a_y-a_x plane. They depend on the bias β and can vary changing this parameter which denotes the longitudinal force distribution between rear and front tyre.

Rear wheel drive motorcycles

Traditional rear wheel drive motorcycles are represented by $\beta=0$, so (5.7b) becomes:

$$\frac{a_x^2}{g^2}+\left(\frac{a_y^2}{g^2}-\mu^2\right)\left(\frac{w-b}{w}+\frac{h}{w}\frac{a_x}{\sqrt{g^2+a_y^2}}\right)^2\leq 0, \tag{5.8}$$

whereas (5.7a) may be discarded because it is now included in (5.8). In addition to tyres adherence, it is also necessary to consider the pitch-over constraints, i.e.

$$N_f=\left(\frac{b}{w}-\frac{h}{w}\frac{a_x}{\sqrt{g^2+a_y^2}}\right)mg>0 \tag{5.9}$$

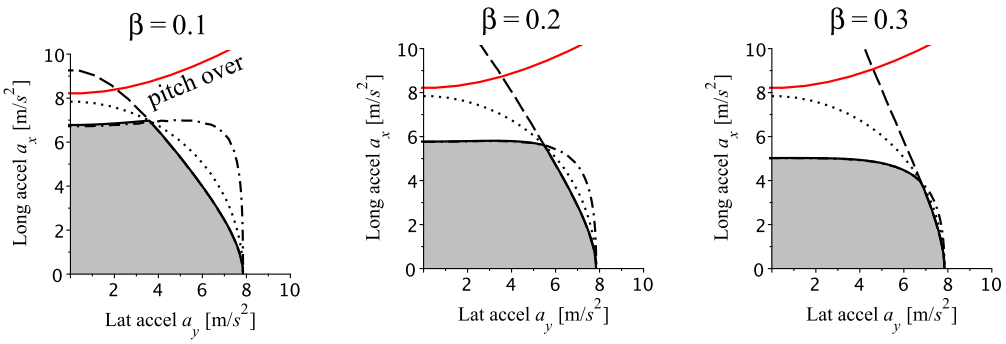

Figure 5.3: $g-g$ performance of an all wheel drive motorcycle with constant front/rear traction bias for $\mu = 0.8$. Different style lines for: adherence ellipse (dot), rear adherence (dash), front adherence (dash dot). Grey areas denote feasible motions.

which may be rewritten as:

$$a_x < \frac{b}{h}\sqrt{g^2 + a_y^2} \tag{5.10}$$

and implies (5.8) is strictly less than 0. Inequalities (5.8) and (5.10) are illustrated in Figure 5.2, which shows circles of radii $g\mu$ too. These circles denote the impassable friction limit beyond which no tyre adherence is. However, the set of feasible motions does not cover the whole adherence ellipse by activating traction force only by the rear wheel; moreover, the lower friction coefficient is, the smaller the region of feasible couples (a_x, a_y) becomes, especially in high longitudinal accelerations, as shown in Figure 5.2 for $\mu = 0.4$. On the other hand, in high friction coefficient (diagram with $\mu = 1.2$ in Figure 5.2) high lateral accelerations with medium - high longitudinal accelerations are not achievable and this means some cornering manoeuvres are not feasible. In addition, in this friction scenario, due to the wheeling, the maximum longitudinal acceleration is reached in combination with lateral ones (i. e. when the motorbike rolls) and not in pure traction. In fact, the roll angle lowers the vehicle CoM reducing the load transfer between rear and front wheels. Thus, maximum traction performance is achieved when the bike is exiting a curve, i.e. it is slightly tilted.

All wheel drive motorcycles

Performance may be improved trying to achieve unfeasible steady-state cornering longitudinal and lateral accelerations (a_x, a_y) by using $\beta > 0$. For example, Figure 5.3 shows motorcycle performance for different constant values of β. In each diagram front and rear adherence limits are also visible to find out what tyre saturates in different accelerations scenarios: for high lateral accelerations rear tyre reaches its

limit before the front one because when motorcycle is tilted the CoM is lower and a front load transfer is generated, whereas for high longitudinal accelerations the front wheel saturates before the rear one because of the load transfer on the rear body of the bike. However, if an amount of traction torque is applied to the front wheel, motorcycle can achieve a set of high lateral accelerations a_y (Figure 5.3 with $\beta = 0.3$) that are not feasible for a RWD motorbike (Figure 5.2 with $\mu = 0.8$), but the same action is not convenient for high longitudinal acceleration manoeuvres where a RWD configuration is better due to a higher load transfer to rear wheel when $\beta > 0$.

This preliminary analysis suggests best performance requires a variable β. In order to calculate the optimal traction bias β as function of a_x and a_y, it is assumed that both front and rear tyre are equally engaged, i.e. work at maximum combined adherence limit. Indeed, tyres adherence has to be maximized as much as possible and reasonably rear and front contact points have same friction coefficient. Therefore, it is imposed

$$\frac{X_f^2}{N_f^2} + \frac{Y_f^2}{N_f^2} = \frac{X_r^2}{N_r^2} + \frac{Y_r^2}{N_r^2}. \tag{5.11}$$

Lateral forces terms can be neglected in the above equality; indeed, according to tyre forces (5.5), the ratios $Y_f/N_f = Y_r/N_r = a_y/g$, therefore (5.11) becomes independent from lateral forces. Since both longitudinal and vertical forces are nonnegative, the equation can be further simplified as:

$$\frac{X_f}{N_f} = \frac{X_r}{N_r}, \tag{5.12}$$

i.e.

$$\frac{\beta a_x}{\left(\frac{b}{w} - \frac{h}{w}\frac{a_x}{\sqrt{g^2 + a_y^2}}\right)} = \frac{(1-\beta)a_x}{\left(\frac{w-b}{w} + \frac{h}{w}\frac{a_x}{\sqrt{g^2 + a_y^2}}\right)} \tag{5.13}$$

and in conclusion one obtains the following expression for the bias:

$$\beta_{opt} = \frac{b}{w} - \frac{h}{w}\frac{a_x}{\sqrt{g^2 + a_y^2}}. \tag{5.14}$$

Such bias is *optimal* in the sense that both rear and front tyre are equally engaged and reach the adherence limit simultaneously, exploiting the whole tyre adherence, (except when wheeling condition occurs first). There is a net gain in performances of AWD with respect to RWD bike, especially in cornering, as shown in Figure 5.4a,

where the $g-g$ diagram of AWD motorcycle with the driving strategy (5.14) is wider than the RWD one ($\beta = 0$). Indeed, if substituting the parameter β in (5.7a) and (5.7b) with the expression of β_{opt} (5.14), both rear and front tyre adherence inequalities become

$$\frac{a_x^2}{g^2} + \frac{a_y^2}{g^2} \leq \mu^2, \tag{5.15}$$

that should be compared with the rear wheel drive motorcycle inequality (5.8). Inequality (5.15) is exactly the equation of a circle of radius $g\mu$ whose border is represented by the "ellipse" line in Figure 5.4a and coincides with maximum feasible limit of tyre adherence, except when wheeling condition occurs. In Figure 5.4b some contour plots of β_{opt} show the percentage of total longitudinal thrust applied at the front wheel: the blue lines are almost flat in the a_y axis direction and this means lateral acceleration a_y does not influence so much the traction bias calculation. Notice that the range of β_{opt} is typically between 0 for high longitudinal accelerations to 0.5 for null longitudinal acceleration that is when vehicle moves at constant speed. Steady state maps with other varying friction coefficients from 1.0 to 0.2 show that higher gains in AWD motorbike performances are obtained in low adherence conditions (see Figure 5.5), hence the proposed open loop control strategy is especially useful and works better in low friction or off-road scenarios. Noticeably, the optimal bias (5.14) depends only from the vehicular accelerations (a_x, a_y) and does not require the knowledge of the tyre adherence, which would be very difficult to estimate.

5.2.1 The significance of speed

So far it has not been considered the effect of aerodynamics forces, which at high speed have a significant effect on vehicle dynamics. Lift force F_L and drag resistance F_D read

$$F_L = \frac{1}{2}\rho C_L A V^2 \tag{5.16}$$

$$F_D = \frac{1}{2}\rho C_D A V^2 \tag{5.17}$$

where V is the vehicle speed, A the frontal area, ρ the air mass density, and C_L, C_D aerodynamics constants that depend on vehicle geometry. Motorbikes are designed with $C_L \simeq 0$ because F_L is not a pure lift force, but follows the roll motion, which under cornering would interfere with the lateral dynamics. In regards of the drag resistance, the aerodynamics factor $C_D A$ is typically comprised between 0.15 and 0.50 m^2, so for an average motorcycle the drag resistance at 100 km/h may be

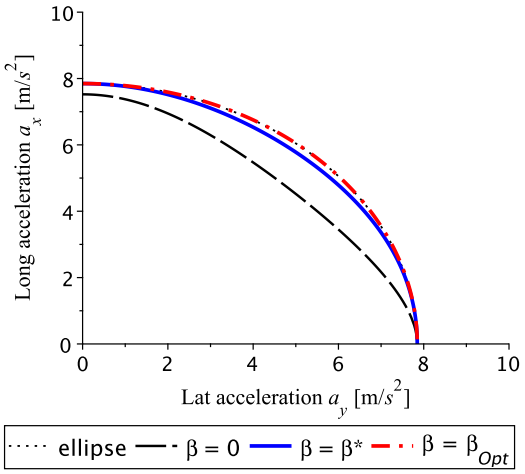

(a) $g - g$ diagram.

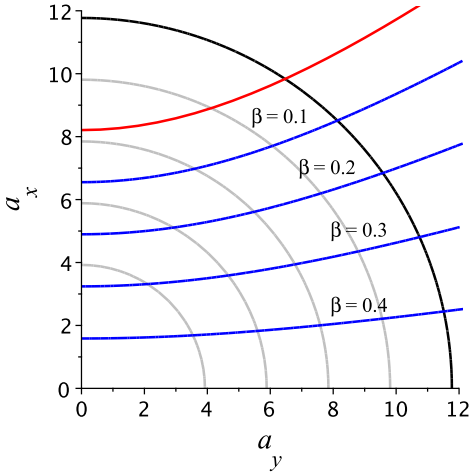

(b) Contour plots of β_{opt}: blue lines denote percentage of torque applied at front wheel and the red one is the wheeling condition. Grey line are friction ellipses at different friction coefficients.

Figure 5.4: All wheel drive motorcycle with optimal bias β_{opt} traction torque repartition.

estimated to be approximately 150 N, which becomes 600 N at 200 km/h and so on. While resistance force grows with the square of the speed, the power increases with the cube, passing from 4.2 to 33.3 kW as the speed increases from 100 to 200 km/h. More in detail, the balance between propulsion power P and driving resistance reads

$$P = \left(ma_x + \frac{1}{2}\rho C_D A V^2 \right) V, \tag{5.18}$$

which in turn gives the following expression of the maximum acceleration as a function of the vehicle speed

$$a_{x,max} = \frac{P_{max}}{V} - \frac{1}{2}\rho C_D A V^2. \tag{5.19}$$

However, even if the acceleration performance significantly decreases as the speed increases, there is little consequence on the optimal distribution of the driving force between rear and front wheel. Indeed, if the *acceleration factor* is defined as follows

$$\tilde{a}_x = \frac{X_r + X_f}{m} = \frac{X}{m} \tag{5.20}$$

where X is the overall traction force, the equation (5.1a) may now be rewritten as

$$ma_x + F_D = m\tilde{a}_x. \tag{5.21}$$

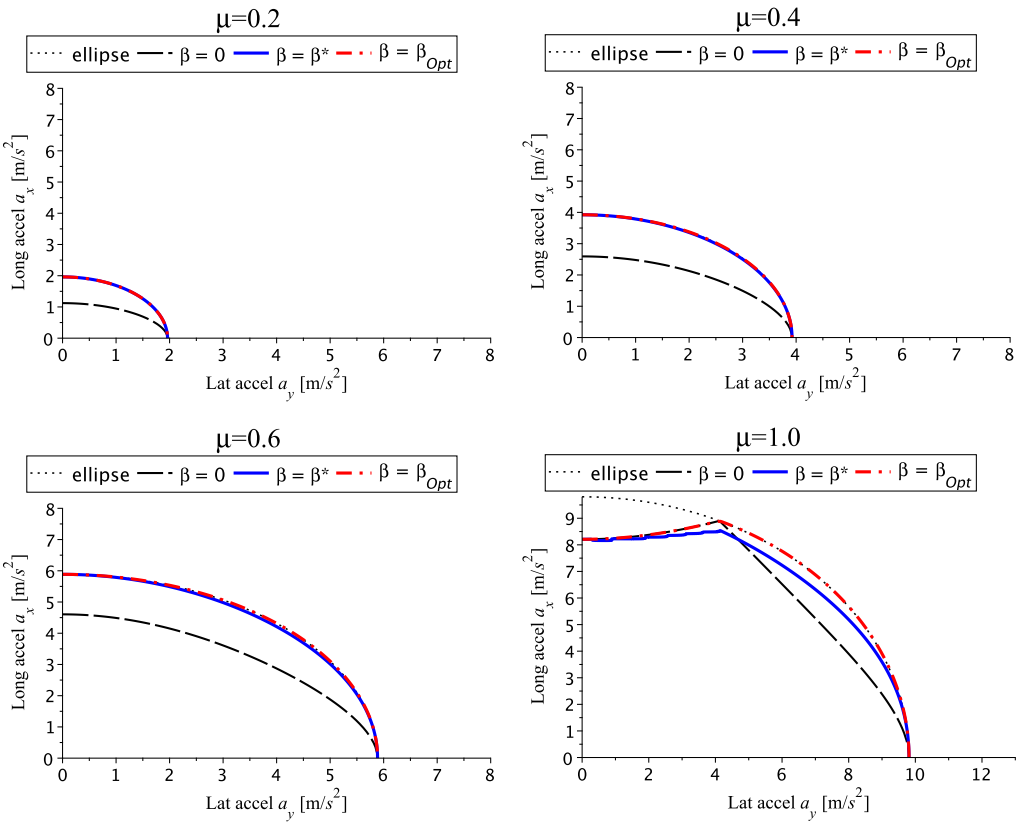

Figure 5.5: All wheel drive motorcycle with optimal bias β_{opt} traction torque repartition and its implementable version β^* for different friction coefficient μ. The AWD advantages over the RWD increases at low adherence.

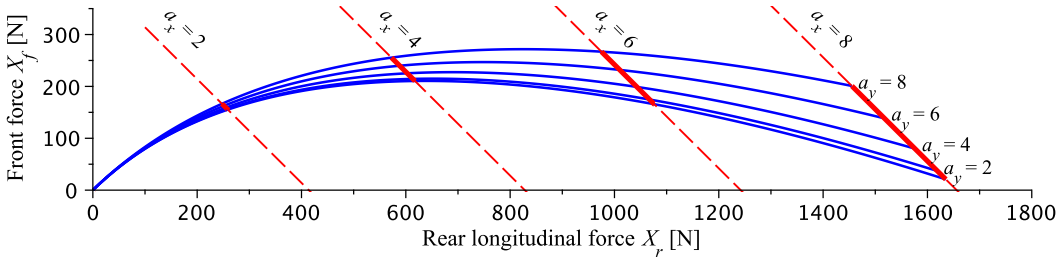

Figure 5.6: Front and rear driving forces as functions of longitudinal a_x and lateral a_y accelerations.

From this point on, the whole analysis from (5.2) through (5.14) can be repeated, obtaining

$$\beta_{opt} = \frac{b}{w} - \frac{h}{w}\frac{\tilde{a}_x}{\sqrt{g^2 + a_y^2}} = \frac{b}{w} - \frac{h}{w}\frac{X/m}{\sqrt{g^2 + a_y^2}}. \tag{5.22}$$

This expression shows that the optimal front/rear force distribution depends on the overall traction force available, rather than on the acceleration and speed. This important result is valid under the assumption that the aerodynamic centre coincides with the centre of gravity, which is approximately true. According to (5.3), the optimal force distribution between front and rear wheels can be finally calculated as:

$$X_{f,opt} = \beta_{opt} X \tag{5.23a}$$

$$X_{r,opt} = (1 - \beta_{opt}) X. \tag{5.23b}$$

Distribution law (5.23) is depicted in Figure 5.6 in the plane $X_r - X_f$.

The optimal thrust force distribution has a great dependence from the longitudinal acceleration $\tilde{a}_x$ as well as little from the lateral one a_y. More precisely, the greater the longitudinal acceleration, the greater the rear force and for any constant value of longitudinal acceleration, a greater amount of overall traction force is transferred on the front wheel for greater lateral accelerations. Nonetheless, the maximum front driving force is much lower than the rear one and this plays a key role for designing and choosing the front motor especially regarding power and weight. Furthermore, from the same picture it can be noticed that the proposed traction repartition law (5.23) actuates the greatest amount of force on the front wheel when the lateral acceleration is maximum, but the longitudinal one is about

between 4 and 6 m/s^2 instead in its maximum value.

In conclusion, the simple traction strategy developed so far can improve the motorcycle performance in steady-state conditions with respect to a traditional motorbike, filling completely the ellipse of adherence under traction.

5.2.2 Traction control implementation

It is now discussed how the open loop traction strategy (5.23) proposed in this Chapter can be actually implemented in a real AWD motorcycle, in particular with a low-cost sensor configuration. The optimal bias (5.22) does not require the knowledge of the actual tyre adherence, which would be difficult to estimate, but needs a real time measurement of the involved quantities, that are the lateral acceleration a_y and the overall longitudinal traction force X.

In order to measure the lateral acceleration, an accelerometer could be installed on the transversal vehicle axis that is the axis orthogonal to bike trajectory. However, in turning the vehicle is tilted as well as the sensor, hence the measure includes an undesired extra component due to the gravity g which affects the lateral acceleration value. This component can be further increased or decreased when the vehicle moves on an incline or when the road has non null banking. To obtain correct values of the effective lateral acceleration, the disturbances in the measured signal need to be compensated. Consequently, methods based on a single inertial measurement are affected by errors introduced by road inclination and cannot be successfully used for our purpose.

An alternative solution for lateral acceleration a_y is to measure indirectly this quantity by the value of the motorcycle roll angle, which is related to it by (5.4) $a_y = tan(\varphi)g$. A direct sensor for roll angle is not in the market for commercial vehicles, but just for racing bikes because it can be measured only by means of expensive optical sensors [144]. For this reason it is important to devise an efficient estimation method. Some solutions about this topic can be found in literature. A pertinent example is presented in [145] where the roll angle estimation is based on a minimum set of sensors which includes two gyrometers plus a wheel encoder for vehicle speed measurement. However, the speed signal can be affected by uncertainties when large accelerations or decelerations occur as explained in [146] where a roll angle estimation method that does not require this signal is described. This approach uses two accelerometers, two additional gyroscopes and a specific method for data fusion of different sensors. A quite different solution for roll angle estimation is a video based system that evaluates this angle based on digital image processing and in particular on the analysis of gradient estimation histograms [147].

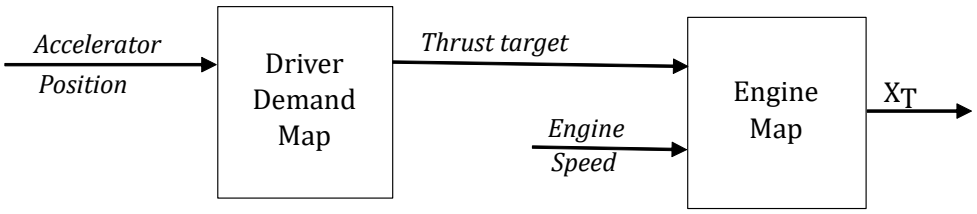

Figure 5.7: Driver demand map and engine map to convert the thrust force target request by the driver by means of the accelerator lever into the total thrust force X_T provided by the engine.

This kind of approaches need a training phase and it is unclear if they perform well on real world data or in low light scenarios such as foggy days or during night.

Most of the previous methods need expensive sensor systems or are not capable of providing measures in real time. Due to the explained limitations and possible errors in the sensors signals induced by noise such as chassis vibrations, last considered alternative is a sensorless solution. As highlighted earlier, the optimal rear and front traction force distribution plotted in Figure 5.6 as well as the β_{opt} contour plots suggest a little dependence of the thrust force repartition by the lateral acceleration a_y. Consequently, the idea is to neglect its effect by setting $a_y = 0$ and to consider a simplified expression of the optimal bias

$$\beta = \frac{b}{w} - \frac{h}{w}\frac{X/m}{g}. \tag{5.24}$$

Moreover, the rider's intention should be considered, thus the overall traction force X has been replaced by the driver traction force demand X_T, which it can be directly related to the accelerator position by means of engine and driver maps stored by vehicle manufacturers inside the Electronic Control Unit (ECU) to control all the engine parameters, as explained by block scheme depicted in Figure 5.7. As a result, the proposed bias reads

$$\beta^* = \frac{b}{w} - \frac{h}{w}\frac{X_T/m}{g}. \tag{5.25}$$

The traction repartition formula β^* (5.25) is the proposed sensorless solution that can be easily and quickly calculated by the ECU after the engine torque output because it is neither time consuming nor costly in terms of online memory. Figure 5.4a quantifies the performance of an AWD motorcycle equipped with this driving strategy ($\beta = \beta^*$): the difference in performances with the control law β_{opt} defined

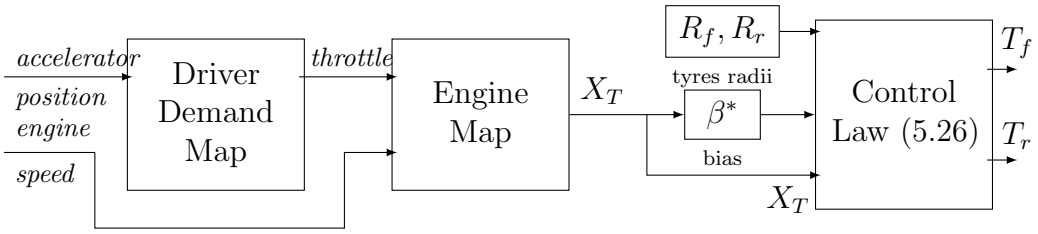

Figure 5.8: Block diagram for the implementation of repartition law (5.26). All these maps are stored into the ECU.

in (5.22) is minimal, becoming almost null at low adherence (see Figure 5.5) and, most important, the AWD motorcycle with the simplified traction distribution law β^* still significantly outperforms the RWD bike.

Because the thesis considers a full electric motorcycle, the adoption of an AWD architecture can be easily achieved by two electric motors, one for each wheel, thus the expression of a control law based on the motor torque rather than the overall traction force makes more sense. If it is indicated by T the motor torque, the optimal rear and front wheel torque distribution is

$$T_{f,opt} = \beta^* X_T R_f \tag{5.26a}$$

$$T_{r,opt} = (1 - \beta^*) X_T R_r \tag{5.26b}$$

which depends on the rider force demand X_T obtained from accelerator position by engine maps, as explained in the control scheme in Figure 5.8. This is the final traction repartition law proposed in the work to improve the motorcycle performances and used now on in AWD motorcycle for comparison with the single track one.

For completeness about the distribution strategy implementation, it is now briefly explained how to map the rider intention expressed by accelerator rotation into the engine torque. Refer to block scheme in Figure 5.8. The force demand, as requested by the driver by the accelerator rotation, is indirectly calculated by the Driver Demand Map: the input variables is the accelerator position, given by the drive by wire potentiometer and the output variable will be the throttle position, actuated from the ECU by hydraulic or electric actuators on the engine intake butterflies or barrels. Then electronic throttle control can be accomplished in one of two ways. The first is by using an open-loop, map-style programming of the ECU (the Engine Map): knowing the torque produced by the engine at any given combination of rpm and throttle position, an electronic butterfly's programming can be modified to react accordingly, based on what the driver is asking for. The

second is to use a closed-loop system, with a torque sensor providing feedback to the ECU. For a review on the topic see [148].

Despite the simplification made, the proposed algorithm is the most convenient way because it does not need any further expensive sensor. In addition, it has been proved neglecting the lateral acceleration in the traction repartition formula does not affect so much the performances of the AWD motorcycle in cornering situations, on the contrary a net gain versus the benchmark remains. In conclusion, the repartition β^* that does not require the employment of any specific sensor in face of a only little loss in performance constitutes a technical solution towards industrial application. Moreover, the rider fully controls the vehicle because the optimal traction torque distribution calculated inside the ECU depends only by the rider's overall traction demand and some geometrical parameters.

5.3 Numerical validation and analysis of results

In this Section the reference RWD motorcycle is compared to the novel AWD one and the results obtained in the simple model are validated using a multibody software. The whole analysis developed through the Chapter as well as the numerical results has been collected in a paper [149].

Driving strategy presented in (5.25) is obtained by the simplest model, thus a validation of the presented results using a more complex one is required. Assessment is done through multibody simulations. The validation process consists in two parts: firstly the steady state contour map are generated to understand whether outperformances of AWD motorcycle hold in the complex model, then some time domain dynamical simulations of rectilinear and cornering critical manoeuvres are carried out for transient analysis and compared to the RWD benchmark motorcycle. For $g-g$ performances a kinetostatic model is derived by the validation dynamical one.

5.3.1 Motorcycle model

The optimal traction strategy is validated through the second version of the multibody software FastBike for real-time dynamic analysis of two wheel vehicles presented in Section 2.5. Remember that the motorcycle mathematical model is fully nonlinear and consists in all relevant components of a motorbike (chassis, brake calipers, other unsprung masses, chain powertrain, etc.) as well as front fork and rear swingarm suspension which are a must for off-road bikes. Front and rear wheel torque (to model the AWD motorcycle) and steering torque are the control

inputs of the model used both to simulate the virtual rider and apply the driving torque strategy (5.26). Moreover, for off-road bikes, it is important to considerer rough roads in addition to a perfectly smooth ones. A random road profile can be generated with typical spectral characteristics and used in a selected subset of simulations.

An accurate nonlinear tyre model is necessary for a reliable validation dealing with off-road motorcycles. it is worth underlining forces formulas must model the effects of the combined lateral and longitudinal slips, essential for scenarios under our attention. These effects are included into the Full Tyre Model described Section 3.7, obtained as a simplification of the MF-Tyre 6.2 Magic Formula version. The influence of tyre relaxation length is also included in motorcycle model to a more realistic analysis of the transient manoeuvres. Furthermore, it is assumed that rear and front tyres work in the same way.

Finally, the rider's ability cannot be neglected in the study of optimal traction strategy performance, and thus a virtual rider capable of generating challenging manoeuvres is designed, based on the rider model of the Section 2.6. The virtual rider is modelled as a steering torque controller, neglecting body movements, able to activate of course also the engine torque and of following prescribed speed and roll angle profiles. Each of these control objectives is achieved by a PID controller tuned by trial and errors.

5.3.2 Performance envelope

As first step to validate the presented traction strategy the steady state contour map of the simple model in Figure 5.4a can be compared with the same one generated using the multibody model. In order to plot this diagram and get motorcycles performances it is necessary to reduce the Simulink multibody dynamic model to a steady state one (as in [150]), or in other words to solve a kinetostatic problem for any given value of the longitudinal and lateral acceleration.

Kinetostatic problem

The first step is to identify the set s of static variables starting from the dynamic one x_C. The overall system of FastBike has seventeen state variables to describe the relative motion of the bodies: the roll φ and pitch μ angles, the height of CoM z, the steer angle δ and steer rate $\dot{\delta}$, the front fork travel f_s and swingarm angle s_a and their rate $\dot{f}_s$, $\dot{s}_a$, the body speeds V_x, V_y and V_z and the angular speeds Ω_x, Ω_y

and Ω_z and the wheel angular speeds ω_r and ω_f. Summarizing,

$$\begin{aligned} x_C = [&1 = \varphi,\ 2 = \mu,\ 3 = z,\ 4 = \delta,\ 5 = f_s,\ 6 = s_a,\ 7 = V_x,\ 8 = V_y,\\ &9 = V_z,\ 10 = \Omega_x,\ 11 = \Omega_y,\ 12 = \Omega_z,\ 13 = \dot{\delta},\ 14 = \dot{f}_s,\ 15 = \dot{s}_a,\\ &16 = \omega_r,\ 17 = \omega_f] \end{aligned} \tag{5.27}$$

They are in chassis reference frame.

Considering that in the kinetostatic model the derivatives of the state variables are equal to zero, it holds $\dot{\varphi} = 0$, $\dot{\mu} = 0$, $\dot{z} = V_z = 0$, $\dot{\delta} = 0$, $\dot{f}_s = 0$, $\dot{s}_a = 0$, thus they cannot be static ones, restricting the set. Moreover, instead of the quantities in chassis reference frame, we want the angular speed in body fixed reference frame. Since both $\dot{\varphi}$, $\dot{\mu}$ are null in steady state motion, the dynamic variables Ω_x, Ω_y and Ω_z are replaced by the static variable $\dot{\psi}$. All the other dynamic variables in x_C vector (5.27) can be set as static ones. With these considerations, the following thirteen static variables have been chosen for the steady state model: the roll angle, the pitch angle, the steer angle, the CoM height, the fork travel and the swingarm angle, CoM translational velocities V_x and V_y in the body fixed reference frame, the yaw rate, the rear and front wheel angular velocities, the steer torque, and the total driving force:

$$\begin{aligned} s = [&1 = \varphi,\ 2 = \mu,\ 3 = z,\ 4 = \delta,\ 5 = f_s,\ 6 = s_a,\ 7 = V_x,\ 8 = V_y,\\ &9 = \dot{\psi},\ 10 = \omega_r,\ 11 = \omega_f,\ 12 = T_s,\ 13 = X_T] \end{aligned} \tag{5.28}$$

The latter is then split between the rear and front wheel torques based on (5.26) when considering the AWD motorcycle configuration. Before each iteration of the solver kinematics quantities, road contact forces, and rear swingarm and front fork suspension forces are separately calculated by their specific equations and formulas, then used inside the multibody mathematical model. For further details see the Matlab function reported in Appendix B. The final result of this reduction is an algebraic system of nonlinear equations, which are numerically solved in Matlab for assigned values of longitudinal and lateral acceleration and vehicle speed. A couple (a_x, a_y) is declared admissible if the solution is physical acceptable, i.e. it respects the physical and dynamical constraints such as roll and steer angles less than 90 degrees or nonnegative tyre vertical load. If the steady state longitudinal and lateral acceleration couple (a_x, a_y) is an admissible motion, it can be included in the $g - g$ diagram of the motorcycle to visualize its performances. Usually just a few iterations of the solver are enough to converge to the solution, but for border values of the $g - g$ diagram the number of iterations can increase.

The numerical results presented in this work refer to an enduro electric motorcycle; its geometric and mass properties and tyre constants are listed in Appendix A. If not stated otherwise, the longitudinal vehicle speed is 20 m/s and the friction coefficient is $\mu = 0.8$.

The $g - g$ diagram of the multibody model labelled as "Reference diagram" in Figure 5.9b has a behaviour qualitatively similar to its correspondent of the simple model in Fig. 5.4a (that for simplicity of comparison is also reported in Figure 5.9a, again as "Reference diagram"): also in the highly nonlinear mathematical model the AWD equipped with traction strategy (5.26) outperforms the RWD motorcycle configuration, confirming and validating the advantages found out with the simple model. Moreover, the positive results of AWD on RWD also hold in case of different friction coefficients, especially for lower tyre adherences.

Summarizing, both under cornering and in a straight line motion an appropriate repartition of the traction torque can help the rider to carry out some manoeuvres impossible with a standard motorcycle. More precisely, an AWD motorcycle can make the difference in all the manoeuvres that involve lateral and longitudinal accelerations inside the area between dashed black and solid blue lines of the "Reference diagram" in Fig. 5.9b. The accelerations couples (a_x, a_y) into this region are typically reached by a rider exiting a curve, thus in these situations the proposed driving strategy can become a benefit, especially during races. For example exiting the same curve with a higher longitudinal acceleration means to gain time on the race. However, the analysis carried out so far is incomplete because the torque distribution formula β^* (5.25) involves some geometrical parameters such as the CoM position (b, h) and the overall vehicle mass m, thus a sensitivity analysis is required.

5.3.3 Sensitivity analysis of motorcycle design parameters

Because of the variability between riders, it is not possible to know a priori neither the overall vehicle mass nor the precise location of CoG. Moreover, the position of motorcycle centre of mass (b, h) is not constant during riding due to suspension motion, especially for off-road motorcycles. Its variation affects the performance of the optimal traction strategy which depends by these parameters.

Figure 5.9 shows the influence of different CoG positions both in theoretical and multibody $g - g$ diagrams. In all steady state contour maps (5.25) is evaluated with the same CoG position. Their values are equal to its position in nominal configuration (see (b_0, h_0) in Table A.3 Moving forward the longitudinal position b of CoG will reduce the load transfer in straight runs and allow for higher longitudinal

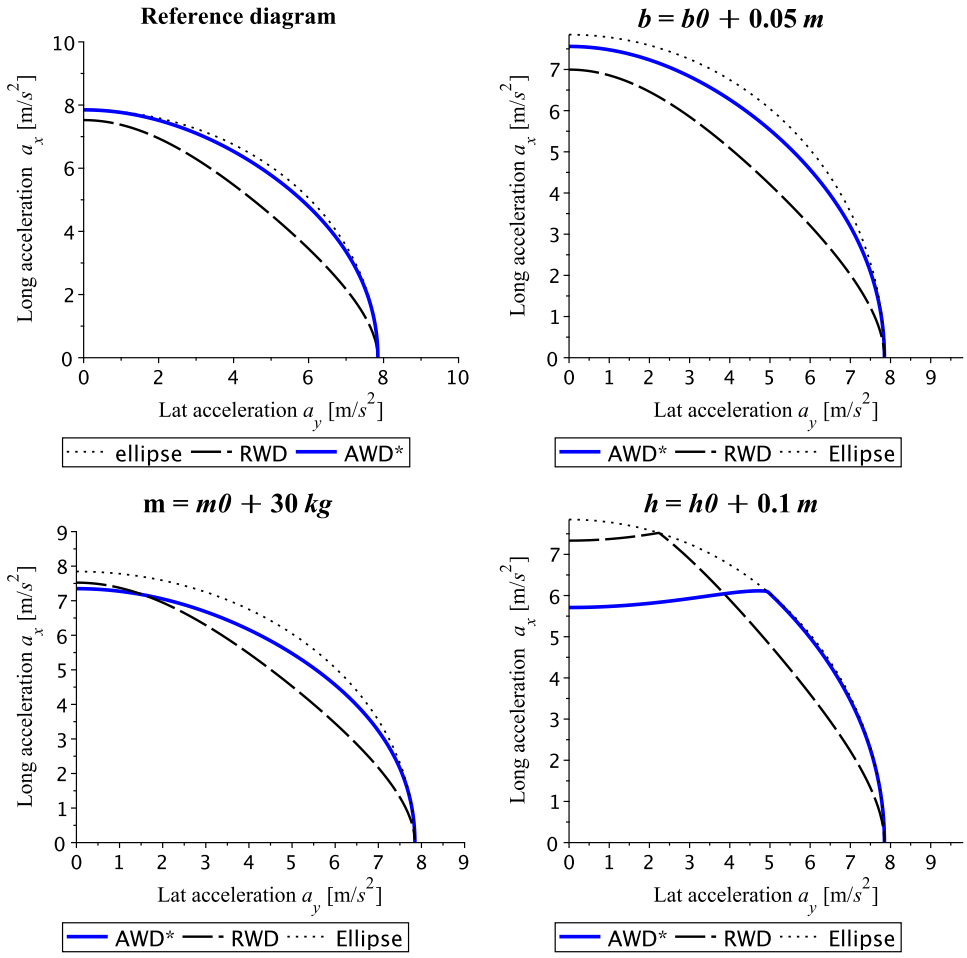

(a) $g-g$ diagrams for the simplified model.

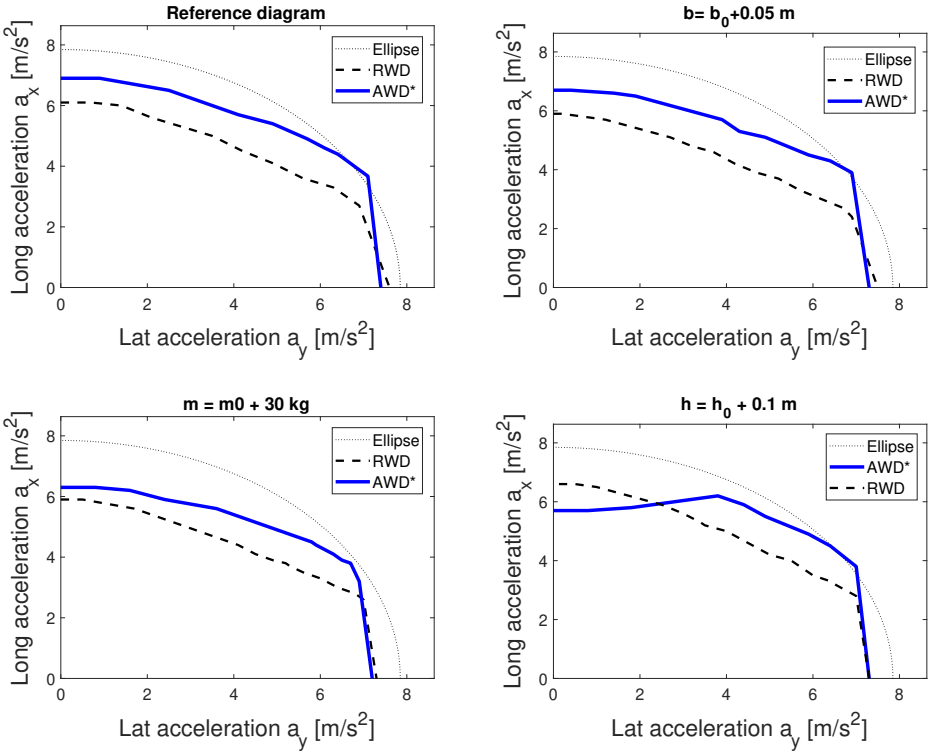

(b) Multibody $g-g$ diagrams.

Figure 5.9: Sensitivity analysis of traction distribution formula β^* (5.25) for CoG position (b_0, h_0) and overall mass m_0 variation.

acceleration than in single track case (see Figure 5.9a labelled as $b = b_0 + 0.05$ m). A similar behaviour is registered when the CoG is lower than its position in nominal configuration, whereas if it is higher, the load transfer will be increased in rectilinear motion reducing longitudinal acceleration as well as the acceleration performances in cornering will be improved, as shown in diagram where $h = h_0 + 0.1$ m of the same figure. This effect also happens when the CoG is moved back and it may be beneficial in motorcycles with low engine power that in any case prevent the vehicle to lift the front wheel in acceleration. Furthermore, punctual comparison of plots in Figure 5.9a and 5.9b reveals again a good match in dynamical behaviour between simple and multibody models and it constitutes another proof in the validation process of the presented control law.

In addition to a CoG position variation, the traction distribution formula (5.25) needs an estimation of the unknown rider weight which can vary about from 60 to 110 kg. This issue can be partially solved setting a mass selector in the motorcycle to inform the vehicle about this quantity. Anyway, a sensitivity analysis on this parameter is also conducted. The comparison of AWD and RWD motorcycles visualized in m_0 variation diagrams of Figure 5.9a and 5.9b reveals that rider mass variation does not significantly affect solutions and relationship between the two bike configurations mainly because the rider uncertainty mass with respect the reference one $m_r = 70$ kg is lighter than the overall mass and the difference is still applied at the vehicle centre of gravity. Especially in cornering manoeuvres, a net gain of the traction repartition control law β^* (5.25) over the single track motorcycle is visualized.

5.3.4 Transient analysis

Previous analysis in the complex multibody model confirms the superiority of the AWD with respect to a conventional motorcycle, at least in steady motion. However, it is incomplete because it has not considered any transient and it is essential to validate and guarantee the strategy works in steady turning as well as in transient manoeuvres. In this perspective, time domain simulations of few manoeuvres are carried out in Simulink. The rider consists in two PID algorithms, as described earlier which act on the control inputs of the multibody motorcycle block.

First of all a pure straight acceleration motion is analysed, applying a total drive torque ramp: numerical results are reported in Figure 5.10. We notice from the rear longitudinal slip plot that the single track motorcycle loses adherence when it achieves its maximum longitudinal acceleration of 6 m/s^2. Conversely, the AWD

motorcycle equipped with the proposed control law (5.26) is capable of reaching a higher longitudinal acceleration of 7 m/s^2. The maxima longitudinal accelerations achieved by the two motorcycle configurations agree with the maxima longitudinal ones reported in the steady state $g - g$ reference diagram of Figure 5.9b. The wheel drive torque repartition worths a specific remark. The front wheel torque is approximately equal to the difference between the rear wheel torque applied to the single track motorcycle and the rear wheel one of the AWD bike. It is just an approximation because the tyres radii of considered motorbike are not the same. From rear wheel torque plot, we see that in the acceleration phase this quantity does not increase linearly and this result is in agreement with the thrust force distribution at $a_y = 0$ discussed in force plane of Figure 5.6. A further interesting feature of the applied driving strategy is that it transfers in percentage less and less of the total thrust force on the front wheel when acceleration increases, so the torque repartition between wheels is not constant in time, but changes, see beta traction repartition plot in Fig. 5.10. This makes sense and is coherent with controller scheme (5.22) that induces a rear load transfer when rider desires high longitudinal accelerations. However, even in strongly high longitudinal accelerated straight motion at least a little quantity of the total drive torque is transferred to the front wheel and this means that a torque distribution should be adopted in any case for better performances.

The next case study is a cornering manoeuvre (entrance-stationary-exit) with particular focus on the exit phase. The manoeuvre consists in a rectilinear acceleration phase, a stationary cornering and final acceleration for the exit of the turn. In the exit of the selected curve the target profiles are chosen such that the rider carries out the manoeuvre in combined accelerations ($a_x = 5, a_y = 4$) which corresponds to an unfeasible couple for the single track motorcycle, but theoretically achievable by an all wheel drive one equipped with the optimal traction strategy (see Figure 5.9b). Instead, in the stationary turning phase the vehicle travels at 15 m/s tilted by 26° and consequently the rider turns in a curve with radius $R = 50$ meters. These statements and the numerical simulation results of this manoeuvre can be checked in Figure 5.11. The roll angle plot shows the rear wheel drive motorbike loses adherence and falls down at about 18 s, which constitutes the beginning of the exit acceleration phase. On the other hand, the bike with AWD configuration carries out the predefined trajectory without any issue. It is worth analysing the traction repartition plot in Figure 5.11: the torque splitting imposed by the controller in the exit phase of the corner starts exactly at 18 s, the same time when RWD bike falls down, emphasizing the adding worth on the adoption of the traction torque distribution strategy.

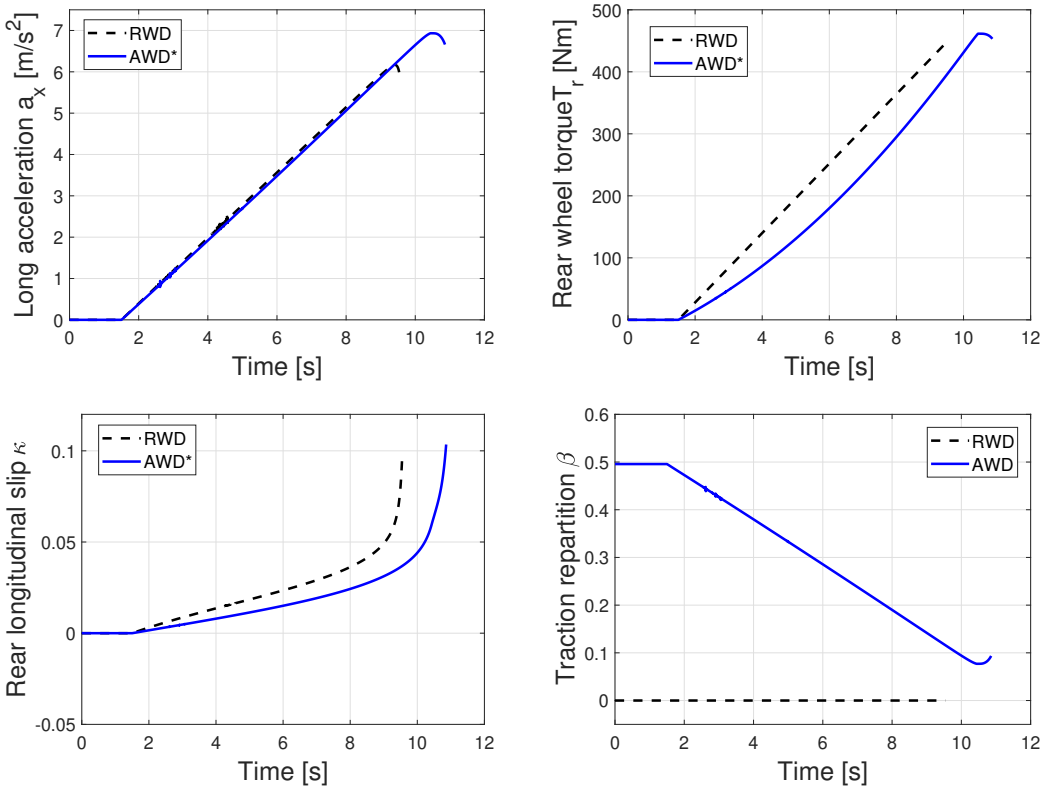

Figure 5.10: Dynamical simulations in a pure longitudinal acceleration manoeuvre, flat road: traditional RWD bike (blue solid line) and AWD bike (black dashed line) with β^* (5.25) as traction repartition bias.

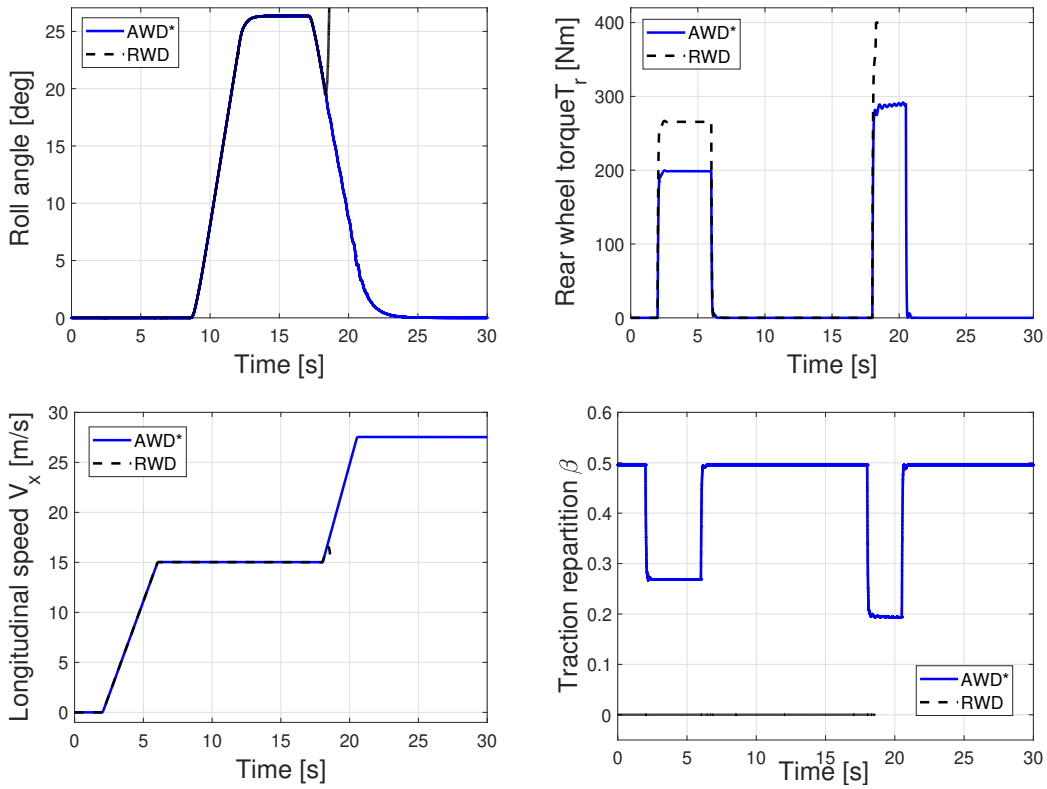

Figure 5.11: Dynamical simulations of a turning manoeuvre: traditional RWD bike (blue solid line) and AWD bike (black dashed line) with β^* (5.25) as traction repartition bias.

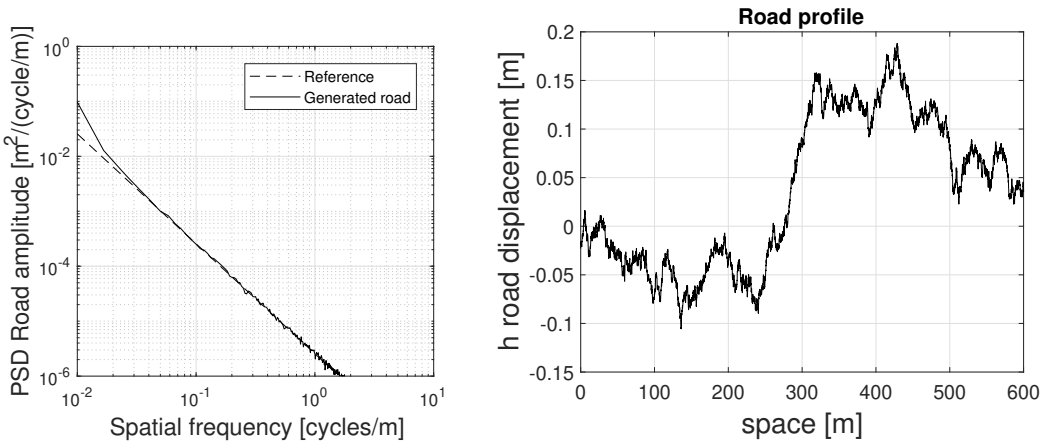

Figure 5.12: Power spectral density of the road profile (on the left) and the road profile of class C (on the right).

In conclusion, dynamical simulations corroborate the steady state results of the kinetostatic model and once again the advantages of engaging a suitable driving strategy.

5.3.5 Effect of road unevenness

For off-road bikes, it is important to considerer rough roads in addition to a perfectly smooth ones and perform simulations on them.

The road considered for the analysis has a random profile. It is modelled according to ISO 8608 [151] which uses the power spectral density (PSD) of the vertical displacement of the road. It describes the amplitude of the road with respect ot the spatial frequency by the equation

$$G_d(n) = G_d(n_0) \left(\frac{n}{n_0} \right)^{-k_r} \tag{5.29}$$

where G_d is the vertical displacement PSD, n_0 (= 0.1 cycles/m) is the reference spatial frequency, n the spatial frequency and k_r is the exponent of the fitted PSD. The parameter $G_d(n_0)$ describes the severity of the irregularities of the road and defines road classes in the standard ISO 8608.

For simulation, road profile is generated based on the procedure described in [152], by assuming $G_d(n_0) = 2^8 \cdot 10^{-6}$ and $k_r = 2$ to obtain a vertical displacement in a range of ± 0.15 m. Figure 5.12 on the left shows the reference power spectral density used to generate the profile which corresponds to a road class C and the power spectral density and on the right the generated road profile, used in dynamical simulations.

The same pure longitudinal acceleration manoeuvre analysed with flat road is

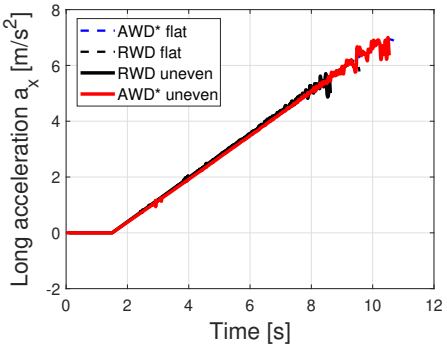

(a) Longitudinal acceleretion response.

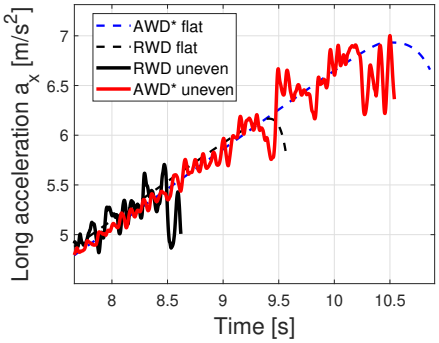

(b) Zoom in maxima longitudinal acceleration.

Figure 5.13: Dynamical simulation of a straight running manoeuvre with uneven road profile of Figure 5.12: uneven road (solid line) and flat road (dashed line); RWD bike is represented by black lines.

simulated along a rough road profile. Although no significant differences in the dynamical behaviour of AWD and RWD motorcycles are detected at low longitudinal acceleration with respect to the same simulation in flat road, the same is not valid at high longitudinal accelerations any more. As shown in Figure 5.13b, in an uneven road profile the RWD bike achieves a lower maximum acceleration than in a flat road, thus the effect of driving on a rough road looks similar to riding a motorcycle on a lower variable friction road. Nonetheless, the AWD motorbike configuration controlled by (5.26) does not seem to be significantly conditioned by the difference in road profile: indeed, the bike can achieve the same maximum longitudinal acceleration as in a flat road.

From this analysis it can concluded that as the effect of road irregularities can be compared to a friction reduction, the proposed traction wheel torque repartition is particularly convenient in uneven roads because our algorithm does not require the friction knowledge and it is not influenced by it.

5.4 Conclusions

This study has proposed a novel optimal traction torque repartition law for all wheel drive motorcycles, which is derived by a simple model and then validated in a multibody one. The $g - g$ diagrams of both models have highlighted better performances of the all wheel drive motorcycle than the single track one. Major improvements are registered on off road low adherence terrains and in cornering manoeuvres when vehicle runs in combined longitudinal and lateral acceleration, especially during the exit of a curve. This means that a motorcycle controlled by

a suitable driving strategy can achieve higher accelerations and, in general, more lateral acceleration through a given corner or more longitudinal acceleration on a straight corresponds to quicker lap times. The steady state analysis has also been confirmed by time domain dynamical simulations.

Additionally, the investigation has explored and proved the possibility of implementing the presented driving strategy on any commercial motorcycle provided with an electric motor for each wheel without requiring any further sensor. The work has referred to an all wheel drive motorcycle with two electric motors just as an example, but the solution can be also applied if the front wheel is driven by mechanical or hydraulic systems. At least theoretically the choice of a feedforward control law based on the throttle required by the driver and its implementation by means of a sensorless solution makes easier and smoother the motorcycle handling and follows the drive desires of the pilot improving his driving feeling. This represents a further point in favour of the presented traction strategy.

To complete the work last step would be to carry out experimental tests of the presented torque repartition strategy on a real all wheel drive electric motorcycle.

Chapter 6

Final discussion and conclusions

History has shown that improvements in traction, handling and stability of motorcycle can be made through better control over the individual wheel torques, where control was traditionally achieved through the reduction of the overall drive torque, or the application of a brake at one, or both of the wheels. Electronically controlled systems include the Traction Control System and the Motorcycle Stability Control (MSC) developed by Bosch or the Antilock Brake System. Improvements in one performance aspect of a vehicle often come at the expense of worse performance in another; for example, when stability in a corner is improved through the application of a brake, the vehicle speed might suffer.

Most current electronic enhancements are active only when the system detects that the vehicle is in danger of becoming unstable, at which point it will interfere with the driver's request of the vehicle. The issues with this method of working are twofold: the system is not active most of the time, leading to expensive components being idle, and when they are active, they might interfere with the driver's intentions. A benefit of a system that aims to influence vehicle performance through active distribution of the rear and front drive torque or the activation of the front wheel torque is that they can be permanently active, and thus utilised by a rider in a way that is not imposing. Additionally, they can be used in parallel with existing stability enhancements when a dangerous situation is detected or the vehicle moves under the critical speed in the unstable region, increasing the rider ability to safely negotiate rough terrains. Some researchers have considered the potential for torque distribution systems or all wheel drive traction architecture to improve the handling of automobiles. Similar research related to motorcycle has not registered a significant spread until now, maybe due to the very limited number of manufactured motorbikes that can apply drive torque to the front wheel [31–34]. However, currently the use of electric motors solves many the technical issues about front torque traction and applicability of wheel torque distribution on motorcycle,

thus this area of research related to all wheel drive motorcycles becomes interesting, starting from understanding whether this architecture is beneficial in some way over the traditional one until exploring the effect it has on handling and stability.

This thesis provided details of investigations that have been made in the areas of motorcycle stability at low speed and active wheel torque distribution. In this Chapter, conclusions drawn from those investigations will be summarised. Work that represents original contributions will also be highlighted. Finally, recommendations for further work will be made.

6.1 Conclusions

Contributions in both modelling and control system of the analysed problems have conducted to interesting results, thus, conclusions will be sectioned according to corresponding chapters in the thesis, and supplement the more detailed summaries at the end of each chapter. Chapters 1 presented an introduction to the topic and a review of the current technology thus will not be subject matter of further discussion.

6.1.1 Motorcycle modelling

Chapter 2 presented the modelling of the motorcycle for both control design and validation. Simple driver models, capable of controlling the roll angle and longitudinal speed of the vehicle were created.

First of all, to study whether the front wheel torque can affect the self-balancing of a motorcycle, without any steering action, a simplified mathematical model oriented to the control has been derived, which captures roll dynamics of the motorcycle. The vehicle has been modelled as a single body that can move on the plane and has four degrees of freedom (x and y rear contact point position, roll angle and yaw angle). The model has two control inputs, the rear and front wheel torque and takes into account the presence of a driving front wheel torque, instead of the usual front braking torque; it could be used to design Multi Input Multi Output (MIMO) control systems. Both these features make the model itself interesting, especially for the increasing attention in electronic active safety systems, which can be easier implemented in electric and all-wheel drive motorcycles. To gain a better insight how front wheel torque affects the stability of the bike, the model does not include the steer torque among its control inputs, handling the steer angle as a model parameter, unlike most of literature models. However, to generate a stabilizing torque around the roll axis applying the front wheel torque, the

steering column is rotated and locked at its maximum, a specific peculiarity of the developed model. Equations of motion has been obtained applying the Lagrangian approach and then, the model has been implemented in Matlab/Simulink to use it as starting point for designing the self-balancing control system. The derived model is a nonlinear second order ODE system with a dynamical behaviour similar to an inverted pendulum, tailored for control purposes.

On the other hand, the optimal traction strategy has been derived by the Newton-Euler approach considering the motorcycle as a lumped mass. Both models have been used to design control strategies that have to be tested. Thus, a sufficiently detailed representation of the motorcycle for model and control validation is required. In this view point multibody models can provide accurate description of the vehicle and use for in-depth analysis. As multibody motorcycle model, a commercial software, named FastBike, has been chosen because it is validated against experimental data, confirming high reliability and fidelity of the model itself, essential features for handling and performance investigations. Moreover, it can be easily integrated as a block into a Simulink diagram and most important, it is not computationally expensive. The software codes a nonlinear mathematical model based on literature [59], but it has been customized to account the front drive torque and work at very low speed both forward and backward. The multibody model includes the individual rotations of the wheel masses, and accounts for dynamic weight transfer, inertial and gyroscopic effects, and aerodynamic drag. Two versions have employed. In the first one the rear and front suspensions have not been included, but for validation in low speed scenario it remains a good approximation af a real motorcycle. However, suspension motion is a must for transient analysis in accelerating manoeuvres. Thus, the updated version of eleven degrees of freedom has been used in traction torque distribution investigations. This multibody model represented an essential tool for developed study.

Simple Proportional–Integral controllers control speed and steer inputs, if required, to allow simulated motorcycles to undertake similar manoeuvres, and, thus, the different vehicles can be directly compared.

Together, these components form advanced models of a motorcycle that are suitable for detailed investigations into the effects of the front wheel motorization.

6.1.2 Tyre modelling

Various tyre models has been coded for use with the vehicle models. The tyre models presented include a linear model, and two Magic Formula models, specifically declined for motorcycles.

The first linear model and its simplified nonlinear generalization founded on Magic Formula are based on [92] and work in pure slip condition. They are appropriate for motorcycle investigations at low speed.

The most complex of the tyre models calculates all six principle forces and moments, and includes the effects of the vertical load and combined slip situations. It has been proposed a simplification of MF-Tyre 6.2 Magic Formula version [103], the last one available until now which can handle both car and motorcycle tyres. The main drawback of MF-Tyre 6.2 model is that it includes more than a hundred of parameters not easy to manage; for this reason, it has been proposed a simplified version which considers a reduced subset of parameters without losing the aforementioned features. The proposed tyre model has been implemented in Simulink in a format designed to be reusable and adaptable to different tyres, since the user can select model parameters from a mask.

The three presented tyre models can be employed for different levels of accuracy in the whole motorcycle control design process: from system modelling oriented to control, to control design until numerical validation phase.

6.1.3 Low speed stability

At low speed the study investigated whether and how the front wheel torque helps the stabilization of the vehicle around the upright position, without any rider action required and possibly in a small bounded area.

At first, the second objective has been neglected and a control system has been designed, based on the developed analytical model, with the aim to pursue a null roll angle, i.e. the vehicle stabilization in the upright position. Since the front wheel torque has a greater authority on the roll angle than the rear wheel one, at the beginning a single wheel torque as control input (the front one) has been used, setting the rear one equal to zero. This choice also allows to analyse how the front torque affects the vehicle stabilization.

Two control techniques have been tested and compared on the system:

- a PID controller, for its simplicity;
- a sliding mode control, a nonlinear control technique with two main advantages: a simple implementation and robustness to match model uncertainties.

Simulation results have shown that vehicle stabilization is achieved with both controllers: a first positive answer to the thesis investigation. Plots of state variables with the first method have shown that the vehicle is balanced in a shorter

trajectory than the sliding mode controller, even tough it applies a higher front wheel torque. This condition is preferred for real applications.

Previous analysis remains into theoretical framework. Then, both the mathematical model and the designed single input PID and sliding mode controllers have been validated with the first version of the multibody model, that one without suspensions. Validation tests have been carried out comparing analytical model response to the multibody software one. Simulations have shown a good match in roll angles: the same controller can stabilize the complex motorcycle multibody model of the software as well, behaving in a similar way with respect to the response of the simple analytical one. This means that the mathematical model captures the main roll dynamics and can be used for other model-based control systems.

For application in real situations such as in red traffic light, the second priority is to control the stabilization in a small bounded area. To achieve this second control objective two separate feedback loops for rear and front wheel torque using two PID controllers have been designed; the rear wheel controller has been employed to bound longitudinal vehicle motion as much as possible controlling the rear contact point speed. The attempt of designing a MIMO sliding mode controller has been also discussed, but some structural issues and possible singularities on sliding hypothesis have been highlighted. The designed MIMO control system with PID architecture slightly reduces the path with respect to SISO simulations, but the results are not so satisfactory as expected. Indeed, to confine the self-standing action in a small bounded area around the rear contact point a swaying motion forward and backward similar to the inverted pendulum control was expected, but such a motion has not been realized in numerical simulations. Furthermore, the validation tests highlighted some discrepancies, especially in velocity variable and the trajectory as direct consequence. A possible cause of these difficulties could be the excessive simplicity of the controller or the presence of other fundamental dynamics not captured by the simplified model.

Concluding, the conducted study in this topic remains still preliminary. However, despite the difficulties of confining the self-balancing action into a small bounded area, the sliding mode controller as well as the PID control strategy have proved the front wheel traction torque affects the stability of the vehicle, thus it can be involved as support into other motorcycle safety systems.

6.1.4 Optimal traction strategy

A second way to investigate other possible benefits of having active front wheel torque is to explore how and how much the traction torque repartition can

improve continuously the vehicle performances in combined longitudinal and lateral acceleration situations, such as the exit of a curve, especially in those conditions where a traditional motorcycle falls down because it overcomes tyre adherence limits.

Advantages of AWD configuration over the classical rear wheel drive one have been measured comparing $g - g$ diagrams, i.e. the plot of the longitudinal versus lateral accelerations of the vehicle which depicts the motorcycle admissible motions and is strictly related to tyre adhesion: if in same manoeuvres the AWD bike with a braking or traction torque repartition does not lose the grip, whereas the RWD overcomes tyre adhesion and falls down, the AWD architecture has clear benefits.

In order to derive a simplified $g - g$ diagram, the motorcycle has been modelled as a lumped mass, which is subjected to steady-state longitudinal and lateral accelerations and from it the optimal traction strategy has been derived, as function of the longitudinal and lateral acceleration. These accelerations can be directly related to the overall traction demand and roll angle.

Following the general approach, then the presented traction strategy has been validated in a steady state analysis with a more complex model: the steady state contour map of the simple model has been compared with the same one generated using an updated version of the multibody model, because the first one had no suspensions, a must for off-road bikes and accelerating manoeuvres. In order to plot this diagram and get motorcycles performances it has been necessary to reduce the multibody dynamic model to a steady state one. Furthermore, for a better analysis also some improvements in the tyre model would have been beneficial, thus the simplified version of MF-Tyre 6.2 Magic Formula has been applied as tyre model. The steady state analysis on the multibody model has confirmed the superiority of AWD motorcycle over a conventional motorcycle, at least in steady motion and a sensitivity analysis proved the robustness of the control strategy.

However, it is essential to guarantee the strategy works in steady turning as well as in transient manoeuvres. In this perspective, time domain simulations of few manoeuvres has been carried out in Simulink, both in straight running and cornering. Dynamical simulations have corroborated the steady state results of the kinetostatic model and once again the advantages of engaging a suitable driving strategy. Finally, for off-road bikes, it is important to considerer rough roads in addition to the perfectly smooth ones. So a random road profile has been generated with typical spectral characteristics and used in a selected subset of simulations, concluding the work.

This second aspect of the general problem about the optimal traction strategy for an all-wheel drive motorcycle has yielded interesting results. Indeed, if important

advantages of changing the distribution of power between the wheels for higher control on the vehicle have already been identified and applied in braking manoeuvres and many braking repartition strategies such as for example the ABS cornering already exists for motorcycles, all encouraged by the matter of fact all motorcycles have both front and rear brakes, the same it is not true in traction any more. The optimal traction strategy derived throughout this thesis has no equivalent in literature based on author's knowledge, at least that simultaneously

- works both in straight running and in cornering;
- is scientifically based on a model, instead of an empirical law;
- does not use a fixed ratio between rear and front wheel torque;
- takes into account the driving conditions.

It has been proved that major improvements of an AWD bike on the traditional one are registered on off road low adherence terrains and in cornering manoeuvres when vehicle runs in combined longitudinal and lateral acceleration. This means that a motorcycle controlled by a suitable driving strategy can achieve higher accelerations and in general, more lateral acceleration through a given corner or more longitudinal acceleration on a straight corresponds to quicker lap times.

Additionally, the investigation has explored and proved the possibility of implementing the presented driving strategy on any commercial motorcycle provided with an electric motor for each wheel without requiring any further sensor. The fact that it does not require the a priori knowledge of tyre friction coefficient is crucial in this perspective. The implementable solution is a simplification of the optimal one because it neglects the lateral acceleration term. However, numerical simulations have proved that despite slightly losing on performances with respect to the optimal solution, the advantage over RWD bike remains high. The work has referred to an AWD motorcycle with two electric motors, but the solution can be also applied if the front wheel is driven by mechanical or hydraulic systems. Furthermore, at least theoretically the choice of a feedforward control law based on the throttle required by the driver and its implementation by means of a sensorless solution makes easier and smoother the motorcycle handling and follows the driving desires of the pilot improving his driving feeling. All these features make the presented method applicable to real motorcycles and industrially appealing. For these reasons, it has been decided to try to patent the formula of traction repartition.

6.1.5 Overall conclusions

Currently, powering the front wheel of a motorcycle mechanically or hydraulically is difficult and expensive: such motorcycles are sold at a premium for speciality purposes. Furthermore, the change of bike design adds weight and cost to the vehicle; thus, for most situations, it is difficult to justify the added expense. However, with electric motors becoming cheaper and more common in automotive, it is foreseeable that vehicles with drive sources at each wheel will become available. In this situation, it would be sensible to take advantages of the gains that active front wheel torque and drive or brake torque repartition can provide in handling, stability and vehicle performances. As for automobiles, if the trend is towards electric propulsion, and powering the front wheel becomes easier, this research has shown the on and off-road handling and stability characteristics will not be adversely affected by the front drive torque; conversely, they are actually facilitated, and the power on the front wheel could be utilized to support other rider assist systems, for example in emergency situations. Furthermore, improvements in low-friction traction could be realised.

Concluding, since the electric propulsion is the energy of the next future, the research represents a good starting point to understand how this technology and the front wheel power can be utilized, not only to the advantage of the environment, but also as a benefit to vehicle performances, riding and driver's safety in potentially dangerous situations such as close to tyre adherence limit.

6.2 Original contributions to knowledge

This Section outlines the elements of work contained in this thesis that, in the author's opinion, represent original contributions to knowledge.

- For the self-balancing problem, a four degrees of freedom nonlinear mathematical model with two control inputs – the rear and front wheel torques - for an all-wheel drive electric motorcycle has been derived in the perspective of stability control system design. Two feature distinguish the presented model from the others proposed into the literature: it takes into account the presence of a driving front wheel torque, instead of the usual front braking torque; it works when vehicle moves at low speed (0.1-1 m/s). The model validation with a complex multibody software has highlighted a good match in the roll angle response, which means the presented analytical model captures the main roll motion dynamics and can be used for other more advanced nonlinear model-based control systems, both SISO and MIMO.

- The possible influence of the front wheel torque on self-balancing process of the motorcycle, without any rider action or steer torque actuation, has been investigated by means of two control systems: a PID controller and a sliding mode one. The analysis of control strategies on both analytical and multibody model has shown the possibility to generate a stabilizing momentum around the roll axis of motorcycle with the front wheel torque.

- A complex tyre model that includes the effects of vertical load variation, combined slip, and camber angle on tyre forces and moments has been proposed. It is a simplified version of MF-Tyre 6.2 Magic Formula: the proposed model requires a reduced subset of parameters instead of more than a hundred of parameters of the original one, without losing the aforementioned features. It has been included into the multibody model to carry out more reliable numerical simulations for the optimal traction strategy validation, but it is reusable in other multibody models when high level of accuracy in tyre model is required.

- A novel optimal traction torque distribution law has derived based on a simplified model instead of on empirical laws. It does not require the knowledge of the road friction coefficient and takes into account the driving conditions (longitudinal and lateral accelerations). Its implementation on a real motorcycle has been discussed and a simplified sensorless solution is proposed, neglecting the lateral acceleration term. The final traction repartition strategy again outperforms the traditional single track motorcycle, in face of a slight loss of performances over the optimal one.

- The motorcycle has been analysed in straight line and cornering situations, both in steady state and transient manoeuvres as well as in uneven roads in order to find out the effect of wheel torque distribution on vehicle performances. Real all-wheel drive motorcycles are rare; this investigation considers one of the advantages they might offer.

6.3 Future works

This work provides a foundation for many further interesting research topics. This Section aims to provide recommendations for areas of future work that would build on the current understanding of the all-wheel drive architecture adoption in motorcycles and its influences.

- The way in which traction torque distribution coexists with other stability and safety systems should be investigated. Integrated chassis control has the potential to integrate existing brake-based stability control (such as ABS cornering) with traction torque repartition and other possible future trends, such as active steering and active suspension.

- Many optimal braking distribution strategies exist in literature [139, 140]: it would be interesting to understand if strategies at low and high speed can be integrated in a single law and applied for braking repartition too.

- Experimental tests with an all wheel drive motorcycle should be carried out to validate results and provide human feedback on the quality of such a architecture and control method, which is hard, if not impossible, to calculate.

- With an electric motor at each wheel, it is feasible that energy could be recovered from one wheel and applied to another; thus, a torque imbalance could be generated regardless of the torque request from the driver. It would be interesting to see the effect of this additional torque difference in motorcycles, especially at low speeds.

- A control law should be developed, capable of calculating the torque that would, for example, minimise slip power, or understeer behaviour. The effect on the minimum lap time of an AWD-equipped race motorcycle would be particularly interesting.

- The performance on loose or low friction ground have more potential for improvement than high friction road situations, as theoretically shown in this thesis. More in-depth analyses in this sense should be undertaken.

- Further studies should be also undertaken to investigate the influences of the front wheel torque on the stability process.

- A more advanced controller should be developed, capable of self-balancing the motorcycle at low speed in a small bounded area and reduce the chattering effects on the control inputs in order to apply it into real situations such as when the vehicle stops during a red traffic light.

Bibliography

[1] L. De Novellis, A. Sorniotti, and P. Gruber. "Optimal wheel torque distribution for a four-wheel-drive fully electric vehicle". In: *SAE International Journal of Passenger Cars-Mechanical Systems* 6.2013-01-0673 (2013), pp. 128–136 (cit. on p. 3).

[2] J. N. Ross. *All-wheel-drive vehicle sales flourishing*. Ed. by Autoblog. URL: `https://www.autoblog.com/2013/12/12/all-wheel-drive-vehicle-sales-rise` (cit. on p. 5).

[3] J.W. Griffin and A.A. Popov. "Multibody dynamics simulation of an all-wheel-drive motorcycle for handling and energy efficiency investigations". In: *Vehicle system dynamics* 56.7 (2018), pp. 983–1001 (cit. on pp. 5, 124).

[4] A. Clerc. "Physique et chimie populaires, t. 2". In: *Paris: Jules Rouff, ss* (1883), pp. 48–50 (cit. on p. 6).

[5] O. Bolton. "Electrical bicycle". Pat. US552271A. 1895 (cit. on p. 6).

[6] Popular Mechanics. "Hearst Magazines 10/1911". In: *ISSN* 32.4558 (), p. 560 (cit. on p. 6).

[7] *"Ransomes, Sims and Jefferies"*. URL: `www.gracesguide.co.uk` (cit. on p. 7).

[8] Erwin Tragatsch. "Alle Motorräder 1894-1981, Bd. 1, 9". In: *Aufl., Stuttgart* (1992) (cit. on p. 7).

[9] National Museum of American History Smithsonian Institution. *Alikli fuel cell history*. 2016. URL: `americanhistory.si.edu` (cit. on p. 7).

[10] AMA Motorcycle Hall of Fame. *Mike Corbin*. URL: `motorcyclemuseum.org` (cit. on p. 7).

[11] A. Łebkowski. "Electric motorcycle powertrain analysis". In: (2016) (cit. on pp. 7, 8).

[12] J. Blissett et al. “Design of electrical system for racing electric motorcycles”. In: *2016 International Conference on Electrical Systems for Aircraft, Railway, Ship Propulsion and Road Vehicles & International Transportation Electrification Conference (ESARS-ITEC)*. IEEE. 2016, pp. 1–5 (cit. on p. 7).

[13] Y. Matsuda, T. Murase, and D. Kawai. *The feasibility study of a design concept of electric motorcycle*. Tech. rep. SAE Technical Paper, 2015 (cit. on p. 7).

[14] E. Drummond et al. “Design and Construction of an Electric Motorcycle”. In: *2019 Systems and Information Engineering Design Symposium (SIEDS)*. IEEE. 2019, pp. 1–6 (cit. on p. 7).

[15] R. Nasiri-Zarandi and M. Ebrahimi. “Extracting requirements for design a two-wheels electric vehicle and proposing a design procedure”. In: *2018 9th Annual Power Electronics, Drives Systems and Technologies Conference (PEDSTC)*. IEEE. 2018, pp. 462–468 (cit. on p. 7).

[16] T. Bäuml. “Modelling, simulation and validation of an electrical zero emission off-road motorcycle”. In: *2010 IEEE Vehicle Power and Propulsion Conference*. IEEE. 2010, pp. 1–5 (cit. on pp. 7, 11).

[17] S. Uberti et al. “An eco-innovation and technical contaminated approach for designing a low environmental impact off-road motorcycle”. In: *International Journal on Interactive Design and Manufacturing (IJIDeM)* 12.1 (2018), pp. 281–295 (cit. on p. 7).

[18] Department of applied Chemistry. *Applied physical chemistry laboratory*. Ed. by Waseda University. URL: `http://www.ec.appchem.waseda.ac.jp/researche/introe_energy.htm` (cit. on p. 9).

[19] V. A. Katić et al. “Electrification of the vehicle propulsion system–an overview”. In: *Facta Universitatis, Series: Electronics and Energetics* 27.2 (2014), pp. 299–316 (cit. on pp. 9, 11).

[20] A. Khaligh and Z. Li. “Battery, ultracapacitor, fuel cell, and hybrid energy storage systems for electric, hybrid electric, fuel cell, and plug-in hybrid electric vehicles: State of the art”. In: *IEEE transactions on Vehicular Technology* 59.6 (2010), pp. 2806–2814 (cit. on p. 9).

[21] F. Un-Noor et al. “A comprehensive study of key electric vehicle (EV) components, technologies, challenges, impacts, and future direction of development”. In: *Energies* 10.8 (2017), p. 1217 (cit. on pp. 9–12).

[22] C. C. Chan and et al. “The state of the art of electric and hybrid vehicles”. In: *Proceedings of the IEEE* 90.2 (2002), pp. 247–275 (cit. on p. 11).

[23] D. Tokunaga and K. Kesamaru. “Development of novel PM motors for sport type electric motorcycles”. In: *2012 15th International Conference on Electrical Machines and Systems (ICEMS)*. IEEE. 2012, pp. 1–4 (cit. on p. 11).

[24] J. Y. Yong et al. “A review on the state-of-the-art technologies of electric vehicle, its impacts and prospects”. In: *Renewable and Sustainable Energy Reviews* 49 (2015), pp. 365–385 (cit. on p. 12).

[25] P. Y. Xuan, M. Henz, and J. Weigl. “Environmental impact of converted electrical motorcycle”. In: *World Electric Vehicle Journal* 6.4 (2013), pp. 1136–1143 (cit. on p. 12).

[26] P. Kerdlap and S. H. Gheewala. “Electric motorcycles in Thailand: A life cycle perspective”. In: *Journal of Industrial Ecology* 20.6 (2016), pp. 1399–1411 (cit. on p. 12).

[27] N. Sheng, X. Zhou, and Y. Zhou. “Environmental impact of electric motorcycles: Evidence from traffic noise assessment by a building-based data mining technique”. In: *Science of the Total Environment* 554 (2016), pp. 73–82 (cit. on p. 12).

[28] F. M. Ibanez et al. “Extending the Autonomy of a Battery for Electric Motorcycles”. In: *IEEE Transactions on Vehicular Technology* 68.4 (2019), pp. 3294–3305 (cit. on p. 13).

[29] OECD/IEA. *Global EV Outlook 2017*. 2017 (cit. on p. 13).

[30] M. E. Lawson and W. E. Lawson. *All wheel drive motorcycle with enhanced soft terrain capabilities*. US Patent 9,828,062. 2017 (cit. on p. 13).

[31] *Christini Technologies Inc. The basics of AWD.* URL: `https://www.christini.com/awd-technology/about-the-tech` (cit. on pp. 13, 14, 151).

[32] *About Rokon. History.* URL: `https://www.rokon.com/about-rokon` (cit. on pp. 13, 151).

[33] L. J. Öhlins. *2WD - the complete story.* 2013. URL: `https://www.ohlins.com/about/history/` (cit. on pp. 13, 16, 151).

[34] *Visionar srl, Armotia - 2WD motorcycle.* URL: `http://www.armotia.com/en/history/` (cit. on pp. 13, 19, 151).

[35] C. H. Fehn. *Motorcycle having two driven wheels*. US Patent 3,268,025. 1966 (cit. on pp. 13, 14).

[36] K. Yamauchi. *Front and rear wheel drive motorcycle*. US Patent 5,113,964. 1992 (cit. on p. 14).

[37] S. J. Christini and M. J. Dunn. *Two-wheel drive two-wheeled vehicle*. US Patent 8,689,957. 2014 (cit. on p. 14).

[38] S. Hieble. *Motorcycle with adjustable-power front wheel drive (all wheel drive)*. US Patent 5,894,903. 1999 (cit. on p. 16).

[39] S. Ohshita, L. Jansson, and L. Gustafsson. *Two wheel drive motorcycle*. European Patent Office EP0779205B1. 2002 (cit. on p. 16).

[40] Z. Inokay. *Hydromechanical front wheel drive for motorcycles*. WIPO (PCT) WO2005075285A1. 2005 (cit. on p. 16).

[41] L. Gustafsson. *Arrangement and device for driving a vehicle wheel, preferably a motorcycle front wheel*. WIPO (PCT) WO2003070554A1. 2003 (cit. on p. 16).

[42] P. H. Southwell. "MECHANICAL, ELECTRICAL OR HYDRAULIC TRANSMISSION?" In: *Canadian Agricultural Engineering* 2.1 (1960), pp. 24–27 (cit. on p. 17).

[43] *BMW Motorrad launches the R 1200 GS xDrive Hybrid*. URL: `https://www.press.bmwgroup.com/global/article/detail/T0269445EN/bmw-motorrad-launches-the-r-1200-gs-xdrive-hybrid-world-premiere-of-the-first-travel-enduro-featuring-hybrid-all-wheel-drive?language=en` (cit. on p. 18).

[44] B. C. Chen et al. "Modeling and control of hybrid electric motorcycle with direct-driven wheel motor". In: *SAE transactions* (2004), pp. 785–791 (cit. on p. 18).

[45] V. T. Nguyen, P. Hwang, and T. Huynh. "Computational analysis on Hybrid Electric Motorcycle with front wheel electric motor using Lithium Ion battery". In: *2017 International Conference on System Science and Engineering (ICSSE)*. IEEE. 2017, pp. 355–359 (cit. on p. 18).

[46] A. Badgujar et al. "Hybrid two wheel drive motorcycle with range extend". In: *IJSRD International Journal for Scientific Rsearch & Development* 4.3 (2016) (cit. on p. 19).

[47] J. Trunkenpolz. *Vehicle*. US Patent App. 12/449,407. 2010 (cit. on p. 19).

[48] R. L. Nicoson. *Electric Front Wheel Drive System for Motorcycle*. US Patent App. 12/539,756. 2011 (cit. on p. 19).

[49] T. Eguchi. *Drive control system and drive control method for front-and rear-wheel drive vehicle*. US Patent App. 15/336,159. 2017 (cit. on p. 19).

[50] E. A. Werner et al. *Motorcycle with an Electrically Driveable Front Wheel*. US Patent App. 15/868,485. 2018 (cit. on p. 19).

[51] L. Cheng et al. "Ring Motor Front Wheel for Electric Motorcycle". In: *2019 IEEE Power and Energy Conference at Illinois (PECI)*. IEEE, pp. 1–8 (cit. on p. 19).

[52] M. Baumann, M. Buchholz, and K. Dietmayer. "A two-wheel driven power train for improved safety and efficiency in electric motorbikes". In: *World Electric Vehicle Journal* 8.1 (2016), pp. 102–111 (cit. on p. 19).

[53] E. V. Meyers. *Two wheeled vehicle with all wheel drive system*. WIPO (PCT) Patent WO2011150366A1. 2012 (cit. on p. 19).

[54] R. S. Sharp. "The stability and control of motorcycles". In: *Journal of mechanical engineering science* 13.5 (1971), pp. 316–329 (cit. on pp. 22, 32, 35, 93).

[55] Y. Zhang et al. "Balance control and analysis of stationary riderless motorcycles". In: *2011 IEEE International Conference on Robotics and Automation*. IEEE. 2011, pp. 3018–3023 (cit. on pp. 22, 93).

[56] M. Yokomori, K. Higuchi, and T. Ooya. "Rider's operation of a Motorcycle Straight at Low Speed". In: *JSME international journal. Ser. 3, Vibration, control engineering, engineering for industry* 35.4 (1992), pp. 553–559 (cit. on p. 22).

[57] M. Baumann et al. "Model-based corner braking control for electric motorcycles". In: *IFAC-PapersOnLine* 49.11 (2016), pp. 291–296 (cit. on pp. 27, 30, 96, 123).

[58] P. De Filippi et al. "Electronic stability control for powered two-wheelers". In: *IEEE transactions on control systems technology* 22.1 (2013), pp. 265–272 (cit. on pp. 27, 30, 96, 123).

[59] V. Cossalter and R. Lot. "A motorcycle multi-body model for real time simulations based on the natural coordinates approach". In: *Vehicle system dynamics* 37.6 (2002), pp. 423–447 (cit. on pp. 28, 32, 50, 53, 153).

[60] K.A. Seffen, G.T. Parks, and P.J. Clarkson. "Observations on the controllability of motion of two-wheelers". In: *Proceedings of the institution of mechanical engineers, part I: journal of systems and control engineering* 215.2 (2001), pp. 143–156 (cit. on p. 29).

[61] M. Tanelli et al. “Control-oriented steering dynamics analysis in sport motorcycles: modeling, identification and experiments”. In: *IFAC Proceedings Volumes* 42.10 (2009), pp. 468–473 (cit. on p. 29).

[62] N. H. Getz. “Dynamic inversion of nonlinear maps with applications to nonlinear control and robotics”. PhD thesis. University of California, Berkeley, 1995 (cit. on p. 29).

[63] A. Saccon, J. Hauser, and A. Beghi. “Trajectory exploration of a rigid motorcycle model”. In: *IEEE Transactions on Control Systems Technology* 20.2 (2011), pp. 424–437 (cit. on p. 29).

[64] J. Yi, Y. Zhang, and D. Song. “Autonomous motorcycles for agile maneuvers, part I: dynamic modeling”. In: *Proceedings of the 48h IEEE Conference on Decision and Control (CDC) held jointly with 2009 28th Chinese Control Conference*. IEEE. 2009, pp. 4613–4618 (cit. on p. 30).

[65] M. Corno et al. “Control-oriented modeling of motorcycle dynamics”. In: *IFAC Proceedings Volumes* 45.16 (2012), pp. 769–774 (cit. on p. 30).

[66] P. De Filippi et al. “Enhancing active safety of two-wheeled vehicles via electronic stability control”. In: *IFAC Proceedings Volumes* 44.1 (2011), pp. 638–643 (cit. on pp. 30, 98).

[67] S. Singhania, I. Kageyama, and V. M. Karanam. “Study on Low-Speed Stability of a Motorcycle”. In: *Applied Sciences* 9.11 (2019), p. 2278 (cit. on pp. 30, 93).

[68] C. Yang and T. Murakami. “Full-speed range self-balancing electric motorcycles without the handlebar”. In: *IEEE Transactions on Industrial Electronics* 63.3 (2015), pp. 1911–1922 (cit. on pp. 30, 31, 94).

[69] C. Koenen. “The dynamic behaviour of a motorcycle when running straight ahead and when cornering”. PhD thesis. PhD thesis, Delft University, 1983 (cit. on pp. 32, 33).

[70] J. P. Meijaard and A. A. Popov. “Multi-body modelling and analysis into the non-linear behaviour of modern motorcycles”. In: *Proceedings of the institution of mechanical engineers, part K: journal of multi-body dynamics* 221.1 (2007), pp. 63–76 (cit. on pp. 32, 61, 62).

[71] V. Cossalter. *Motorcycle dynamics*. Lulu. com, 2006 (cit. on pp. 32, 35, 36, 38, 42, 90, 93).

[72] A. L. Schwab, J. P. Meijaard, and J. M. Papadopoulos. "Benchmark results on the linearized equations of motion of an uncontrolled bicycle". In: *Journal of mechanical science and technology* 19.1 (2005), pp. 292–304 (cit. on p. 32).

[73] W. Ooms, I.J.M. Besselink, and H. Nijmeijer. "Motorcycle modelling and control". PhD thesis. Master's Thesis, Technische Universiteit Eindhoven, 2011 (cit. on p. 32).

[74] A. Bonci et al. "Modelling of all-wheel-drive motorcycle for dymanics analysis and control". In: *Bicycle and Motorcycle Dynamics 2019 (BMD 2019), Symposium on the Dynamics and Control of Single Track vehicles* (University of Padua, Italy). Poster (cit. on p. 32).

[75] D. J.N. Limebeer and R. S. Sharp. "Bicycles, motorcycles, and models". In: *IEEE Control Systems Magazine* 26.5 (2006), pp. 34–61 (cit. on p. 32).

[76] The Mathworks. *Simscape Multibody -Model and simulate multibody mechanical systems*. URL: `https://www.mathworks.com/products/simmechanics.html` (cit. on p. 32).

[77] Mechanical Simulation Corporation. *Mechanical simulation: home page*. URL: `http://www.carsim.com/` (cit. on p. 32).

[78] Dessault Systemes. *Industry solutions - Modelica Libraries*. URL: `https://www.3ds.com/products-services/catia/products/dymola/industry-solutions/` (cit. on p. 32).

[79] MSC Software. *Adams the multibody dynamics simulation solution*. URL: `http://www.mscsoftware.com/product/adams` (cit. on p. 32).

[80] L. T. Ooms W. abd Scharbrodt. *13 degrees of freedom motorcycle model*. URL: `https://it.mathworks.com/matlabcentral/fileexchange/67975-13-dof-motorcycle-model-w-ooms` (cit. on p. 32).

[81] R. S. Sharp and D. J. N. Limebeer. "A motorcycle model for stability and control analysis". In: *Multibody system dynamics* 6.2 (2001), pp. 123–142 (cit. on p. 33).

[82] R. S. Sharp, S. Evangelou, and D. J. N. Limebeer. "Advances in the modelling of motorcycle dynamics". In: *Multibody system dynamics* 12.3 (2004), pp. 251–283 (cit. on p. 33).

[83] H. Pacejka. *Tire and vehicle dynamics*. Elsevier, 2005 (cit. on pp. 33, 42, 60, 61, 68, 70, 72, 77, 90).

[84] The Modelica Association. *Modelica Language*. URL: `https://www.modelica.org/` (cit. on p. 33).

[85] T. Schmitt. "Modeling of a motorcycle in Dymola/Modelica". PhD thesis. Master's thesis, Vorarlberg University of Applied Sciences, 2009 (cit. on p. 33).

[86] R. Capitani et al. "Handling analysis of a two-wheeled vehicle using MSC. ADAMS/motorcycle". In: *Vehicle system dynamics* 44.sup1 (2006), pp. 698–707 (cit. on p. 33).

[87] A. Nakamura and T. Murakami. "A stabilization control of two wheels driven wheelchair". In: *2009 IEEE/RSJ International Conference on Intelligent Robots and Systems*. IEEE. 2009, pp. 4863–4868 (cit. on p. 35).

[88] M. Bruschetta et al. "Design and implementation of a high performance non linear MPC- virtual motorcycle rider". In: *Bicycle and Motorcycle Dynamics 2019 (BMD 2019), Symposium on the Dynamics and Control of Single Track vehicles* (University of Padua, Italy) (cit. on pp. 35, 54).

[89] L. D. Metz and L. G. Metz. "Vehicle Dynamics Terminology". In: *SAE Recommended Practice J670e* () (cit. on p. 39).

[90] Verdiana Del Rosso et al. "Self-balancing electric motorcycle moelling at low speed: preliminary results". In: *Proceeding of 6th European Conference on Computational Mechanics (Solids, Structures and Coupled Problems) ECCM 6 7th European Conference on Computational Fluid Dynamics ECFD 7*. CIMNE. 2018, pp. 3699–3710 (cit. on p. 43).

[91] G. R. Fowles and G. L. Cassiday. *Analytical mechanics*. Belmont, CA: Thomson Brooks/Cole, 2005 (cit. on p. 43).

[92] R. Lot. *FastBikeRT software - User Manual Version 1.1. Multibody software for dynamics analysis of two wheel vehicles*. Dynamotion (cit. on pp. 50, 51, 67, 72, 154).

[93] J. Garcia De Jalon and E. Bayo. *Kinematic and dynamic simulation of multibody systems: the real-time challenge*. Springer Science & Business Media, 2012 (cit. on p. 50).

[94] *MBSymba*. URL: `http://www.multibody.net/mbsymba/` (cit. on p. 50).

[95] R. Lot. "A motorcycle tire model for dynamic simulations: Theoretical and experimental aspects". In: *Meccanica* 39.3 (2004), pp. 207–220 (cit. on pp. 52, 90, 91).

[96] A. Saccon, J. Hauser, and A. Beghi. "A virtual rider for motorcycles: Maneuver regulation of a multi-body vehicle model". In: *IEEE Transactions on Control Systems Technology* 21.2 (2012), pp. 332–346 (cit. on p. 54).

[97] V. Cossalter et al. “A general method for the evaluation of vehicle manoeuvrability with special emphasis on motorcycles”. In: *Vehicle system dynamics* 31.2 (1999), pp. 113–135 (cit. on p. 54).

[98] R. Lot, M. Massaro, and R. Sartori. “Advanced motorcycle virtual rider”. In: *Vehicle System Dynamics* 46.S1 (2008), pp. 215–224 (cit. on p. 54).

[99] B. Li, X. Yang, and J. Yang. “Tire model application and parameter identification-a literature review”. In: *SAE International Journal of Passenger Cars-Mechanical Systems* 7.2014-01-0872 (2014), pp. 231–243 (cit. on p. 60).

[100] E. Fiala. *Seitenkrafte am rollenden luftreifen'Z. VDI bd. 96, no. 29*. 1954 (cit. on p. 60).

[101] G. Gim. “An analytical model of pneumatic tyres for vehicle dynamic simulations. Part 2: Comprehensive slips”. In: *International journal of vehicle design* 12.1 (1991), pp. 19–39 (cit. on p. 60).

[102] H. B. Pacejka and R. S. Sharp. “Shear force development by pneumatic tyres in steady state conditions: a review of modelling aspects”. In: *Vehicle system dynamics* 20.3-4 (1991), pp. 121–175 (cit. on pp. 60, 61).

[103] TNO. *MF-tyre/MF-Swift 6.2 manual*. 2013 (cit. on pp. 61, 75–77, 82, 86, 154).

[104] F. Farroni et al. “A real-time thermal model for the analysis of tyre/road interaction in motorcycle applications”. In: *Proceedings, Bicycle and Motorcycle Dynamics 2019 (BMD 2019), Symposium on the Dynamics and Control of Single Track vehicles* (University of Padua, Italy) (cit. on p. 61).

[105] E. Leo et al. “Effects of tire wear on motorcycle dynamics”. In: *Proceedings, Bicycle and Motorcycle Dynamics 2019 (BMD 2019), Symposium on the Dynamics and Control of Single Track vehicles* (University of Padua, Italy) (cit. on p. 61).

[106] E.V.O.J. Kuiper and J.J.M. Van Oosten. “The PAC2002 advanced handling tire model”. In: *Vehicle system dynamics* 45.S1 (2007), pp. 153–167 (cit. on p. 61).

[107] J. E. Bernard and C. L. Clover. “Tire modeling for low-speed and high-speed calculations”. In: *SAE transactions* (1995), pp. 474–483 (cit. on p. 61).

[108] E. J. H. De Vries and H. B. Pacejka. “Motorcycle tyre measurements and models”. In: *Vehicle System Dynamics* 29.S1 (1998), pp. 280–298 (cit. on p. 77).

[109] J.D.G. Kooijman et al. “A bicycle can be self-stable without gyroscopic or caster effects”. In: *Science* 332.6027 (2011), pp. 339–342 (cit. on p. 93).

[110] R.S. Sharp and Y. Watanabe. “Chatter vibrations of high-performance motorcycles”. In: *Vehicle System Dynamics* 51.3 (2013), pp. 393–404 (cit. on p. 93).

[111] H. Sakai. *Theoretical and Fundamental Consideration to Accord between Self-Steer Speed and Rolling in Maneuverability of Motorcycles*. Tech. rep. SAE Technical Paper, 2018 (cit. on p. 93).

[112] Y. Takenouchi, T. Sekine, and M. OKANO. *Study on condition of stability of motorcycle at low speed*. Tech. rep. SAE Technical Paper, 2002 (cit. on p. 93).

[113] A.L. Schwab, J.P. Meijaard, and J.D.G. Kooijman. “Some recent developments in bicycle dynamics”. In: *Proceedings of the 12th World Congress in Mechanism and Machine Science*. 2007, pp. 1–6 (cit. on p. 93).

[114] Y. Zhang and J. Yi. “Dynamic modeling and balance control of human/bicycle systems”. In: *2010 IEEE/ASME International Conference on Advanced Intelligent Mechatronics*. IEEE. 2010, pp. 1385–1390 (cit. on p. 93).

[115] C. F. Huang, Y. C. Tung, and T. Yeh. “Balancing control of a robot bicycle with uncertain center of gravity”. In: *2017 IEEE International Conference on Robotics and Automation (ICRA)*. IEEE. 2017, pp. 5858–5863 (cit. on p. 94).

[116] L. Keo et al. “Experimental results for stabilizing of a bicycle with a flywheel balancer”. In: *2011 IEEE international conference on robotics and automation*. IEEE. 2011, pp. 6150–6155 (cit. on p. 94).

[117] Y. Tanaka and T. Murakami. “Self sustaining bicycle robot with steering controller”. In: *The 8th IEEE International Workshop on Advanced Motion Control (AMC04)*. IEEE. 2004, pp. 193–197 (cit. on p. 94).

[118] H. Niki and T. Murakami. “An approach to self stabilization of bicycle motion by handle controller”. In: *IEEJ Transactions on Industry Applications* 125 (2005), pp. 779–785 (cit. on p. 94).

[119] Y. Feng, R. Du, and Y. Xu. “Steering angle balance control method for riderless bicycle based on ADAMS”. In: *International Conference on Intelligent Transportation*. Springer. 2016, pp. 15–31 (cit. on p. 94).

[120] J. Yi, Yizhai Zhang, and D. Song. "Autonomous motorcycles for agile maneuvers, part II: Control systems design". In: *Proceedings of the 48h IEEE Conference on Decision and Control (CDC) held jointly with 2009 28th Chinese Control Conference*. IEEE. 2009, pp. 4619–4624 (cit. on p. 94).

[121] T. Kimura, Y. Ando, and E. Tsujii. "Development of new concept two-wheel steering system for motorcycles". In: *SAE International Journal of Passenger Cars-Electronic and Electrical Systems* 7.2013-32-9106 (2013), pp. 36–40 (cit. on p. 94).

[122] M. Araki, K. Akimoto, and T. Takenaka. "Study of Riding Assist Control Enabling Self-Standing in Stationary State". In: *SAE International Journal of Vehicle Dynamics, Stability, and NVH* 3.10-03-01-0004 (2018) (cit. on p. 95).

[123] Y. Yavin. "Stabilization and control of the motion of an autonomous bicycle by using a rotor for the tilting moment". In: *Computer methods in applied mechanics and engineering* 178.3-4 (1999), pp. 233–243 (cit. on p. 95).

[124] S. Lee and W. Ham. "Self stabilizing strategy in tracking control of unmanned electric bicycle with mass balance". In: *IEEE/RSJ international conference on intelligent robots and systems*. Vol. 3. IEEE. 2002, pp. 2200–2205 (cit. on p. 95).

[125] M. Tsuchiya and E. Tsujii. "Motorcycle Dynamics and control of the MOTOROiD that stands upright even when stopped". In: *Bicycle and Motorcycle Dynamics 2019 (BMD 2019), Symposium on the Dynamics and Control of Single Track vehicles* (University of Padua, Italy). Poster (cit. on p. 95).

[126] R. Lot and J. Fleming. "Gyroscopic stabilisers for powered two-wheeled vehicles". In: *Vehicle System Dynamics* 57.9 (2019), pp. 1381–1406 (cit. on p. 95).

[127] A.V. Beznos et al. "Control of autonomous motion of two-wheel bicycle with gyroscopic stabilisation". In: *Proceedings. 1998 IEEE International Conference on Robotics and Automation (Cat. No. 98CH36146)*. Vol. 3. IEEE. 1998, pp. 2670–2675 (cit. on p. 95).

[128] H. Yetkin et al. "Gyroscopic stabilization of an unmanned bicycle". In: *2014 American Control Conference*. IEEE. 2014, pp. 4549–4554 (cit. on p. 95).

[129] S.V. Emelyanov and V.A. Taran. "On a class of variable structure control systems". In: *Proc. of USSR Academy of Sciences, Energy and Automation*. Vol. 3. 1962 (cit. on p. 100).

[130] S.V. Emel'yanov, V.I. Utkin, V.A. Taran, et al. "Theory of systems with variable structure [in Russian]". In: *Science, Moscow* (1970) (cit. on p. 100).

[131] V. I. Utkin. "Sliding Modes and Their Application in Variable Structure Systems [in Russian]". In: *Moscow, Nauka* (1974) (cit. on p. 100).

[132] U. Itkis. *Control systems of variable structure*. Wiley New York, 1976 (cit. on p. 100).

[133] V. Utkin. "Variable structure systems with sliding modes". In: *IEEE Transactions on Automatic control* 22.2 (1977), pp. 212–222 (cit. on p. 100).

[134] C. Edwards and S. Spurgeon. *Sliding mode control: theory and applications*. Crc Press, 1998 (cit. on pp. 101, 102, 107).

[135] L. Keo and M. Yamakita. "Controlling balancer and steering for bicycle stabilization". In: *2009 IEEE/RSJ International Conference on Intelligent Robots and Systems*. IEEE. 2009, pp. 4541–4546 (cit. on p. 101).

[136] C. Vecchio and A. Ferrara. "Sliding Mode Control: theoretical developments and applications to uncertain mechanical systems". Master's thesis in Automatic Control and Robotics. Università degli studi di Pavia, Dipartimento di Informatica e Sistemistica, 2008 (cit. on p. 101).

[137] Verdiana Del Rosso et al. "Modelling and Control of a Self-Balancing Electric Motorcycle: Preliminary Results". In: *2018 26th Mediterranean Conference on Control and Automation (MED)*. IEEE. 2018, pp. 867–872 (cit. on p. 108).

[138] Verdiana Del Rosso et al. "Self-balancing two-wheel drive electric motorcycle modelling and control: preliminary results". In: *2018 5th International Conference on Control, Decision and Information Technologies (CoDIT)*. IEEE. 2018, pp. 358–363 (cit. on pp. 108, 114).

[139] M. Corno et al. "On optimal motorcycle braking". In: *Control Engineering Practice* 16.6 (2008), pp. 644–657 (cit. on pp. 123, 124, 160).

[140] F. Biral and R. Lot. "An interpretative model of gg diagrams of racing motorcycle". In: *Proceedings of the 3rd ICMEM International Conference on Mechanical Engineering and Mechanics. Beijing, Repubblica Popolare Cinese, Ottobre*. 2009, pp. 21–23 (cit. on pp. 123, 160).

[141] A. Bonci et al. "A Smooth Traction Control Design for Two-Wheeled electric vehicles". In: *2018 14th IEEE/ASME International Conference on Mechatronic and Embedded Systems and Applications (MESA)*. IEEE. 2018, pp. 1–6 (cit. on p. 124).

[142] T. Abumi and T. Murakami. "Slip ratio control considering road condition for Two-Wheel drive electric motorcycle". In: *2014 10th France-Japan/8th Europe-Asia Congress on Mecatronics (MECATRONICS2014-Tokyo)*. IEEE. 2014, pp. 53–57 (cit. on p. 124).

[143] F. Maggio, F. Biral, and M. Da Lio. *How Gearbox Ratios Influence Lap Time and Driving Style. An Analysis Based on Time-Optimal Maneuvers.* Tech. rep. SAE Technical Paper, 2003 (cit. on p. 124).

[144] M. Norgia et al. "Optical sensors for real-time measurement of motorcycle tilt angle". In: *IEEE Transactions on Instrumentation and Measurement* 58.5 (2009), pp. 1640–1649 (cit. on p. 135).

[145] R. Lot, V. Cossalter, and M. Massaro. "Real-time roll angle estimation for two-wheeled vehicles". In: *ASME 2012 11th Biennial Conference on Engineering Systems Design and Analysis*. American Society of Mechanical Engineers. 2012, pp. 687–693 (cit. on p. 135).

[146] I. Boniolo, S. M. Savaresi, and M. Tanelli. "Lean angle estimation in two-wheeled vehicles with a reduced sensor configuration". In: *2012 IEEE International Symposium on Circuits and Systems*. IEEE. 2012, pp. 2573–2576 (cit. on p. 135).

[147] M. Schlipsing et al. "Roll angle estimation for motorcycles: Comparing video and inertial sensor approaches". In: *2012 IEEE Intelligent Vehicles Symposium*. IEEE. 2012, pp. 500–505 (cit. on p. 135).

[148] B. Ashok, S. D. Ashok, and C. R. Kumar. "A review on control system architecture of a SI engine management system". In: *Annual Reviews in Control* 41 (2016), pp. 94–118 (cit. on p. 138).

[149] R. Lot et al. "Optimal Traction Strategy for All-Wheel Drive Electric Motorcycles". In: *IEEE Transactions on Vehicular Technology* (2019). under review (cit. on p. 138).

[150] V. Cossalter, A. Doria, and R. Lot. "Steady turning of two-wheeled vehicles". In: *Vehicle system dynamics* 31.3 (1999), pp. 157–181 (cit. on p. 139).

[151] Inter. Org. for Standardization and Technical Committee ISO/TC and Mechanical Vibration and Shock. Subcommittee SC2 Measurement and Evaluation of Mechanical Vibration and Shock as Applied to Machines. *Mechanical Vibration–Road Surface Profiles–Reporting of Measured Data*. 2nd. International Organization for Standardization, 2016 (cit. on p. 147).

[152] M. Agostinacchio, D. Ciampa, and S. Olita. “The vibrations induced by surface irregularities in road pavements–a Matlab® approach”. In: *European Transport Research Review* 6.3 (2014), p. 267 (cit. on p. 147).

Appendix A

Motorcycle model parameters

This Appendix lists the parameters used for both analytical and multibody models of the motorcycle and for tyre models. Values given here are used in the numerical simulations unless otherwise stated in the text. They has been got from a real motorcycle.

A.1 Motorcycle parameters

Table A.1: Geometrical properties.

Symbol	Value	Unit	Description
w	1.416	m	wheelbase
ε	24	deg	caster angle
a_n	0.107	m	mechanical trail
R_f, R_r	0.347, 0.318	m	front and rear tyre radius
ρ_f, ρ_r	0.04, 0.05	m	tyre cross-sectional radius of curvature
l_{sa}	0.596	m	swingarm
s_a	16.8	deg	nominal swingarm angle

Table A.2: Inertial motorcycle properties of analytical model (2.32)-(2.35) for self-balancing problem. The motorcycle is modelled as a lumped mass with the steering axis rotated at its maximum angle. The rider is not included.

Symbol	Value	Unit	Description
m	130.5	kg	overall mass
(b, h)	(0.745,0.601)	m	$x-z$ position of the overall CoM G
I_{xx}, I_{yy}, I_{zz}	8.268, 27.945, 21.025	kg m^2	principle moments of inertia
I_{xy}, I_{xz}, I_{yz}	-0.552 0.19, -0.016	kg m^2	products of inertia
N_f, N_r	678.69,600.69	N	front and rear tyre load

Table A.3: Inertial motorcycle properties of multibody model in FastBike code (see Section 2.5) for the optimal traction strategy.

Symbol	Value	Unit	Description
m_0	207.7	kg	overall mass
m_f, m_r	29.2, 108.5	kg	front and rear chassis mass
m_{rid}	70	kg	rider mass
(b_0, h_0)	(0.704, 0.842)	m	$x-z$ position of centre of mass
(b_f, h_f)	(1.301, 0.563)	m	$x-z$ position of front centre of mass
(b_r, h_r)	(0.604, 0.884)	m	$x-z$ position of rear centre of mass
e	0.0288	m	front eccentricity
$I_{fxx}, I_{fyy}, I_{fzz}$	3.11, 3.97, 1.212	kg m^2	front principle moments of inertia
$I_{rxx}, I_{ryy}, I_{rzz}$	29.1, 37.1, 11.1	kg m^2	rear principle moments of inertia
I_{wf}, I_{wr}	0.666, 0.867	kg m^2	front, rear wheel spin moments of inertia

Table A.4: Other parameters

Symbol	Value	Unit	Description
$C_D A$	0.4	m^2	drag coefficient
c_δ	6	Nm/rad s^{-1}	steering column damping
δ	40	degree	steering rotation in self-balance problem
g	9.806	m/s^2	gravity acceleration

A.2 Tyre models parameters

Table A.5: Linear and Basic Tyre Model parameters.

Symbol	Value	Unit	Description
D_x	1.0		longitudinal adherence
K_κ	10.0	1/rad	longitudinal stiffness
D_y	1.0		lateral adherence
K_α	10.0	1/rad	sideslip stiffness
K_γ	0.8	1/rad	camber stiffness
a_t	0.02	m	pneumatic trail
c_γ	0.02	m	twisting stiffness
K_ψ			rotational slip stiffness
a_0	0.2	rad	self-aligning non-linear coefficient
t_w	0		twisting non-linear coefficient

Table A.6: Full Tyre Model parameters of torques. The model uses non dimensional parameters.

Symbol	**Value**	**Description**
R_0	0.3 [m]	nominal unloaded tyre radius
Yaw torque		
B_t	8.0	trail stiffness
C_t	0.95	trail shape factor
q_{Dz1}	0.12	pneumatic trail peak with load
E_t	-15	trail curvature factor
B_r	0.2	twisting stiffness
q_{Dz8}	0.06	var peak twisting with camber
q_{Dz10}	-0.02	var peak twisting with squared camber
Rolling resistance		
q_{sy1}	0.01	rolling friction
q_{sy2}	0.02	rolling friction with long force

Table A.7: Full Tyre Model parameters of longitudinal and lateral forces. The model uses non dimensional parameters.

Symbol	**Value**	**Description**
F_{z0}	1000 [N]	nominal tyre load
Longitudinal force		
p_{Cx1}	1.606	longitudinal shape
p_{Dx1}	1.2	longitudinal friction
p_{Dx2}	-0.092	variation long friction with load
p_{Dx3}	0.85	variation long friction with camber
p_{Ex3}	0.026	longitudinal curvature
p_{Kx1}	25.94	longitudinal stiffness
p_{Kx2}	-4.233	longitudinal stiffness with load
r_{Bx1}	13.476	slope factor for combined slip reduction F_x
r_{Bx2}	1.0	influence of camber of stiffness for combined
r_{Cx1}	1.0	long shape factor for combined
Lateral force		
p_{Cy1}	8.0	lateral shape factor
p_{Dy1}	1.2	lateral friction
p_{Dy2}	-0.05	variation of lateral friction with load
p_{Dy3}	0.0	variation of lateral friction with camber
p_{Ey1}	-0.946	lateral curvature at F_{z0}
p_{Ky1}	20.0	lateral sideslip stiffness
p_{Ky2}	1.0	sideslip stiffness with load
p_{Ky3}	0.0	variation of sideslip stiffness with camber
p_{Ky4}	0.6	peak slip stiffness with load
p_{Ky6}	1.3	camber stiffness
p_{Ky7}	0.0	camber stiffness load dependency
r_{By1}	7.786	slope factor for combined slip reduction F_y
r_{By2}	8.169	variation of slope reduction with sideslip
r_{Cy1}	1.0	lateral shape factor for combined
Relaxation length		
σ_r	0.14 [m]	rear relaxation length
σ_f	0.07 [m]	front relaxation length

Appendix B

Matlab code: kinetostatic model

```
function res = FastBike_stationary(s)
% takes the static variables and returns the residuals of FastBike model
global speed ax ay % independent variables
global myMotoPar RearTyrePar FrontTyrePar bike % model and tyre parameters
global k_velx k_omegar k_omegaf weight scalecenter % scaling factors
global paranalysis b0_n h0_n m0_n % nominal CoG position

% The Matlab FastBike files use a set of 19 state variables
% but the static one has 15.
% steady state vars
% s= [1=phi, 2=mu, 3=z, 4=delta, 5=fs, 6=sa, 7=Vgx, 8=Vgy, 9=yaw_rate, 10=omega_r, 11=omega_f, 12=SteerTorque, 13=DrivingForce, 14 = Ry/weight, 15 = Fy/weight]
% where Vgx, Vgy and yawrate are CoG speeds in body fixed reference frame
% Ry and Fy are rear and front tyre lateral forces
% state variables of motorcycle model (in chassis reference frame)
% xC = [1=phi, 2=mu, 3=z, 4=delta, 5=fs, 6=sa, 7=V_x, 8=V_y, 9=V_z, 10=Omega_x, 11=Omega_y, 12=Omega_z, 13=delta_dot = 0, 14=fs_dot = 0, 15=sa_dot = 0, 16=omega_r, 17=omega_f, 18=yr, =19yf]

%% conversion from steady state vars <s> to dynamic states <xC>

% scaling factors
    scalecenter = 1; % centre of variable scale
    k_velx = speed;
    % wheel angular velocities
    k_omegar = speed/myMotoPar.P_R__r; %s(10) omega_r
    k_omegaf = speed/myMotoPar.P_R__f; %s(11) omega_f

```

```
26      weight = myMotoPar.P_m*9.806; % 2000; s(13) % driving force
27
28  % model internal state variables
29  xC(1) = s(1);  %phi, roll angle
30  xC(2) = s(2);  %mu, pitch angle
31  xC(3) = s(3);  %h, CoG position
32  xC(4) = s(4);  %delta, steer angle
33  xC(5) = s(5);  %fs, fork travel
34  xC(6) = s(6);  %sa, swingarm angle
35
36  % CoG speed in chassis reference frame
37  Vxg=k_velx*(s(7)+scalecenter*0); Vyg=s(8); Vzg=0; %psi=0;
38  % xC(7) = (cos(psi) * sin(xC(1)) * Vyg - sin(xC(1)) * sin(psi) * Vxg
        - cos(xC(1)) * Vzg) * sin(xC(2)) + cos(xC(2))*(cos(psi)*Vxg +sin(
        psi)*Vyg);
39  % xC(8) = -Vxg * sin(psi) * cos(xC(1)) + Vyg * cos(psi) * cos(xC(1))
        + Vzg * sin(xC(1));
40  % xC(9) = (-cos(psi) * sin(xC(1)) * Vyg + sin(xC(1)) * sin(psi) * Vxg
         + cos(xC(1)) * Vzg) * cos(xC(2)) + sin(xC(2))*(cos(psi)*Vxg +sin(
        psi)*Vyg);
41
42  xC(7) = (sin(xC(1)) * Vyg  - cos(xC(1))*Vzg)*sin(xC(2)) + cos(xC(2))*
        Vxg;
43  xC(8) = Vyg * cos(xC(1)) + Vzg * sin(xC(1));
44  xC(9) = (-sin(xC(1)) * Vyg + cos(xC(1))*Vzg)*cos(xC(2)) + sin(xC(2))*
        Vxg;
45
46  % chassis angular speed in body fixed reference frame
47  %Omega__x = -sin(mu) * cos(phi) * yaw_rate + cos(mu) * roll_rate;
48  %Omega__y = sin(phi) * yaw_rate + pitch_rate;
49  %Omega__z = yaw_rate * cos(phi) * cos(mu) + roll_rate * sin(mu);
50  xC(10) = -sin(s(2)) * cos(s(1)) * s(9);  %Omega_x,
51  xC(11) = sin(s(1)) * s(9);  %Omega_y,
52  xC(12) = s(9) * cos(s(1)) * cos(s(2));  %Omega_z,
53
54  xC(13) = 0; % delta_dot = 0, steer rate
55  xC(14) =  0; % fs_dot = 0, fork travel rate
56  xC(14) =  0; %  sa_dot = 0, swingarm angle rate
57  xC(16) = k_omegar*(s(10)+scalecenter); % omega_r
58  xC(17) = k_omegaf*(s(11)+scalecenter); % omega_f
59  %Ry = s(14)*weight; Fy = s(15)*weight; % rear and front lateral tyre
        forces
60  xC(18) = s(14); % equations are discarded
61  xC(19) = s(15); % equations are discarded
62
```

```
63
64 %% model derivatives calculation
65 [StateVariables,RearTyreContact_pre,RearTyreKinematics1,
       FrontTyreContact_pre, FrontTyreKinematics1,
       RearSuspensionKinematics,FrontSuspensionKinematics] =
       FastBikeRTv3_outputs(xC,myMotoPar);
66
67 RearTyreContact  = 150e3*RearTyreContact_pre;
68 FrontTyreContact = 150e3*FrontTyreContact_pre;
69
70 % Tyre forces with Full Tyre Model
71 [RearTyreForce, RearSlip] = TyreMagic2013(RearTyreContact,RearTyrePar
       .RearTyrePressure,RearTyreKinematics1,RearTyrePar);
72 [FrontTyreForce, FrontSlip] = TyreMagic2013(FrontTyreContact,
       FrontTyrePar.FrontTyrePressure,FrontTyreKinematics1,FrontTyrePar);
73
74 % rear swingarm and front fork suspension forces
75 RearSuspensionForce = SpringDamperFcn(RearSuspensionKinematics,
       myMotoPar.cr,myMotoPar.kr);
76 FrontSuspensionForce = SpringDamperFcn(FrontSuspensionKinematics,
       myMotoPar.cf,myMotoPar.kf);
77
78 % dynamical system
79 SteerTorque1 = s(12);
80 EngineWheelTorque = 0.0;
81
82 switch bike
83     case 'AWD'
84         gg = 9.81; % gravity
85         if paranalysis % set b0 e h0 for par analysis equals to
               nominal position
86             b0 = b0_n;
87             h0 = h0_n;
88         else
89             b0 = myMotoPar.P_b0;
90             h0 = myMotoPar.P_h0;
91         end
92         % AWD optimal traction bias
93         beta = 1-(b0-h0*ax/sqrt(gg^2+ay^2))/myMotoPar.P_w;
94     case 'AWD_star'
95         gg = 9.81; % gravity
96         if paranalysis % set b0 e h0 for parametric analysis
97             b0 = b0_n;
98             h0 = h0_n;
99             m0 = m0_n;
```

```
100         else
101             b0 = myMotoPar.P_b0;
102             h0 = myMotoPar.P_h0;
103             m0 = myMotoPar.P_m;
104         end
105          % AWD optimal traction bias with ay = 0 and ax = (Xr+Xf)/m
106           beta = 1-(b0-h0*(RearTyreForce.Fx+FrontTyreForce.Fx)/(m0*gg
                ))/myMotoPar.P_w;
107     case 'RWD'
108         beta = 1; % RWD traction bias
109 end
110
111 RearWheelTorque1 =     beta *s(13)*weight*myMotoPar.P_R__r;
112 FrontWheelTorque1= (1-beta)*s(13)*weight*myMotoPar.P_R__f;
113 %absolute frame
114 FxI = -myMotoPar.P_m*ax; FyI =0; FzI=0; % inertial force
115 %chassis frame
116 FxC = (sin(xC(1)) * FyI - cos(xC(1)) * FzI) * sin(xC(2)) + cos(xC(2))
        *FxI;
117 FyC = FyI * cos(xC(1)) + FzI * sin(xC(1));
118 FzC = (- sin(xC(1)) * FyI + cos(xC(1)) * FzI) * cos(xC(2)) + sin(xC
        (2))*FxI;
119 ExternalChassisForce = [FxC FyC FzC];
120 ExternalChassisTorque = [0 0 0];
121
122 % dynamic system
123 dxdt = FastBikeRTv3_derivatives(SteerTorque1, EngineWheelTorque,
        RearWheelTorque1, FrontWheelTorque1, ExternalChassisForce,
        ExternalChassisTorque, RearTyreForce, FrontTyreForce,
        RearSuspensionForce, FrontSuspensionForce, StateVariables,
        myMotoPar);
124
125
126 %% residuals: kinetostatic problem
127 % select the derivatives of static variables
128 % roll_rate = 0 = dxdt(1) %d(phi)/dt
129 % pitch_rate = 0 = dxdt(2)%d(mu)/dt,
130 % dxdt(3)=dh/dt=0  %d(h)/dt,
131 % steer_rate = 0 = dxdt(4)%d(delta)/dt,
132 % fs_dot = 0 = dxdt(5)%d(fs)/dt,
133 % sa_dot = 0 = dxdt(6)%d(sa)/dt,
134 res(1) = dxdt(7);%d(V_x)/dt,  Newton X
135 res(2) = dxdt(8);%d(V_y)/dt,  Newton Y
136 res(3) = dxdt(9);%d(V_z)/dt   Newton Z
137 res(4) = dxdt(10);%d(Omega_x)/dt,   Euler X
```

```
138 res(5) = dxdt(11);%d(Omega_y)/dt,    Euler Y
139 res(6) = dxdt(12);%d(Omega_z)/dt,    Euler Z
140 res(7) = dxdt(13);%d(delta_dot)/dt   Euler steer
141 res(8) = dxdt(14);%d(fs_dot)/dt      Suspension equation
142 res(9) = dxdt(15);%d(sa_dot)/dt      Suspension equation
143 res(10) = dxdt(16);%d(omega_r)/dt,   Wheel spin equation
144 res(11) = dxdt(17);%d(omega_f)/dt,   Wheel spin equation
145 res(14) = dxdt(18); %d(yr)/dt,   not considered
146 res(15) = dxdt(19); %d(yf)/dt    not considered
147
148 % additional equations to set desired speed and lateral acceleration
      as independent variables instead of Steering Torque and Rear Wheel
      Torque
149 % s(7) = Vxg; s(9) = yaw rate
150 res(12) = k_velx*(s(7)+scalecenter*0)-speed;
151 res(13) = speed*s(9)-ay;
152
153 end
```